
JSCSEN 87(3)293–399(2022)

ISSN 1820-7421(Online)

Journal of the Serbian Chemical Society

electronic

VOLUME 87

No 3

BELGRADE 2022



Available on line at



www.shd.org.rs/JSCS/

The full search of JSCS
is available through

DOAJ DIRECTORY OF
OPEN ACCESS
JOURNALS
www.doaj.org

The **Journal of the Serbian Chemical Society** (formerly Glasnik Hemijskog društva Beograd), one volume (12 issues) per year, publishes articles from the fields of chemistry. The **Journal** is financially supported by the **Ministry of Education, Science and Technological Development of the Republic of Serbia**.

Articles published in the **Journal** are indexed in **Clarivate Analytics products: Science Citation Index-Expanded™** – accessed via **Web of Science®** and **Journal Citation Reports®**.

Impact Factor announced 2021: **1.240; 5-year Impact Factor: 1.144.**

Articles appearing in the **Journal** are also abstracted by: **Scopus, Chemical Abstracts Plus (CAplus™), Directory of Open Access Journals, Referativni Zhurnal (VINITI), RSC Analytical Abstracts, EuroPub, Pro Quest and Asian Digital Library.**

Publisher:

Serbian Chemical Society, Karnegijeva 4/III, P. O. Box 36, 1120 Belgrade 35, Serbia
tel./fax: +381-11-3370-467, E-mails: **Society** – shd@shd.org.rs; **Journal** – jscs@shd.org.rs
Home Pages: **Society** – <http://www.shd.org.rs/>; **Journal** – <http://www.shd.org.rs/JSCS/>
Contents, Abstracts and full papers (from Vol 64, No. 1, 1999) are available in the electronic form at the Web Site of the **Journal** (<http://www.shd.org.rs/JSCS/>).

Internet Service:

Former Editors:

Nikola A. Pušin (1930–1947), **Aleksandar M. Leko** (1948–1954),
Panta S. Tutundžić (1955–1961), **Miloš K. Mladenović** (1962–1964),
Dorđe M. Dimitrijević (1965–1969), **Aleksandar R. Despić** (1969–1975),
Slobodan V. Ribnikar (1975–1985), **Dragutin M. Dražić** (1986–2006).

Editor-in-Chief:

BRANISLAV Ž. NIKOLIĆ, Serbian Chemical Society (E-mail: jscs-ed@shd.org.rs)

Deputy Editor:

DUŠAN SLADIĆ, Faculty of Chemistry, University of Belgrade

Sub editors:

Organic Chemistry

DEJAN OPSENICA, Institute of Chemistry, Technology and Metallurgy, University of Belgrade

Biochemistry and Biotechnology

JÁNOS CSANÁDI, Faculty of Science, University of Novi Sad

Inorganic Chemistry

OLGICA NEDIĆ, INEP – Institute for the Application of Nuclear Energy, University of Belgrade

Theoretical Chemistry

MILOŠ ĐURAN, Serbian Chemical Society

Physical Chemistry

IVAN JURANIĆ, Serbian Chemical Society

Electrochemistry

LJILJANA DAMJANOVIĆ-VASILIĆ, Faculty of Physical Chemistry, University of Belgrade

Analytical Chemistry

SNEŽANA GOJKOVIĆ, Faculty of Technology and Metallurgy, University of Belgrade

Polymers

SLAVICA RAŽIĆ, Faculty of Pharmacy, University of Belgrade

Thermodynamics

BRANKO DUNJIĆ, Faculty of Technology and Metallurgy, University of Belgrade

Chemical Engineering

MIRJANA KIJEVČANIN, Faculty of Technology and Metallurgy, University of Belgrade

Materials

TATJANA KALUDEROVIĆ RADOIČIĆ, Faculty of Technology and Metallurgy, University of Belgrade

Metallic Materials and Metallurgy

RADA PETROVIĆ, Faculty of Technology and Metallurgy, University of Belgrade

Environmental and Geochemistry

ANA KOSTOV, Mining and Metallurgy Institute Bor, University of Belgrade

History of and Education in Chemistry

VESNA ANTIĆ, Faculty of Agriculture, University of Belgrade

English Language Editors:

DRAGICA TRIVIĆ, Faculty of Chemistry, University of Belgrade

Technical Editors:

LYNNE KATSIKAS, Serbian Chemical Society

Journal Manager & Web Master:

VLATKA VAJS, Serbian Chemical Society

Office:

JASMINA NIKOLIĆ, Faculty of Technology and Metallurgy, University of Belgrade

VLADIMIR PANIĆ, ALEKSANDAR DEKANSKI, VUK FILIPOVIĆ, Institute of Chemistry, Technology and Metallurgy, University of Belgrade

ALEKSANDAR DEKANSKI, Institute of Chemistry, Technology and Metallurgy, University of Belgrade

VERA ĆUŠIĆ, Serbian Chemical Society

Editorial Board

From abroad: **R. Adžić**, Brookhaven National Laboratory (USA); **A. Casini**, University of Groningen (The Netherlands); **G. Cobb**, Baylor University (USA); **D. Douglas**, University of British Columbia (Canada); **G. Inzelt**, Etvos Lorand University (Hungary); **N. Katsaros**, NCSR “Demokritos”, Institute of Physical Chemistry (Greece); **J. Kenny**, University of Perugia (Italy); **Ya. I. Korenman**, Voronezh Academy of Technology (Russian Federation); **M. D. Lechner**, University of Osnabrueck (Germany); **S. Macura**, Mayo Clinic (USA); **M. Spiteller**, INFU, Technical University Dortmund (Germany); **M. Stratakis**, University of Crete (Greece); **M. Swart**, University de Girona (Cataluna, Spain); **G. Vunjak-Novaković**, Columbia University (USA); **P. Worsfold**, University of Plymouth (UK); **J. Zagal**, Universidad de Santiago de Chile (Chile).

From Serbia: **B. Abramović**, **V. Antić**, **V. Beškoski**, **J. Csanadi**, **Lj. Damjanović-Vasić**, **A. Dekanski**, **V. Dondur**, **B. Dunjić**, **M. Duran**, **S. Gojković**, **I. Gutman**, **B. Jovančević**, **I. Juranić**, **T. Kaluderović Radiočić**, **L. Katsikas**, **M. Kijevčanin**, **A. Kostov**, **V. Leovac**, **S. Milonjić**, **V.B. Mišković-Stanković**, **O. Nedić**, **B. Nikolić**, **J. Nikolić**, **D. Opsićica**, **V. Panić**, **M. Petkovska**, **R. Petrović**, **I. Popović**, **B. Radak**, **S. Ražić**, **D. Sladić**, **S. Sovilj**, **S. Šerbanović**, **B. Solaja**, **Z. Tešić**, **D. Trivić**, **V. Vajs**.

Subscription: The annual subscription rate is **150.00 €** including postage (surface mail) and handling. For Society members from abroad rate is **50.00 €**. For the proforma invoice with the instruction for bank payment contact the Society Office (E-mail: shd@shd.org.rs) or see JSCS Web Site: <http://www.shd.org.rs/JSCS/>, option Subscription.

Godišnja pretplata: Za članove SHD: **2.500,00 RSD**, za penzionere i studente: **1000,00 RSD**, a za ostale: **3.500,00 RSD**; za organizacije i ustanove: **16.000,00 RSD**. Uplate se vrše na tekući račun Društva: **205-13815-62**, poziv na broj **320**, sa naznakom “pretplata za JSCS”.

Nota: Radovi čiji su svi autori članovi SHD prioritetno se publikuju.

Odlukom Odbora za hemiju Republičkog fonda za nauku Srbije, br. 66788/1 od 22.11.1990. godine, koja je kasnije potvrđena odlukom Saveta Fonda, časopis je uvršten u kategoriju međunarodnih časopisa (M-23). Takođe, aktom Ministarstva za nauku i tehnologiju Republike Srbije, 413-00-247/2000-01 od 15.06.2000. godine, ovaj časopis je proglašen za publikaciju od posebnog interesa za nauku. **Impact Factor** časopisa objavljen 2021. godine iznosi **1,240**, a petogodišnji **Impact Factor 1,144**.

The **Journal of the Serbian Chemical Society** (formerly Glasnik Hemijskog društva Beograd), one volume (12 issues) per year, publishes articles from the fields of chemistry. The **Journal** is financially supported by the **Ministry of Education, Science and Technological Development of the Republic of Serbia**.

Articles published in the **Journal** are indexed in **Clarivate Analytics products: Science Citation Index-Expanded™** – accessed via **Web of Science®** and **Journal Citation Reports®**.

Impact Factor announced 2020: **1.097; 5-year Impact Factor: 1.023.**

Articles appearing in the **Journal** are also abstracted by: **Scopus, Chemical Abstracts Plus (CAplusSM), Directory of Open Access Journals, Referativnii Zhurnal (VINITI), RSC Analytical Abstracts, EuroPub, Pro Quest and Asian Digital Library.**

Publisher:

Serbian Chemical Society, Karnegijeva 4/III, P. O. Box 36, 1120 Belgrade 35, Serbia
tel./fax: +381-11-3370-467, E-mails: **Society** – shd@shd.org.rs; **Journal** – jscs@shd.org.rs
Home Pages: **Society** – <http://www.shd.org.rs/>; **Journal** – <http://www.shd.org.rs/JSCS/>
Contents, Abstracts and full papers (from Vol 64, No. 1, 1999) are available in the electronic form at the Web Site of the **Journal** (<http://www.shd.org.rs/JSCS/>).

Internet Service:

Nikola A. Pušin (1930–1947), **Aleksandar M. Leko** (1948–1954),

Panta S. Tutundžić (1955–1961), **Miloš K. Mladenović** (1962–1964),

Dorđe M. Dimitrijević (1965–1969), **Aleksandar R. Despić** (1969–1975),

Slobodan V. Ribnikar (1975–1985), **Dragutin M. Dražić** (1986–2006).

BRANISLAV Ž. NIKOLIĆ, Serbian Chemical Society (E-mail: jscs-ed@shd.org.rs)

DUŠAN SLADIĆ, Faculty of Chemistry, University of Belgrade

Editor-in-Chief:

DEJAN OPSENICA, Institute of Chemistry, Technology and Metallurgy, University of Belgrade

Biochemistry and

JÁNOS CSANÁDI, Faculty of Science, University of Novi Sad

Biochemistry

OLGICA NEDIĆ, INEP – Institute for the Application of Nuclear Energy, University of Belgrade

Inorganic Chemistry

MILOŠ ĐURAN, Serbian Chemical Society

Theoretical Chemistry

IVAN JURANIĆ, Serbian Chemical Society

Physical Chemistry

LJILJANA DAMJANOVIĆ-VASILIĆ, Faculty of Physical Chemistry, University of Belgrade

Electrochemistry

SNEŽANA GOJKOVIĆ, Faculty of Technology and Metallurgy, University of Belgrade

Analytical Chemistry

SLAVICA RAŽIĆ, Faculty of Pharmacy, University of Belgrade

Polymers

BRANKO DUNJIĆ, Faculty of Technology and Metallurgy, University of Belgrade

Thermodynamics

MIRJANA KIJEVČANIN, Faculty of Technology and Metallurgy, University of Belgrade

Chemical Engineering

TATJANA KALUDEROVIĆ RADOIČIĆ, Faculty of Technology and Metallurgy, University of Belgrade

Materials

RADA PETROVIĆ, Faculty of Technology and Metallurgy, University of Belgrade

Metallic Materials and

METALLURGY

Environmental and

VESNA ANTIĆ, Faculty of Agriculture, University of Belgrade

Geochemistry

DRAGICA TRIVIĆ, Faculty of Chemistry, University of Belgrade

History of and

EDUCATION IN CHEMISTRY

English Language

LYNNE KATSIKAS, Serbian Chemical Society

Editors:

VLATKA VAJS, Serbian Chemical Society

Technical Editors:

JASMINA NIKOLIĆ, Faculty of Technology and Metallurgy, University of Belgrade

Journal Manager &

VLADIMIR PANIĆ, ALEKSANDAR DEKANSKI, VUK FILIPOVIĆ, Institute of

Web Master:

Chemistry, Technology and Metallurgy, University of Belgrade

Office:

ALEKSANDAR DEKANSKI, Institute of Chemistry, Technology and Metallurgy,

University of Belgrade

VERA ĆUŠIĆ, Serbian Chemical Society

Editorial Board

From abroad: **R. Adžić**, Brookhaven National Laboratory (USA); **A. Casini**, University of Groningen (The Netherlands); **G. Cobb**, Baylor University (USA); **D. Douglas**, University of British Columbia (Canada); **G. Inzelt**, Etvos Lorand University (Hungary); **N. Katsaros**, NCSR “Demokritos”, Institute of Physical Chemistry (Greece); **J. Kenny**, University of Perugia (Italy); **Ya. I. Korenman**, Voronezh Academy of Technology (Russian Federation); **M. D. Lechner**, University of Osnabrueck (Germany); **S. Macura**, Mayo Clinic (USA); **M. Spiteller**, INFU, Technical University Dortmund (Germany); **M. Stratakis**, University of Crete (Greece); **M. Swart**, University de Girona (Cataluna, Spain); **G. Vunjak-Novaković**, Columbia University (USA); **P. Worsfold**, University of Plymouth (UK); **J. Zagal**, Universidad de Santiago de Chile (Chile).

From Serbia: **B. Abramović**, **V. Antić**, **V. Beškoski**, **J. Csanadi**, **Lj. Damjanović-Vasilić**, **A. Dekanski**, **V. Dondur**, **B. Dunjić**, **M. Đuran**, **S. Gojković**, **I. Gutman**, **B. Jovančević**, **I. Juranić**, **L. Katsikas**, **M. Kijevečanin**, **V. Leovac**, **S. Milonjić**, **V.B. Mišković-Stanković**, **O. Nedić**, **B. Nikolić**, **J. Nikolić**, **D. Opsenica**, **V. Panić**, **M. Petkovska**, **R. Petrović**, **I. Popović**, **B. Radak**, **T. Kaluderović Radiočić**, **N. Radović**, **S. Ražić**, **D. Sladić**, **S. Sovilj**, **S. Šerbanović**, **B. Šolaja**, **Z. Tešić**, **D. Trivić**, **V. Vajs**.

Subscription: The annual subscription rate is **150.00 €** including postage (surface mail) and handling. For Society members from abroad rate is **50.00 €**. For the proforma invoice with the instruction for bank payment contact the Society Office (E-mail: shd@shd.org.rs) or see JSCS Web Site: <http://www.shd.org.rs/JSCS/>, option Subscription.

Godišnja pretplata: Za članove SHD: **2.500,00 RSD**, za penzionere i studente: **1000,00 RSD**, a za ostale: **3.500,00 RSD**; za organizacije i ustanove: **16.000,00 RSD**. Uplate se vrše na tekući račun Društva: **205-13815-62**, poziv na broj **320**, sa naznakom “pretplata za JSCS”.

Nota: Radovi čiji su svi autori članovi SHD prioritetno se publikuju.

Odlukom Odbora za hemiju Republičkog fonda za nauku Srbije, br. 66788/1 od 22.11.1990. godine, koja je kasnije potvrđena odlukom Saveta Fonda, časopis je uvršten u kategoriju međunarodnih časopisa (M-23). Takođe, aktom Ministarstva za nauku i tehnologiju Republike Srbije, 413-00-247/2000-01 od 15.06.2000. godine, ovaj časopis je proglašen za publikaciju od posebnog interesa za nauku. **Impact Factor** časopisa objavljen 2020. godine iznosi **1,097**, a petogodišnji **Impact Factor 1,023**.

INSTRUCTIONS FOR AUTHORS (2021)

GENERAL

The *Journal of the Serbian Chemical Society* (the *Journal* in further text) is an international journal publishing papers from all fields of chemistry and related disciplines. Twelve issues are published annually. The Editorial Board expects the editors, reviewers, and authors to respect the well-known standard of professional ethics.

Types of Contributions

Original scientific papers	(up to 15 typewritten pages, including Figures, Tables and References) report original research which must not have been previously published.
Short communications	(up to 8 pages) report unpublished preliminary results of sufficient importance to merit rapid publication.
Notes	(up to 5 pages) report unpublished results of short, but complete, original research
Authors' reviews	(up to 40 pages) present an overview of the author's current research with comparison to data of other scientists working in the field
Reviews ^a	(up to 40 pages) present a concise and critical survey of a specific research area. Generally, these are prepared at the invitation of the Editor
Surveys	(about 25 pages) communicate a short review of a specific research area.
Book and Web site reviews	(1 - 2 pages)
Extended abstracts	(about 4 pages) of Lectures given at meetings of the Serbian Chemical Society Divisions
Letters to the Editor	report miscellaneous topics directed directly to the Editor

^aGenerally, Authors' reviews, Reviews and Surveys are prepared at the invitation of the Editor.

Submission of manuscripts

Manuscripts should be submitted using the **OnLine Submission Form**, available on the JSCS Web Site (<http://www.shd-pub.org.rs/index.php/JSCS>). The manuscript must be uploaded as a Word.doc or .rtf file, with tables and figures (including the corresponding captions – above Tables and below Figures), placed within the text to follow the paragraph in which they were mentioned for the first time.

Please note that **Full Names** (First Name, Last Name), **Full Affiliation** and **Country** (from drop down menu) of **ALL OF AUTHORS** (written in accordance with English spelling rules - the first letter capitalized) must be entered in the manuscript Submission Form (Step 3). Manuscript Title, authors' names and affiliations, as well as the Abstract, **WILL APPEAR** in the article listing, as well as in **BIBLIOGRAPHIC DATABASES (WoS, SCOPUS...)**, in the form and in the order entered in the author details

Graphical abstract

Graphical abstract is a one-image file containing the main depiction of the authors work and/or conclusion and must be supplied along with the manuscript. It must enable readers to quickly gain the main message of the paper and to encourage browsing, help readers identify which papers are most relevant to their research interests. Authors must provide an image that clearly represents the research described in the paper. The most relevant figure from the work, which summarizes the content, can also be submitted. The image should be submitted as a separate file in **Online Submission Form - Step 2**.

Specifications: The graphical abstract should have a clear start and end, reading from top to bottom or left to right. Please omit unnecessary distractions as much as possible.

- **Image size:** minimum of 500×800 pixels (W×H) and a minimum resolution of 300 dpi. If a larger image is sent, then please use the same ratio: 16 wide × 9 high. Please note that your image will be scaled proportionally to fit in the available window in TOC; a 150x240 pixel rectangle. Please be sure that the quality of an image cannot be increased by changing the resolution from lower to higher, but only by resampling or exporting the image with a higher resolution, which can be set in usual "settings" option.
- **Font:** Please use Calibri and Symbol font with a large enough font size, so it is readable even from the image of a smaller size (150 × 240 px) in TOC.
- **File type:** JPG and PNG only.
No additional text, outline or synopsis should be included. Please do not use white space or any heading within the image.

Cover Letter

Manuscripts must be accompanied by a cover letter (strictly uploaded in **Online Submission Step 2**) in which the type of the submitted manuscript and a warranty as given below are given. The Author(s) has(have) to warranty that the manuscript submitted to the *Journal* for review is original, has been written by the stated author(s) and has not been published elsewhere; is currently not being considered for publication by any other journal and will not be submitted for such a review while under review by the *Journal*; the manuscript contains no libellous or other unlawful statements and does not contain any materials that violate any personal or proprietary rights of any other person or entity. All manuscripts will be acknowledged on receipt (by e-mail).

Illustrations

Illustrations (Figs, schemes, photos...) in TIF or EPS format (JPG format is acceptable for colour and greyscale photos, only), must be additionally uploaded (Online Submission Step 2) as a separate file or one archived (.zip, .rar or .arj) file. Figures and/or Schemes should be prepared according to the **Artwork Instructions** - http://www.shd.org.rs/JSCS/jscs-pdf/Artwork_Instructions.pdf!

For any difficulties and questions related to **OnLine Submission Form** - <https://www.shdpub.org.rs/index.php/JSCS/submission/wizard>, please refer to **User Guide** - <https://openjournal-systems.com/ojs-3-user-guide/>, Chapter **Submitting an Article** - <https://openjournalsystems.com/ojs-3-user-guide/submitting-an-article/>. If difficulties still persist, please contact JSCS Editorial Office at JSCS@shd.org.rs

A manuscript not prepared according to these instructions will be returned for resubmission without being assigned a reference number.

Conflict-of-Interest Statement*: Public trust in the peer review process and the credibility of published articles depend in part on how well a conflict of interest is handled during writing, peer review, and editorial decision making. A conflict of interest exists when an author (or the author's institution), reviewer, or editor has financial or personal relationships that inappropriately influence (bias) his or her actions (such relationships are also known as dual commitments, competing interests, or competing loyalties). These relationships vary from those with negligible potential to those with great potential to influence judgment, and not all relationships represent true conflict of interest. The potential for a conflict of interest can exist whether or not an individual believes that the relationship affects his or her scientific judgment. Financial relationships (such as employment, consultancies, stock ownership, honoraria, paid expert testimony) are the most easily identifiable conflicts of interest and the most likely to undermine the credibility of the journal, the authors, and of science itself. However, conflicts can occur for other reasons, such as personal relationships, academic competition, and intellectual passion.

Informed Consent Statement*: Patients have a right to privacy that should not be infringed without informed consent. Identifying information, including patients' names, initials, or hospital numbers, should not be published in written descriptions, photographs, and pedigrees unless the information is essential for scientific purposes and the patient (or parent or guardian) gives written informed consent for publication. Informed consent for this purpose requires that a patient who is identifiable be shown the manuscript to be published. Authors should identify individuals who provide writing assistance and disclose the funding source for this assistance. Identifying details should be omitted if they are not essential. Complete anonymity is difficult to achieve, however, and informed consent should be obtained if there is any doubt. For example, masking the eye region in photographs of patients is inadequate protection of anonymity. If identifying characteristics are altered to protect anonymity, such as in genetic pedigrees, authors should provide assurance that alterations do not distort scientific meaning and editors should so note. The requirement for informed consent should be included in the journal's instructions for authors. When informed consent has been obtained it should be indicated in the published article.

Human and Animal Rights Statement* When reporting experiments on human subjects, authors should indicate whether the procedures followed were in accordance with the ethical standards of the responsible committee on human experimentation (institutional and national) and with the Helsinki Declaration of 1975, as revised in 2000 (5). If doubt exists whether the research was conducted in accordance with the Helsinki Declaration, the authors must explain the rationale for their approach, and demonstrate that the institutional review body explicitly approved the doubtful aspects of the study. When reporting experiments on animals, authors should be asked to indicate whether the institutional and national guide for the care and use of laboratory animals was followed.

*International Committee of Medical Journal Editors ("Uniform Requirements for Manuscripts Submitted to Biomedical Journals"), February 2006

PROCEDURE

All contributions will be peer reviewed and only those deemed worthy and suitable will be accepted for publication. The Editor has the final decision. To facilitate the reviewing process, authors are encouraged to suggest up to three persons competent to review their manuscript. Such suggestions will be taken into consideration but not always accepted. If authors would prefer a specific person not be a reviewer, this should be announced. The Cover Letter must be accompanied by these suggestions. Manuscripts requiring revision should be returned according to the requirement of the Editor, within 60 days upon reception of the reviewing comments by e-mail.

The *Journal* maintains its policy and takes the liberty of correcting the English as well as false content of manuscripts **provisionally accepted** for publication in the first stage of reviewing process. In this second stage of manuscript preparation by JSCS Editorial Office, the author(s) may be required to supply some **additional clarifications and corrections**. This procedure will be executed during copyediting actions, with a demand to author(s) to perform corrections of unclear parts before the manuscript would be published OnLine as **finally accepted manuscript (OLF Section of the JSCS website)**. Please note that the manuscript can receive the status of **final rejection** if the author's corrections would not be satisfactory.

When finally accepted manuscript is ready for printing, the corresponding author will receive a request for proof reading, which should be performed within 2 days. Failure to do so will be taken as the authors agree with any alteration which may have occurred during the preparation of the manuscript for printing.

Accepted manuscripts of active members of the Serbian Chemical Society (all authors) have publishing priority.

MANUSCRIPT PRESENTATION

Manuscripts should be typed in English (either standard British or American English, but consistent throughout) with 1.5 spacing (12 points Times New Roman; Greek letters in the character font Symbol) in A4 format leaving 2.5 cm for margins. For Regional specific, non-standard characters that may appear in the text, save documents with Embed fonts Word option: *Save as -> (Tools) -> Save Options... -> Embed fonts in the text*.

The authors are requested to seek the assistance of competent English language expert, if necessary, to ensure their English is of a reasonable standard. The Serbian Chemical Society can provide this service in advance of submission of the manuscript. If this service is required, please contact the office of the Society by e-mail (jscs-info@shd.org.rs).

Tables, figures and/or schemes must be embedded in the main text of the manuscript and should follow the paragraph in which they are mentioned for the first time. **Tables** must be prepared with the aid of the **WORD table function**, without vertical lines. The minimum size of the font in the tables should be **10 pt**. Table columns must not be formatted using multiple spaces. Table rows must not be formatted using any returns (enter key; ↵ key) and are **limited to 12 cm width**. Tables should not be incorporated as graphical objects. **Footnotes to Tables** should follow them and are to be indicated consequently (in a single line) in superscript letters and separated by semi-column.

Table caption must be placed above corresponding Table, while **Captions of the Illustrations** (Figs. Schemes...) must follow the corresponding item. **The captions, either for Tables or Illustrations**, should make the items comprehensible without reading of the main text (but clearly referenced in), must follow numerical order (Roman for Tables, Arabic for Illustrations), and should not be provided on separate sheets or as separate files.

High resolution Illustrations (named as Fig. 1, Fig. 2... and/or Scheme 1, Scheme 2...) in **TIF or EPS format** (JPG format is acceptable for photos, only) **must be additionally uploaded as a separate files or one archived (.zip, .rar) file**.

Illustrations should be prepared according to the [ARTWORK INSTRUCTIONS](http://www.shd.org.rs/JSCS/jscs-pdf/Artwork_Instructions.pdf) - http://www.shd.org.rs/JSCS/jscs-pdf/Artwork_Instructions.pdf !

All pages of the manuscript must be numbered continuously.

DESIGNATION OF PHYSICAL QUANTITIES AND UNITS

IUPAC recommendations for the naming of compounds should be followed. SI units, or other permissible units, should be employed. The designation of physical quantities must be in italic throughout the text (including figures, tables and equations), whereas the units and indexes (except for indexes having the meaning of physical quantities) are in upright letters. They should be in Times New Roman font. In graphs and tables, a slash should be used to separate the designation of a physical quantity from the unit

(example: p / kPa, j / mA cm $^{-2}$, t / °C, T_0 / K, τ /h, $\ln(j / \text{mA cm}^{-2})$...). Designations such as: p (kPa), t [min]..., are not acceptable. However, if the full name of a physical quantity is unavoidable, it should be given in upright letters and separated from the unit by a comma (example: Pressure, kPa; Temperature, K; Current density, mA cm $^{-2}$...). Please do not use the axes of graphs for additional explanations; these should be mentioned in the figure captions and/or the manuscript (example: “pressure at the inlet of the system, kPa” should be avoided). The axis name should follow the direction of the axis (the name of y-axis should be rotated by 90°). Top and right axes should be avoided in diagrams, unless they are absolutely necessary.

Latin words, as well as the names of species, should be in *italic*, as for example: *i.e.*, *e.g.*, *in vivo*, *ibid*, *Calendula officinalis L.*, etc. The branching of organic compound should also be indicated in *italic*, for example, *n*-butanol, *tert*-butanol, etc.

Decimal numbers must have decimal points and not commas in the text (except in the Serbian abstract), tables and axis labels in graphical presentations of results. Thousands are separated, if at all, by a comma and not a point.

Mathematical and chemical equations should be given in separate lines and must be numbered, Arabic numbers, consecutively in parenthesis at the end of the line. All equations should be embedded in the text. Complex equations (fractions, integrals, matrix...) should be prepared with the aid of the **Microsoft Equation 3.0** (or higher) or **MathType** (Do not use them to create simple equations and labels). Using the **Insert -> Equation option, integrated in MS Office 2010 and MS Office 2013, as well as insertion of equation objects within paragraph text IS NOT ALLOWED.**

ARTICLE STRUCTURE

- TITLE PAGE;
- MAIN TEXT – including Tables and Illustrations with corresponding captions;
- SUPPLEMENTARY MATERIAL (optional)

Title page

- **Title** in bold letters, should be clear and concise, preferably 12 words or less. The use of non-standard abbreviations, symbols and formulae is discouraged.
- **AUTHORS' NAMES** in capital letters with the full first name, initials of further names separated by a space and surname. Commas should separate the author's names except for the last two names when ‘and’ is to be used. In multi-affiliation manuscripts, the author's affiliation should be indicated by an Arabic number placed in superscript after the name and before the affiliation. Use * to denote the corresponding author(s).
- *Affiliations* should be written in italic. The e-mail address of the corresponding author should be given after the affiliation(s).
- *Abstract:* A one-paragraph abstract written of 150 – 200 words in an impersonal form indicating the aims of the work, the main results and conclusions should be given and clearly set off from the text. Domestic authors should also submit, on a separate page, an Abstract - Izvod, the author's name(s) and affiliation(s) in Serbian (Cyrillic letters). (Домаћи аутори морају доставити Извод (укупнујући имена аутора и афилијацију) на српском језику, исписане ћирилицом, иза Захвалнице, а пре списка референци.) For authors outside Serbia, the Editorial Board will provide a Serbian translation of their English abstract.
- *Keywords:* Up to 6 keywords should be given. Do not use words appearing in the manuscript title
- **RUNNING TITLE:** A one line (maximum five words) short title in capital letters should be provided.

Main text – should have the form:

- **INTRODUCTION,**
- **EXPERIMENTAL (RESULTS AND DISCUSSION),**
- **RESULTS AND DISCUSSION (EXPERIMENTAL),**
- **CONCLUSIONS,**
- **NOMENCLATURE (optional) and**
- **Acknowledgements: If any.**
- **REFERENCES** (Citation of recent papers published in chemistry journals that highlight the significance of work to the general readership is encouraged.)

The sections should be arranged in a sequence generally accepted for publication in the respective fields. They subtitles should be in capital letters, centred and NOT numbered.

- The INTRODUCTION should include the aim of the research and a concise description of background information and related studies directly connected to the paper.
- The EXPERIMENTAL section should give the purity and source of all employed materials, as well as details of the instruments used. The employed methods should be described in sufficient detail to enable experienced persons to repeat them. Standard procedures should be referenced and only modifications described in detail. On no account should results be included in the experimental section.

Chemistry

Detailed information about instruments and general experimental techniques should be given in all necessary details. If special treatment for solvents or chemical purification were applied that must be emphasized.

Example: Melting points were determined on a Boetius PMHK or a Mel-Temp apparatus and were not corrected. Optical rotations were measured on a Rudolph Research Analytical automatic polarimeter, Autopol IV in dichloromethane (DCM) or methanol (MeOH) as solvent. IR spectra were recorded on a Perkin-Elmer spectrophotometer FT-IR 1725X. ^1H and ^{13}C NMR spectra were recorded on a Varian Gemini-200 spectrometer (at 200 and 50 MHz, respectively), and on a Bruker Ultrashield Advance III spectrometer (at 500 and 125 MHz, respectively) employing indicated solvents (*vide infra*) using TMS as the internal standard. Chemical shifts are expressed in ppm (δ / ppm) values and coupling constants in Hz (J / Hz). ESI-MS spectra were recorded on Agilent Technologies 6210 Time-Of-Flight LC-MS instrument in positive ion mode with $\text{CH}_3\text{CN}/\text{H}_2\text{O}$ 1/1 with 0.2 % HCOOH as the carrying solvent solution. Samples were dissolved in CH_3CN or MeOH (HPLC grade purity). The selected values were as follows: capillary voltage = 4 kV, gas temperature = 350 °C, drying gas flow 12 L min $^{-1}$, nebulizer pressure = 310 kPa, fragmentator voltage = 70 V. The elemental analysis was performed on the Vario EL III- C,H,N,S/O Elemental Analyzer (Elementar Analysensysteme GmbH, Hanau-Germany). Thin-layer chromatography (TLC) was performed on precoated Merck silica gel 60 F254 and RP-18 F254 plates. Column chromatography was performed on Lobar LichroPrep Si 60 (40-63 μm), RP-18 (40-63 μm) columns coupled to a Waters RI 401 detector, and on Biotage SP1 system with UV detector and FLASH 12+, FLASH 25+ or FLASH 40+ columns pre packed with KP-SIL [40-63 μm , pore diameter 6 nm (60 Å)], KP-C18-HS (40-63 μm , pore diameter 9 nm (90 Å) or KP-NH [40-63 μm , pore diameter 10 nm (100 Å)] as adsorbent. Compounds were analyzed for purity (HPLC) using a Waters 1525 HPLC dual pump system equipped with an Alltech, Select degasser system, and dual λ 2487 UV-VIS detector. For data processing, Empower software was used (methods A and B). Methods C and D: Agilent Technologies 1260 Liquid Chromatograph equipped with Quat Pump (G1311B), Injector (G1329B) 1260 ALS, TCC 1260 (G1316A) and Detector 1260 DAD VL+ (G1315C). For data processing, LC OpenLab CDS ChemStation software was used. For details, see Supporting Information.

1. Synthesis experiments

Each paragraph describing a synthesis experiment should begin with the name of the product and any structure number assigned to the compound in the Results and Discussions section. Thereafter, the compound should be identified by its structure number. Use of standard abbreviations or unambiguous molecular formulas for reagents and solvents, and of structure numbers rather than chemical names to identify starting materials and intermediates, is encouraged.

When a new or improved synthetic method is described, the yields reported in key experimental examples, and yields used for comparison with existing methods, should represent amounts of isolated and purified products, rather than chromatographically or spectroscopically determined yields. Reactant quantities should be reported in weight and molar units and for product yields should be reported in weight units; percentage yields should only be reported for materials of demonstrated purity. When chromatography is used for product purification, both the support and solvent should be identified.

2. Microwave experiments

Reports of syntheses conducted in microwave reactors must clearly indicate whether sealed or open reaction vessels were used and must document the manufacturer and model of the reactor, the method of monitoring the reaction mixture temperature, and the temperature-time profile. Reporting a wattage rating or power setting is not an acceptable alternative to providing temperature data. Manuscripts describing work done with domestic (kitchen) microwave ovens will not be accepted except for studies where the unit is used for heating reaction mixtures at atmospheric pressure.

3. Compound characterization

The Journal upholds a high standard for compound characterization to ensure that substances being added to the chemical literature have been correctly identified and can be synthesized in known yield and purity by the reported preparation and isolation methods. For all new compounds, evidence adequate to establish both **identity** and **degree of purity** (homogeneity) must be provided.

Identity - Melting point. All homogeneous solid products (e.g. not mixtures of isomers) should be characterized by melting or decomposition points. The colors and morphologies of the products should also be noted.

Specific rotations. Specific rotations based on the equation $[\alpha]^l; D = (100 \alpha) / (l c)$ should be reported as unitless numbers as in the following example: $[\alpha]^{20}; D = -25.4$ (c 1.93, CHCl_3), where c / g mL^{-1} is concentration and l / dm is path length. The units of the specific rotation, (deg mL) / (g dm), are implicit and are not included with the reported value.

Spectra/Spectral Data. Important IR absorptions should be given.

For all new diamagnetic substances, NMR data should be reported (^1H , ^{13}C , and relevant heteronuclei). ^1H NMR chemical shifts should be given with two digits after the decimal point. Include the number of protons represented by the signal, signal multiplicity, and coupling constants as needed (J italicized, reported with up to one digit after the decimal). The number of bonds through which the coupling is operative, nJ , may be specified by the author if known with a high degree of certainty. ^{13}C NMR signal shifts should be rounded to the nearest 0.01 ppm unless greater precision is needed to distinguish closely spaced signals. Field strength should be noted for each spectrum, not as a comment in the general experimental section. Hydrogen multiplicity (C, CH, CH_2 , CH_3) information obtained from routine DEPT spectra should be included. If detailed signal assignments are made, the type of NOESY or COSY methods used to establish atom connectivity and spatial relationships should be identified in the Supporting Information. Copies of spectra should also be included where structure assignments of complex molecules depend heavily on NMR interpretation. Numbering system used for assignments of signals should be given in the Supporting Information with corresponding general structural formula of named derivative.

HPLC/LCMS can be substituted for biochemistry papers where the main focus is not on compound synthesis.

HRMS/elemental analysis. To support the molecular formula assignment, HRMS data accurate within 5 ppm, or combustion elemental analysis [carbon and hydrogen (and nitrogen, if present)] data accurate within 0.5 %, should be reported for new compounds. HRMS data should be given in format as is usually given for combustion analysis: calculated mass for given formula following with observed mass: (+)ESI-HRMS m/z : [molecular formula + H^+] calculated mass, observed mass. Example: (+)ESI-HRMS m/z : calculated for $[\text{C}_{13}\text{H}_8\text{BrCl}_2\text{N} + \text{H}^+]$ 327.92899, observed 327.92792.

NOTE: in certain cases, a crystal structure may be an acceptable substitute for HRMS/elemental analysis.

Biomacromolecules. The structures of biomacromolecules may be established by providing evidence about sequence and mass. Sequences may be inferred from the experimental order of amino acid, saccharide, or nucleotide coupling, from known sequences of templates in enzyme-mediated syntheses, or through standard sequencing techniques. Typically, a sequence will be accompanied by MS data that establish the molecular weight.

Example: Product was isolated upon column chromatography [dry flash (SiO_2 , eluent EA, EA/MeOH gradient 95/5 → 9/1, EA/MeOH/NH₃ gradient 18/0.5/0.5 → 9/1/1, and flash chromatography (Biotage SP1, RP column, eluent MeOH/H₂O gradient 75/25 → 95/5, N-H column, eluent EA/Hex gradient 6/3 → EA)]. Yield 968.4 mg (95 %). Colorless foam softens at 96–101 °C. $[\alpha]^{20}; D = +0.163$ ($c = 2.0 \times 10^{-3}$ g/mL, CH_2Cl_2). IR (ATR): 3376w, 2949m, 2868w, 2802w, 1731s, 1611w, 1581s, 1528m, 1452m, 1374s, 1331w, 1246s, 1171m, 1063w, 1023m, 965w, 940w, 881w, 850w, 807w, cm^{-1} . ^1H NMR (500 MHz, CDCl_3 , δ): 8.46 (*d*, 1H, $J = 5.4$, H-2'), 7.89 (*s*, 1H, $J = 2.0$, H-8'), 7.71 (*d*, 1H, $J = 8.9$, H-5'), 7.30 (*dd*, 1H, $J_1 = 8.8$, $J_2 = 2.1$, H-6'), 6.33 (*d*, 1H, $J = 5.4$, H-3'), 6.07 (*s*, HN-Boc, exchangeable with D_2O), 5.06 (*s*, 1H, H-12), 4.92–4.88 (*m*, 1H, H-7), 4.42 (*bs*, H-3), 3.45 (*s*, $\text{CH}_3\text{-N}$), 3.33 (*bs*, H-9'), 3.05–2.95 (*m*, 2H, H-11'), 2.70–2.43 (*m*, 2H, H-24) and HN, exchangeable with D_2O), 2.07 (*s*, CH_3COO), 2.04 (*s*, CH_3COO), 1.42 (*s*, 9H, $(\text{CH}_3)_3\text{C-N(Boc)}$), 0.88 (*s*, 3H, CH₃-10), 0.79 (*d*, 3H, $J = 6.6$, CH₃-20), 0.68 (*s*, 3H, CH₃-13). ^{13}C NMR (125 MHz, CDCl_3 , δ): 170.34, 170.27, 151.80, 149.92, 148.87, 134.77, 128.36, 125.11, 121.43, 117.29, 99.98, 75.41, 70.82, 50.43, 49.66, 47.60, 47.33, 44.97, 43.30, 41.83, 41.48, 37.65, 36.35, 35.44, 34.89,

34.19, 33.23, 31.24, 28.79, 28.35, 27.25, 26.45, 25.45, 22.74, 22.63, 21.57, 21.31, 17.85, 12.15. (+)ESI-HRMS (*m/z*): calculated for [C₄₅H₆₇CIN₄O₆ + H]⁺ 795.48219, observed 795.48185. Combustion analysis for C₄₅H₆₇CIN₄O₆: Calculated. C 67.94, H 8.49, N 7.04; found C 67.72, H 8.63, N 6.75. HPLC purity: method A: RT 1.994, area 99.12 %; method C: RT 9.936, area 98.20 %.

Purity - Evidence for documenting compound purity should include one or more of the following:

- a) Well-resolved high field 1D ¹H NMR spectrum showing at most only trace peaks not attributable to the assigned structure and a standard 1D proton-decoupled ¹³C NMR spectrum. Copies of the spectra should be included as figures in the Supporting Information.
- b) Quantitative gas chromatographic analytical data for distilled or vacuum-transferred samples, or quantitative HPLC analytical data for materials isolated by column chromatography or separation from a solid support. HPLC analyses should be performed in two diverse systems. The stationary phase, solvents (HPLC), detector type, and percentage of total chromatogram integration should be reported; a copy of the chromatograms may be included as a figure in the Supporting Information.
- c) Electrophoretic analytical data obtained under conditions that permit observing impurities present at the 5 % level.

HRMS data may be used to support a molecular formula assignment **but cannot be used as a criterion of purity**.

4. Biological Data

Quantitative biological data are required for all tested compounds. Biological test methods must be referenced or described in sufficient detail to permit the experiments to be repeated by others. Detailed descriptions of biological methods should be placed in the experimental section. Standard compounds or established drugs should be tested in the same system for comparison. Data may be presented as numerical expressions or in graphical form; biological data for extensive series of compounds should be presented in tabular form. Tables consisting primarily of negative data will not usually be accepted; however, for purposes of documentation they may be submitted as supporting information. Active compounds obtained from combinatorial syntheses should be resynthesized and retested to verify that the biology conforms to the initial observation.

Statistical limits (statistical significance) for the biological data are usually required. If statistical limits cannot be provided, the number of determinations and some indication of the variability and reliability of the results should be given. References to statistical methods of calculation should be included. Doses and concentrations should be expressed as molar quantities (*e.g.*, mol/kg, μ mol/kg, M, mM). The routes of administration of test compounds and vehicles used should be indicated, and any salt forms used (hydrochlorides, sulfates, *etc.*) should be noted. The physical state of the compound dosed (crystalline, amorphous; solution, suspension) and the formulation for dosing (micronized, jet-milled, nanoparticles) should be indicated. For those compounds found to be inactive, the highest concentration (*in vitro*) or dose level (*in vivo*) tested should be indicated.

- The RESULTS AND DISCUSSION should include concisely presented results and their significance discussed and compared to relevant literature data. The results and discussion may be combined or kept separate.
- The inclusion of a CONCLUSION section, which briefly summarizes the principal conclusions, is recommended.
- NOMENCLATURE is optional but, if the authors wish, a list of employed symbols may be included.
- REFERENCES should be numbered sequentially as they appear in the text. Please note that any reference numbers appearing in the Illustrations and/or Tables and corresponding captions must follow the numbering sequence of the paragraph in which they appear for the first time. When cited, the reference number should be superscripted in Font 12, following any punctuation mark. In the reference list, they should be in normal position followed by a full stop. Reference entry must not be formatted using Carriage returns (enter key; ↵ key) or multiple space key. The formatting of references to published work should follow the *Journal's* style as follows:

- Journals^a: A. B. Surname1, C. D. Surname2, *J. Serb. Chem. Soc.* **Vol** (Year) first page Number (<https://doi.org/doi>)^b
- Books: A. B. Surname1, C. D. Surname2, *Name of Book*, Publisher, City, Year, pp. 100-101 (<https://doi.org/doi>)^b
- Compilations: A. B. Surname1, C. D. Surname2, in *Name of Compilation*, A. Editor1, C. Editor2, Ed(s)., Publisher, City, Year, p. 100 (<https://doi.org/doi>)^b
- Proceedings: A. B. Surname1, C. D. Surname2, in *Proceedings of Name of the Conference or Symposium*, (Year), Place of the Conference, Country, *Title of the Proceeding*, Publisher, City, Year, p. or Abstract No. 100
- Patents: A. B. Inventor1, C. D. Inventor2, (Holder), Country Code and patent number (registration year)
- Chemical Abstracts: A. B. Surname1, C. D. Surname2, *Chem. Abstr.* CA 234 567a; For non-readily available literature, the Chemical Abstracts reference should be given in square brackets: [C.A. 139/2003 357348t] after the reference
- Standards: EN ISO 250: *Name of the Standard* (Year)
- Websites: Title of the website, URL in full (date accessed)

^a When citing Journals, the International Library Journal abbreviation is required. Please consult, e.g., https://images.webofknowledge.com/WOK46/help/WOS/A_abrvjt.html

^b doi should be replaced by doi number of the Article, for example: <http://dx.doi.org/10.2298/JSC161212085B> (as active link). If doi do not exist, provide the link to the online version of the publication.

Only the last entry in the reference list should end with a full stop.

The names of all authors should be given in the list of references; the abbreviation *et al.* may only be used in the text. The original journal title is to be retained in the case of publications published in any language other than English (please denote the language in parenthesis after the reference). Titles of publications in non-Latin alphabets should be transliterated. Russian references are to be transliterated using the following transcriptions:

ж→zh, х→kh, ц→ts, ч→ch, ш→sh, щ→shch, ы→y, ю→yu, я→ya, ё→e, ѕ→i, ъ→’.

Supplementary material

Authors are encouraged to present the information and results non-essential to the understanding of their paper as SUPPLEMENTARY MATERIAL (can be uploaded in Step 4 of Online Submission). This material may include as a rule, but is not limited to, the presentation of analytical and spectral data demonstrating the identity and purity of synthesized compounds, tables containing raw data on which calculations were based, series of figures where one example would remain in the main text, etc. The Editorial Board retain the right to assign such information and results to the Supplementary material when deemed fit. Supplementary material does not appear in printed form but can be downloaded from the web site of the JSCS.

Mathematical and chemical equations should be given in separate lines and must be numbered, Arabic numbers, consecutively in parenthesis at the end of the line. All equations should be embedded in the text. Complex equations (fractions, integrals, matrix...) should be prepared with the aid of the Microsoft Equation 3.0 (or higher) or MathType (Do not use them to create simple equations and labels). Using the Insert -> Equation option, integrated in MS Office 2010 and MS Office 2013, as well as insertion of equation objects within paragraph text IS NOT ALLOWED.

Deposition of crystallographic data

Prior to submission, the crystallographic data included in a manuscript presenting such data should be deposited at the appropriate database. Crystallographic data associated with organic and metal-organic structures should be deposited at the Cambridge Crystallographic Data Centre (CCDC) by e-mail to deposit@ccdc.cam.ac.uk

Crystallographic data associated with inorganic structures should be deposited with the Fachinformationszentrum Karlsruhe (FIZ) by e-mail to crysdata@fiz-karlsruhe.de. A deposition number will then be provided, which should be added to the reference section of the manuscript.

For detailed instructions please visit the JSCS website:
<https://www.shd-pub.org.rs/index.php/JSCS/Instructions>

ARTWORK INSTRUCTIONS

JSCS accepts only **TIFF** or **EPS** formats, as well as **JPEG** format (only for colour and greyscale photographs) for electronic artwork and graphic files. **MS files** (Word, PowerPoint, Excel, Visio) **NOT acceptable**. Generally, scanned instrument data sheets should be avoided. Authors are responsible for the quality of their submitted artwork. Every single Figure or Scheme, as well as any part of the Figure (A, B, C...) should be prepared according to following instructions (every part of the figure, A, B, C..., must be submitted as an independent single graphic file):

TIFF

Virtually all common artwork and graphic creation software is capable of saving files in TIFF format. This 'option' can normally be found under 'the 'Save As...' or 'Export...' commands in the 'File' menu.

TIFF (Tagged Image File Format) is the recommended file format for bitmap, greyscale and colour images.

- Colour images should be in the RGB mode
- When supplying TIFF files, please ensure that the files are supplied at the correct resolution:
 1. Line artwork: minimum of 1000 dpi
 2. RGB image: minimum of 300 dpi
 3. Greyscale image: minimum of 300 dpi
 4. Combination artwork (line/greyscale/RGB): minimum of 500 dpi
- Images should be tightly cropped, without frame and any caption.
- If applicable please re-label artwork with a font supported by JSCS (Arial, Helvetica, Times, Symbol) and ensure it is of an appropriate font size.
- Save an image in TIFF format with LZW compression applied.
- It is recommended to remove Alpha channels before submitting TIFF files.
- It is recommended to flatten layers before submitting TIFF files.

Please be sure that quality of an image cannot be increased by changing the resolution from lower to higher, but only by rescanning or exporting the image with higher resolution, which can be set in usual "settings" facilities.

EPS

Virtually all common artwork creation software, such as Canvas, ChemDraw, CorelDraw, SigmaPlot, Origin Lab..., are capable of saving files in EPS format. This 'option' can normally be found under the 'Save As...' or 'Export...' commands in the 'File' menu.

For vector graphics, EPS (Encapsulated PostScript) files are the preferred format as long as they are provided in accordance with the following conditions:

- when they contain bitmap images, the bitmaps should be of good resolution (see instructions for TIFF files)
- when colour is involved, it should be encoded as RGB
- an 8-bit preview/header at a resolution of 72 dpi should always be included
- embed fonts should always included and only the following fonts should be used in artwork: Arial, Helvetica, Times, Symbol
- the vertical space between the parts of an illustration should be limited to the bare necessity for visual clarity
- no data should be present outside the actual illustration area
- line weights should range from 0.35 pt to 1.5 pt
- when using layers, they should be reduced to one layer before saving the image (Flatten Artwork)

JPEG

Virtually all common artwork and graphic creation software is capable of saving files in JPEG format. This 'option' can normally be found under the 'Save As...' or 'Export...' commands in the 'File' menu.

JPEG (Joint Photographic Experts Group) is the acceptable file format **only for colour and greyscale photographs**. JPEG can be created with respect to photo quality (low, medium, high; from 1 to 10), ensuring file sizes are kept to a minimum to aid easy file transfer. Images should have a minimum resolution of 300 dpi. Image width: minimum 3.0 cm; maximum 12.0 cm.

Please be sure that quality of an image cannot be increased by changing the resolution from lower to higher, but only by rescanning or exporting the image with higher resolution, which can be set in usual "settings" facilities.

SIZING OF ARTWORK

- JSCS aspires to have a uniform look for all artwork contained in a single article. Hence, it is important to be aware of the style of the journal.
- Figures should be submitted in black and white or, if required, colour (charged). If coloured figures or photographs are required, this must be stated in the cover letter and arrangements made for payment through the office of the Serbian Chemical Society.
- As a general rule, the lettering on an artwork should have a finished, printed size of 11 pt for normal text and no smaller than 7 pt for subscript and superscript characters. Smaller lettering will yield a text that is barely legible. This is a rule-of-thumb rather than a strict rule. There are instances where other factors in the artwork, (for example, tints and shadings) dictate a finished size of perhaps 10 pt. Lines should be of at least 1 pt thickness.
- When deciding on the size of a line art graphic, in addition to the lettering, there are several other factors to address. These all have a bearing on the reproducibility/readability of the final artwork. Tints and shadings have to be printable at the finished size. All relevant detail in the illustration, the graph symbols (squares, triangles, circles, *etc.*) and a key to the diagram (to explain the explanation of the graph symbols used) must be discernible.
- The sizing of halftones (photographs, micrographs,...) normally causes more problems than line art. It is sometimes difficult to know what an author is trying to emphasize on a photograph, so you can help us by identifying the important parts of the image, perhaps by highlighting the relevant areas on a photocopy. The best advice that can be given to graphics suppliers is not to over-reduce halftones. Attention should also be paid to magnification factors or scale bars on the artwork and they should be compared with the details inside. If a set of artwork contains more than one halftone, again please ensure that there is consistency in size between similar diagrams.

General sizing of illustrations which can be used for the Journal of the Serbian Chemical Society:

- Minimum fig. size: 30 mm width
- Small fig. size - 60 mm width
- Large fig. size - 90 mm width
- Maximum fig. size - 120 mm width

Pixel requirements (width) per print size and resolution for bitmap images:

	Image width	A	B	C
Minimal size	30 mm	354	591	1181
Small size	60 mm	709	1181	2362
Large size	90 mm	1063	1772	3543
Maximal size	120 mm	1417	2362	4724

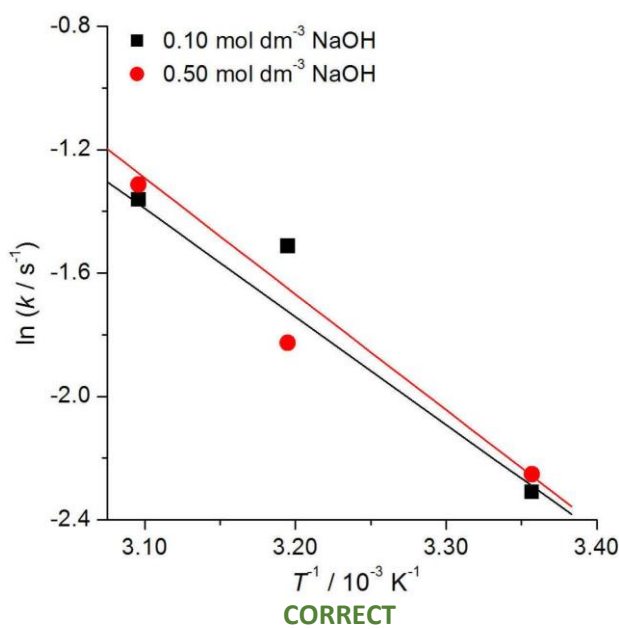
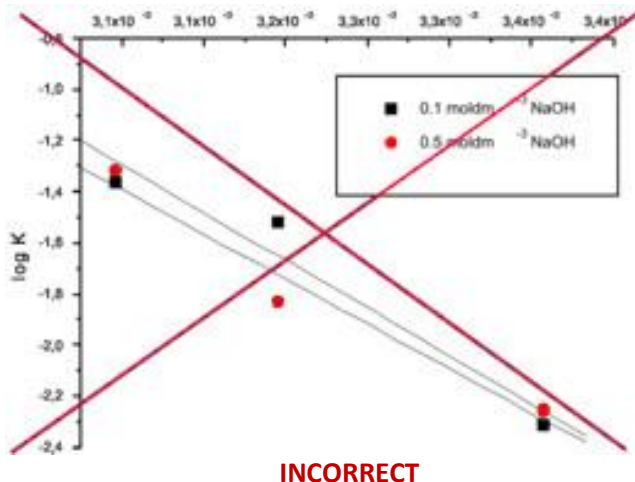
A: 300 dpi > RGB or Greyscale image

B: 500 dpi > Combination artwork (line/greyscale/RGB)

C: 1000 dpi > Line artwork

The designation of physical quantities and graphs formatting

The designation of physical quantities on figures must be in italic, whereas the units are in upright letters. They should be in Times New Roman font. In graphs a slash should be used to separate the designation of a physical quantity from the unit (example: p / kPa , $t / \text{°C}$, T_0 / K , τ / h , $\ln(j / \text{mA cm}^2)$...). Designations such as: $p (\text{kPa})$, $t [\text{min}]$..., are not acceptable. However, if the full name of a physical quantity is unavoidable, it should be given in upright letters and separated from the unit by a comma (example: Pressure, kPa, Temperature, K...). Please do not use the axes of graphs for additional explanations; these should be mentioned in the figure captions and/or the manuscript (example: “pressure at the inlet of the system, kPa” should be avoided). The axis name should follow the direction of the axis (the name of y-axis should be rotated by 90°). Top and right axes should be avoided in diagrams, unless they are absolutely necessary. Decimal numbers must have decimal points and not commas in the axis labels in graphical presentations of results. Thousands are separated, if at all, by a comma and not a point.





Journal of the Serbian Chemical Society

JSCS-info@shd.org.rs • www.shd.org.rs/JSCS

J. Serb. Chem. Soc. Vol. 87, No. 3 (2022)

CONTENTS*

Organic Chemistry

- Y. Dongliang, S. A. Ejaz, M. Aziz, A. Saeed, S. Ejaz, M. Sajjad Bilal, H. M. Kashif Mahmood and S. T. Ejaz:* Benzene-1,3-diol derivatives as the inhibitors of butyryl-cholinesterase: An emergent target of Alzheimer's disease 293

Inorganic Chemistry

- M. V. Rodić, M. M. Radanović, D. V. Gazdić, V. M. Leovac, B. Barta Holló, V. Raičević, S. K. Belošević, B. Krüger and Lj. S. Vojinović-Ješić:* Reactions of copper(II) bromide with 2,6-diacylpyridine bis(phenylhydrazone) (**L**) – Molecular and crystal structures of **L** and its mixed-valence complex $[\text{Cu}^{\text{II}}\text{L}_2][\text{Cu}^{\text{I}}_2\text{Br}_4]$ 307

Theoretical Chemistry

- S. Avram and C. Neanu:* Large-scale comparison between the diffraction-component precision indexes favors Cruickshank's R_{free} function 321

Physical Chemistry

- A. L. de Souza Madureira Felício and H. de Santana:* Structural stability of biofilms produced from silkworm cocoon fibers 331

Electrochemistry

- S. A. Al-Zahrani, V. Jevtovic, K. M. Alenezi, H. El Moll, A. Haque and D. Vidovic:* Electrocatalytic hydrogen evolution upon reduction of pyridoxal semicarbazone and thiosemicarbazone-based Cu(II) complexes 345

Polymers

- I. P. Trifonova, J. A. Rodicheva, A. E. Sheveleva, V. A. Burmistrov and O. I. Koifman:* Flotator Oxal as the plasticizer for suspension PVC 355

Materials

- M. F. Öktem and B. Aydaş:* Flame retardant characteristics of polymerized dopamine hydrochloride coated jute fabric and jute fabric composites 363

Metallic Materials and Metallurgy

- M. Zoraga, T. Yucel, S. İlhan and A. O. Kalpaklı:* Investigation of selective leaching conditions of ZnO, ZnFe₂O₄ and Fe₂O₃ in electric arc furnace dust in HNO₃ 377

Environmental

- H. Güher, B. Öterler, B. Çamur Elipek, O. Yeler and G. Burcu Aydin:* Spatial and temporal evaluation of the physicochemical quality of domestic/industrial water in the Kırklareli Reservoir (Turkish Thrace) 389

Published by the Serbian Chemical Society
Karnegijeva 4/III, P.O. Box 36, 11120 Belgrade, Serbia
Printed by the Faculty of Technology and Metallurgy
Karnegijeva 4, P.O. Box 35-03, 11120 Belgrade, Serbia

* For colored figures in this issue please see electronic version at the Journal Home Page:
<http://www.shd.org.rs/JSCS/>



Benzene-1,3-diol derivatives as the inhibitors of butyrylcholinesterase: An emergent target of Alzheimer's disease

YIN DONGLIANG¹, SYEDA ABIDA EJAZ^{2*}, MUBASHIR AZIZ², AMNA SAEED², SAMINA EJAZ³, MUHAMMAD SAJJAD BILAL², HAFIZ MOHAMMAD KASHIF MAHMOOD² and SYEDA TEHMINA EJAZ⁴

¹Department of Neurointervention, The Third hospital of Jinan, No.1 Wangsheren North Street, Gongye North Road, Licheng District, Jinan City, Shandong Province, 205132, China,

²Department of Pharmaceutical Chemistry, Faculty of Pharmacy, The Islamia University of Bahawalpur, Bahawalpur-63100, Pakistan, ³Department of Biochemistry, Institute of Biochemistry, Biotechnology and Bioinformatics, The Islamia University of Bahawalpur-63100, Bahawalpur, Pakistan and ⁴Department of Mathematics, The Government Sadiq College Women University Bahawalpur, Bahawalpur, Pakistan

(Received 16 April, revised 21 August, accepted 23 August 2021)

Abstract: Molecular docking is a powerful and significant approach for the identification of lead molecules on the basis of virtual screening. With it a large number of compounds can be tested and based on the scoring function and ranking, the conclusion can be made about how the selected compounds can inhibit the targeted protein/receptor. Considering the importance of selective inhibitors of cholinesterase in the treatment of Alzheimer disease, this research is focused on the determination of the mechanism of binding interactions of few benzene-1,3-diol derivatives within the active site of both acetyl-cholinesterase (AChE) and butyrylcholinesterase (BChE). All the selective ligands were found to have a greater binding affinity with the BChE when compared to that of AChE, by an average value of ~ 28.4 and ~ 12.5 kJ/mol, respectively. The results suggested that the identified inhibitors can be used as the lead compounds for the development of novel inhibitors of the targeted enzymes against some specific diseases, thus opening the possibility of new therapeutic strategies.

Keywords: molecular docking; acetyl-cholinesterase (AChE); butyrylcholinesterase (BChE); active pocket.

INTRODUCTION

Alzheimer's disease (AD), a neurodegenerative disorder, is characterized by the significant decrease in the level of acetylcholine (ACh) neurotransmitter.^{1,2}

* Corresponding author. E-mail: abida.ejaz@iub.edu.pk; abida.ejaz@iub.edu.pk
<https://doi.org/10.2298/JSC210416073D>

This neurotransmitter (ACh) plays a significant role in the normal processes of learning and memory, activating muscarinic and nicotinic receptors of the central nervous system.^{3,4} The acetyl-cholinesterase (AChE) and the butyrylcholinesterase (BChE) are well-studied enzymes that are involved in the hydrolysis of ACh to acetate and choline in the synaptic cleft.^{5,6} The major signs and symptoms of AD include dementia, confusion, memory lapses, misinterpreting of the spatial relationships, and the decline in the ability to speak, write, think, reason, making decisions and planning. Personality and behavioural changes have also been observed including depression, anxiety, agitation, social isolation, mood swings, diurnal rhythm disturbances and delusions.^{7,8} AD is characterized by various markers in the brain including a large number of amyloid plaques surrounded by the neurofibrillary tangles, vascular damage from plaque deposition and neuronal cell degradation. The main component of plaques is amyloid β protein and also the major cause of AD. The deposition of this notorious protein leads to the development of other symptoms.^{9,10} Head injuries, progression of age, sequelae of delivery, ataxic fever, paralysis, mania, apoplexy, mercury abuse, wine abuse, political upheavals, unhappy love, dietary excess, masturbation, unfulfilled love, domestic problems, poverty and fears are among the causes of AD that emerged in the last century.^{11,12}

Recent research has revealed that in the brain of patients suffering from AD, the level of AChE is considerably reduced whereas that of BChE increases, thus, aggravating the toxicity of β -amyloid peptide. In such instances, it is possible that BChE may be more suitable target than AChE.¹³ Both AChE and BChE share 53 % amino acid sequence similarities of their active sites.¹⁴ Recently, the increased level of BChE has been studied in AD patients therefore resulted in the increased β -amyloid peptide toxicity.¹⁵ It is not surprising that cholinesterase inhibitors have shown better results in the treatment of AD than any other strategy explored.¹⁶ Hence, the search for the discovery of novel cholinesterase inhibitors (ChE) is expected to continue in future since the current ChEs inhibitors are reported to have some side effects.¹⁷ The availability of several crystal structures of both ChEs (in complexes) with different inhibitors provides the possibility to apply the docking protocol to explore the protein inhibitor complexes in terms of the nature of their interactions.¹⁸ Although there are considerable efforts being made for understanding the etiology of the neurodegenerative disorder (AD) but the development of novel inhibitor of specific target remain as an important concern in the treatment of patient. The main challenge in the development of the inhibitors of the selected targets is their potency, selectivity and drugability. Therefore, there is a need of deep understanding of the structure activity relationships and functions of the selective inhibitors of selected enzymes.¹⁹

Over the past few years, the high-throughput screening (HTS) has become a cornerstone technology of pharmaceutical research²⁰ but it is very expensive and

technically impossible to screen a huge library of chemical compounds using these biochemical techniques (high throughput screening). In this regard, computational methodologies have become a vital element of many drug discovery programmes, from the hit identification to the lead optimization and beyond.²¹ The high throughput computational screening using pharmacophore based virtual screening, molecular docking and quantum computational studies are among the most cost-effective technique through which millions of compounds can be screened rapidly.²² Many heterocyclic compounds have been synthesized and reported for their potential to inhibit the targeted enzymes, but their molecular target was not fully defined. Among those heterocyclic derivatives, quinolones and dibenzooazepine have been found as the most attractive scaffolds due to their broad range of biochemical activities, such as angiotensin converting enzyme (ACE) inhibitor along with anti-convulsant, neuroprotective and anti-inflammatory properties.²³

The current study is designed to relate the interest of some benzene-1,3-diol obtained from natural source as cholinesterase inhibitors, but more selective as BChE inhibitors. The structures were drawn using ACD/ChemSketch 12.01, and 3D optimized.²⁴ The study comprises the smart approach by using computational 4.2 software.²⁶ Moreover, the ADMET studies were also performed using ADMET tools to find value added product in short time without wasting of chemicals. The crystal structure of both enzymes co-crystallized with their inhibitors were obtained from the protein data bank.²⁵ The selected compounds were further explored along with novel inhibitors to determine the possible binding interactions of different amino acids within the active site of both enzymes, respectively, using Autodock LAB 2.0.²⁷ The deep understanding of the structure activity relationships and functions of the identified inhibitors/drug-like molecules provide a great hope for the development of future novel drugs.

EXPERIMENTAL

In order to gain insight into the binding interactions, the molecular docking studies of the selected compounds were performed using AutoDock 4.2.²⁶ The crystal structure of the human AChE (PDB ID 4BDT) bound to standard inhibitor huperzine W and human BChE (PDB ID 4BDS) bound to standard inhibitor tacrine, Fig. 1, were downloaded from RCSB Protein Data Bank and used for docking studies.²⁵ The visual inspection for the binding pattern was done using the Discovery Studio Visualizer software, Version 17.2.²⁸

Docking procedure

Ligand preparation. The selected compound structures were downloaded in Spatial Data File (SDF) format from PubChem.²⁹ The structures of the compounds were drawn using ACD/ChemSketch 12.01, and 3D optimized.²⁴ The 3D structures were converted to PDB format which were further processed by Autodock 4.2. The International Union of Pure and Applied Chemistry (IUPAC) name and InChIKey of the selected compounds are mentioned in Table I and their respective structures are given in the Supplementary material to this paper.

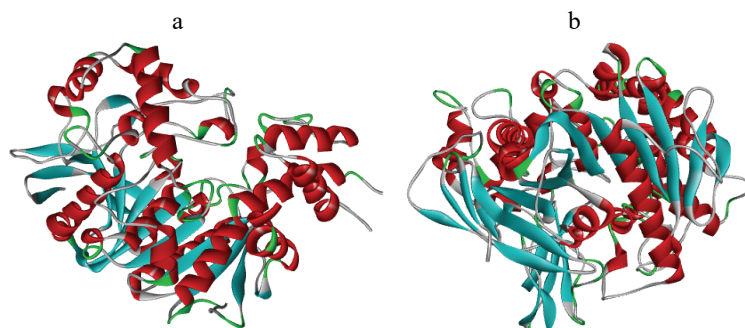


Fig. 1. Crystal structure of: a) human AChE (PDB ID 4BDT) and b) human BChE (PDB ID 4BDS) from Protein Data Bank (<https://www.rcsb.org/search>).²⁵

Table I. List of the selected compounds for study

PubChem CID	Code	IUPAC name	InChIKey
5054	1a	Benzene-1,3-diol	GHMLBKRAJCXXBS-UHFFFAOYSA-N
10333	1b	4-Methylbenzene-1,3-diol	FNYDIAAMUCQQDE-UHFFFAOYSA-N
17927	1c	4-Ethylbenzene-1,3-diol	VGMJYYDKPUPTID-UHFFFAOYSA-N
87874	1d	4-Propylbenzene-1,3-diol	DJDHQJFHXLBJNF-UHFFFAOYSA-N
205912	1e	4-Butylbenzene-1,3-diol	CSHZYWUPJWVTMQ-UHFFFAOYSA-N
3610	1f	4-Hexylbenzene-1,3-diol	WFJIVOKAWHGMBH-UHFFFAOYSA-N
3014087	1g	4-Tert-butylbenzene-1,3-diol	YBKODUYVZRLSOK-UHFFFAOYSA-N
75294	1h	4-Benzylbenzene-1,3-diol	QVFIWTNWKHFVEH-UHFFFAOYSA-N
11171903	1i	4-(1-Phenylethyl)benzene-1,3-diol	PQSXNIMHIHYFEE-UHFFFAOYSA-N
24849532	1j	4-[2-(2,4-Dihydroxyphenyl)ethyl]-benzene-1,3-diol	WKIFTWPZTZUMRN-UHFFFAOYSA-N

Preparation of enzyme (receptor)

Before docking, the protein structure was prepared and refined using Autodock 4.2.²⁶ The standard preparation steps included the removal of co-crystal ligands and water molecules, followed by the addition of hydrogen and gasteiger partial charges to the protein structure. The protein was set to be rigid and ligands were allowed to dock within the activation loop of selected protein. The active site of a protein was determined by selecting a dimension grid of $60 \times 60 \times 60 \text{ \AA}^3$ around the co-crystal ligands, *i.e.*, huperine W in case of AChE and tacrine in case of BChE.

Molecular docking

After preparation of the ligand and the protein files, the Autogrid and Autodock utility of Autodock 4.2 programme were used for docking protocols. The software used the in-house default forcefield and the Lamarckian genetic algorithm (LGA), as a search parameter. LGA is a type of random or stochastic docking. The algorithm, which actually deals with the calculation of random changes in flexible parts of the ligand, further determines its interaction with the amino acid residues of active site pocket. The Autodock 4.2 software calculates the different energy parameters and stores them, accordingly. The number of poses were set to 100 and population size was set upto 300. The high number of poses is a good practice to increase

the accuracy of the result. After the docking, top ten docked conformation with the best ligand–protein interaction and high binding energy were selected for the comparison with co-crystal standard ligand.

Visual inspection

The structures of each selected compound against AChE and BChE were visualized and inspected for the best fit orientation within the active pocket of the enzyme, respectively. This was done using Discovery Studio Visualizer software, version 17.2.

Drug likeness evaluation and calculated ADME properties

The absorption, distribution, metabolism and excretion (ADME) properties for all the tested compounds were calculated using online the integrated tool ADMET LAB 2.0.²⁷ All the synthesized compounds showed moderate ADME properties as shown later on.

RESULTS AND DISCUSSION

Potential binding site in receptors

The commercially available Molecular Operating Environment 2015.10 (MOE) software³⁰ was used for the prediction of the most potential active site where the selected ligand can bind and interact within the activation loop of targeted proteins *i.e.*, both AChE and BchE (Fig. 2).

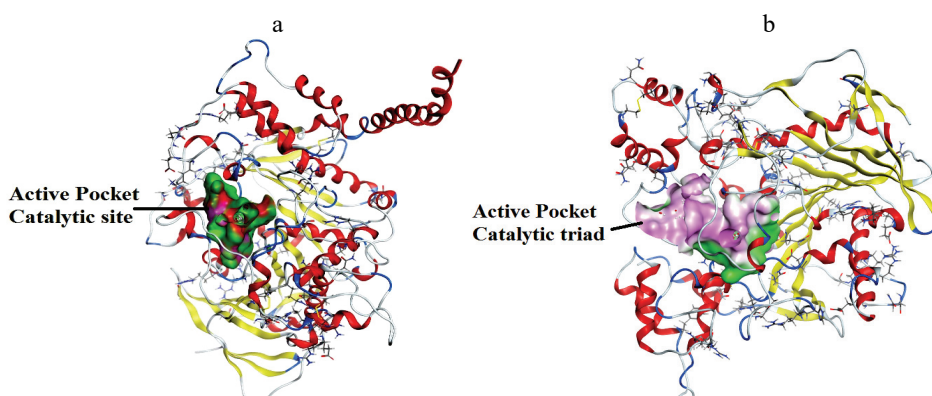


Fig. 2. Binding site prediction of: a) human AChE (PDB ID 4BDT) and b) human BChE (PDB ID 4BDS) using MOE 2015.10.

The active pocket of AChE contained total 36 amino acid residues including; GLN71, TYR72, VAL73, ASP74, GLY82, THR83, TRP86, ASN87, PRO88, TYR119, GLY120, GLY121 GLY122, TYR124, SER125, GLY126, ALA127, LEU130, TYR133, GLU202, SER203, ALA204, TRP236, PHE295, PHE297, SER336, TYR337, PHE338, TYR341, LEU437, TRP439, PRO446, HIS447, GLY448, TYR449 and ILE451. Similarly the active pocket of BChE contained total 45 amino acid residues and includes; GLN67, ASN68, ILE69, ASP70, GLN71, SER72, GLY78, SER79, TRP82, ASN83, PRO84, TYR114, GLY115, GLY116, GLY117, GLN119, THR120, GLY121, THR122, LEU125, TYR128,

GLU197, SER198, TRP231, GLU276, ALA277, VAL280, TYR282, GLY283, THR284, PRO285, LEU286, SER287, VAL288, ASN289, ALA328, PHE329, TYR332, PHE398, TRP430, MET437, HIS431, GLY439, TYR440 and ILE442. The selected ligands formed hydrogen bonding with the amino acid residues of the active pockets. In comparison to AChE, the ligands formed maximum interactions with amino acid residues of BChE, thus ultimately resulted in the improved binding energies.

Docking analysis studies

In-silico study was conducted using Autodock 4.2 and the visualization of docked conformations were carried out using Discovery Studio Visualizer 17.2. The selected derivatives of benzene-1,3-diol were docked within the activation loop of AChE and BChE enzymes. The most possible 2D and 3D binding interactions of the docked conformations were obtained using Discovery Studio visualizer 17.2. All the ligands selected showed comparable interactions and docking scores with both enzymes, when compared to the standard donepezil. The interactions are given in the Figs. 3 and 4 and docking scores are displayed in Table II.

Visual inspection

The structure of each selected compound against AChE and BChE was visualized for best fit orientation within the active pocket of the enzyme, respectively. Particularly the compounds **1h**, **1i** and **1j** formed stable protein-ligand complex with both enzymes. The results are given in Figs. 3 and 4.

AChE docking studies

In terms of the detailed docking interaction studies, only three potent compounds **1h**, **1i** and **1j** are being discussed here. All the detailed discussion of other compounds are provided in Supplementary material to this paper.

The docked conformation of compound **1h**, **1i** and **1j** showed considerable inhibitory potential of AChE enzyme (Fig. 3). The docking scores of these three compounds were found to be best among all other compounds which were -21.68, -22.02 and -22.60 kJ/mol, respectively. It was seen that compound **1h** contain an aromatic ring as a substituent at 4th position of the core aromatic ring. It was notable that the presence of aromatic ring has significantly increased the docking energy. It might be due to the resonance effect of an aromatic ring. Moreover, the substituted aromatic ring was also involved in alkyl interaction with LEU76 and VAL340. Similarly, compound **1i** contain phenyl ethyl as substituent. This substitution has significantly improved the binding energy, which might be due to positive inductive electron donating effect of ethyl group and the interaction of phenyl ring with LEU76 of the active site. Moreover, the resonating π -electrons of the benzene ring was also involved in the binding interactions with amino acid residues which further improved its docking energy. According to the

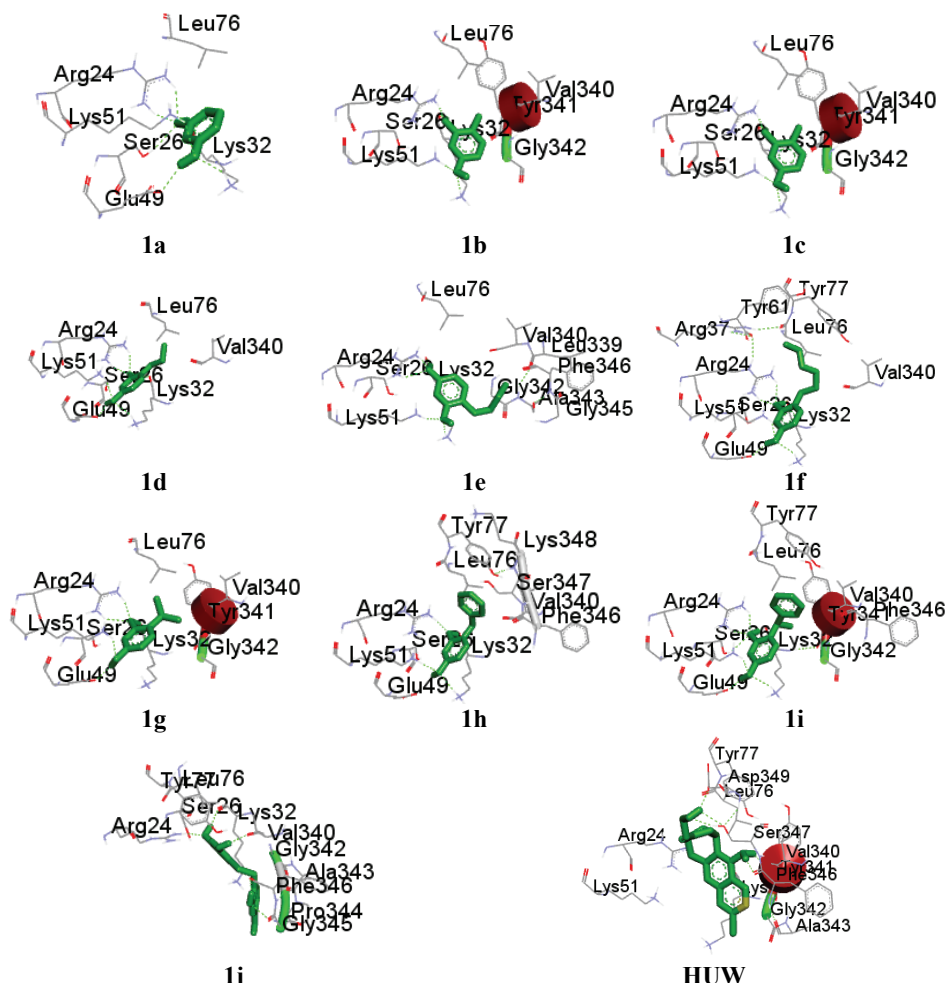


Fig. 3. Protein-ligand complex formed by docked structures of AChE inhibitors.

free binding energy score, compound **1j** was found to be the most potent derivative among all compounds. It was found that the amino acid residues which were involved in bonding and non-bonding interactions with compound **1j** were LYS32, ARG24, VAL340, PHE346, PRO344, LEU76, SER26, TYR77, ALA343 and GLY342. It was observed that the parent compound was substituted with the ethyl phenyl ring which had two hydroxyl groups at ortho position. Previously it was observed that hydroxyl groups were responsible for establishing strong hydrogen bonding with the amino acids of active site. Whereas, the benzene ring was itself involved in strong π -cation and π -sigma bonding with amino acid residues of the active site. Similarly, in the present compound two benzene rings, one ethyl group and 4 hydroxyl groups have significantly contributed to the most pot-

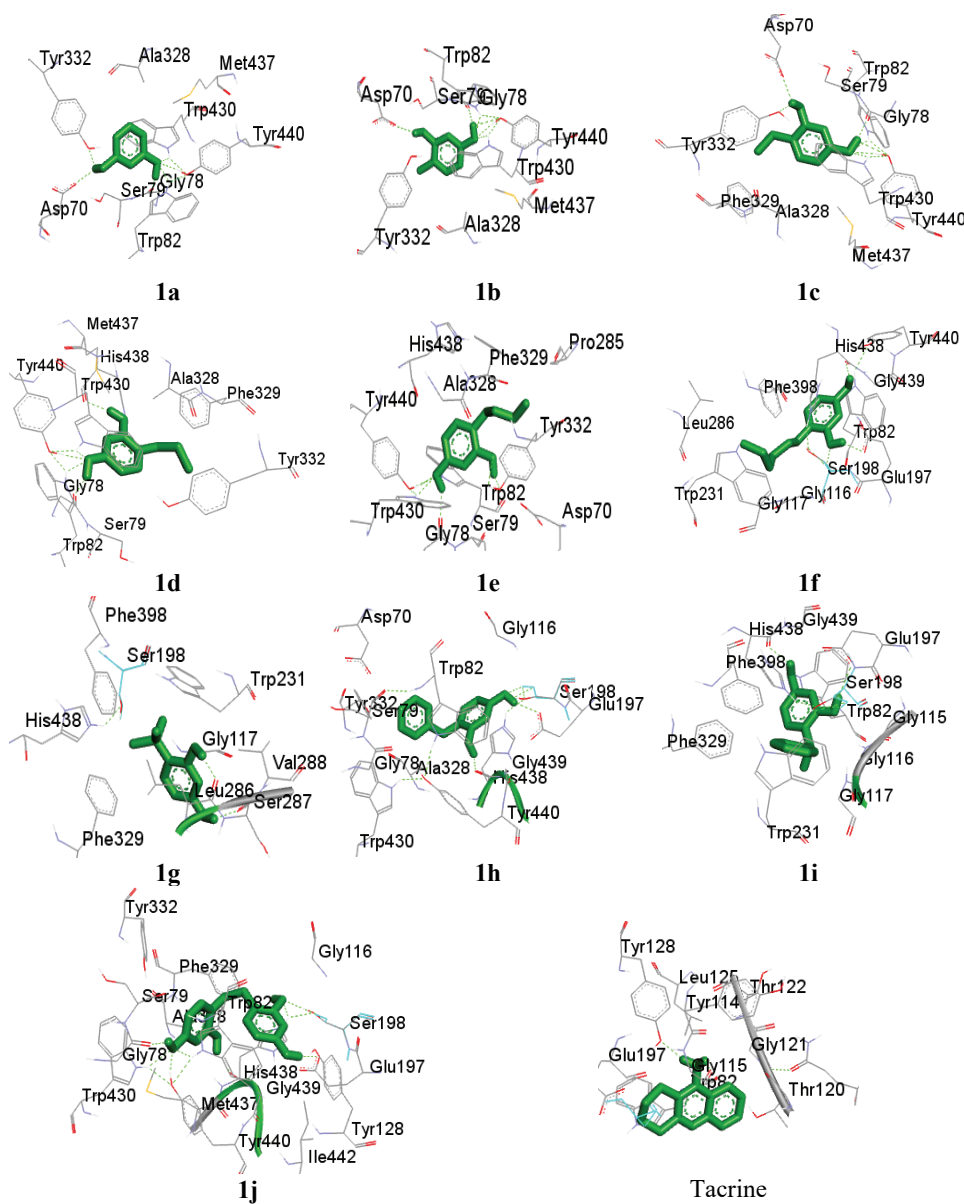


Fig. 4. Protein-ligand complex formed by docked structures of BChE inhibitors.

ent inhibitory potential of the compound. It can be seen that the hydroxyl groups of both rings were involved in hydrogen bonding with LYS32, ARG24, VAL340 and PHE346, respectively. Whereas, the aromatic rings were involved in π -alkyl and π -cation interactions. These factors corresponded to the highest inhibiting

potential of the compound. The detailed 2D interactions of AChE enzyme with all compounds are shown in Supplementary material.

TABLE II. Docking score of selected compounds by considering bound and unbound states of the ligand; **Hup** – huperzine, **Tac** – tacrine, **Don** – donepezil

No.	Code	Acetylcholinesterase (AChE)		Butyrylcholinesterase (BChE)		Selectivity for BChE ^a
		Docking score, kJ/mol	Predicted inhibition constant, μM	Docking score, kJ/mol	Predicted inhibition constant, μM	
1.	1a	-6.69	2300	-17.58	836.67	2.8
2.	1b	-12.60	989.03	-20.68	472.10	2.0
3.	1c	-17.04	527.89	-20.89	309.80	1.7
4.	1d	-17.20	818.97	-23.19	171.02	4.8
5.	1e	-18.50	572.90	-24.82	174.55	3.3
6.	1f	-20.59	247.72	-25.03	81.68	3.0
7.	1g	-20.05	306.32	-23.19	87.16	3.5
8.	1h	-21.68	95.91	-25.07	40.86	2.3
9.	1i	-22.02	43.04	-26.92	27.24	1.5
10.	1j	-22.60	109.61	-29.14	9.30	12.1
11.	Hup	-29.01	8.38	–	–	–
12.	Tac	–	–	-28.84	8.8	–
Ctrl.	Don	-30.14	2.67	-32.65	0.035	89

^aSelectivity index defined as $IC[\text{AChE}]/IC[\text{BChE}]$

Co-crystal ligand of AChE enzyme showed the binding energy of -29.01 kJ/mol. It was notable that the standard compound also possessed the aromatic moiety in its structure, which was responsible for the formation of π -alkyl and π -cation interactions with the amino acids residues. Whereas, the presence of single hydroxyl group was contributing toward the formation of hydrogen bonding with amino acid residue of the active site. So, it is well understood that the presence of hydroxyl group, aromatic ring and electron donating alkyl groups are important determinants of the anti-cholinesterase activity of the compound (see Supplementary material).

BChE docking studies

In the terms of detailed docking interaction studies, only three potent compounds **1h**, **1i** and **1j** are being discussed here. All the detailed discussion of other compounds are provided in separate Supplementary material.

The docked conformation of compound **1h**, **1i** and **1j** showed the significant inhibitory potential against BChE enzyme (Fig. 4). The inhibitory potential of these derivatives were most potent against the BChE enzyme. The docking scores of these three compounds were found to be best among all other compounds, which were -25.07, -26.92 and -29.14 kJ/mol, respectively. These scores were found to be higher than the docking scores obtained with AChE enzyme which further strengthens the fact that these derivatives are more selective and potent

toward the BChE enzyme. Compound **1h** contain the aromatic ring as a substituent. The substituted aromatic ring was involved in an alkyl interaction with GLY115. Similarly, the compound **1i** contained the phenyl ethyl group as a substituent. This substitution has significantly improved the binding energy which might be due to the positive inductive electron donating effect of the ethyl group and the interaction of phenyl ring with ALA328 of the active site. Moreover, the resonating π -electrons of benzene ring were also involved in the binding interactions with amino acid residues, which further improved its docking energy.

According to the free binding energy score, the compound **1j** was found to be the most potent derivative among all compounds which has the docking score of 29.14 kJ/mol, with the predicted inhibitory constant value of 9.30 μ M against BChE enzyme. It was found that the amino acid residues which were involved in bonding and non-bonding interactions with compound **1j** were as follows GLU197, GLY116, GLY117, LEU286, HIS438, TRP231, GLY439, TRP82 and VAL288. It can be observed that the parent compound was substituted with the ethyl phenyl ring, having two hydroxyl groups at *ortho* position. Previously, it was observed that the hydroxyl groups were mainly responsible for establishing strong hydrogen bonding with the amino acids of active site. Whereas, the benzene ring was itself involved in strong π -cation and π -sigma bonding, with the amino acid residues. Similarly, in the present compounds, two benzene rings, one ethyl group and 4 hydroxyl groups significantly contributed to most potent inhibitory potential of the derivative. It can be seen that hydroxyl groups of both rings were involved in hydrogen bonding with GLU197, GLY117, GLY116 and LEU286, respectively. Whereas, the aromatic rings were involved in π -alkyl and π -cation interactions. These factors corresponded to the highest inhibiting potential of **1j** compound. The detailed 2D interactions of BChE enzyme with all compounds are shown in Supplementary material.

The co-crystal ligand tacrine, of BChE enzyme, showed the binding energy of -28.84 kJ/mol. It was notable that the compound **1j** showed much better binding conformation than the standard tacrine. It was evident that the standard and the potent derivatives possessed the aromatic moiety in their structures which was responsible for the formation of stabilizing hydrophobic interactions, *i.e.*, π -alkyl and π -cation interactions with the amino acids residues. Whereas, the presence of hydroxyl group was contributing toward the formation of hydrogen bonding with the amino acid residue of active site. It was observed that the potent 1,3-diol derivatives possessed a larger number of hydroxyl groups, which caused more hydrogen bondings with the amino acid residues of active site. So it was concluded that the presence of hydroxyl group, the aromatic ring and the electron donating alkyl group were the important determinants for the anti-cholinesterase activity of the compounds (see Supplementary material).

Drug likeness evaluation and calculated ADME properties

During the drug discovery process, the determination of ADME properties of drug like molecule is a very important step. These properties were calculated by using online tool ADMET LAB 2.0. The octanol–water distribution coefficients ($S + \log P$ and $M\log P$), the pH dependent octanol–water distribution coefficient ($S + \log D$), the number of hydrogen bond donors ($HBDH$), the hydrogen bond acceptor (the sum of nitrogen and oxygen atoms) MNO and the topological polar surface area ($TPSA$) were determined for each molecule.

Among all the properties, the $TPSA$ is a valuable molecular descriptor, which is used for the calculation of drug absorption properties. The $TPSA$ value of less than 60 \AA^2 gives prediction that the molecule has sufficient bioavailability properties, but if the value exceeds 140 \AA^2 , the molecule is considered as undesirable. Similarly the compounds with the molecular weight <500 , $HBDH < 10$, $MNO < 5$ and $\log P < 5$ are considered to be orally bio-available with a favourable ADME profile. All the selected compounds exhibited promising ADME properties, within the limits of Lipinski's rule of 5. The properties of the selected compounds are displayed in Table III.

TABLE III. Calculated ADME properties of the selected compounds

Compound	MW_t	$S+\log P$	$S+\log D$	$M\log P$	$HBDH$	MNO	$TPSA$
1a	110.11	0.751	0.736	0.893	2	2	40.46
1b	124.14	1.109	1.098	1.246	2	2	40.46
1c	138.16	1.595	1.588	1.58	2	2	40.46
1d	152.19	2.109	2.103	1.897	2	2	40.46
1e	166.22	2.664	2.66	2.2	2	2	40.46
1f	194.27	3.791	3.788	2.773	2	2	40.46
1g	166.22	2.647	2.644	2.2	2	2	40.46
1h	200.23	2.897	2.891	2.786	2	2	40.46
1i	214.261	3.201	3.197	3.05	2	2	40.46
1j	246.26	1.882	1.871	1.942	4	4	80.92

CONCLUSION

The structure based virtual screening was employed to study the protein–ligand interactions for the identification of new BChE inhibitors, which could be a starting point for a promising lead candidate in the treatment of AD. The Pubchem database was filtered, treated, and subsequently screened against both AChE and BChE protein. Moreover, their predicted inhibition constant values were also in correlation with their binding energy values. Among the different derivatives, 4-(1-phenylethyl)benzene-1,3-diol (**1i**) and 4-[2-(2,4-dihydroxyphenyl) ethyl]benzene-1,3-diol (**1j**) showed strong inhibition and strong interactions with BChE. Thus, these compounds could be the starting point for the future development of novel inhibitors of BChE.

SUPPLEMENTARY MATERIAL

Additional data and information are available electronically at the pages of journal website: <https://www.shd-pub.org.rs/index.php/JSCS/article/view/10672>, or from the corresponding author on request.

ИЗВОД

ДЕРИВАТИ БЕНЗЕН-1,3-ДИОЛА КАО ИНХИБИТОРИ БУТИРИЛХОЛИНЕСТЕРАЗЕ:
НОВА МЕТА У АЛЦХАЈМЕРОВОЈ БОЛЕСТИ

YIN DONGLIANG¹, SYEDA ABIDA EJAZ², AMNA SAEED², MUBASHIR AZIZ², SAMINA EJAZ³, MUHAMMAD SAJJAD BILAL², HAFIZ MOHAMMAD KASHIF MAHMOOD² и SYEDA TEHMINA EJAZ⁴

¹Department of Neurointervention, The Third hospital of Jinan, No.1 Wangsheren North Street, Gongye North Road, Licheng District, Jinan City, Shandong Province, 205132, China, ²Department of Pharmaceutical Chemistry, Faculty of Pharmacy, The Islamia University of Bahawalpur, 9 Bahawalpur-63100, Pakistan, ³Department of Biochemistry, Institute of Biochemistry, Biotechnology and Bioinformatics, The Islamia 11 University of Bahawalpur-63100, Bahawalpur, Pakistan и ⁴Department of Mathematics, The Government Sadiq College Women University Bahawalpur, Bahawalpur, Pakistan

Молекулско моделовање (Molecular docking) је снажан и значајан приступ у идентификовању водећих молекула (lead molecules) на основу виртуелног скрининга. На овај начин, велики број једињења може да буде испитан, и на основу добијених резултата једињења могу да буду рангирана и може се претпоставити како одабрана једињења могу инхибирати циљани протеин. Имајући у виду важност постизања селективне инхибиције холинестеразе, у овом истраживању фокусирали смо се на одређивање механизма везивних интеракција неколико деривата бензен-1,3-диола у активном месту ацетилхолинестеразе (AChE) и бутирилхолинестеразе (BChE). Показано је да сви одобрани лиганди имају већи афинитет за везивање са бутирилхолинестеразом (BChE) у поређењу са цетилхолинестеразом (AChE), са просечним вредностима $-28,4$ и $-12,5$ kJ/mol, редом. Резултати нашег истраживања указују да идентификовани инхибитори могу бити узети као водећи кандидати за развој нових инхибитора циљаних ензима у третману специфичних болести, и на тај начин се отвара могућност за нове терапеутске стратегије.

(Примљено 16. априла, ревидирано 21. августа, прихваћено 23. августа 2021)

REFERENCES

1. L. Reguera, D. G. Rivera, *Chem. Rev.* **119** (2019) 9836 (<https://doi.org/10.1021/acs.chemrev.8b00744>)
2. U. K. Sharma, P. Ranjan, E. V. Van der Eycken, S.-L. You, *Chem. Soc. Rev.* **49** (2020) 8721 (<https://doi.org/10.1039/D0CS00128G>)
3. R. C. Cioc, E. Ruijter, R. V. Orru, *Green Chem.* **16** (2014) 2958 (<https://doi.org/10.1039/C4GC00013G>)
4. H. Pellissier, *Adv. Synth. Catal.* **358** (2016) 2194 (<https://doi.org/10.1002/adsc.201600462>)
5. M. Ashe, *Master Thesis*, University of Southampton, Faculty of Natural and Environmental Sciences, Southampton, 2016 (<http://eprints.soton.ac.uk/id/eprint/397980>)
6. S. M. Xu, L. Wei, C. Shen, L. Xiao, H. Y. Tao, C. J. Wang, *Nature Commun.* **10** (2019) 5553 (<https://doi.org/10.1038/s41467-019-13529-z>)
7. M. Wang, Z. Shi, *Chem. Rev.* **120** (2020) 7348 (<https://doi.org/10.1021/acs.chemrev.9b00384>)

8. H. A. Younus, M. Al. Rashida, A. Hameed, M. Uroos, U. Salar, S. Rana, K. M. Khan, *Expert Opin. Ther. Pat.* **31** (2021) 267 (<https://doi.org/10.1080/13543776.2021.1858797>)
9. X. Xiao, T. R. Hoye, *Nat. Chem.* **10** (2018) 838 (<https://doi.org/10.1038/s41557-018-0075-y>)
10. M. H. Cao, N. J. Green, S. Z. Xu, *Org. Biomol. Chem.* **15** (2017) 3105 (<https://doi.org/10.1039/C6OB02761J>)
11. X. Ji, C. Zhou, K. Ji, R. E. Aghoghovbia, Z. Pan, V. Chittavong, B. Ke, B. Wang, *Angew. Chem. Int. Ed.* **55** (2016) 15846 (<https://doi.org/10.1002/anie.201608732>)
12. Y. Yamashita, T. Yasukawa, W. J. Yoo, T. Kitanosono, S. Kobayashi, *Chem. Soc. Rev.* **47** (2018) 4388 (<https://doi.org/10.1039/C7CS00824D>)
13. J. Hu, M. Bian, H. Ding, *Tetrahedron Lett.* **57** (2016) 5519 (<https://doi.org/10.1016/j.tetlet.2016.11.007>)
14. J. F. Allochio Filho, B. C. Lemos, A. S. de Souza, S. Pinheiro, S. J. Greco, *Tetrahedron* **73** (2017) 6977 (<https://doi.org/10.1016/j.tet.2017.10.063>)
15. B. L. Oliveira, Z. Guo, G. J. L. Bernardes, *Chem. Soc. Rev.* **46** (2017) 4895 (<https://doi.org/10.1039/C7CS00184C>)
16. P. L. Wang, S. Y. Ding, Z. C. Zhang, Z. P. Wang, W. Wang, *J. Am. Chem. Soc.* **141** (2019) 18004 (<https://doi.org/10.1021/jacs.9b10625>)
17. W. Gati, H. Yamamoto, *Acc. Chem. Res.* **49** (2016) 1757 (<https://doi.org/10.1021/acs.accounts.6b00243>)
18. C. He, J. Hu, Y. Wu, H. Ding, *J. Am. Chem. Soc.* **139** (2017) 6098 (<https://doi.org/10.1021/jacs.7b02746>)
19. E. Sánchez-Larios, J. M. Holmes, C. L. Daschner, M. Gravel, *Org. Lett.* **12** (2010) 5772 (<https://doi.org/10.1021/o1102685u>)
20. J. Wang, H. Li, H. Xie, L. Zu, X. Shen, W. Wang, *Angew. Chem.* **119** (2007) 9208 (<https://doi.org/10.1002/ange.200703163>)
21. B. C. Hong, R. Y. Nimje, A. A. Sadani, J. H. Liao, *Org. Lett.* **10** (2008) 2345 (<https://doi.org/10.1021/o18005369>)
22. W. Notz, F. Tanaka, C. F. Barbas, *Acc. Chem. Res.* **37** (2004) 580 (<https://doi.org/10.1021/ar0300468>)
23. A. Cordova, C. F. Barbas, *Tetrahedron Lett.* **44** (2003) 1923 ([https://doi.org/10.1016/S0040-4039\(03\)00019-4](https://doi.org/10.1016/S0040-4039(03)00019-4))
24. F. Tanaka, C. F. Barbas III, *J. Syn. Org. Chem. Jpn.* **63** (2005) 709 (<https://doi.org/10.5059/yukigoseikyokaishi.63.709>)
25. S. Mukherjee, J. W. Yang, S. Hoffmann, B. List, *Chem. Rev.* **107** (2007) 5471 (<https://doi.org/10.1021/cr0684016>)
26. N. Campillo, J. A. Paez, P. Goya, *Helv. Chim. Acta* **86** (2003) 139 (<https://doi.org/10.1002/hlca.200390003>)
27. D. B. Ramachary, K. Anebouselvy, N. S. Chowdari, C. F. Barbas, *J. Org. Chem.* **69** (2004) 5838 (<https://doi.org/10.1021/jo049581r>)
28. R. Thayumanavan, B. Dhevalapally, K. Sakthivel, F. Tanaka, C. F. Barbas III, *Tetrahedron Lett.* **43** (2002) 3817 ([https://doi.org/10.1016/S0040-4039\(02\)00686-X](https://doi.org/10.1016/S0040-4039(02)00686-X))
29. N. S. Chowdari, C. F. Barbas, *Org. Lett.* **7** (2005) 867 (<https://doi.org/10.1021/o1047368b>)
30. E. M. Carreira, T. C. Fessard, *Chem. Rev.* **114** (2014) 8257 (<https://doi.org/10.1021/cr500127b>)
31. L. Hong, R. Wang, *Adv. Synth. Catal.* **355** (2013) 1023 (<https://doi.org/10.1002/adsc.201200808>)

32. J. Tellenbröker, D. Kuck, *Eur. J. Org. Chem.* **2001** (2001) 1483 ([https://doi.org/10.1002/1099-0690\(200104\)2001:8<1483::AID-EJOC1483>3.0.CO;2-U](https://doi.org/10.1002/1099-0690(200104)2001:8<1483::AID-EJOC1483>3.0.CO;2-U))
33. A. Boudhar, M. Charpenay, G. Blond, J. Suffert, *Angew. Chem. Int. Ed.* **52** (2013) 12786 (<https://doi.org/10.1002/anie.201304555>)
34. L. Porcelli, D. Stolfa, A. Stefanachi, R. Di Fonte, M. Garofoli, R. Iacobazzi, N. Silvestris, A. Guarini, S. Cellamare, A. Azzariti, *Cancer Lett.* **445** (2019) 1 (<https://doi.org/10.1016/j.canlet.2018.12.013>)
35. D. B. Ramachary, C. F. Barbas III, *Chem. Eur. J.* **10** (2004) 5323 (<https://doi.org/10.1002/chem.200400597>)
36. M. W. Schmidt, K. Baldridge, J. A. Boatz, S. T. Elbert, M. S. Gordon, J. H. Jensen, S. Koseki, N. Matsunaga, K. A. Nguyen, S. Su, T. L. Windus, M. Dupuis, J. A. Montgomery, *J. Comput. Chem.* **14** (1993) 1347 (<https://doi.org/10.1002/jcc.540141112>)
37. Y. Zhao, D. G. Truhlar, *Theor. Chem. Acc.* **120** (2008) 215 (<https://doi.org/10.1007/s00214-007-0310-x>)
38. A. Castro-Alvarez, H. Carneros, D. Sanchez, J. Vilarrasa, *J. Org. Chem.* **80** (2015) 11977 (<https://doi.org/10.1021/acs.joc.5b01814>)
39. M. Head-Gordon, J. A. Pople, M. J. Frisch, *J. Chem. Phys. Lett.* **153** (1988) 503 ([https://doi.org/10.1016/0009-2614\(88\)85250-3](https://doi.org/10.1016/0009-2614(88)85250-3))
40. Y. Zhao, N. E. Schultz, D. G. Truhlar, *J. Chem. Phys.* **123** (2005) 161103 (<https://doi.org/10.1063/1.2126975>)
41. S. B. Trickey, *Int. J. Quantum Chem.* **59** (1996) 259 (<https://doi.org/10.1002/qua.560590302>)
42. M. Attarbashi, N. Zabarjad Shiraz, M. Samadizadeh, *J. Theor. Comput. Chem.* **19** (2020) 2050005 (<https://doi.org/10.1142/S0219633620500054>)
43. M. Girod, B. Grammaticos, *Nucl. Phys., A* **330** (1979) 40 ([https://doi.org/10.1016/0375-9474\(79\)90535-9](https://doi.org/10.1016/0375-9474(79)90535-9)).

SUPPLEMENTARY MATERIAL TO
**Benzene-1,3-diol derivatives as the inhibitors of
butyrylcholinesterase: An emergent target of
Alzheimer's disease**

YIN DONGLIANG¹, SYEDA ABIDA EJAZ^{2*}, MUBASHIR AZIZ², AMNA SAEED²,
SAMINA EJAZ³, MUHAMMAD SAJJAD BILAL², HAFIZ MOHAMMAD KASHIF
MAHMOOD² and SYEDA TEHMINA EJAZ⁴

¹Department of Neurointervention, The Third hospital of Jinan, No.1 Wangsheren North Street, Gongye North Road, Licheng District, Jinan City, Shandong Province, 205132, China,

²Department of Pharmaceutical Chemistry, Faculty of Pharmacy, The Islamia University of Bahawalpur, Bahawalpur-63100, Pakistan, ³Department of Biochemistry, Institute of Biochemistry, Biotechnology and Bioinformatics, The Islamia University of Bahawalpur-63100, Bahawalpur, Pakistan and ⁴Department of Mathematics, The Government Sadiq College Women University Bahawalpur, Bahawalpur, Pakistan

J. Serb. Chem. Soc. 87 (3) (2022) 293–306

Table S-I. Structures of the selected compounds for study

PubChem CID	Codes	Compound structure	PubChem CID	Codes	Compound structure
5054	1a		3610	1f	
10333	1b		3014087	1g	
17927	1c		75294	1h	
87874	1d		11171903	1i	
205912	1e		24849532	1j	

*Corresponding author. E-mail: abida.ejaz@iub.edu.pk; abida.ejaz@iub.edu.pk

AChE docking studies

Bonding and non-bonding interaction of the amino acid residues of AChE enzyme with benzene-1,3-diol derivatives are shown in Fig. S-1. The amino acid residues which were involved in bonding and non-bonding interactions with, the compound **1a** were SER26, ARG24, LYS32, GLU49, LEU76 and LYS51. It was notable that the highly electronegative oxygen atom of OH group present at 1st position of benzene ring was making strong hydrogen bond with SER26 and ARG24 amino acid residues of AChE, whereas LYS32 was making hydrogen bond with hydrogen atom of OH group at position 1st of the benzene ring. It is evident that the OH group has strong electronegativity difference which can exert strong electrostatic force of attraction. Moreover, it was also involved in imparting positive inductive effect (+I). Similarly, LYS32 and GLU49 were involved in making hydrogen bond with the OH group present at 3rd position of the benzene ring. The LYS32 was also involved in making π -sigma bond with the benzene ring of resorcinol. Moreover, LYS51 was involved in strong π -cation interaction with the core benzene ring of interacting compound. Docking score of the current conformation was found to be -6.69 kJ/mol.

The amino acid residues, which were involved in bonding and non-bonding interactions with the compound **1b**, were ARG24, LYS32, LEU76, VAL340, TYR341, LYS51, GLY342 and SER26. It was observed that the interacting compound exhibited binding energy of -12.60 kJ/mol, which was due to the presence of methyl group at 4th position of benzene ring. It is well known that methyl group imparts the positive mesomeric effect, by donating electrons to the core of the benzene ring. It was also observed that OH groups present at 1st and 3rd position of the benzene ring were involved in making a strong hydrogen bond with LYS32 and ARG24 of activation loop. Furthermore, it was notable that the parent benzene ring had also showed major contribution toward interacting amino acid residues, through the formation of strong π -sigma and π -alkyl bond with LYS32 and LEU76 residues, respectively. Other interacting amino acid residues like VAL340, TYR341 and SER26 were involved in the formation of Van der Waals interactions with the interacting compound.

The docked conformations of compound **1c** with AChE enzyme showed that SER26, LYS32, ARG24, GLU49, LYS51, LEU76, GLY342 and TYR341 amino acid residues were involved in bonding and non-bonding interactions, (Fig. 4). It was notable that the substituted ethyl group had the electron donating tendency, which was imparting the positive mesomeric effect (+M). The substituted ethyl group was also involved in the formation of strong π -alkyl bond with LYS32 and LEU76 residues of active site. Furthermore, it was observed that the OH groups played the vital role in forming strong inhibiting interactions with amino acid residues of the active site. It was found that the carboxylate end of LYS32 and GLU49 was forming a hydrogen bond with the hydrogen atom of hydroxyl

group, which is present at position 1st and 3rd, respectively. Moreover, SER26 and ARG24 was found to be involved in the hydrogen bond with oxygen atoms of both hydroxyl group. In terms of binding energies, it was calculated as -17.04 kJ/mol. Another major interaction was a strong π -cation bond between benzene ring and LYS51. This π -cation was stabilizing the electrostatic interaction between a cation and a polarizable electronic cloud of the aromatic ring. Moreover, the aromatic ring was also involved in the π -sigma bonding with LYS32. Other amino acid residues which were involved in the Van der Waals interactions were GLY342 and TYR341.

The amino acid residues which were involved in bonding and non-bonding interactions with compound **1d** were ARG24, SER26, LYS32, GLU49, LYS51, LEU76 and VAL340. It can be seen that the propyl group was substituted at 4th position of benzene ring, due to which docking score was slightly better than compound **1c**. The docking score was appeared to be -17.20 kJ/mol. The substituted propyl group had the ability to donate electrons and imparted the positive mesomeric effect (+M). Another significance of propyl group included the strong π -alkyl interaction with LEU76 residue of the active site. It was obvious that hydroxyl groups played the vital role in the determination of the inhibiting potential of benzene 1,3 diol derivatives. Both OH groups were involved in making strong hydrogen bond with SER26, ARG24, GLU49 and LYS32. Most particularly, SER32 and ARG24 predominantly formed hydrogen bond with the negative end of the hydroxyl group, whereas other two formed hydrogen bond with the positive hydrogen atom. The presence of core aromatic ring also played a significant role in the inhibitory potential of these derivatives, as aromatic ring was itself involved in two major interactions *i.e.*, π -sigma and π -cation with LYS32 and LYS51, respectively. Amino acid residues like VAL340 and TYR341 were involved in Van der Waals interactions.

The amino acid residues which were involved in bonding interactions with **1e** were PHE346, GLY345, ALA343, LEU339, VAL340, LYS32, ARG24, GLU49, SER26, LYS51 and LEU76 (Figure 4). The compound **1e** had the substitution of butyl group at 4th position of aromatic ring. It was surprising to be seen that the butyl group was theo nly exposed to Van der Waals interactions, with few amino acid residues *i.e.*, ALA343, GLY345, PHE346 and VAL340. Whereas, the hydroxyl group was involved in making hydrogen bond with ARG24 and LYS32. Previously, it was seen that SER26 and GLU49 were also involved in the hydrogen bond formation, with the both hydroxyl groups, but in present case it was not observed. Moreover, LYS32 was again involved in forming π -sigma bond with the core aromatic ring. This π -sigma bonding significantly stabilizes the protein-ligand complex. The binding score for the compound **1e** was found to be -18.50 kJ/mol.

The amino acid residues which were involved in bonding and non-bonding interactions with compound **1f** were TYR77, TYR61, LEU76, VAL340, SER26, LYS32, ARG24, GLU49, LYS51 and ARG37. The last compound showed the significant docking score, -20.59 kJ/mol, and it can be suggested that it might be due to presence of long chain hexyl substituent.

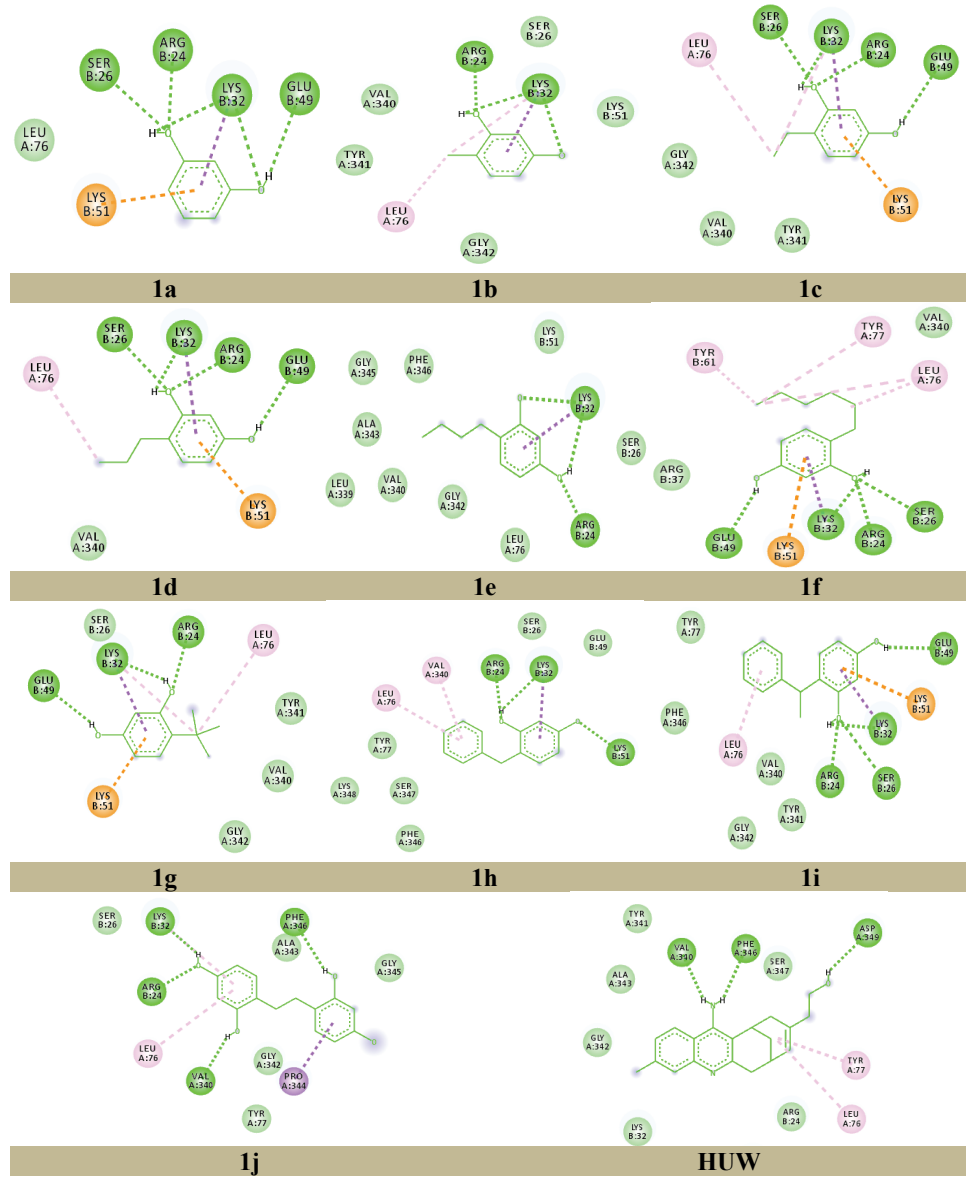


Fig. S-1. 2D interactions of benzene 1,3 diol derivatives with in active site of AChE enzyme.

It is well known that alkyl groups showes the inductive electron donating effect in all medium. The electron donation causes the shielding effect due to which carbon and hydrogen atoms of the benzene ring resonate at higher frequency. It was observed that the hexyl substituent was involved in the formation of π -alkyl bonding with TYR77, TYR61 and LEU76. Furthermore, the hydroxyl group of compound **1f** formed strong hydrogen bond with SER26, ARG24, GLU49 and LYS32. Moreover, the parent aromatic ring formed π -sigma interaction with LYS32, which stabilized the protein-ligand complex. In addition to π -sigma bonding, aromatic ring was involved in strong π -cation interaction with LYS51. The π -cation interaction was involved in stable electrostatic interaction between a cation and polarizable cloud of π electrons. Other interaction included Van der Waals interaction with VAL340. The compound **1g** was substituted with the tertiary butyl substituent, which didn't show any significant difference with **1f**. It was observed that the branched chain butyl group substituent had no significant effect on the interaction with amino acid residues, in fact the current substitution decreased the free binding energy to -20.05 kJ/mol. The overall binding interactions were similar to the compound **1f**.

BChE docking studies

Bonding and non-bonding interaction of amino acid residues of BChE enzyme with benzene-1,3-diol derivatives are shown in Fig. S-2. It was found that the docked conformation of compound **1a** showed reasonable bonding and non-bonding interactions with BChE than AChE. The amino acid residues which were involved in bonding and non-bonding interactions were as follows: ASP70, GLY78, TRP430, ALA328, TYR440, MET437, and SER78. It was notable that the highly electronegative oxygen atom of OH group present at 1st position of benzene ring was involved in making strong hydrogen bond with TRP430 residue. Whereas, GLY78 was involved in making hydrogen bond with electropositive hydrogen atom of OH group at 1st position of benzene ring. It is evident that the OH group have strong electronegativity difference, which can exert strong electrostatic force of attraction. Moreover, it was also involved in imparting positive inductive effect (+I). Similarly, ASP70 was involved in hydrogen bond formation with OH group present at 3rd position of benzene ring. It was noticed that TYR332 was involved in a π -donor hydrogen bond with benzene ring of resorcinol. Moreover, ALA328 was involved in strong π -alkyl bonding with core benzene ring of interacting compound. π -alkyl bonding is significant as it was involved in an interaction of π -electronic cloud of benzene ring and alkyl group of amino acid residue. The docking score of current conformation was found to be -17.58 kJ/mol.

The amino acid residues which were involved in bonding and non-bonding interactions with compound **1b** were as follows; ASP70, GLY78, TYR440,

MET437, ALA328, TYR332, TRP430 and SER79 (Figure 6). It was observed that the interacting compound exhibited the binding energy of -20.68 kJ/mol with the value of 472 μM , which was due to presence of methyl group at 4th position of benzene ring. It is well known that the methyl group imparts the positive mesomeric effect by donating electrons to the core benzene ring. Furthermore, the substituted methyl group had strong π -alkyl and alkyl interactions with π -electronic cloud of TYR440, MET437 and ALA328. Moreover, it was also observed that OH groups present at 1st and 3rd position of benzene ring were involved in a strong hydrogen bond with GLY78 and ASP70 of the activation loop. Furthermore, it was notable that the parent benzene ring also showed major contribution toward the interaction of the amino acid residues through the formation of strong π - π stacked and π -alkyl bond with TYR332 and ALA328 residues, respectively. The other interacting amino acid residues like HIS438, TRP82 and SER79 were involved in the formation of Van der Waals interactions with that compound.

The docked conformation of compound **1c** with BChE enzyme showed that the following amino acid residues were involved in bonding and non-bonding interactions: ASP70, GLY78, TYR440, TRP430, TYR332, PHE329, ALA328 and SER79. It was notable that the substituted ethyl group has approximately the same electron donating tendency as that of the methyl group, due to which it was imparting positive mesomeric effect (+M). The docking score of the compound **1c** *i.e.*, -20.89 kJ/mol didn't show any significant difference with the compound **1b**. Moreover, the substituted ethyl group was also involved in the formation of strong π -alkyl, alkyl and π -sigma bonding with ALA328, TYR332 and PHE329, respectively. Furthermore, it was observed that OH groups played vital role in forming the strong inhibiting interactions with the amino acid residues of the active site. It was found that the carboxylate end of ASP70 and GLY78 formed the hydrogen bond with the electropositive hydrogen atom of hydroxyl group present at 1st and 3rd position of benzene ring, respectively. Moreover, TRP430 and TYR440 was found to be involved in hydrogen bond formation with the oxygen atoms of hydroxyl group. Another major interaction was the formation of strong π - π stacked bonding between the benzene ring and TYR332. Moreover, the aromatic ring was also involved in π -alkyl bonding with ALA328. The other amino acid residues, which were involved in van der Waals interactions with compound **1c**, were MET437 and MET81.

The amino acid residues which were involved in bonding and non-bonding interactions with compound **1d** were as follows; GLY78, ASP70, ALA328, PHE329, TYR332, SER79 and MET437. In the present compound, the propyl group was substituted at 4th position of benzene ring, due to which docking score was slightly better than compound **1c**. The docking score of **1d** was calculated as -23.19 kJ/mol, with the predicted inhibitory constant value of 171 μM . The

substituted propyl group has the ability to donate electrons and impart the positive mesomeric effect ($+M$). Another significance of propyl group was the formation of strong π -sigma and π -alkyl interaction with TYR332 and PHE329 residues of the active site. It was obvious that the hydroxyl groups played vital role in determining the inhibiting potential of benzene 1,3 diol derivatives. It was found that both OH groups formed strong hydrogen bond with ASP70 and GLY78. The presence of core aromatic ring was also playing a significant role in the inhibitory potential of these derivatives, as it was involved in π -alkyl interaction with ALA328. SER79 and TRP 430 were involved in Van der Waals interaction.

The docked conformation of another 1,3 diol derivative, *i.e.*, **1e** was observed to show strong bonding and non-bonding interactions with the amino acid residues of active site of enzyme. The following amino acid residues were involved; SER287, LEU286, HIS438, PHE329, TRP231, PHE398, ALA199, GLY116 and GLY117. Compound **1e** had the substitution of butyl group at 4th position of aromatic ring. It was observed that the substituted butyl group was making strong π -sigma with TRP231 and π -alkyl bonding with HIS438, PHE239, PHE398 and ALA199 of BChE enzyme, but the same compound lacked these important interactions with AChE enzyme, which suggested that these compounds had better inhibitory potential against BChE enzyme, with docking score of -24.82 kJ/mol. Furthermore, the hydroxyl groups were involved in forming hydrogen bond with SER287 and LEU286. Moreover, LEU286 also formed π -alkyl bond with the core aromatic ring. This π -alkyl bonding significantly stabilized the protein-ligand interaction.

The amino acid residues, which were involved in bonding and non-bonding interactions with compound **1f**, were as follows; HIS438, GLU197, SER198, TRP82, PHE398, TRP231, GLY116, GLY117 and GLY439. The present compound showed significant docking score that was -25.03 kJ/mol. It might be due to the presence of long chain hexyl substituent. It is well known that alkyl groups show the inductive electron donating effect in every medium. The electron donation causes the shielding effect due to which carbon and hydrogen of benzene ring resonate at higher frequency. It was observed that the hexyl substituent was involved in the formation of π -sigma, π -alkyl and π - π T-shaped interactions with TRP231, PHE298, HIS438 and TRP82, respectively. Furthermore, the hydroxyl group of compound **1f** formed a strong hydrogen bond with SER198, GLU197 and HIS438. Moreover, the parent aromatic ring formed the π -cation interaction with HIS438. The π -cation interaction was stabilizing the electrostatic interaction between a cation and the polarizable cloud of π -electrons. The other interactions were included Van der Waals interaction with GLY116 and GLY117. The compound **1g** was substituted with the tertiary butyl group which didn't show significant difference with compound **1e**, which was substituted with *n*-butyl chain. It was observed that the branched chain butyl

substituent had no significant effect on the interacting amino acid residues, in fact the current substitution decreased the free binding energy to -23.19 kJ/mol, therefore it was concluded that tertiary butyl had the negative impact on docking energy. The overall binding interactions of compound **1f** was similar to compound **1e**.

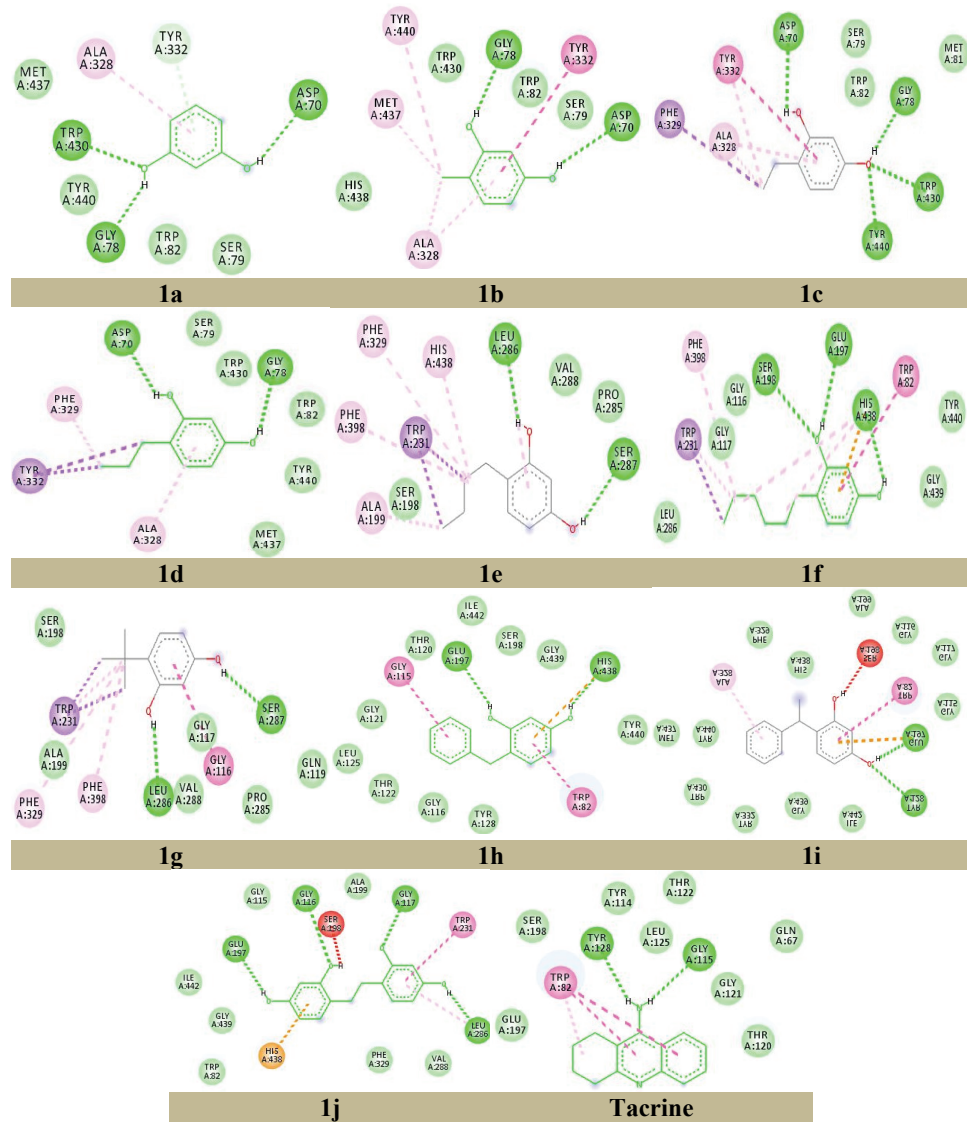


Fig. S-2. 2D interactions of benzene1,3 diol derivatives with in active site of BChE enzyme.



Reactions of copper(II) bromide with 2,6-diacetylpyridine bis(phenylhydrazone) (**L**) – Molecular and crystal structures of **L** and its mixed-valence complex $[\text{Cu}^{\text{II}}\text{L}_2][\text{Cu}^{\text{I}}_2\text{Br}_4]$

MARKO V. RODIĆ^{1*}, MIRJANA M. RADANOVIĆ^{1#}, DRAGANA V. GAZDIĆ¹,
VUKADIN M. LEOVAC^{1#}, BERTA BARTA HOLLÓ^{1#}, VIDAK RAIČEVIĆ^{1#},
SVETLANA K. BELOŠEVIĆ^{2#}, BILJANA KRÜGER³
and LJILJANA S. VOJINOVIĆ-JEŠIĆ^{1#}

¹University of Novi Sad, Faculty of Sciences, Trg Dositeja Obradovića 3, 21000 Novi Sad, Serbia

²Faculty of Technical Sciences, University of Priština, Knjaza Miloša 7, 38220 Kosovska Mitrovica, Serbia and ³University of Innsbruck, Institute of Mineralogy and Petrography, Innrain 52, 6020 Innsbruck, Austria

(Received 27 November, revised 14 December, accepted 20 December 2021)

Abstract: Utilizing X-ray crystallography, the crystal and molecular structures of 2,6-diacetylpyridine bis(phenylhydrazone) (**L**) were determined. The energetics of the intermolecular interactions in the crystal structure were assessed with computational methods, revealing that dispersion interactions are dominant. The basic structural unit of the crystal packing was revealed to be the herring-bone type arrangement of **L** molecules. Assignment of the IR spectrum of **L** with the aid of DFT calculations was performed. Furthermore, new reactions of **L** with CuBr_2 in different solvents are described, which led to the synthesis of the mixed Cu(II)–Cu(I) complex with the formula $[\text{Cu}^{\text{II}}\text{L}_2][\text{Cu}^{\text{I}}_2\text{Br}_4]$ (**1**), and its structural characterization. In the complex cation, two molecules of tridentate N_3 ligand are meridionally arranged in a very distorted octahedral environment of a Cu(II) ion. In $[\text{Cu}_2\text{Br}_4]^{2-}$, the bromide ions are arranged in a trigonal-planar geometry around each copper(I) atom. Finally, for ligand, **1**, and the previously synthesized complex $[\text{CuL}_2]\text{Br}_2$, the thermal properties were examined. The thermal stability of the complexes were lower than that of the ligand and decrease in the order: **L** (250 °C) > $[\text{CuL}_2]\text{Br}_2$ (221 °C) > $[\text{Cu}^{\text{II}}\text{L}_2][\text{Cu}^{\text{I}}_2\text{Br}_4]$ (212 °C). The differences in thermal stability of the complexes are due to differences in the packing efficacy of the constitutional ions.

Keywords: copper(I); Schiff bases; tridentate coordination mode; X-ray crystallography; DFT.

* Corresponding author. E-mail: marko.rodic@dh.uns.ac.rs

Serbian Chemical Society member.

<https://doi.org/10.2298/JSC211127112R>

INTRODUCTION

Hydrazones represent a large group of organic compounds formed by the condensation of carbonyl compounds with hydrazine or its derivatives. Considering the variety of both carbonyl compounds and hydrazine derivatives, the large number of reported hydrazones is not surprising. These compounds are interesting for research not only from the theoretical point of view but also due to the possibility of their application in different areas (wide range of biological activity, analytical reagents, catalysis, *etc.*). This resulted in the publication of numerous scientific papers, reviews, and monographs concerning this group of compounds.^{1–9}

Having different donor atoms (N, O, S, P, *etc.*) to coordinate the metal ions rendered this group of compounds a very interesting topic for coordination chemists.^{2,10} For coordination chemists, a significant ligand precursor is 2,6-diacetylpyridine, which, depending on the hydrazine derivative it is condensed with, can yield bis(hydrazones) of differing denticity. The most numerous are those that act as tridentate and pentadentate ligands.^{11–14}

Some time ago, synthesis, spectroscopic and magnetic characterization of mono- and bis(ligand) complexes of Fe(II), Co(II), Ni(II) and Cu(II) with the tridentate N₃ ligand, 2,6-diacetylpyridine bis(phenylhydrazone) of general formulae [M(L)Cl₂] and [ML₂](ClO₄)₂ were described.¹¹ Recently, complexes with the title ligand, *i.e.*, [CoL₂]I₂¹⁵ and [CuL₂]Br₂,¹⁶ have been synthesized and structurally characterized, which represent the only metal complexes with this ligand to be characterized by SC-XRD so far. As a continuation of research on the coordinating properties of 2,6-diacetylpyridine bis(phenylhydrazone), in this paper, its new reactions with CuBr₂ in different solvents are described, which led to the synthesis, structure, and characterization of a mixed Cu(II)–Cu(I) complex with the formula [Cu^{II}L₂][Cu^I₂Br₄]. Thermal properties were also examined, both for the ligand and the complex [CuL₂]Br₂ synthesized earlier.

EXPERIMENTAL

Reagents

All chemicals used were commercially available products of analytical reagent grade and were used without further purification. The ligand, 2,6-diacetylpyridine bis(phenylhydrazone), L, was synthesized according to a previously described procedure.¹⁵

Preparation of single-crystals of 2,6-diacetylpyridine-bis(phenylhydrazone) (L)

Single crystals suitable for X-ray crystallographic analysis were obtained by diffusion of Et₂O to a concentrated acetonnic solution of the ligand.

Synthesis of the complex [Cu^{II}L₂]/[Cu^I₂Br₄] (I)

To 20 cm³ of Me₂CO, 44 mg (0.2 mmol) of CuBr₂ was added and slightly heated. To this greenish suspension, 34 mg (0.1 mmol) of L was added and the heating was continued for 5 min, during which the solution obtained a red color. The resulting solution was left at room temperature and after three days, red needle-like microcrystals of undefined composition and

black prismatic single crystals of complex **1** were filtered off and washed with Me₂CO. Yield of the mixture: 50 mg.

*Synthesis of the complex [Cu^{II}**L**₂][Cu^I₂Br₄] (**1**) (from MeOH solution)*

A mixture of 34 mg (0.1 mmol) of **L** and 44 mg (0.2 mmol) of CuBr₂ was dissolved in 10 cm³ of warm MeOH and evaporated to a small volume. The obtained black ribbed-plate-like crystals were filtered off and washed with MeOH. Yield: 30 mg (50 %).

Analytical methods

Elemental analyses (C, H and N) of air-dried compounds were performed by standard micro-methods. Molar conductivity measurements of a freshly prepared DMF solution of the complex (*c* = 1 mmol dm⁻³) were performed on a Jenway 4010 conductivity meter. IR spectra were recorded on a Nicolet iS20 (Thermo Scientific) FTIR spectrophotometer, in the range of 400–4000 cm⁻¹, using the KBr pellet technique. ¹H- and ¹³C{¹H}-NMR spectra were acquired on a Bruker Avance III spectrometer equipped with a CryoProbe Prodigy probe-head, operating at 400 and 100.6 MHz, respectively. The spectra were assigned using 2D techniques (gradient ¹H-¹H COSY, HSQC and HMBC), which were recorded using the built-in Bruker pulse sequences. Coupling constants were determined using spin simulation. Thermal data were collected using a TA Instruments SDT Q600 thermal analyzer coupled to a Hiden Analytical HPR20/QIC mass spectrometer. The decomposition was followed from room temperature to 700 °C at a heating rate of 20 °C min⁻¹ under a nitrogen carrier gas (flow rate = 100 cm³ min⁻¹). Sample holder/reference: alumina crucible/empty alumina crucible. Sample mass 2.5–3 mg. TG–MS measurements were performed from room temperature to 350 °C at a heating rate of 10 °C min⁻¹ under an argon carrier gas (flow rate = 50 cm³ min⁻¹). Selected ions for *m/z* 1–58 were monitored in the multiple ion detection mode (MID).

Analytical and spectral data of the synthesized compounds are given in Supplementary material to this paper.

Crystal structure determination

Diffraction experiments were performed on a dual source (MoK α and CuK α X-radiation) Gemini R Ultra diffractometer, equipped with a Ruby CCD detector (Oxford Diffraction). Single crystals were cooled to 170 K by a flux of dry air. The CrysAlisPro was used for the experiment setup and data reduction.¹⁷ Crystal structures were solved with SHELXT¹⁸ and refined by using SHELXL-2018¹⁹ interfaced with ShelXle.²⁰ Pertinent crystallographic and refinement details are listed in Table S-I of the Supplementary material. The crystallographic data are deposited at the Cambridge Crystallographic Data Centre. CCDC Nos.: 2123008 for **L** and 2123007 for **1**. These data are available free of charge via <https://www.ccdc.cam.ac.uk/structures/>.

Hirshfeld surface analysis and intermolecular interaction energies estimate

Hirshfeld surface calculations were performed with Crystal Explorer 2020.²¹ Intermolecular interaction energies were calculated, and parsed to electrostatic, dispersion, polarization, and repulsion terms, using CE-B3LYP model energies²² with Crystal Explorer 2020,²¹ and utilizing TONTO²³ as a backend. Calculations were performed for intermolecular dimers comprised of a selected molecule and all its nearest neighbors defined by the Hirshfeld surface.

Computational methods

All density functional calculations (DFT) calculations were performed with GAMESS US.²⁴ Equilibrium geometry of an isolated 2,6-diacetylpyridine bis(phenylhydrazone) molecule was optimized using B3LYP exchange-correlation functional, and 6-31G(d,p) basis set.

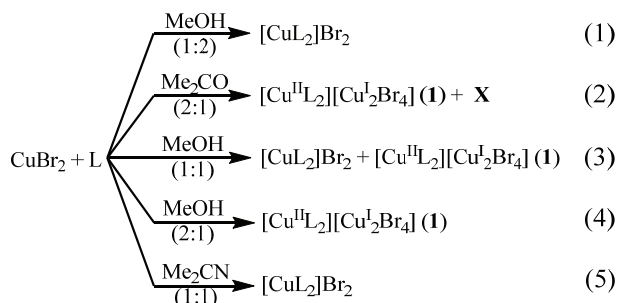
The initial structure was chosen to represent the molecular conformation found in the crystal structure. The ground state was confirmed by the fact that vibrational analysis resulted only in positive frequencies. Partial assignment of IR bands was performed by visual inspection of molecular vibrations with MacMolPlt.²⁵

RESULTS AND DISCUSSION

Syntheses and characterization

A previously described synthesis of the ligand was performed,¹⁵ *i.e.*, warm EtOH solutions of stoichiometric amounts of 2,6-diacetylpyridine and phenylhydrazine hydrochloride were reacted in the presence of an excess of LiOAc. This resulted in the formation of microcrystals of the ligand. Crystals suitable for X-ray diffraction were prepared by slow vapor diffusion of Et₂O into a concentrated acetonnic solution of the ligand.

In a previous paper,¹⁵ the synthesis of the Cu(II) complex with 2,6-diacetylpyridine bis(phenylhydrazone) of the formula [CuL₂]Br₂ was reported. This complex was obtained in the reaction of MeOH solutions of CuBr₂ and L in a 1:2 mole ratio (Scheme 1). Herein, the observation that the composition of the obtained complexes depends not only on the mole ratio of the reactants but also on the nature of the solvent is reported, which is corroborated by results achieved by examining different reaction conditions (Scheme 1).



Scheme 1. Reactions of CuBr₂ and L.

The reaction of CuBr₂ and L in a 2:1 mole ratio in warm Me₂CO gave a mixture of black prismatic single crystals of the formula [Cu^{II}L₂][Cu^I₂Br₄] (**1**) and thin red needle-like crystals of undefined composition (X). Crystals of **1** were suitable for SC-XRD, by which the structure of the obtained complex was unambiguously proven (*vide infra*). Based on elemental analysis and IR spectra, it was not possible to unequivocally propose a molecular formula for X.

When the reaction was performed in MeOH in a 2:1 mole ratio, only black ribbed-plate-like crystals of **1** were formed. The quality of these was not sufficiently high for SC-XRD, but based on the results of elemental analysis and

identity of its IR spectrum with the spectrum of **1**, the same composition and coordination formula was proposed.

A mixture of the crystals of **1** and previously characterized $[\text{CuL}_2]\text{Br}_2$ was formed in the reaction of a MeOH solution of the reactants present in a 1:1 mole ratio. Finally, if acetonitrile was used as the solvent instead of MeOH in mole ratio 1:1, only the bis(ligand) complex $[\text{CuL}_2]\text{Br}_2$ formed.

Complex **1** is stable at higher temperatures (decomp. 212 °C) and shows appreciable solubility in DMF, while it is only partially soluble in alcohols and acetone, and virtually insoluble in H₂O. The molar conductivity of a DMF solution of the complex had a value of 134 S cm² mol⁻¹ and corresponds to 2:1 type of electrolytes,²⁶ which could be explained by the partial decomposition of the complex anion.

In the IR spectrum of the ligand, as well as the spectrum of the complex in the high-energy region (>3000 cm⁻¹), there was only one band that could undoubtedly be ascribed to $\nu(\text{NH})$ vibrations; it is located at 3342 cm⁻¹ in the spectrum of the ligand and at 3271 cm⁻¹ in the spectrum of the complex.

The presence of an IR band corresponding to C=N(imine) stretching is often taken as an indication of whether coordination of the imine nitrogen had occurred.²⁷ Therefore, it is of importance to assign this vibration to an appropriate band(s) in the IR spectrum of **L**. In this study, this step was performed using the results of DFT calculations, along with the assignment of some other characteristic IR bands. The optimized geometry of **L** closely matches the experimentally determined one, as mean absolute deviations of non-hydrogen involved bond lengths and valence angles are 0.011 Å and 0.61°, respectively. Therefore, the calculated vibrational frequencies derived from a theoretical molecular structure may be regarded as reliable.

The very strong band at 1602 cm⁻¹ corresponds to C–C stretching modes of phenyl rings. The stretching of the C=N fragment is coupled both to phenyl rings valence vibrations and pyridine ring valence vibrations, and appears as a shoulder in the IR spectrum at 1592 cm⁻¹ and a strong band at 1563 cm⁻¹, respectively. The strong sharp band at 1508 cm⁻¹ corresponds to in-plane N–H deformations, and the presence of this band may be used to assign the ionic state of **L** in complexes. A medium-intensity band at 1491 cm⁻¹ corresponds to phenyl rings C–H in-plane deformations. Stretching vibration of the hydrazine N–N fragment corresponds to a very strong band at 1165 cm⁻¹. Two strong bands, inherent of monosubstituted benzene rings (*i.e.*, phenyl group), associated with $\nu(\text{C–H})$ vibrations, can be found at 748 and 694 cm⁻¹.²⁸ Finally, in-plane pyridine ring deformation, which is metal-sensitive and can reveal coordination of the pyridine nitrogen if shifted to higher wavenumbers,²⁹ corresponds to the band at 647 cm⁻¹. Other bands in the IR spectrum of the ligand are of little importance for studies of its coordination chemistry and are not discussed.

In the IR spectrum of **1**, the mentioned shoulder at 1592 cm^{-1} is nonexistent, but more importantly, the band at 1563 cm^{-1} is shifted to lower wavenumbers (1518 cm^{-1}), which is in agreement with the observation that coordination of both the imine nitrogen atom and pyridine nitrogen atom lowers the strengths of these bonds.

*Crystal structure of 2,6-diacetylpyridine bis(phenylhydrazone) (**L**)*

The molecular structure of **L** is depicted in Fig. 1. 2,6-Diacetylpyridine bis(phenylhydrazone) displays roughly planar conformation in the crystal structure, with an *s-trans* arrangement of substituents around C1–C6, C5–C8, as well as N1–N3 and N4–N5 bonds (an *all-trans* conformation). The structures in the Cambridge Structural Database (CSD)³⁰ KEWWOB³¹ and URINOZ³² correspond to compounds $[\text{HL}]NO_3$ and $[\text{HL}]ClO_4$ containing protonated **L**, in which both hydrazone moieties are in a conformation in which the arrangement around equivalent C–C bonds is *s-cis*, implying that conformations of **L** in its neutral and protonated forms are significantly different.

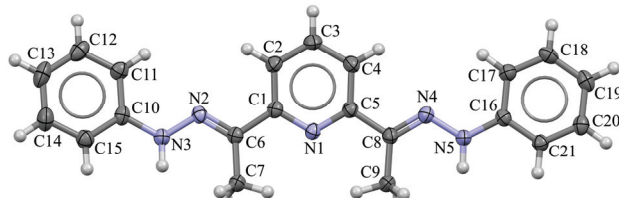


Fig. 1. Molecular structure of **L** with the atom numbering scheme.

Mogul validation of all structural parameters of **L** (bond lengths, valence, and torsions angles as well as ring conformations) against CSD structures having similar fragments indicated that they are completely within the expected range.

The analysis of atom–atom specific contacts by Hirshfeld surface decomposition reveals that major intermolecular contacts are of the type H···H (50.8 %), C···H (21.2 %) and N···H (14.6 %). Enrichment ratios³³ represent an elegant way to judge the propensity of pairs of chemical species to form crystal-packing interactions. Their values for the crystal structure of **L** are listed in Table S-II of the Supplementary material. It can be seen that C···C, N···N and C···N contacts are strongly avoided, while H···H contacts are slightly depressed in the crystal structure ($E_{HH} = 0.90$), even though H···H contacts comprise the majority of the Hirshfeld surface of the molecule. On the contrary, enrichment ratios for C···H and N···H contacts are significantly higher than unity ($E_{CH} = 1.31$, $E_{NH} = 1.31$), indicating that these interatomic contacts are favored in the crystal structure. It is interesting to note that, even though **L** has two potential hydrogen-bond donors (hydrazine nitrogen atoms), and three potential acceptors (pyridine and imine nitrogen atoms), these hydrogen bonds are not realized in the crystal structure.

It is the lack of common atom–atom intermolecular contacts, and related intermolecular features, such as $\text{CH}\cdots\pi$ or stacking interactions, that causes difficulties in recognizing the structural determinants of the crystal packing. To overcome this hurdle, the assessment of pairwise intermolecular energies was performed by CE-B3LYP model energies, and the results are summarized in Table I and Fig. S-1 of the Supplementary material.

TABLE I. Summary of intermolecular interaction energies (kJ mol^{-1}) of the unique molecular pairs constituting the first coordination sphere for **L** calculated using CE-B3LYP model energy; N , the number of interactions equals 2; R is the distance between molecular centroids. The relevant space group symmetry operation is reported without translation. Total interaction energy is calculated by addition of scaled individual components: $E_{\text{tot}} = k_{\text{ele}}E_{\text{ele}} + k_{\text{pol}}E_{\text{pol}} + k_{\text{dis}}E_{\text{dis}} + k_{\text{rep}}E_{\text{rep}}$, where $k_{\text{ele}} = 1.057$, $k_{\text{pol}} = 0.740$, $k_{\text{dis}} = 0.871$, and $k_{\text{rep}} = 0.618^{22}$

Symmetry operation	$R / \text{\AA}$	Energy				
		E_{ele}	E_{pol}	E_{dis}	E_{rep}	E_{tot}
x, y, z	5.35	-13.3	-2.6	-56.0	29.3	-46.7
$x + \frac{1}{2}, -y + \frac{1}{2}, -z$	6.44	-13.9	-2.0	-55.5	35.2	-42.7
$-x, y + \frac{1}{2}, -z + \frac{1}{2}$	9.99	-8.1	-2.2	-24.6	19.3	-19.8
$-x + \frac{1}{2}, -y, z + \frac{1}{2}$	11.63	-4.1	-1.0	-23.2	10.0	-19.1
$x + \frac{1}{2}, -y + \frac{1}{2}, -z$	14.41	12.9	-2.7	-30.1	0.0	-14.6
$-x, y + \frac{1}{2}, -z + \frac{1}{2}$	10.07	-2.8	-0.7	-19.5	12.3	-12.8
$-x + \frac{1}{2}, -y, z + \frac{1}{2}$	12.74	0.5	-0.3	-9.3	0.0	-7.7

In general, it is dispersion interactions that are dominant within the crystal structure, which is in line with the mentioned absence of hydrogen bonds. The basic structural unit of the crystal packing is revealed to be the herring-bone type arrangement of **L** molecules, forming a double-layered column lying parallel to the $(0\ 2\ -1)$ crystallographic plane, and infinitely propagating along the crystallographic a axis, as depicted in Fig 2a.

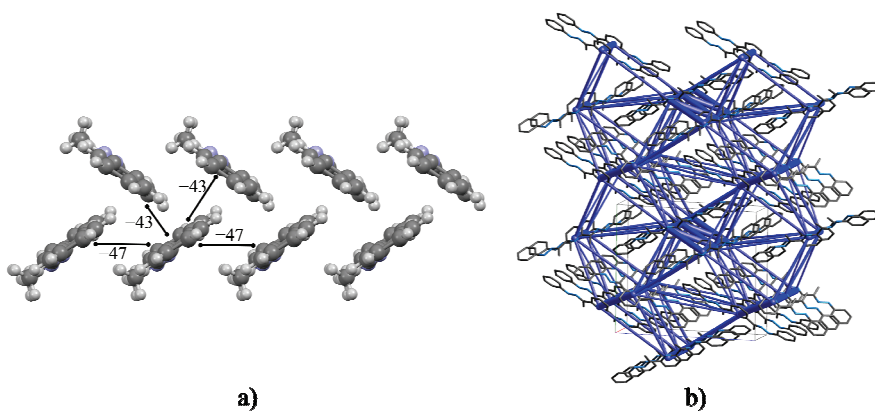


Fig. 2. a) Side view of the herring-bone type arrangement of **L** molecules; numbers indicate interaction energy in kJ mol^{-1} . b) Energy framework of the crystal structure of **L**.

From the perspective of an **L** molecule, the motif is realized by two different interactions, each forming two pairs. These interactions are dispersion dominated, but it is noteworthy that they are the only ones that make any significant electrostatic contribution to the stabilizing energy.

A stabilizing interaction of the energy of -47 kJ mol^{-1} is formed between two partner molecules, related by pure translations along crystallographic *a* axis. The molecules mutually form a stacking arrangement with significant offset. An energetically comparable (-43 kJ mol^{-1}) interaction is formed between the selected molecule of **L** from one sub-layer and two molecules belonging to the second sub-layer of the double layer motif. These molecules and **L** from the first sub-layer are related by 2_1 screw rotation along the crystallographic *b* axis, coupled to additional translations. Overview of crystal packing energetics is presented on an energy framework diagram (Fig. 2b), constructed from the calculated intermolecular energies.

Crystal structure of $[\text{Cu}^{II}\text{L}_2][\text{Cu}^I_2\text{Br}_4]$ (1)

The crystal structure of complex **1** is comprised of isolated complex cations $[\text{CuL}_2]^{2+}$ and dinuclear complex anions $[\text{Cu}_2\text{Br}_4]^{2-}$. The molecular structure of the formula unit is shown in Fig. 3. The structure of the complex cation $[\text{CuL}_2]^{2+}$ was already described in a structurally characterized compound, $[\text{CuL}_2]\text{Br}_2$.¹⁶ While the complex cation in $[\text{CuL}_2]\text{Br}_2$ has crystallographic two-fold symmetry, in **1** this symmetry is only approximate (two-fold pseudosymmetry axis bisects N2A–Cu1–N4B angle). Allowing for a large tolerance margin, the cation has D_2 point group symmetry, with additional two-fold axes passing through the N1A–Cu1–N1B bonds and cutting across the N2A–Cu1–N2B angle, respectively.

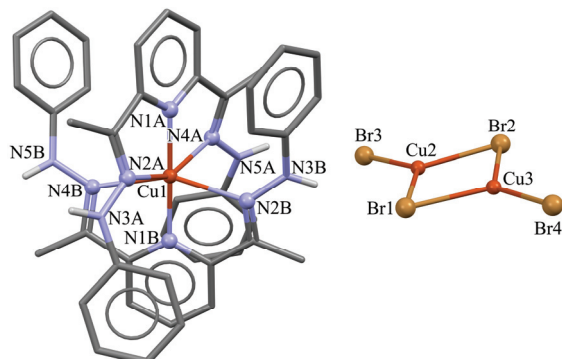


Fig. 3. Molecular structure of the formula unit of $[\text{Cu}^{II}\text{L}_2][\text{Cu}^I_2\text{Br}_4]$ (1).

The ligand is coordinated as a tridentate, through the pyridine nitrogen atom and two imine nitrogen atoms, analogous to the mode found in $[\text{CoL}_2]\text{I}_2$ (CSD refcode ZIXSOR),¹⁵ and resembling that of a structurally related ligand 2,6-di-

formylpyridine bis(phenylhydrazone), **L'**, in $[\text{Zn}(\text{L}')_2](\text{CF}_3\text{O}_3\text{S})_2$ (CSD refcode GUKTOW).³⁴ Two ligands are meridionally arranged in a very distorted octahedral environment of a Cu(II) ion, so that the dihedral angle is enclosed by mean planes through the Cu1, N1A, N2A and N4A atoms, and Cu1, N1B, N2B and N4B atoms, amounts $72.94(8)^\circ$, reflecting the deformation of the coordination polyhedron by its deviation from 90° . A deviation from the ideal octahedron is also manifested through *trans*-valence angles deviating from their ideal values of 180° , as shown in Table II.

TABLE II. Selected structural parameters of $[\text{Cu}^{\text{II}}\text{L}_2][\text{Cu}^{\text{I}}_2\text{Br}_4]$ (**1**), $[\text{CuL}_2]\text{Br}_2$ and **L**

Bond	Bond length, Å	
	$[\text{Cu}^{\text{II}}\text{L}_2][\text{Cu}^{\text{I}}_2\text{Br}_4]$ (1)	$[\text{CuL}_2]\text{Br}_2^{16}$
Cu1–N1A	1.936(3)	1.9451(18)
Cu1–N1B	1.944(3)	–
Cu1–N2A	2.258(3)	2.2170(18)
Cu1–N2B	2.288(3)	–
Cu1–N4A	2.308(3)	2.3736(18)
Cu1–N4B	2.334(4)	
Valence angle, °		
N1A–Cu1–N1B	176.75(14)	
N2A–Cu1–N4A	152.59(13)	
N2B–Cu1–N4B	152.58(13)	
Bond length, Å		
$[\text{Cu}^{\text{II}}\text{L}_2][\text{Cu}^{\text{I}}_2\text{Br}_4]$ (1)		
Ligand A	Ligand B	L
N1–C1	1.352(5)	1.358(5)
N1–C5	1.347(5)	1.348(5)
C1–C6	1.475(6)	1.461(6)
C5–C8	1.464(6)	1.461(6)
C6–N2	1.297(5)	1.294(6)
C8–N4	1.300(5)	1.305(6)
N2–N3	1.357(5)	1.349(5)
N4–N5	1.353(5)	1.357(5)

Metal–ligand bond lengths belonging to two ligand molecules, designated A and B in the atom enumeration scheme, are not equivalent. The shortest coordination bonds involve pyridine nitrogen atoms N1A and N1B, which have a comparable length with the one found in $[\text{CuL}_2]\text{Br}_2$. Mid-length bonds are longer in **1** than in $[\text{CuL}_2]\text{Br}_2$, while the longest bonds in **1** are shorter than the corresponding ones in $[\text{CuL}_2]\text{Br}_2$, thus manifesting the flexibility of the $[\text{CuL}_2]^{2+}$ cation. Intraligand bond lengths do not show significant differences between coordinated and free **L**, as shown in Table II.

In $[\text{Cu}_2\text{Br}_4]^{2-}$, the bromide ions are arranged in a trigonal-planar geometry around each copper(I) atom. By virtue of edge sharing, a four-membered metal-

locycle is formed, with two bromide ions in a bridging mode, and a Cu···Cu separation of 2.9477(8) Å. The four-membered ring Cu₂–Br₁–Cu₃–Br₂ can be regarded as flat for all practical purposes.

Thermal properties of L, [CuL₂]Br₂ and [Cu^{II}L₂]/[Cu^I₂Br₄] (1)

The ligand, and both complexes were analyzed by simultaneous TG-DSC measurements. In an inert atmosphere, the ligand was stable up to relatively high temperature (Fig. 4). It melted at 220 °C and began to decompose at 250 °C, onset. Above this temperature, L loses about 80 % of its mass in one step up to 600 °C with a DTG maximum at 322 °C. The heat effect of thermal decomposition is exothermic with a peak maximum at 322 °C.

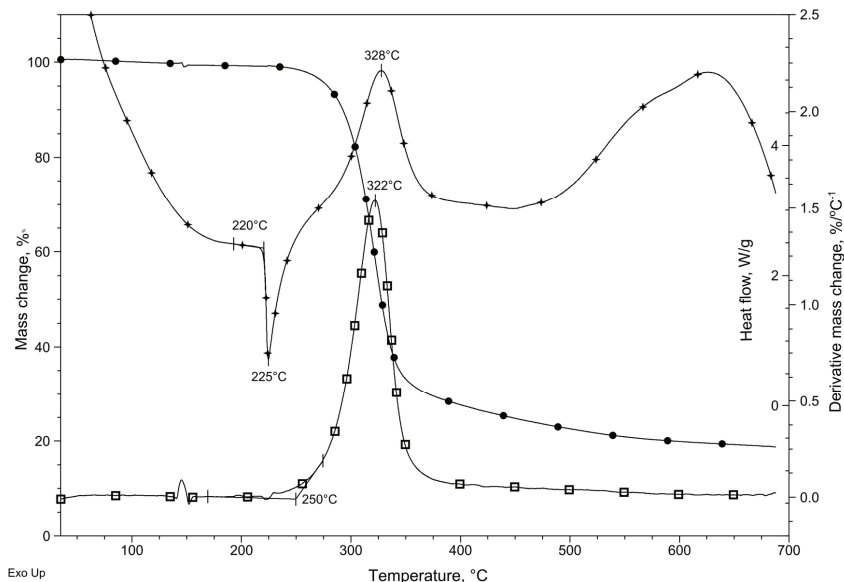


Fig. 4. TG (●), DTG (□) and DSC (+) curves of L in nitrogen.

The thermal stability of complexes is lower than that of the ligand and decreases in order: L (250 °C) > [CuL₂]Br₂ (221 °C) > [Cu^{II}L₂]/[Cu^I₂Br₄] (212 °C). The mass loss in 1 began at 83 °C, onset and the mass decrease is 3.4 % (Fig. 5). The rate maximum of this process is achieved at 150 °C. By coupled TG–MS measurements, it was determined that this mass loss corresponds to evaporation of absorbed water (Fig. S-2 of the Supplementary material). The thermal decomposition of the complex started at 212 °C, onset, before the solvent loss was finished. This compound loses about 20 % of its mass up to 300 °C in a well-defined step with DTG maximum at 228 °C. Above this temperature, the decomposition was continuous, and its steps could not be distinguished. Only a small intensity DTG peak could be observed at 408 °C.

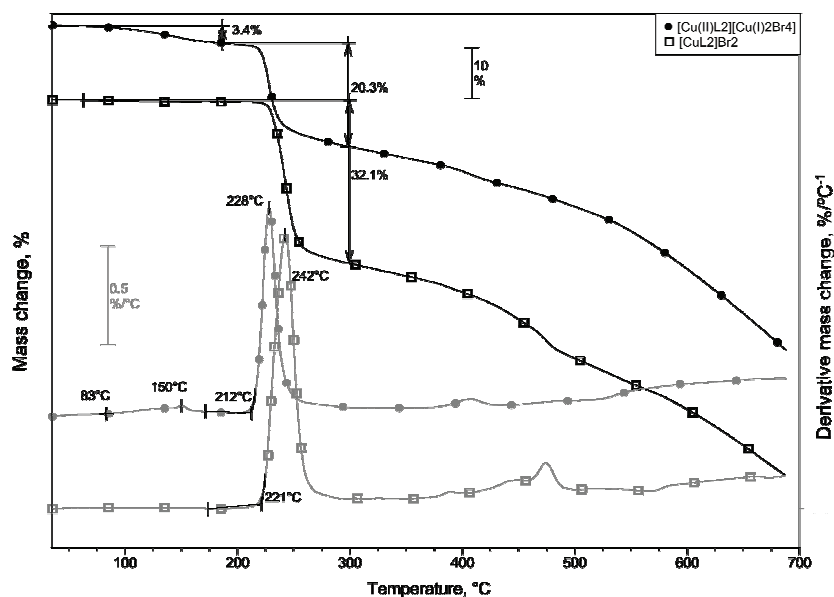


Fig. 5. TG and DTG curves of $[\text{Cu}^{II}\text{L}_2]\text{[Cu}^{I_2}\text{Br}_4$ (●) and $[\text{CuL}_2]\text{Br}_2$ (□) in nitrogen.

The thermal stability of $[\text{CuL}_2]\text{Br}_2$ is higher than that of $[\text{Cu}^{II}\text{L}_2]\text{[Cu}^{I_2}\text{Br}_4$, but also lower than the stability of the ligand. The sample of this compound did not contain any solvent and began to decompose at 221 °C, onset. Similarly to **1**, only one decomposition step was observed with a mass loss of 32.1 % and a DTG maximum at 242 °C. At higher temperatures, the decomposition processes are completely overlapped with a low intensity DTG peak at 475 °C.

The high thermal stability of the ligand and lower stabilities of the complexes show that coordination decreases the stability of the ligand. As the cation is the same in both complexes, their different thermal stabilities (comparing **1** after water loss) can be attributed to their counterions.

Complex **1** has the bulky tetracyclic $[\text{Cu}_2\text{Br}_4]^{2-}$ anion, as opposed to $[\text{CuL}_2]\text{Br}_2$, which possesses only two bromide ions, resulting in a significantly smaller counterion volume. Due to the voluminous complex anion, the packing of **1** is less compact than that of $[\text{CuL}_2]\text{Br}_2$. Therefore, the empty space in the crystal lattice of **1** is larger and water molecules are capable of occupying it.

The heat flow curves of the compounds (Fig. S-3 of the Supplementary material) show the same tendency. Namely, the solvent loss of **1** was endothermic. After that, the beginning of its thermal decomposition was also endothermic with a small peak at 220 °C, which almost immediately turned exothermic (233 °C). Above 300 °C, the decomposition was followed by an exothermic heat effect. Only slight differences were observed on the heat flow curve of $[\text{CuL}_2]\text{Br}_2$. Its decomposition also started with a small endothermic peak at 231 °C, followed by an

intensive exothermic one at 250 °C. The thermal decomposition processes above 300 °C were mostly exothermic (peak maxima at 441 and 479 °C) with a small endothermic peak at 471 °C.

CONCLUSIONS

The molecular structure of **L** revealed that the ligand adopts a conformation quite common to those of structurally related compounds. An assessment of the energetics of the intermolecular interactions in the crystal structure by computational methods revealed that dispersion interactions are dominant. The basic structural unit of the crystal packing is the herring-bone type arrangement of **L** molecules.

The composition of the obtained complexes depended not only on the CuBr₂ to **L** mole ratio, but also on the nature of the reaction solvent involved. In the complex cation of **1**, the ligand is coordinated as a tridentate N₃, and two ligand molecules are meridionally arranged in a very distorted octahedral environment around the Cu(II) ion. In [Cu₂Br₄]²⁻, bromides are arranged in a trigonal-planar geometry around each copper(I) atom; with two bromides in a bridging mode, forming a four-membered metallacycle.

The relatively high thermal stability of the ligand decreases on coordination to the Cu^{II} ion. As the cation is identical in both complexes, the difference in their thermal stability could be ascribed to the anions present. Due to the bulky [Cu₂Br₄]²⁻ anion, the packing of **1** is less compact than that of [CuL₂]Br₂.

SUPPLEMENTARY MATERIAL

Additional data and information are available electronically at the pages of journal website: <https://www.shd-pub.org.rs/index.php/JSCS/article/view/11422>, or from the corresponding author on request.

Acknowledgments. The authors acknowledge the financial support of the Ministry of Education, Science, and Technological Development of the Republic of Serbia, & Austrian Federal Ministry of Education, Science and Research (Project No. 451-03-02141/2017-09/14; WTZ project No. SRB 14/2018); The Ministry of Education, Science and Technological Development of the Republic of Serbia (Grant No. 451-03-9/2021-14/ 200125).

ИЗВОД

РЕАКЦИЈЕ БАКАР(II)-БРОМИДА СА БИС(ФЕНИЛХИДРАЗОНОМ)
2,6-ДИАЦЕТИЛПИРИДИНА (**L**) – МОЛЕКУЛСКА И КРИСТАЛНА СТРУКТУРА
L И ЊЕГОВОГ МЕШОВИТО-ВАЛЕНТНОГ КОМПЛЕКСА [Cu^{II}L₂][Cu^I₂Br₄]

МАРКО В. РОДИЋ¹, МИРЈАНА М. РАДАНОВИЋ¹, ДРАГАНА В. ГАЗДИЋ¹, ВУКАДИН М. ЛЕОВАЦ¹,
БЕРТА БАРТА ХОЛО¹, ВИДАК РАИЧЕВИЋ¹, СВЕТЛАНА К. БЕЛОШЕВИЋ², БИЉАНА КРИГЕР³
и ЛИЉАНА С. ВОЛИНОВИЋ-ЈЕШИЋ¹

¹Универзитет у Новом Саду, Природно-математички факултет, Трг Д. Обрадовића 3, 21000
Нови Сад, ²Факултет техничких наука, Универзитет у Приштини, Књаза Милоша 7, 38220
Косовска Митровица и ³University of Innsbruck, Institute of Mineralogy and Petrography,
Innrain 52, 6020 Innsbruck, Austria

Кристална и молекулска структура бис(фенилхидразона) 2,6-диацетилпирдина, **L**, одређене су рентгенском структурном анализом. Енергије интермолекулских интеракција

у кристалној структури су процењене рачунарским методама и имају доминантно дисперзиони карактер. Основна структурна јединица кристалног паковања настаје слагањем молекула **L** у мотив облика рибље кости. Асигнација IR спектра **L** је извршена помоћу DFT прорачуна. У раду су описане нове реакције **L** са CuBr₂ у којима настаје валентномешовити Cu(II)-Cu(I) комплекс формуле [Cu^{II}L₂][Cu^I₂Br₄] (**1**), који је структурно окарактерисан. У комплексном катјону су два молекула лиганда меридијално распоређена око Cu(II), градећи веома деформисано октаедарско окружење. У анјону су бромидни јони распоређени тригонално-планарно око јона Cu(I). Описана су термичка својства лиганда, комплекса **1** и претходно синтетисаног комплекса [CuL₂]Br₂. Термичка стабилност комплекса је низка од термичке стабилности лиганда: **L** (250 °C) > [CuL₂]Br₂ (221 °C) > > [Cu^{II}L₂][Cu^I₂Br₄] (212 °C). Разлика у термичкој стабилности комплекса може да се припише различитој ефикасности паковања јона у кристалним структурама.

(Примљено 27. новембра, ревидирано 14. децембра, прихваћено 20. децембра 2021)

REFERENCES

1. D. G. Guimarães, L. A. Rolim, A. de A. Gonsalves, C. R. M. Araújo, *Rev. Virtual Química* **9** (2017) 2551 (<https://dx.doi.org/10.21577/1984-6835.20170151>)
2. C. Bonaccorso, T. Marzo, D. La Mendola, *Pharmaceuticals* **13** (2020) (<https://dx.doi.org/10.3390/ph13010004>)
3. S. Rollas, S. Küçükgüzel, S. Rollas, S. G. Küçükgüzel, *Molecules* **12** (2007) 1910 (<https://dx.doi.org/10.3390/12081910>)
4. M. M. E. Shakdofa, M. H. Shtaiwi, N. Morsy, T. M. A. Abdel-rassel, *Main Gr. Chem.* **13** (2014) 187 (<https://dx.doi.org/10.3233/MGC-140133>)
5. A.-M. Stadler, J. Harrowfield, *Inorg. Chim. Acta* **362** (2009) 4298 (<https://dx.doi.org/10.1016/j.ica.2009.05.062>)
6. M. Katyal, Y. Dutt, *Talanta* **22** (1975) 151 ([https://dx.doi.org/10.1016/0039-9140\(75\)80161-5](https://dx.doi.org/10.1016/0039-9140(75)80161-5))
7. Y. P. Kitaev, *Khimiya gidrazonov*, Nauka, Moscow, 1977
8. Y. P. Kitaev, B. I. Buzykin, *Gidrazony*, Nauka, Moscow, 1974
9. I. D. Kostas, B. R. Steele, *Catalysts* **10** (2020) art. no. 1107 (<https://dx.doi.org/10.3390/catal10101107>)
10. V. V. Kogan, V.A., Zelentsov, V.V., Larin, G. M., Lukov, *Kompleksy perekhodnykh metallov s gidrazonami*, Nauka, Moscow, 1990
11. J. D. Curry, M. A. Robinson, D. H. Busch, *Inorg. Chem.* **6** (1967) 1570 (<https://dx.doi.org/10.1021/ic50054a032>)
12. I. Ivanović-Burmazović, K. Andđelković, in *Advances in Inorganic Chemistry*, R. van Eldik, Ed., Academic Press, Cambridge, MA, 2004, p. 315 ([https://dx.doi.org/10.1016/S0898-8838\(03\)55006-1](https://dx.doi.org/10.1016/S0898-8838(03)55006-1))
13. C. A. Brown, W. Kaminsky, K. A. Claborn, K. I. Goldberg, D. X. West, *J. Braz. Chem. Soc.* **13** (2002) 10 (<https://dx.doi.org/10.1590/S0103-50532002000100003>)
14. T. S. Lobana, R. Sharma, G. Bawa, S. Khanna, *Coord. Chem. Rev.* **253** (2009) 977 (<https://dx.doi.org/10.1016/J.CCR.2008.07.004>)
15. S. Belošević, M. Rodić, M. Radanović, V. Leovac, *Univ. Thought - Publ. Nat. Sci.* **8** (2018) 33 (<https://dx.doi.org/10.5937/UNIVTHO8-19451>)
16. S. Belošević, M. M. Radanović, M. V. Rodić, V. M. Leovac, *Bull. Nat. Sci. Res.* **11** (2021) 24 (<https://dx.doi.org/10.5937/BNSR11-30567>)
17. Rigaku Oxford Diffraction, *CrysAlisPro Software system*, Rigaku Corporation, Wroclaw, 2021

18. G. M. Sheldrick, *Acta Crystallogr., A* **71** (2015) 3 (<https://dx.doi.org/10.1107/S2053273314026370>)
19. G. M. Sheldrick, *Acta Crystallogr., C* **71** (2015) 3 (<https://dx.doi.org/10.1107/S2053229614024218>)
20. C. B. Hübschle, G. M. Sheldrick, B. Dittrich, *J. Appl. Crystallogr.* **44** (2011) 1281 (<https://dx.doi.org/10.1107/S0021889811043202>)
21. P. R. Spackman, M. J. Turner, J. J. McKinnon, S. K. Wolff, D. J. Grimwood, D. Jayatilaka, M. A. Spackman, *J. Appl. Crystallogr.* **54** (2021) 1006 (<https://dx.doi.org/10.1107/S1600576721002910>)
22. C. F. Mackenzie, P. R. Spackman, D. Jayatilaka, M. A. Spackman, *IUCrJ* **4** (2017) 575 (<https://dx.doi.org/10.1107/S205225251700848X>)
23. D. Jayatilaka, D. J. Grimwood, in *Proceeding of International Conference on Computational Science*, 2003, Melbourne, Australia and St. Petersburg, Russia, 2003 Proceedings, Part IV, Springer, 2003, p. 142 (https://dx.doi.org/10.1007/3-540-44864-0_15)
24. G. M. J. Barca, C. Bertoni, L. Carrington, D. Datta, N. De Silva, J. E. Deustua, D. G. Fedorov, J. R. Gour, A. O. Gumina, E. Guidez, T. Harville, S. Irle, J. Ivanic, K. Kowalski, S. S. Leang, H. Li, W. Li, J.J. Lutz, I. Magoulas, J. Mato, V. Mironov, H. Nakata, B.Q. Pham, P. Piecuch, D. Poole, S.R. Pruitt, A.P. Rendell, L.B. Roskop, K. Ruedenberg, T. Sattasathuchana, M.W. Schmidt, J. Shen, L. Slipchenko, M. Sosonkina, V. Sundriyal, A. Tiwari, J.L. Galvez Vallejo, B. Westheimer, M. Włoch, P. Xu, F. Zahariev, M.S. Gordon, *J. Chem. Phys.* **152** (2020) 154102 (<https://dx.doi.org/10.1063/5.0005188>)
25. B. M. Bode, M. S. Gordon, *J. Mol. Graph. Model.* **16** (1998) 133 ([https://dx.doi.org/10.1016/s1093-3263\(99\)00002-9](https://dx.doi.org/10.1016/s1093-3263(99)00002-9))
26. W. J. Geary, *Coord. Chem. Rev.* **7** (1971) 81 ([https://dx.doi.org/10.1016/S0010-8545\(00\)80009-0](https://dx.doi.org/10.1016/S0010-8545(00)80009-0))
27. L. S. Vojinović-Ješić, M. M. Radanović, *Coordination chemistry of aminoguanidine and its Schiff bases*, Faculty of Sciences, Novi Sad, 2017 (in Serbian)
28. H. Günzler, H.-U. Gremlich, *IR-Spektroskopie: Eine Einführung*, Fourth Edition, John Wiley & Sons, Ltd., Weinheim, 2003, pp. 157–264 (<https://dx.doi.org/10.1002/9783527662852.ch6>)
29. K. Nakamoto, *Infrared and Raman Spectra of Inorganic and Coordination Compounds*, John Wiley & Sons, Inc., Hoboken, NJ, 2008
30. C. R. Groom, I. J. Bruno, M. P. Lightfoot, S. C. Ward, *Acta Crystallogr., B* **72** (2016) 171 (<https://dx.doi.org/10.1107/S2052520616003954>)
31. W. Clegg, R. W. Harrington, *CSD Commun.*, Database Identifier KEWWOB, Deposition Number 1836923 (2018) (<https://dx.doi.org/10.5517/ccdc.csd.cc1znqlp>)
32. W. Radecka-Paryzek, M. Kubicki, E. Luks, *Struct. Chem.* **21** (2010) 299 (<https://dx.doi.org/10.1007/s11224-009-9532-y>)
33. C. Jelsch, K. Ejsmont, L. Huder, *IUCrJ* **1** (2014) 119 (<https://dx.doi.org/10.1107/S2052252514003327>)
34. F. Dumitru, Y.-M. Legrand, M. Barboiu, E. Petit, A. van der Lee, *Cryst. Growth Des.* **9** (2009) 2917 (<https://dx.doi.org/10.1021/cg9002466>).

SUPPLEMENTARY MATERIAL TO

Reactions of copper(II) bromide with 2,6-diacetylpyridine bis(phenylhydrazone) (L**) – Molecular and crystal structures of **L** and its mixed-valence complex $[Cu^{II}L_2][Cu^I_2Br_4]$**

MARKO V. RODIĆ^{1*}, MIRJANA M. RADANOVIĆ¹, DRAGANA V. GAZDIĆ¹,
VUKADIN M. LEOVAC¹, BERTA BARTA HOLLÓ¹, VIDAK RAIČEVIĆ¹,
SVETLANA K. BELOŠEVIĆ², BILJANA KRÜGER³
and LJILJANA S. VOJINOVIC-JEŠIĆ¹

¹University of Novi Sad, Faculty of Sciences, Trg Dositeja Obradovića 3, 21000 Novi Sad, Serbia,

²Faculty of Technical Sciences, University of Priština, Knjaza Miloša 7, 38220 Kosovska Mitrovica, Serbia and ³University of Innsbruck, Institute of Mineralogy and Petrography, Innrain 52, 6020 Innsbruck, Austria

J. Serb. Chem. Soc. 87 (3) (2022) 307–320

2,6-diacetylpyridine-bis(phenylhydrazone) (L**)**

Selected IR bands [wavenumber, cm^{-1}]: 3442(w), 1602(vs), 1563(s), 1508(s), 1491(m), 1454(s), 1435(s), 1363(m), 1329(w), 1293(w), 1247(s), 1165(s), 1141(m), 1090(w), 842(m), 815(m), 755(m), 748(s), 694(m). $^1\text{H-NMR}$ [DMSO- d_6 , δ / ppm]: 9.51 (2H, s, NH), 8.01 (2H, d, $J = 7.8$ Hz, H-2, H-4), 7.76 (1H, dd, $J = 7.8$ Hz, J = 7.8 Hz, H-3), 7.32 (4H, ddd, $^3J = 8.0$ Hz, $^3J = 1.0$ Hz, $^4J = 0.8$ Hz, H-11, H-15, H-17, H-21), 7.26 (4H, ddd, $^3J = 8.0$ Hz, $^3J = 7.2$ Hz, $^4J = 1.5$ Hz, H-12, H-14, H-18, H-20), 6.81 (2H, dddd, $^3J = 7.2$ Hz, $^4J = 1.3$ Hz, H-13, H-19), 2.44 (6H, s, CH_3). $^{13}\text{C-NMR}$ [DMSO- d_6 , δ / ppm]: 155.4 (C-1, C-5), 146.1 (C-10, C-16), 142.0 (C-6, C-8), 136.7 (C-3), 129.4 (C-12, C-14, C-18, C-20), 119.8 (C-13, C-19), 117.9 (C-2, C-4), 113.5 (C-11, C-15, C-17, C-21), 11.7 (C-7, C-9).

$[Cu^{II}L_2][Cu^I_2Br_4]$ (I**)**

Anal. Calc. for the black prismatic single crystals of $\text{C}_{42}\text{H}_{42}\text{Br}_4\text{Cu}_3\text{N}_{10}$: C, 42.14; H, 3.48; N, 11.70. Found: C, 42.34; H, 3.53; N, 11.59 %. Conductivity in DMF, $\Lambda = 134 \text{ S cm}^2 \text{ mol}^{-1}$. Selected IR bands [$\tilde{\nu}$ / cm^{-1}]: 3446(w), 3272(m), 1597(vs), 1518(m), 1494(s), 1435(m), 1262(s), 1170(m), 750(m), 693(m).

$[Cu^{II}L_2][Cu^I_2Br_4]$ (I**) (from MeOH solution)**

Anal. Calc. for $\text{C}_{42}\text{H}_{42}\text{Br}_4\text{Cu}_3\text{N}_{10}$: C, 42.14; H, 3.48; N, 11.70 %. Found: C, 42.47; H, 3.29; N, 11.64 %. Selected IR bands [$\tilde{\nu}$ / cm^{-1}]: 3446(w), 3272(m), 1597(vs), 1517(m), 1494(s), 1435(m), 1262(s), 1170(m), 751(m), 693(m).

*Corresponding author. E-mail: marko.rodic@dh.uns.ac.rs

TABLE S-I. Crystallographic and refinement details

Crystal data	L	[Cu ^{II} L ₂][Cu ^I ₂ Br ₄] (1)
Chemical formula	C ₂₁ H ₂₁ N ₅	C ₄₂ H ₄₂ Br ₄ Cu ₃ N ₁₀
M _r	466.05	1197.11
Crystal system	Orthorhombic	Orthorhombic
Space group	P2 ₁ 2 ₁ 2 ₁	Pbca
Temperature, K	170	170
a / Å	5.3545(2)	21.9263(19)
b / Å	17.3224(6)	16.8642(10)
c / Å	19.3856(7)	23.8799(18)
V / Å ³	1798.07(11)	8830.1(11)
Z	4	8
Radiation type	Cu K α	Mo K α
Radiation wavelength	1.54184	0.71073
μ / mm ⁻¹	0.615	5.10
Crystal size, mm	0.62 × 0.24 × 0.11	0.49 × 0.35 × 0.14
 Data collection		
Absorption correction	Multiscan	Gaussian
T _{min} , T _{max}	0.651, 1	0.258, 0.773
Measured reflections	8671	50087
Independent reflections	3205	9054
Observed [I > 2σ(I)] reflections	2960	5901
R _{int}	0.058	0.081
(sin θ/λ) _{max} / Å ⁻¹	0.600	0.627
 Refinement		
R[F ² > 2σ(F ²)]	0.045	0.042
wR(F ²)	0.107	0.072
S	1.13	1.01
No. of reflections	3205	9054
No. of parameters	246	536
No. of restraints	0	0
H-atom treatment	Mixed	Constrained
Δρ _{max} , Δρ _{min} , e Å ⁻³	0.20, -0.29	0.71, -0.85
Flack x	0.2(2)	N.A.

TABLE S-II. Decomposition of the Hirshfeld surface of **L** into specific atom–atom contacts, expressed as a percentage of the Hirshfeld surface occupied by such contacts, and calculated enrichment ratios

Observed contact surface area ratio, %			
Inside Atom	Outside Atom		
	C	N	H
C	0.1	0.1	21.1
N	0.1	0.0	7.1
H	14.6	6.1	50.8

Enrichment ratios			
Inside Atom	Outside Atom		
	C	N	H
C	<0.01		
N	0.08	/	
H	1.31	1.31	0.90

Enrichment ratios were not listed when the ‘random contacts’ were lower than 0.9%, as they are not meaningful (/ written instead).

TABLE S-III. Hydrogen-bond parameters of $[\text{Cu}^{\text{II}}\text{L}_2][\text{Cu}^{\text{I}}_2\text{Br}_4]$ (**1**)

D–H···A	$d(\text{D–H}) / \text{\AA}$	$d(\text{H}\cdots\text{A}) / \text{\AA}$	$d(\text{D}\cdots\text{A}) / \text{\AA}$	$\angle(\text{D–H}\cdots\text{A}) / {}^\circ$	Symmetry operation on A
N3A–H3A···Br2	0.88	3.01	3.632(4)	129.4	$-\text{x}+\frac{1}{2}, -\text{y}+1, \text{z}+\frac{1}{2}$
N3A–H3A···Br4	0.88	3.05	3.735(4)	136.7	$-\text{x}+\frac{1}{2}, -\text{y}+1, \text{z}+\frac{1}{2}$
N3B–H3B···Br1	0.88	2.84	3.479(4)	130.6	
N3B–H3B···Br3	0.88	3.10	3.749(4)	132.3	
N5A–H5A···Br3	0.88	2.89	3.659(4)	147.5	
N5B–H5B···Br4	0.88	2.93	3.645(4)	139.7	$-\text{x}+\frac{1}{2}, -\text{y}+1, \text{z}+\frac{1}{2}$

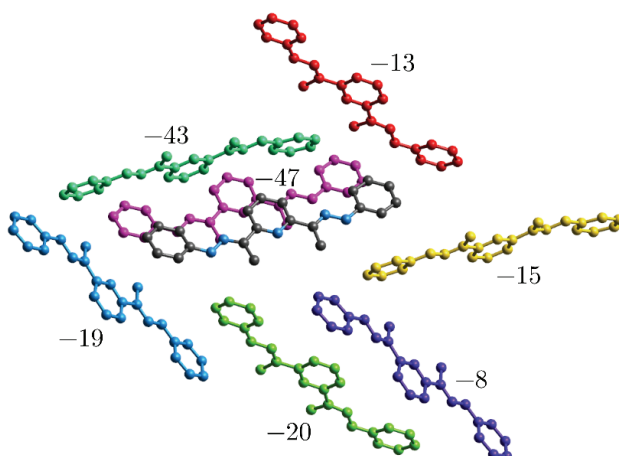


Fig. S-1. Arrangement of molecules and their interaction energies in kJ mol^{-1} . For clarity, only one of two molecular pairs is displayed for every unique interaction. The central molecule is color-coded by element-type, while partner molecules are decorated with different colors.

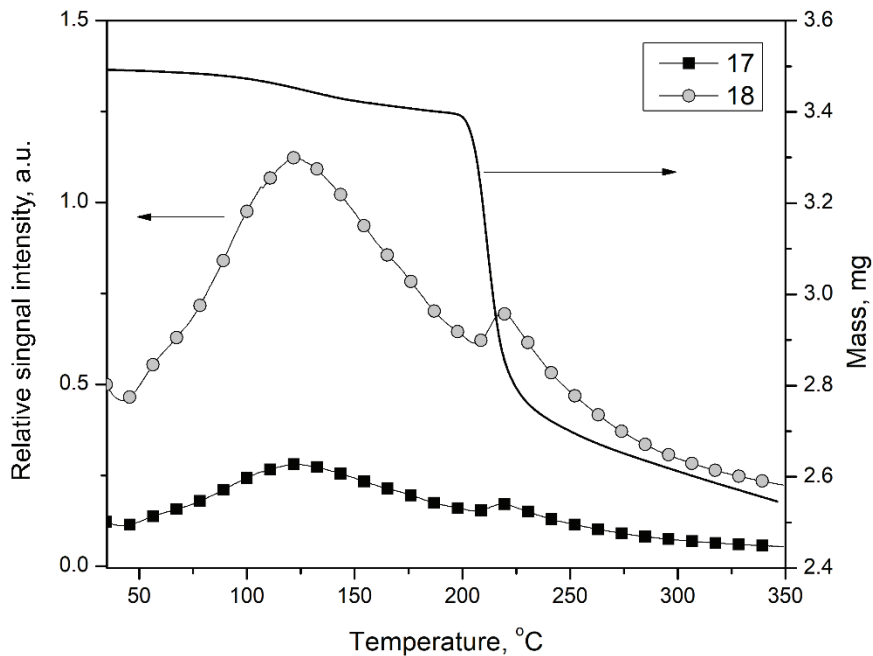


Fig. S-2. TG and MS curves of $[\text{Cu}^{\text{II}}\text{L}_2]\text{[Cu}^{\text{I}}_2\text{Br}_4]$ for signals $m/z = 17$ and 18 in argon.

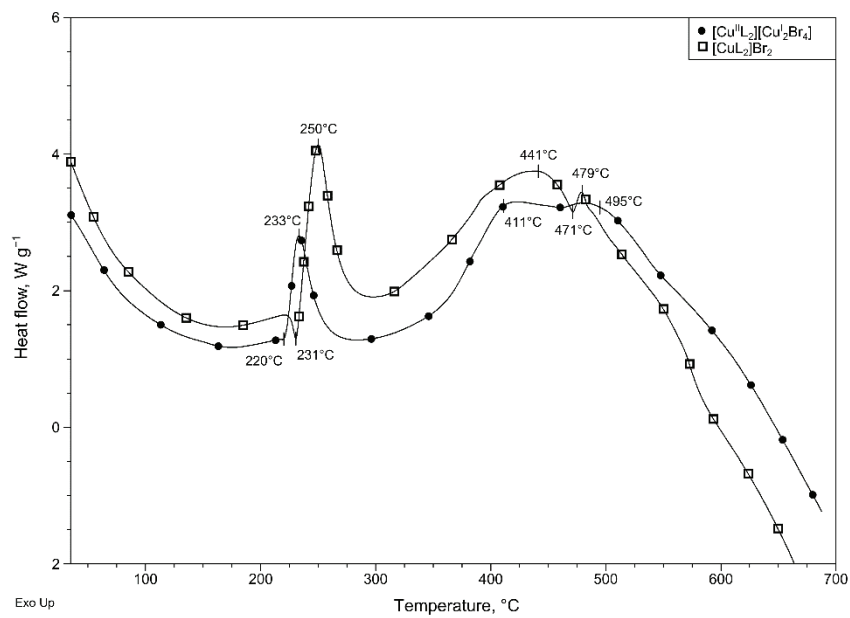
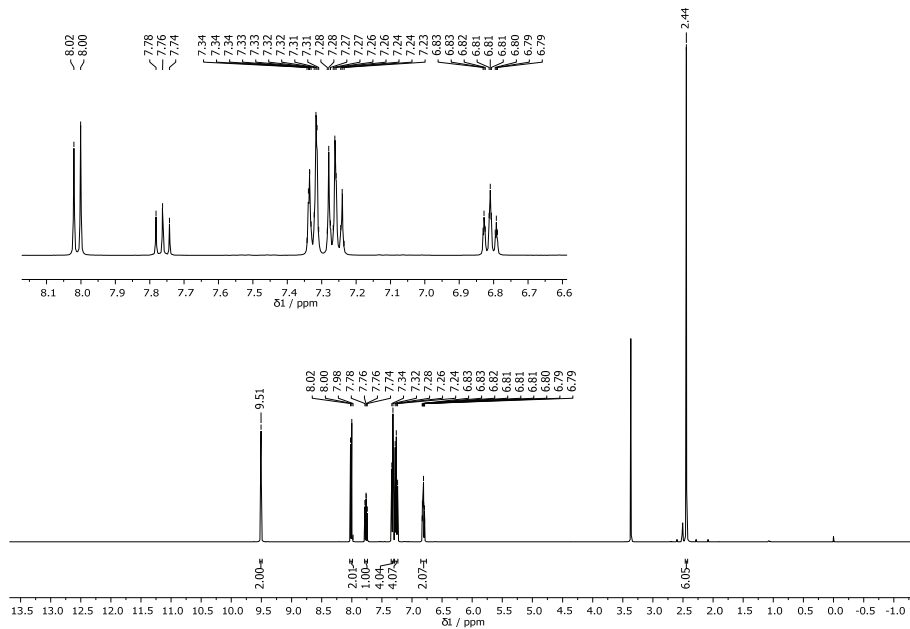
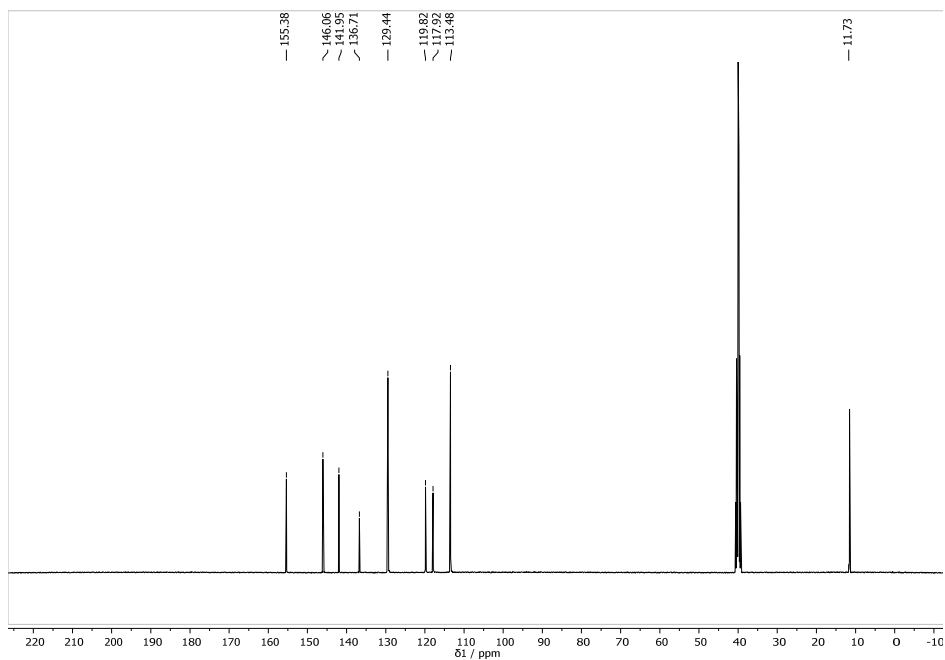


Fig. S-3. DSC curve of $[\text{Cu}^{\text{II}}\text{L}_2]\text{[Cu}^{\text{I}}_2\text{Br}_4]$ and $[\text{CuL}_2]\text{Br}_2$ in nitrogen.

Fig. S-4. ^1H -NMR spectrum of **L**.Fig. S-5. ^{13}C -NMR spectrum of **L**.

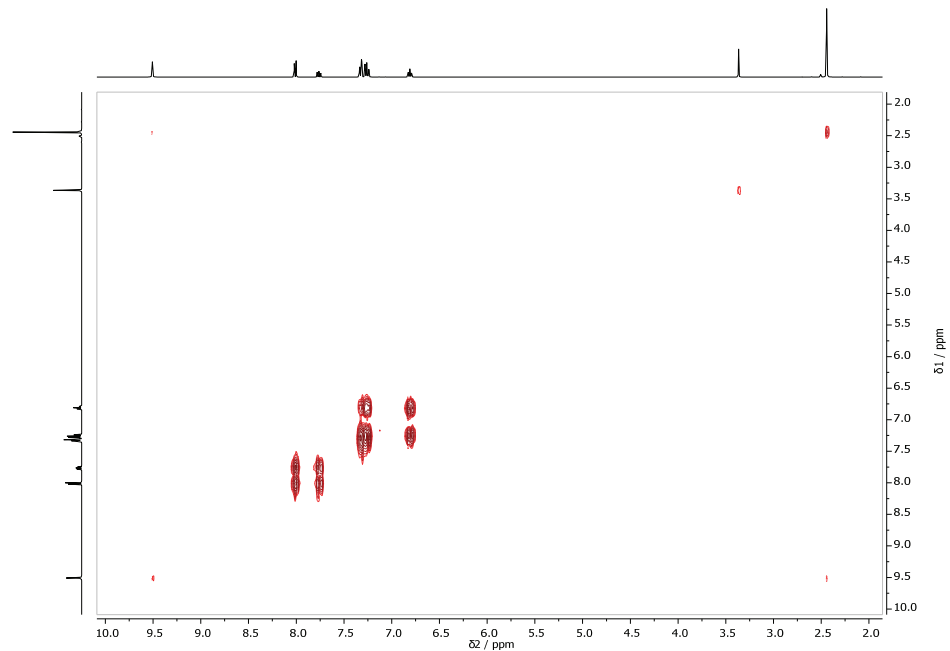
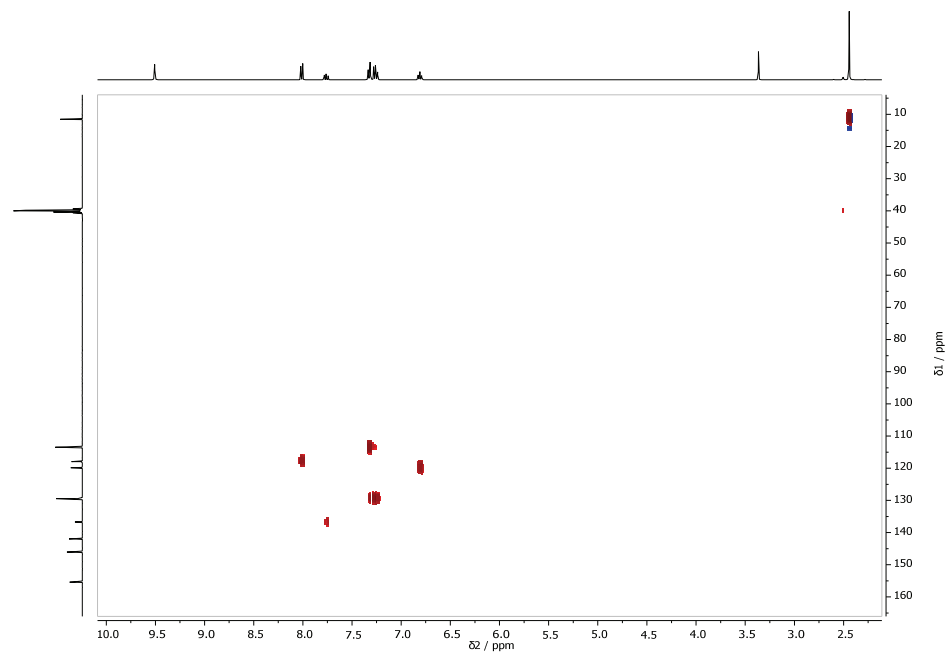
Fig. S-6. Gradient ^1H - ^1H COSY NMR spectrum of L.

Fig. S-7. HSQC NMR spectrum of L.

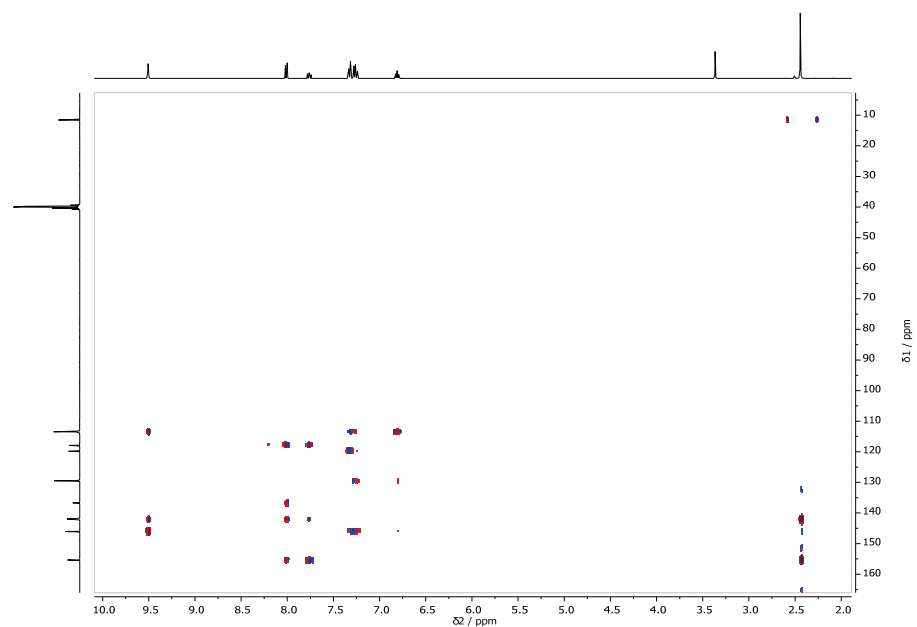


Fig. S-8. ¹HMBC NMR spectrum of **L**.



Large-scale comparison between the diffraction-component precision indexes favors Cruickshank's R_{free} function

SORIN AVRAM* and CRISTIAN NEANU**

Department of Computational Chemistry, "Coriolan Dragulescu" Institute of Chemistry,
Timișoara, Romania

(Received 18 May, revised 31 August, accepted 25 September 2021)

Abstract: This study aims to provide a first large-scale comparison between the various diffraction-component precision index (*DPI*) equations, assess the applicability of the parameter, and make recommendations on *DPI* computation. The *DPI* estimates the average accuracy of the atomic coordinates obtained by the structural refinement of protein diffraction data, with application in crystallography and cheminformatics. Although, Cruickshank and Blow proposed *DPI* equations based on R and R_{free} in order to calculate *DPI* values, which remain scarcely employed in the quality assessment of the Protein Data Base (PDB) files, due to the unclear data extraction protocols (to assign variables), the complex equations, the lack of extensive applicability studies and the limited access to automated computations. In order to address these shortcomings, the entire RCSB PDB database was evaluated using Cruickshank's and Blow's R and R_{free} *DPI* variations. Computations of 143070 X-ray structures indicate that R_{free} -based *DPI* equations apply to 30 % more protein structures compared to R -based *DPI* equations, with Cruickshank R_{free} -based *DPI* (CRF) exceeding the number of successful Blow's R_{free} -based *DPI* (BRF) computations. Although our results indicate that, in general, the resolutions $< 2 \text{ \AA}$ assure consistency among the various *DPIs* computations (differences $< 0.05 \text{ \AA}$), we recommend the use of CRF *DPI* because of its wider applicability.

Keywords: cheminformatics; drug discovery; protein structure; docking; crystallography.

INTRODUCTION

Cheminformatics has become an indispensable component of modern drug discovery.¹ Three-dimensional protein structures (or ligand-protein complexes) serve as the primary input for the structure-based methods, such as ligand

*•** Correspondence E-mail: (*)sorin.avram@acad-icht.tn.edu.ro;
(**)cristian.neanu@gmail.com
<https://doi.org/10.2298/JSC200518076A>

docking, pharmacophore, and ligand design methods.^{1,2} Different types of the PDB data mining analysis have been performed in the past, for example, to facilitate modelling of the synthetic protein structures with desired properties,³ to study the cation-pi interactions in proteins,⁴ etc. Additionally, protein-target homology modelling, molecular dynamics, and molecular mechanics simulations are state-of-the-art tools to build protein models, simulate and evaluate the conformational space of proteins, and ultimately detect and understand protein mechanisms and protein-protein and protein-ligand interactions.²

Beyond the limitations concerning the algorithms, the output of structure-based computational methods is a subject to the quality of the crystallographic protein structures, *i.e.*, the quality of the models fitting the experimental diffraction data.⁵ The deposition of a new macromolecular structure in RCSB PDB (<https://www.rcsb.org/>)^{6,7} is accompanied by multiple indicators describing experimental results and model validation (<https://www.wwpdb.org/>),^{8–10} but lack the unanimous definitions for high-quality structures.¹¹ With more than 166 thousand macromolecular structures, the PDB database is among the most commonly employed digital resources for protein structures, impacting multiple scientific disciplines, *e.g.*, materials sciences, physics, computer science, chemistry, engineering, and mathematics.¹²

The essential indicators to assess the suitability of crystallographic biomolecules for structure-based methods were extensively reviewed by Warren *et al.*⁵ The authors observed that PDB entry selection is often reasoned by the resolution of the X-ray crystal structure, a measure of data (electron density) quantity, misleadingly used as a measure of data quality. Additionally, model quality can be calculated using *R*-factors (*R* or *R*_{free})¹³ measuring the difference between measured data and data predicted from the model.⁵ Warren *et al.*⁵ pointed towards the diffraction-component precision index,¹⁴ as a global criterion to computational outputs (such as protein-ligand docking).⁵ Depending on the availability of input parameters, Cruickshank proposed an *R*- and *R*_{free}-based version of *DPI*.¹⁴ To make *DPI* computation more accessible, a few years later, Blow¹⁵ rearranged Cruickshank's formulas in a simplified version (*vide infra*). assess both model and data quality.

The diffraction-component precision index (*DPI*), developed by Cruickshank,¹⁴ estimates the coordinate error of atoms in protein crystal structures, providing means to select highly precise data, as well as to determine the accuracy limit of them.

Several studies have underlined the importance of *DPI* in the evaluation of the quality of PDB structures supplied to computational approaches,^{5,16–21} but *DPI* continues to be scarcely employed, due to the unclear data extraction protocols (to assign variables), the complex equations, the lack of extensive applicability studies, and the limited access to automated computations. To date,

we identified only the free online resources offered by K. Sekar's laboratory facilitating the computation of Cruickshank *DPI*.¹⁹ Moreover, to our knowledge, no comparative studies on large numbers of PDB files between Cruickshank and Blow *DPI* equations (for *R* and *R*_{free}) were reported in the literature.

This study aims to provide a first large-scale comparison between the various *DPI* equations, assess the applicability of the parameter, and make recommendations on *DPI* computation.

EXPERIMENTAL

PDB data and variables

The entire RCSB PDB database was downloaded (159678 PDB files; accessed on Jan 28, 2020) and 143070 X-ray structures were retained (NMR and 3D electron microscopy-based determined structures were discarded). The PDB files were used to extract (and compute) the variables in Table I.

TABLE I. Variables extracted from Protein Data Base (PDB) files employed for diffraction-component precision index (*DPI*) calculations.

Name ^a	Description	Observations
<i>N</i> _i	Number of occupied atoms	Count of non-hydrogen atoms with occupancy of 1.0 (from ATOM and HETATM)
<i>N</i> _{prot}	Number of protein atoms	Count of non-hydrogen protein atoms in the PDB file (from ATOM) from REMARK 3
<i>n</i> _{obs}	Number of observations/reflections	
<i>q</i>	Number of parameters to be refined for each non-H	For fully anisotropic refinement <i>q</i> = 9 For isotropic refinement, <i>q</i> = 4 ¹⁴
<i>p</i>	Number of free parameters	<i>p</i> = <i>n</i> _{obs} - <i>n</i> _{param} ¹⁴
<i>n</i> _{param}	Number of parameters to be refined	<i>n</i> _{param} = <i>N</i> _i <i>q</i> ¹⁵
<i>C</i> / %	Completeness	from REMARK 3
<i>R</i> / %	The normalized linear residual between observed and calculated structure factor amplitudes	Protein atomic model refinement <i>R</i> factor (from REMARK 3)
<i>R</i> _{free} / %	Cross-validation <i>R</i> value (<i>R</i> value calculated for the cross-validation data excluded from refinement) ¹³	Protein atomic model refinement <i>R</i> _{free} factor (from REMARK 3)
<i>V</i> / Å ³	Crystal asymmetric unit volume	i. <i>V</i> = <i>V</i> _M 14.12 <i>N</i> _{prot} , ¹⁵ <i>V</i> _M is Matthews coefficient (from REMARK 280) ii. volume of the asymmetric unit computed from the crystal unit description iii. (from CRYST1) from REMARK 2 or REMARK 3: RESOLUTION RANGE HIGH
<i>d</i> _{min} / Å	Resolution	

^aA list of variables, extracted (and computed) from PDB files, to calculate *DPI* values is displayed

DPI computations

Based on the parameters described in Table I, the *DPI* was computed according to the Cruickshank and Blow equations as described in Table II.

TABLE II. Diffraction-component precision index (*DPI*) equations computed using the variables described in Table I; *CR*: *DPI* computed with *R*-based *DPI* Cruickshank formula, *CRF*: *DPI* computed with *R_{free}*-based *DPI* Cruickshank formula, *BR*: *DPI* computed with *R*-based *DPI* Blow formula; *BRF*: *DPI* computed with *R_{free}*-based *DPI* Blow formula (see Table I for variable definitions)

<i>DPI</i> Equation ^a		Ref.
$CR = \left(\frac{N_i}{p} \right)^{-1/2} C^{-1/3} R d_{\min}$	(1)	14
$CRF = \left(\frac{N_i}{n_{\text{obs}}} \right)^{-1/2} C^{-1/3} R_{\text{free}} d_{\min}$	(2)	14
$BR = 1.28 N_i^{1/2} \left(1 - \frac{q N_i}{n_{\text{obs}}} \right)^{-1/2} V^{1/3} n_{\text{obs}}^{-5/6} R$	(3)	15
$BRF = 128 N_i^{1/2} V^{-1/3} n_{\text{obs}}^{-5/8} R_{\text{free}}$	(4)	15

For proteins containing several unique protein chains (*e.g.*, 5DIS – 4 unique protein chains: A, B, C, D) we have taken in to account and processed only the data from the “A” chain.

Therefore, in order to calculate the Blow-*DPI* (Eqs. (3) and (4)), the crystal volume for all proteins was evaluated by processing the number of atoms from the “A” chain.

Following Gurusaran’s *et al.* suggestion,²⁰ we retained 120594 structures which met the following 2 criteria: completeness $C > 75\%$ and the percentage of fully occupied atoms in the protein structure $> 90\%$.

RESULTS AND DISCUSSION

Comparative analysis of DPI computations

The results indicate that for 120484 PDB IDs (*i.e.*, 84 % of the number of X-ray entries available), at least one *DPI* value was calculated according to the equations in Table II using the parameters extracted from the PDB files as described in Table I. In the case of 87451 entries (*i.e.*, 62 % of the number of X-ray structures) the *DPI* values were successfully determined by all four equations. Following Gurusaran *et al.*,²⁰ we focused on *DPI* values $< 1 \text{ \AA}$, which we considered a reasonable cutoff for the analysis of relevant *DPI* computations. Thereby, 3338 entries (2.8 %) with *DPI* values $> 1 \text{ \AA}$, obtained through either of the equations, were discarded.

R_{free}-based *DPIs* showed larger applicability (117562 PDB entries) compared to *R*-based *DPIs* (88620 PDB entries). The distribution of the values followed very similar trends with 90 % showing *DPI* values $< 0.5 \text{ \AA}$. Cruickshank *DPIs* indicated median values of 1.7 \AA , similar to Blow *DPIs* (1.6 \AA), as it can be seen in Fig. 1A.

Further, the pairwise correlation between *DPI* computations at *DPI* cutoffs ranging stepwise from < 1 to $< 0.1 \text{ \AA}$ (Fig. 1B) were calculated. Very strong correlations (Pearson > 0.97) were found in (*CR*, *BR*) pairs as well as (*CRF*, *BRF*) pairs independent of the *DPI* cutoffs. Contrary to that, the *R*-based and *R_{free}*-based *DPI* outputs coincided more at smaller *DPI* values (Fig. 1B), e.g., the correlation of (*CR*, *CRF*) and (*BR*, *BRF*) pairs increased from 0.85 for *DPI* values $< 1 \text{ \AA}$, to 0.96 \AA at *DPI* values $< 0.1 \text{ \AA}$. These results suggested that, in general, either Cruikshank or Blow equations should be used, and differences between *R* and *R_{free}* *DPIs* values are more likely to be encountered at lower *DPI* values.

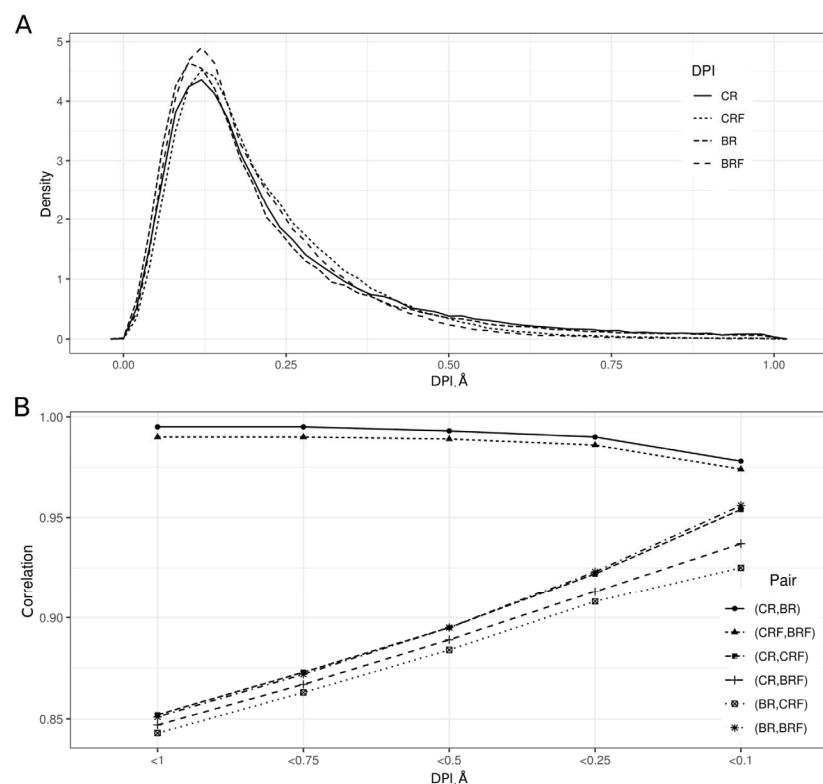


Fig. 1. A) Distribution of *DPI* values computed by 4 equations. B) Pairwise correlation between *DPI* computations at *DPI* cutoffs ranging stepwise from 1 to $< 0.1 \text{ \AA}$.

The *R_{free}* equations were calculated for $\sim 30\%$ more protein structures compared to *R*-based *DPI*, a significant advantage. Surprisingly, more proteins (2685 PDB structures) allowed *CRF* calculations compared to *BRF*. Although this difference is small, it was expected that Blow's equation would be more applicable due to fewer input variables, commonly contained in the header of a PDB file.¹⁶

In the next sections, it was aimed to find the source of inconsistency between the outputs of the *DPI* computations and further the limiting factors in *DPI* calculations.

Key variables for DPI consistency

To identify the parameters responsible for the variations in *DPI* calculations (obtained with the equations in Table II), *CR* was used as a reference and the PDB entries for which $CR < 1 \text{ \AA}$ were explored. The absolute difference (Δ) between *CR* values and the outputs of each *DPI* of the other equations was computed pair-wisely. Consistency has been defined around a threshold of 0.05. Accordingly, the data were split into two groups: *DPI* differences $\leq 0.05 \text{ \AA}$ were considered “Consistent *DPIs*” and *DPI* differences $> 0.05 \text{ \AA}$ “Inconsistent *DPIs*”. For example, $\Delta CRF_i = |CR_i - CRF_i|$ defines the difference between CR_i and CRF_i *DPI* values obtained for PDB entry i . If $\Delta CRF_i \leq 0.05 \text{ \AA}$, i is labeled as “consistent *DPIs*”, and otherwise as “inconsistent *DPIs*” in the ΔCRF set. Similarly, ΔBR and ΔBRF using *CR* were computed as a reference. The size of the sets and the number of class representatives are reported in Table III.

TABLE III. Important variables for diffraction-component precision index (*DPI*) consistency in ΔBR , ΔCRF and ΔBRF sets (see Table I for variable definitions)

<i>DPI</i> Comparison	Inconsistent/consistent <i>DPI</i> counts	Variable	Threshold value ^{a,b}	Retrieval, %		
				Inconsistent <i>DPI</i> ^c	Consistent <i>DPI</i> ^c	Overall
ΔBR	5027/81289	$d_{\min} / \text{\AA}$	2.3	86.2	81.6	85.9
		p	10000	71.2	73.1	71.3
		$R / \%$	0.2	68.4	74.6	68.7
ΔCRF	28645/58143	$d_{\min} / \text{\AA}$	2	78.5	75.9	77.6
		p	13000	77.3	75.5	76.8
		$R_{\text{free}} / \%$	0.235	67.2	64.8	66.4
ΔBRF	32850/51800	$d_{\min} / \text{\AA}$	2	83.9	75.8	80.8
		p	15000	74.8	76.0	75.3
		$R_{\text{free}} / \%$	0.235	70.8	64.7	68.4

^aInconsistent *DPI* identified for $d_{\min} >$, $R_{\text{free}} >$, $p <$ threshold values (see Figs. S-1–S-3 of the Supplementary material to this paper); ^b p is nondimensional, R and R_{free} are equivalent with percentages; ^cconsistent *DPIs* is when the difference between *R-based Cruickshank DPI* values (*CR*) and the output of each *DPI* from the other equations is ≤ 0.05 ; Inconsistent *DPIs* is when the difference between *R-based Cruickshank DPI* values (*CR*) and the output of each *DPI* from the other equations is > 0.05 (see 3.2 Key variables for *DPI* consistency)

Based on the *DPI* consistency assessment, each variable required for the computation of *DPIs* was explored. According to the largest shifts between the distributions of the classes (see Figs. S-1–S-3 of the Supplementary material to this paper), the first 3 most important variables for each set: d_{\min} , p , and R for ΔBR ; d_{\min} , p and R_{free} for ΔCRF and ΔBRF , respectively (Table III) were retrieved. For each variable, a range of values to find the threshold that best dis-

criminations between the classes, *i.e.*, the best trade-off between the retrieval of “Consistent *DPIs*” and “Inconsistent *DPIs*” class members (Figs. S-4–S-6 of the Supplementary material) was systematically explored.

The results pointed towards d_{\min} to be the major factor contributing to the differences in *DPI* results. In fact, in 81.6 % of the cases, consistent *DPI* values between *CR* and *BR* results were obtained for $d_{\min} < 2.3 \text{ \AA}$. For 76 % of the structures, $d_{\min} < 2 \text{ \AA}$ identified consistent *DPIs* in the ΔCRF and the ΔBRF sets. The another important variable is p . The threshold values of $p < 10000$, < 13000 and < 15000 , retrieved were 73.1, 75.5 and 76 %, respectively, of the ‘Consistent *DPI*’ group in ΔBR , ΔCRF and ΔBRF sets, respectively.

Based on the current results, for most PDB files, consistent *DPI* values are expected to appear at $d_{\min} < 2 \text{ \AA}$. The resolution of the PDB structure serves as input only for *CR* and *CRF* calculation and describes the level of detail present in the diffraction pattern. Although, in general, high-resolution structures (*e.g.*, $d_{\min} < 2 \text{ \AA}$) ensure sufficient density to obtain good models, this is not always true.^{5,16}

Failures in DPI computations

Out of 143070 structures, *DPI* computation failed for 3125 due to missing variables or inadequate component values, such as $p = n_{\text{obs}} - qN_i$ or $(1 - qN_i/n_{\text{obs}})$ in Eqs. (1) and (3), respectively (see Table II). In the case of 41262 entries, *i.e.*, 30 % of the PDB, *DPI* computations by all 4 equations were not possible (Gurusaran *et al.*²⁰ filters were not applied here).

Two major variables that impaired the computation of *DPIs*, *i.e.*, p and qN_i/n_{obs} (Table IV) were identified. Values of $p \leq 0$ or $qN_i/n_{\text{obs}} \geq 1$ made *CR* and *BR* calculation impossible and showed a relatively high prevalence (~22 %, *i.e.*, ~32000 entries) in the PDB database. This explained the limited *R*-based *DPI* applicability compared to *R_{free}*-based *DPIs*. The later ones were predominantly affected by the availability of the *R_{free}* factor (in 6021 PDB entries).

TABLE IV. Percentages of Protein Data Base entries with missing/inadequate variable values (see Table I) involved in diffraction-component precision index computations (see Table II)

Variable	p	qN_i/n_{obs}	R_{free}	V	C	n_{obs}	V_M	N_{prot}	R	Other ^a
PDB entries, %	24.28	22.64	4.25	2.87	2.53	1.65	1.63	1.49	0.29	<0.1

^a N_i , V_a and d_{\min}

Errors in the calculation of the volume V (present in the Blow *DPI* equations eq 3 and eq 4) affected 2.87 % (4068) structures. In this particular case, V can be computed using the unit cell lengths and angles (see Table I), providing very similar values to the V_M -based volume (Pearson correlation of 0.858, Fig. S-7). Consequently, the corresponding *DPI* values indicated very strong correlations of 0.997 and 0.995 with *BR* and *BRF* *DPIs*, respectively. Moreover, it can be applied to 2788 more PDB compared to *BR* and 3310 more compared to *BRF*.

(*DPI* cutoff < 1 Å). Larger values of *DPI*, e.g., > 2 Å, are encountered in cases with disproportionate n_{obs} relative to the volume or the number of atoms. In these cases, small n_{obs} can generate large *DPI* values.

CONCLUSION

In drug discovery studies crystallographic protein structures are used extensively for protein-ligand docking and molecular dynamics. Using a reliable measure to prioritize the fittest structures (if multiple is available) is of significant importance for the outcome of the experiments as recently shown by Halip *et al.*²² *DPI* is one potentially valuable indicator, but difficulties in computation might have decreased its application in medicinal chemistry and cheminformatics.

Our comprehensive exploration of four *DPI* variants, showed that R_{free} -based *DPI* computations (*CRF* and *BRF*) can be determined for the vast majority of the currently available PDB entries and provide similar outputs to *R*-based *DPI* types (*BR* and *CR*), especially in structures with small *DPI* values. Zero or negative values for p or $1 - qN_i/n_{\text{obs}}$ are the major sources of computational failures in *R*-based computations. The differences in *DPI* results are strongly influenced by the resolution (d_{\min}) and the number of parameters (p). In general, *DPI* computations in structures with resolutions < 2 Å will result in small differences between the outputs of the four approaches

NOMENCLATURE

DPI: Diffraction-component precision index

CR: *DPI* computed with *R*-based *DPI* Cruickshank formula,

CRF: *DPI* computed with R_{free} -based *DPI* Cruickshank formula,

BR: *DPI* computed with *R*-based *DPI* Blow formula

BRF: *DPI* computed with R_{free} -based *DPI* Blow formula

SUPPLEMENTARY MATERIAL

Additional data and information are available electronically at the pages of journal website: <https://www.shd-pub.org.rs/index.php/JSCS/article/view/10775>, or from the corresponding author on request.

Acknowledgements. We wish to thank Dr. Ana Borota for her constructive comments and suggestions regarding the manuscript. This work was supported by “Coriolan Drăgulescu” Institute of Chemistry, Timisoara, Romanian Academy, Romania, project number 1.1.4/2019/2020.

И З В О Д

ОБИМНО ПОРЕЂЕЊЕ ИНДЕКСА ПРЕЦИЗНОСТИ ДИФРАКЦИОНИХ КОМПОНЕНТИ
ДАЈЕ ПРЕДНОСТ CRUICKSHANK R_{free} ФУНКЦИЈИ

SORIN AVRAM и CRISTIAN NEANU

Department of Computational Chemistry, “Coriolan Dragulescu” Institute of Chemistry, Timișoara, Romania

Ова студија тежи да обезбеди прво обимно поређење различитих једначина индекса прецизности дифракционих компоненти (*DPI*), процени применљивост параметра, и направи препоруке за израчунавање *DPI*. *DPI* процењује просечну поузданост атомских

координата добијених финим-структурним подешавањем података дифракције за протеине, са применом у кристалографији и хеминформатици. Мада су Cruickshank и Blow предложили *DPI* једначине засноване на R и R_{free} за израчунавање *DPI* вредности, оне су нису погодне за коришћење за процену квалитета фајлова протеинске базе података (PDB), због нејасних протокола за издавање података (да би им се приписале варијабле), сложености једначина, недостатка екстензивних студија применљивости и ограниченог приступа аутоматизованим израчунавањима. Да би превазишли ове недостатке целокупна RCSB PDB база података је проверена користећи Cruickshank и Blow R и R_{free} *DPI* варијације. Израчунавања на 143070 кристалних структура указују на то да су R_{free} -засноване *DPI* једначине применљиве на 30 % више протеинских структура у поређењу са R -заснованим *DPI* једначинама, са Cruickshank R_{free} -заснованим *DPI* (CRF) израчунавањима која превазилаže број успешних Blow R_{free} -заснованих *DPI* (BRF) израчунавања. Иако приказани резултати указују да, опште узвеши, резолуција структуре $<2\text{ \AA}$ обезбеђују конзистентност различитих *DPI* израчунавања (разлике су $<0,05\text{ \AA}$), препоручује се да се користи CRF *DPI* због његове шире применљивости.

(Примљено 18. маја, ревидирано 31. августа, прихваћено 25. септембра 2021)

REFERENCES

1. P. Willett, *WIREs Comput. Mol. Sci.* **1** (2011) 10 (<https://doi.org/10.1002/wcms.1>)
2. G. Sliwoski, S. Kothiwale, J. Meiler, E.W. Lowe Jr., *Pharmacol. Rev.* **66** (2014) 334 (<https://doi.org/10.1124/pr.112.007336>)
3. D. M. Popović, S. D. Zarić, B. Rabenstein, E.-W. Knapp, *J. Am. Chem. Soc.* **25** (2001) 6040 (<https://doi.org/10.1021/ja003878z>)
4. S. Zarić, D. Popović, E.-W. Knapp, *Chem. Eur. J.* **6** (2000) 3935 ([https://doi.org/10.1002/1521-3765\(20001103\)6:21%3C3935::AID-CHEM3935%3E3.0.CO;2-J](https://doi.org/10.1002/1521-3765(20001103)6:21%3C3935::AID-CHEM3935%3E3.0.CO;2-J))
5. G. L. Warren, T. D. Do, B. P. Kelley, A. Nicholls, S. D. Warren, *Drug Discov. Today* **17** (2012) 1270 (<https://doi.org/10.1016/j.drudis.2012.06.011>)
6. H. M. Berman, J. Westbrook, Z. Feng, G. Gilliland, T. N. Bhat, H. Weissig, I. N. Shindyalov, P. E. Bourne, *Nucleic Acids Res.* **28** (2000) 235 (<https://doi.org/10.1093/nar/28.1.235>)
7. S. K. Burley, H. M. Berman, C. Bhikadiya, C. Bi, L. Chen, L. Di Costanzo, C. Christie, K. Dalenberg, J. M. Duarte, S. Dutta, Z. Feng, S. Ghosh, D. S. Goodsell, R. K. Green, V. Guranovic, D. Guzenko, B. P. Hudson, T. Kalro, Y. Liang, R. Lowe, H. Namkoong, E. Peisach, I. Periskova, A. Prlic, C. Randle, A. Rose, P. Rose, R. Sala, M. Sekharan, C. Shao, L. Tan, Y. P. Tao, Y. Valasatava, M. Voigt, J. Westbrook, J. Woo, H. Yang, J. Young, M. Zhuravleva, C. Zardecki, *Nucleic Acids Res.* **47** (2019) D464 (<https://doi.org/10.1093/nar/gky1004>)
8. H. Berman, K. Henrick, H. Nakamura, *Nat. Struct. Biol.* **10** (2003) 980 (<https://doi.org/10.1038/nsb1203-980>)
9. H. Berman, K. Henrick, H. Nakamura, J. L. Markley, *Nucleic Acids Res.* **35** (2007) D301 (<https://doi.org/10.1093/nar/gkl971>)
10. wwPDB consortium, *Nucleic Acids Res.* **47** (2019) D520 (<https://doi.org/10.1093/nar/gky949>)
11. M. J. Domagalski, H. Zheng, M. D. Zimmerman, Z. Dauter, A. Wlodawer, W. Minor, *Structural Genomics. Methods in Molecular Biology*, Vol. 1091, Humana Press, Totowa, NJ, 2014, p. 297 (https://doi.org/10.1007/978-1-62703-691-7_21)
12. N. V. Zukang Feng, Luigi Di Costanzo, D. S. Goodsell, J. D. Westbrook, S. K. Burley, C. Zardecki, *Data Sci. J.* **19** (2020) 25 (<http://doi.org/10.5334/dsj-2020-025>)

13. A. T. Brunger, *Nature* **355** (1992) 472 (<https://doi.org/10.1038/355472a0>)
14. D .W. Cruickshank, *Acta Cryst., D* **55** (1999) 1108 (<https://doi.org/10.1107/s0907444999004308>)
15. D .M. Blow, *Acta Crystallogr., D* **58** (2002) 792 (<https://doi.org/10.1107/s0907444902003931>)
16. P. C. Hawkins, A. G. Skillman, G. L. Warren, B. A. Ellingson, M. T. Stahl, *J. Chem. Inf. Model.* **50** (2010) 572 (<https://doi.org/10.1021/ci100031x>)
17. P. C. Hawkins, G. L. Warren, A. G. Skillman, A. Nicholls, *J. Comput.-Aided Mol. Des.* **22** (2008) 179 (<https://doi.org/10.1007/s10822-007-9166-3>)
18. S. I. Avram, L. Crisan, L. M. Pacureanu, A. Bora, E. Seclaman, M. Balint, L. G. Kurunczi, *Med. Chem. Res.* **22** (2012) 3589 (<https://doi.org/10.1007/s00044-012-0367-5>)
19. K. S. D. Kumar, M. Gurusaran, S. N. Satheesh, P. Radha, S. Pavithra, K. P. S. Thulaa Tharshan, J. R. Helliwell, K. Sekar, *J. Appl. Crystallogr.* **48** (2015) 939 (<https://doi.org/10.1107/s1600576715006287>)
20. M. Gurusaran, M. Shankar, R. Nagarajan, J. R. Helliwell, K. Sekar, *IUCrJ* **1** (2014) 74 (<https://doi.org/10.1107/S2052252513031485>)
21. J. Goto, R. Kataoka, N. Hirayama, *J. Med. Chem.* **47** (2004) 6804 (<https://doi.org/10.1021/jm0493818>)
22. L. Halip, S. Avram, C. Neanu, *Struct. Chem.* **32** (2021) 1693 (<https://doi.org/10.1007/s11224-021-01751-9>).

SUPPLEMENTARY MATERIAL TO
**Large-scale comparison between the diffraction-component
precision indexes favors Cruickshank's R_{free} function**

SORIN AVRAM* and CRISTIAN NEANU**

*Department of Computational Chemistry, “Coriolan Dragulescu” Institute of Chemistry,
Timișoara, Romania*

J. Serb. Chem. Soc. 87 (3) (2022) 321–330

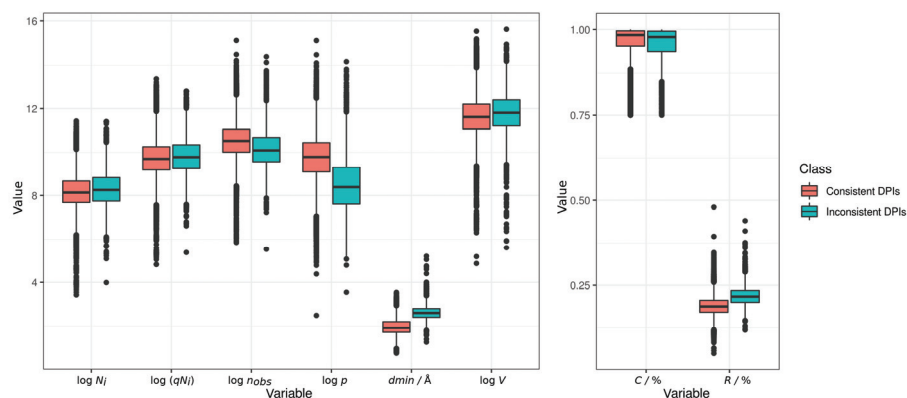


Fig. S-1. Boxplot showing the distribution of variables for consistent and inconsistent DPI values in CR and BR computations (see TABLE I for variables definitions).

*•** Correspondence E-mail: (*)sorin.avram@acad-icht.tm.edu.ro;
(**)cristian.neanu@gmail.com

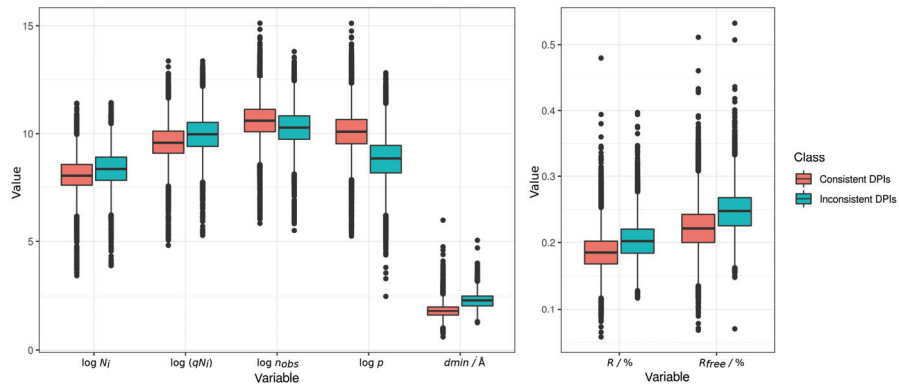


Fig. S-2. Boxplot showing the distribution of variables for consistent and inconsistent *DPI* values in *CR* and *CRF* computations (see Table I for variables definitions).

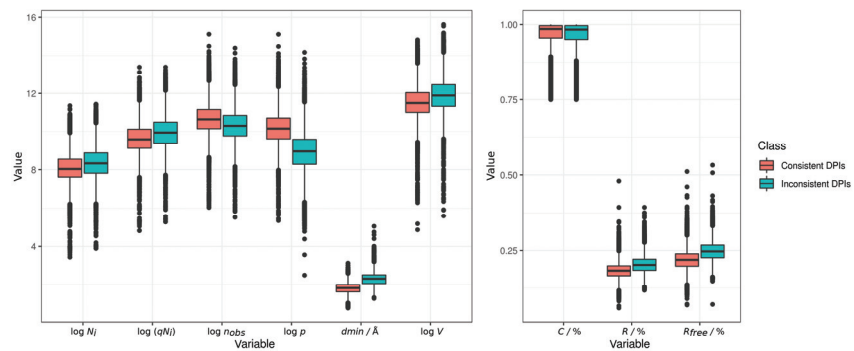


Fig. S-3. Boxplot showing the distribution of variables for consistent and inconsistent *DPI* values in *CR* and *BRF* computations (see Table I for variables definitions).

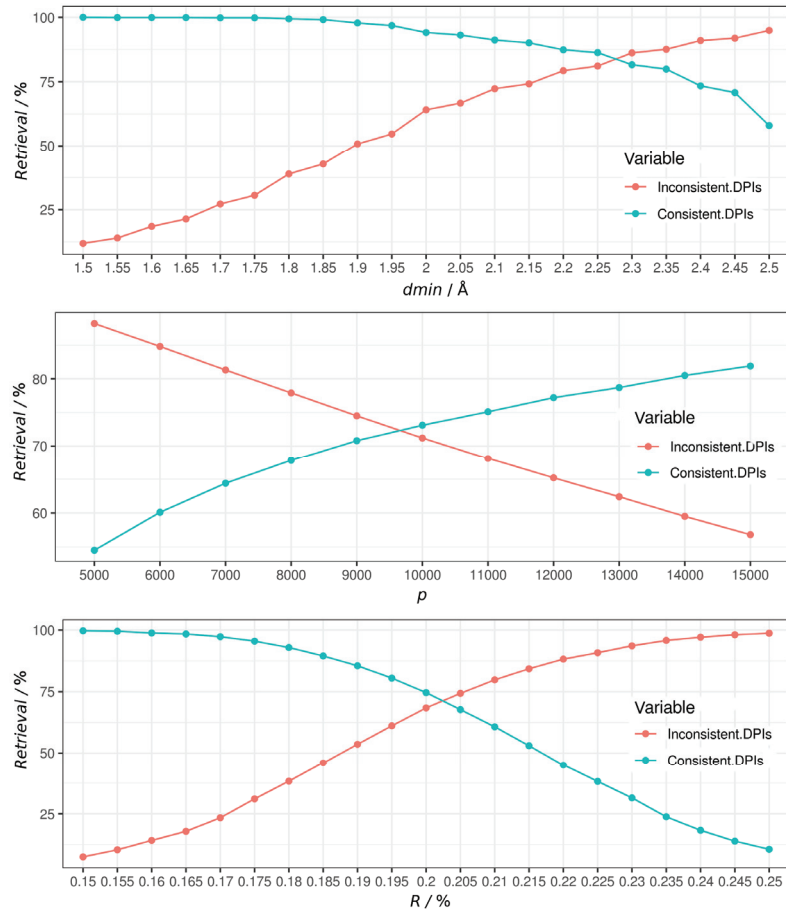


Fig. S-4. Retrieval percentages of consistent and inconsistent *DPI* class instances in *CR* and *BR* computation, at various thresholds for d_{\min} , p and R (see TABLE I for variables definitions).

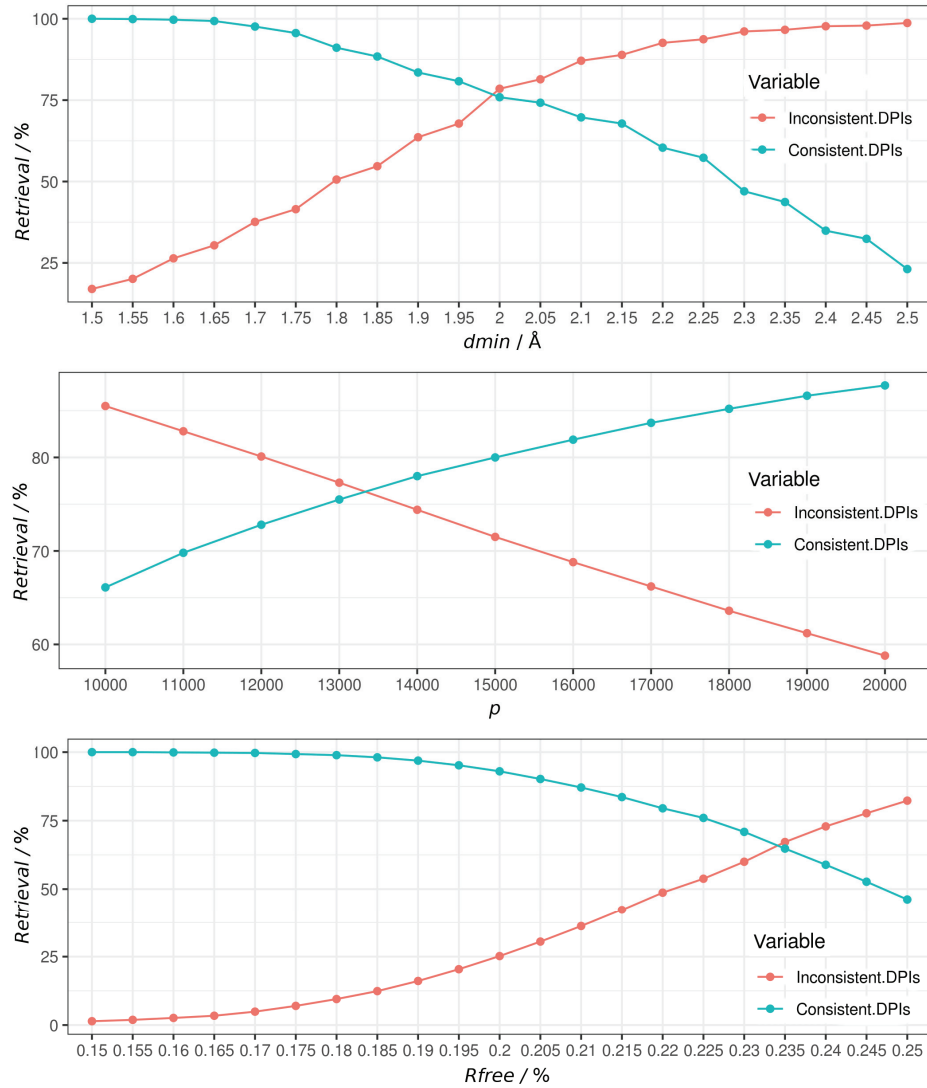


Fig. S-5. Retrieval percentages of consistent and inconsistent *DPI* class instances in *CR* and *CRF* computation, at various thresholds for d_{\min} , p , and R_{free} (see Table I for variables definitions).

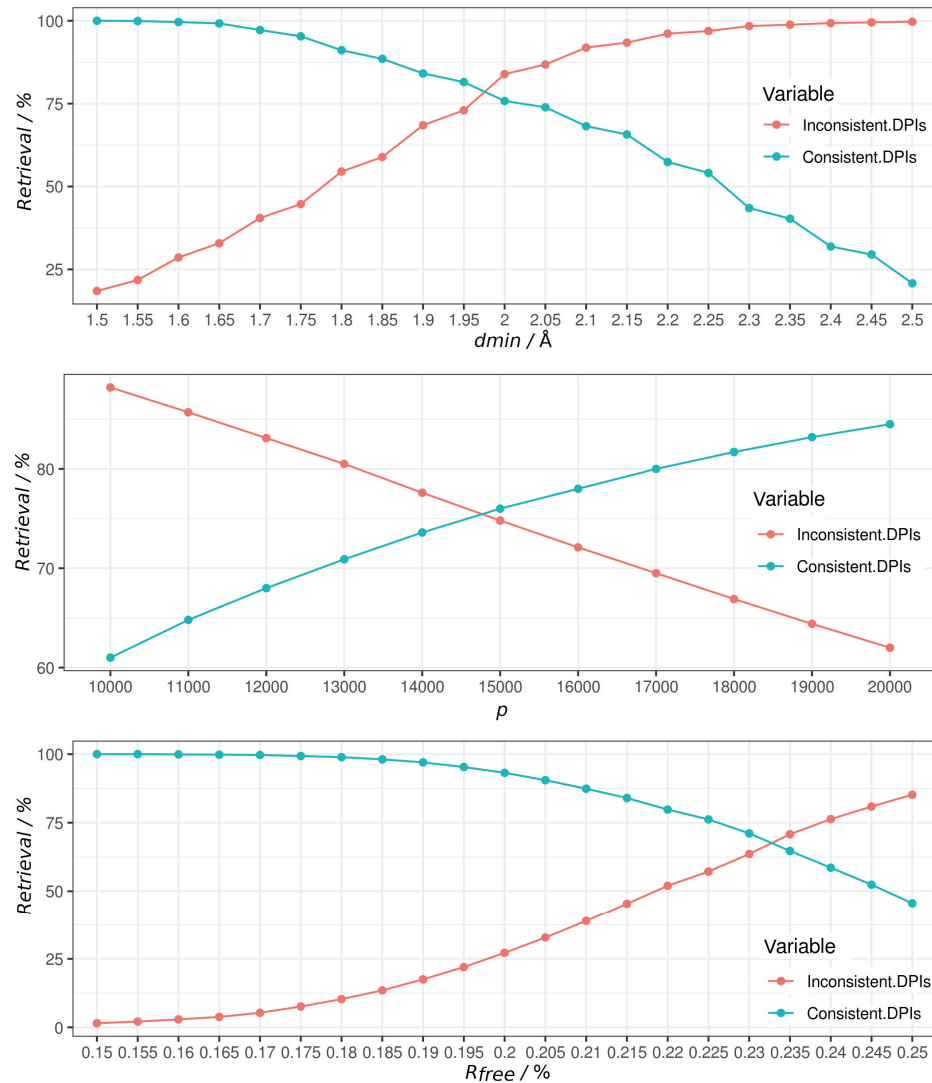


Fig. S-6. Retrieval percentages of consistent and inconsistent *DPI* class instances in *CR* and *BR* computation, at various thresholds for d_{min} , p , and R_{free} . (see Table I for variables definitions).

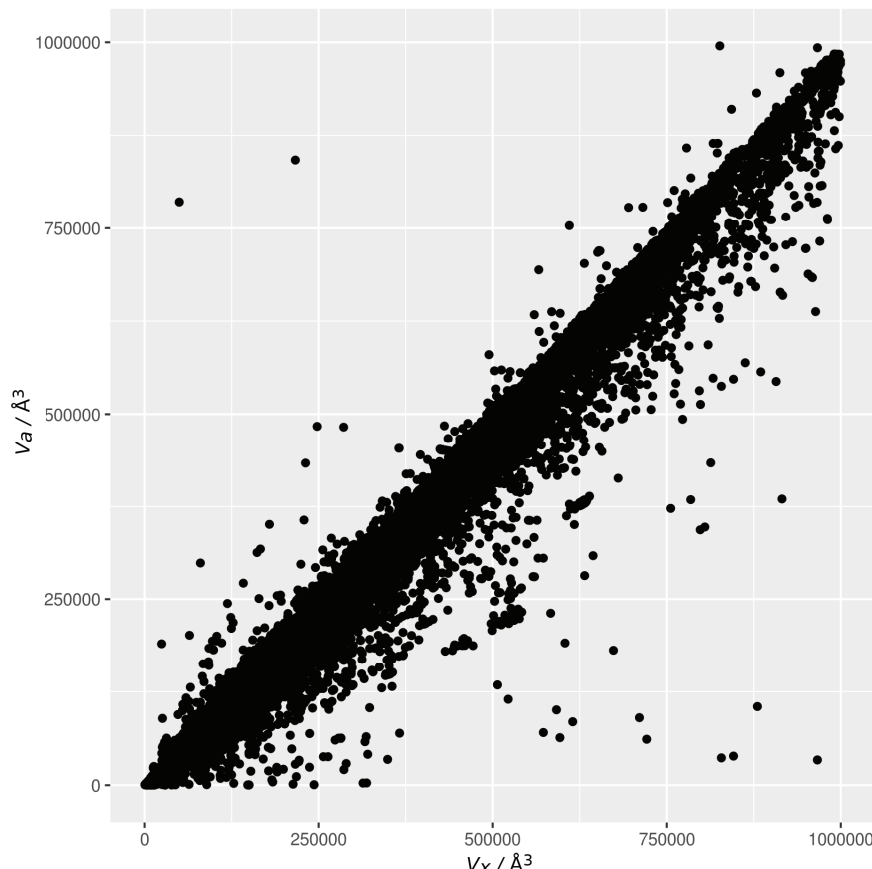


Fig. S-7. Plot of V_a , i.e. protein structure volume computed from Matthews coefficient, versus V_x , i.e. protein structure volume computed from the crystal asymmetric unit data.

Analysis of the DPI data and corresponding variables for the subsets of alpha- and beta-helical PDB structures

The general workflow which was used to assess the the alpha helix (AP) and beta sheets (BP) proteins was the following (Fig. S-8):

From our PDB downloaded database, 117,829 PDB structures passed the following criteria:

- Completeness $\geq 75\%$
- Number of occupied atoms $\geq 90\%$
- *DPI_CRF* computed and > 0

The lists of alpha helix (AP) and beta sheets (BP) proteins were downloaded from the RCSB PDB database (<https://www.rcsb.org/>)

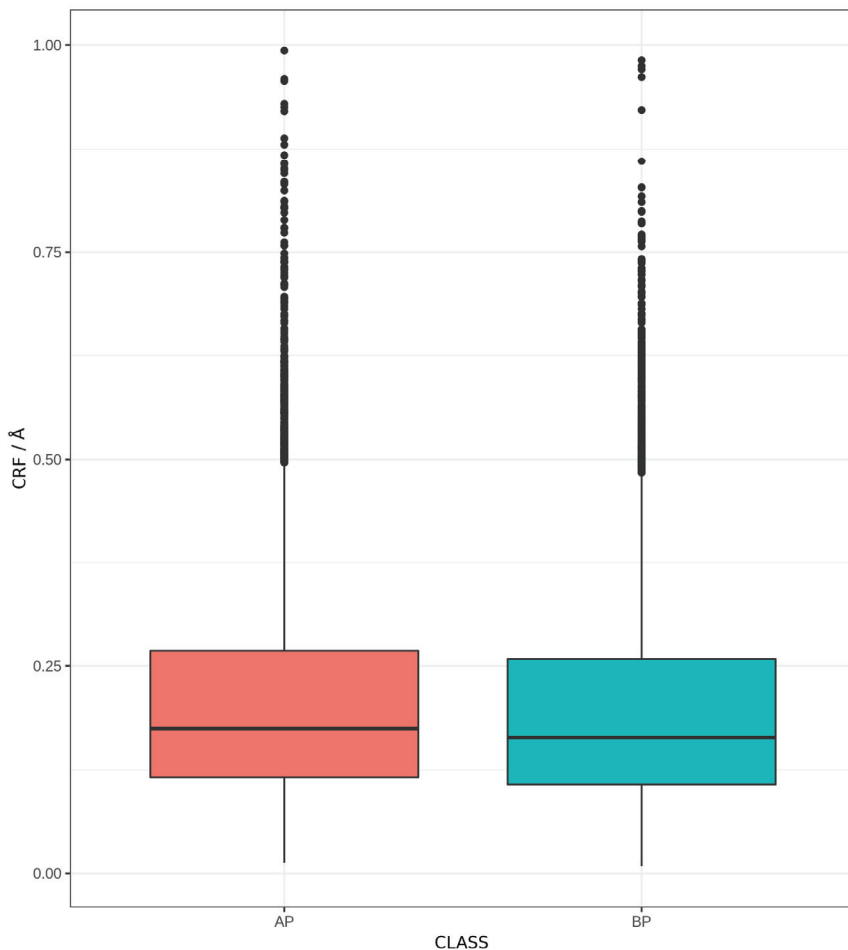


Fig. S-8. Boxplot showing the distribution of variables for AP (alpha helix proteins) and BP (beta helix proteins) *DPI* values in *CRF* computations.

The overlapping PDBs (1,648) between the APs (17,034 PDBs) and BP (26,893 PDBs) were removed from both sets, leaving a total of 40,631 PDB (37.9 % APs and 62.1 % BPs). For 29,802 PDBs *CRF_DPI* values were successfully computed (12,077 APs and 17,725 BPs).

The comparative analysis between alfa and beta proteins in terms of *DPI* revealed no significant differences (Figure S-8). This could be explained by the fact that the technology applied to obtain crystals and models is the same for lipo-soluble, water-soluble, alpha-helical or beta-chain structures, and consequently the accuracy of the positions of atoms is similar.



Structural stability of biofilms produced from silkworm cocoon fibers

ANA LÚCIA DE SOUZA MADUREIRA FELÍCIO and HENRIQUE DE SANTANA*

Departamento de Química, CCE, Universidade Estadual de Londrina, Londrina,
PR 86051-990, Brazil

(Received 11 June, revised 21 July, accepted 23 July 2021)

Abstract: Biofilms were obtained from cocoons of the silkworm, *Bombyx mori*, involving the removal of sericin, extraction and solubilization of fibroin fibers, dialysis of fibroin dispersions and preparation of biofilms by the casting process. Biofilm transparency was verified by UV–Vis spectroscopy and thermal stability by thermogravimetric/differential scanning calorimetry (TG/DSC). Soon after preparation, the solidification of the fibroin solution prepared from the cocoons and extracted by the Ajisawa method was monitored until the biofilm stabilized, using attenuated total reflectance-Fourier transform infrared spectroscopy (ATR-FTIR) as a function of time. The results showed that there was a change in the conformation from the silk I structure (α -helix) to silk II (β -sheet). In order to improve the characterization of the biofilms obtained by the Ajisawa method and LiBr solubilization of fibroin fibers, Raman spectroscopy was used to verify the stabilization of the different possible molecular conformations for the fibers in these materials, by comparison with the cocoon spectra and those of the solid (freeze-dried precipitated by dialysis for 72 h. By comparing the Raman spectra of the biofilms in terms of the intensities of the broadened band characteristic of amide I, it was possible to assess the conformational changes in both materials based on the possible transitions between β -sheet conformations and flexible α -helix and β -turn structures. The results showed a dispersion of these conformations in the biofilms generated and in the solid freeze-dried hydrogel spectrum, and the β -sheet conformation was found to be predominant. The TG and DSC curves showed that the materials with higher β -sheet content exhibited higher thermal stability. Thus, the data obtained further elucidated the properties of these materials that are widely used in various processes.

Keywords: silk fibroin; Raman spectroscopy; *Bombyx mori*; molecular conformation.

* Corresponding author. E-mail: hensan@uel.br
<https://doi.org/10.2298/JSC210611054F>

INTRODUCTION

The search for sustainable materials with applications in various fields has become the focal point of various studies in pursuit of process innovation. One such material is the fiber produced and synthesized in the glands of the silkworm, *Bombyx mori*.^{1–18} At the end of the larval stage, the silkworm produces silk fibers to form a cocoon by a complex spinning process. Most of the cocoon consists of fibroin fibers cemented together by another protein, sericin, that acts as an adhesive.¹

The sericin is removed by degumming the cocoon, and the silk fibroin (SF) can be processed using various methods. Conventional degumming entails boiling the cocoons in an aqueous solution, the efficiency of which can be improved by adding substances such as sodium carbonate, high lipid soaps, citric acid, urea, tartaric acid or various enzymes to remove the sericin and other impurities.²

After degumming, the fibroin fibers can be dissolved in various concentrated salt solutions, such as lithium bromide (LiBr), calcium chloride (CaCl₂), calcium nitrate Ca(NO₃)₂, Ajisawa reagent (CaCl₂:EtOH:H₂O) and formic acid. The salt concentration, temperature and dissolution time can directly affect the degree of peptide bond decomposition and consequently the solubility of the fibroin. The salts involved in both degumming and dissolution are removed by dialysis to obtain an aqueous SF solution.^{1,3–5}

The aqueous SF solution can be used as is or to produce versatile forms of fibroin, such as powder, nanofibers, films, hydrogels and sponges, according to the field of application, and by virtue of its biocompatibility, controllable degradation, ease of processing and availability in the sericulture industry.^{3,6}

SF biofilms are one of the most important and valuable support biomaterials with applications in fields such as biomedicine, electronics, textile engineering, optoelectronics, energy collection/storage, biosensors, food coatings, *etc.* They can be obtained by simple evaporation of the aqueous solution (a process known as casting), or by more complex techniques, such as vertical deposition, spin-assisted layer-by-layer assembly, spin coating or electrospinning.⁷

SF has two main molecular conformations (silk I and silk II) in the secondary structure. Silk I is a non-crystalline, metastable, water soluble form and is mainly made up of random coils and α -helix conformations. Silk II is a highly stable, organized, non-water-soluble structure, characterized by a sheet formation. The structures can be transformed under appropriate conditions. The molecular conformation of the SF is an important parameter in the production of medical devices.^{8–11}

In fact, native SF can be solubilized and processed as regenerated silk in a wide variety of geometrical shapes. Several studies have shown that chemical treatments, such as immersion in high salt concentration organic solvents, can break the hydrogen bond between the β -sheets to transition the SF conformation

from silk II to silk I and transform fibroin fibers into a water-soluble random coil conformation.^{19,20}

Motta *et al.*²¹ report on the thermal and dynamic mechanical properties of three different regenerated silk fibroin films cast from water solutions, characterized by differential scanning calorimetry (DSC). DSC revealed the presence of a lower temperature endothermic phenomenon centered at about 70 °C for the as-prepared room temperature cast film, and other typical material thermal parameters – glass transition, crystallization, and thermal degradation – more or less pronounced depending on the specific preparation procedure and the thermal or solvent treatment. These results were interpreted assuming progressive evolution of the random coil regions from the more stable β -sheet conformation, as induced by different applied preparation conditions or treatment.

The aim of this study was to examine the structural organization and thermal stability of biofilms with a view to elucidating the properties of this material. Attenuated total reflectance-Fourier transform infrared (ATR-FTIR) and Raman spectroscopy were used to characterize the segment arrangements in the polypeptide matrices for generation to produce biofilms, and thermogravimetric (TG) and differential scanning calorimetry (DSC) to monitor the effect of temperature on the various materials. The results show that the β -sheet conformation plays a crucial role in the so-called secondary fibroin structures of biofilms, determining the rigidity and thermal stability of the material.

EXPERIMENTAL

Materials

The silkworm cocoons (*Bombyx mori*) used in this study were imported from China. Fibers were extracted and solubilized using anhydrous Na₂CO₃ (Sigma-Aldrich, 99.0 %), ultrapure water (Milli-Q, Milipore), CaCl₂·2H₂O (Dinâmica, 99 %) and ethanol (Qhemis, 99.5 %).

Cocoon classification

First, the cocoon samples were cut along the top to remove the pupae and other internal impurities. Then they were cut into small pieces of approximately 1 cm² and washed in ultrapure water.

Fibroin extraction – sericin removal (degumming)

A quantity of 1.06 g Na₂CO₃ was dissolved in a beaker containing 500 mL of ultrapure water heated to 95 °C on a hotplate. Next, 1.5 g of chopped cocoons were added. The apparatus was constantly stirred and kept at 95 °C for 40 min.

After heating and stirring, the fibers were taken out of the solution and excess water removed by manual wringing. The fibers were then washed in ultrapure water at 25 °C and stirred for 20 min. The washing was repeated 3 times and the excess water then removed by manual wringing. The resulting fibers were placed in a Petri dish and left in an oven at 50 °C for 24 h.

This degumming stage resulted in an average drop in the initial cocoon weight of 27.6 %, representing the amount of sericin removed during the process.

Solubilization of the fibroin fibers

Fiber solubilization can be achieved by different methods using different salts and solvents. In this study, two fiber solubilization methods were used.

First, a ternary solution (Ajisawa reagent) consisting of calcium chloride, ethanol and water ($\text{CaCl}_2 \cdot 2\text{H}_2\text{O} : \text{CH}_3\text{CH}_2\text{OH} : \text{H}_2\text{O}$, 1:2:6 mole ratio) was prepared. The fibers obtained in the previous stage were cut into smaller pieces and added to the solution at 1 g of chopped fiber to 10 mL ternary solution (1:10).

The beaker containing the solution was then placed in a thermostat-controlled bath at 80 °C for 40 min, stirring manually every 5 min. The beaker was then removed from the bath and left to cool to a temperature of 25 °C. The fibers were completely solubilized in the ternary solution, resulting in low-viscosity, slightly bleached dispersions.

In the second method, a 9.3 mol L⁻¹ aqueous solution of lithium bromide (LiBr) was prepared. Care is required in the preparation of this solution, since the reaction produces a lot of heat. The dry fibers were also cut into smaller pieces and added to the solution at 1 g of fiber to 4 mL solution (1:4).

The solution was then placed in a thermostat-controlled bath at 60 °C for approximately 4 h, stirring manually every 5 min for the first hour, and then every 15 min until the fibers were fully dissolved. Next, the beaker was removed from the bath and left to cool to 25 °C, as in the Ajisawa method, whereby a similar dispersion was obtained.

Dialysis

The fibroin dispersions obtained using the two methods were transferred to pre-hydrated cellulose membranes, then dialyzed in ultrapure water for 48 h. The temperature was kept at 25 °C with continuous stirring, and the initial water was replaced after 1 h, and subsequently every 8 h, at 1:30 volume ratio fibroin dispersion:water.

After dialysis, the dispersion was transferred to 50 mL Falcon tubes for centrifugation at 6000 rpm (Centurion Pro-Analytical centrifuge) for 40 min to remove impurities. The supernatant was transferred to another tube and the process repeated.

The dispersions dialyzed for 24 h were transparent and colorless, and the bleached particles precipitated by centrifugation adhered to the wall and bottom of the tube. The supernatant of the dispersion was collected and transferred to another tube, completely eliminating these particles. The fibroin solution was stored at 4 °C before use.

A volume of 0.5 mL of each dispersion was placed in weighing boats and kept in an oven at 60 °C for 24 h. The weight after drying was checked by calculating the weight/volume of dialyzed cocoon fibroin, resulting in an average of 5.0 %.

To check whether the dialysis time influenced purification, another part of the fiber dispersion was left to dialysis for a further 24 h, totaling 72 h. In this case, it formed a hydrogel precipitate on the inside of the membrane. This material was removed, centrifuged under the conditions applied to the 48 h dispersion, and subsequently freeze-dried to remove the water, leaving a solid residue.

Biofilm preparation

Biofilms were prepared by casting the fibroin solution dialyzed for 48 h. A volume of 0.8 mL fibroin solution was transferred to 23 mm acrylic plates, placed in a fan oven and kept at 50 °C for 8 h. Next, the films were carefully removed using tweezers and characterized.

After drying, the biofilms were transparent and looked like plastic. There was some flexibility and no breaks were observed.

Spectroscopic characterization

To check the transparency of the as prepared biofilms, UV–Vis transmittance spectra in the 220–800 nm range were obtained using a UV–Vis 2600 spectrophotometer (Shimadzu).

Infrared spectra were taken on a Fourier transform IR spectrophotometer (FTIR, Frontier MIR/NIR, PerkinElmer®) in the attenuated total reflectance (ATR) mode, using a UATR® accessory with diamond crystal and zinc selenide focusing, scan between 4000 and 650 cm⁻¹, resolution of 2 cm⁻¹ and 32 accumulated scans. The biofilm was formed over the crystal, and the spectra acquired over a period of 60 min in a gaseous nitrogen atmosphere to speed up the drying process.

Raman spectra were obtained using an Alpha300+ WITec® confocal Raman microscope system (excitation at 785 nm), with a ZEISS 50× lens.

Thermal analysis

Biofilm fragments with a total weight of 1.8 g were used in differential scanning calorimetry (DSC) and thermogravimetric (TG) analysis. Samples were placed on hermetically sealed aluminum (DSC) and platinum (TG) supports. The DSC curves were obtained using a Shimadzu DSC-60, and the heating rate was 10 °C min⁻¹ in the 230–300 °C range. TG curves were obtained using a Shimadzu TGA-50 and the heating rate was 10 °C min⁻¹ in the 20–1000 °C range. The gas flow for both procedures was 50 mL min⁻¹ nitrogen.

RESULTS AND DISCUSSION

The UV–Vis spectra of the biofilms obtained by the two extraction methods, a) Ajisawa and b) LiBr, are shown in Fig. S-1 of the Supplementary material to this paper. High incidences of transparency in the visible region (300–800 nm) and a characteristic band at 277 nm were observed for both analyzed biofilms. This peak could be ascribed to the $\pi\rightarrow\pi^*$ electron transition of aromatic, tyrosine, phenylalanine and tryptophan amino acid residues in the fibroin chain.^{4,9}

The elevated transparency of the biofilms was a desired characteristic given the various possible applications of this kind of material, whether in optics or even biomedical fields (encapsulating drugs, colorants, nanoparticles, *etc.*). Some studies in the literature show that transparency can be directly associated with the method used to obtain the fibroin solution. Biofilms obtained using regenerated fibroin from cocoons exhibit transparency indices above 95 %, whereas for biofilms from native fibroin extracted directly from the silkworm glands, this index was between 70 and 90 %, and in addition to opacity, the films may exhibit yellowish hues.²⁰

The ATR FT-IR spectra as a function of the structural stabilization time of the biofilm prepared by Ajisawa extraction are shown in Fig. 1. Initially (up to 4 min after preparation) low intensity bands were observed at 1643, 1546 and 1246 cm⁻¹, attributed respectively to amides I, II and III.⁵ Amide I is the result of asymmetric coupling of C=O and C–N bond stretching, and the band related to amides II and III are the result of symmetric coupling of C–N bond stretching and angular deformation in the N–H plane.¹⁰ All these bands in the IR spectrum are sensitive to changes in the conformation.¹¹

After 45 min, an increase in the intensity of these bands was observed, with broadened bands between 1650/1639, 1531/1514 and 1240/1231 cm^{-1} . After 60–65 min, the spectra remained unchanged. Bands were defined at 1639, 1514 and 1231 cm^{-1} and shoulders were observed at 1650 and 1531 cm^{-1} .

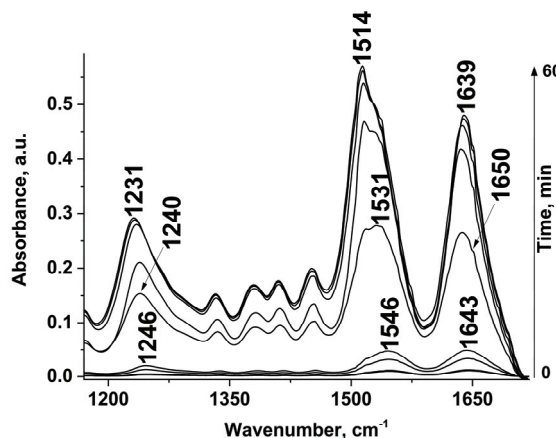


Fig. 1. Changes in the FTIR spectra as a function of the structural stabilization time of the biofilm prepared by the Ajisawa extraction method, obtained by ATR.

According to the literature,¹¹ the bands at 1610–1630 cm^{-1} (amide I) and 1510–1520 cm^{-1} (amide II) are characteristic of silk II (β -pleated sheet) secondary structure, whereas absorption at 1640–1660 cm^{-1} (amide I) and 1535–1542 cm^{-1} indicate that the conformation contains silk I (α -form). These results could indicate that after 60–65 min, a biofilm stabilized with a predominance of the β -sheet rather than the α -form.^{11,12}

With the aim of further investigating the changes observed in the IR spectra, Raman spectra were recorded. This was necessary in view of the work performed by Lefèvre *et al.*¹³ who used polarized Raman spectroscopy to show the molecular organization in the silk cocoon produced by *B. mori*, with a mixture of different quantities of β -sheets and flexible structures (β -turns and α -helices).

The Raman spectra of the cocoon, the biofilms prepared by the LiBr and Ajisawa methods, and the freeze-dried hydrogel are shown in Fig. 2.

The Raman spectra of the cocoon (Fig. 2), obtained at an excitation wavelength of 785 nm, exhibit main bands at around 1672, 1622, 1560, 1455, 1407, 1270 and 1239 cm^{-1} .¹⁴ The frequencies at 1672, 1560 and 1270/1239 cm^{-1} were respectively ascribed to amides I, II and III, related to the different contributions of C=O stretching, angular N–H in-plane deformation and C–N stretching in the polypeptide chains of the cocoon primary structure. The band at 1622 cm^{-1} was related to vibrations in the amino acid side-chain of the silk fibroin. The band at 1407 cm^{-1} was related to the presence of sericin, and the band at 1455 cm^{-1} was ascribed to fibroin.^{15,18}

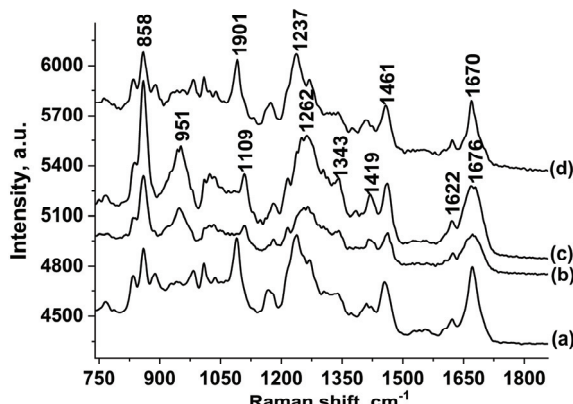


Fig. 2. Raman spectra of: a) cocoon, b) biofilms prepared by the LiBr method and c) Ajisawa method, and d) the freeze-dried hydrogel, at excitation of 785 nm.

The biofilm spectra exhibited marked variations compared to the spectrum of the cocoon sample. The spectra in Fig. 2b and c show band displacement and broadening compared to the cocoon spectra at 1674, 1461 and 1419 cm⁻¹, as well as the presence of a broadened band at 1262 cm⁻¹. These spectral variations were considered to be associated with structural changes in the material. The spectrum of the freeze-dried hydrogel (Fig. 2d), was fairly similar to that obtained for the cocoon, exhibiting preferential ordering of the materials that was different from that observed in the spectra of the biofilms.

To better assess whether the biofilms prepared were or were not identical at molecular level, the work of Lefèvre *et al.*¹³ was taken into account. The deconvolution of the amide I band in the Raman spectrum revealed that the frequencies at 1655, 1666 and 1678/1693 cm⁻¹ could be related to different conformations of the α -helix, β -sheet and β -turn structures, respectively.

With the aim of studying the Raman spectra of the biofilms, deconvolution was implemented in the spectra between 1620/1640 and 1700/1710 cm⁻¹, as shown in Fig. 3. Fig. 3 shows the four bands in the spectra analyzed, compared to the different conformations proposed by Lefèvre *et al.*¹³ The cocoon spectrum (Fig. 3a) shows that the band at 1671 cm⁻¹ was of higher intensity and broader compared to the bands at 1652 and 1687 cm⁻¹, revealing that the cocoon structure has a tendency to incorporate a higher quantity of β -sheet conformations. However, the deconvoluted spectrum of the biofilm produced by extraction with LiBr (Fig. 3b), that there were more α -helices and β -turns than β -sheets because of the higher relative intensity and broadening of the bands at 1660 and 1679/1689 cm⁻¹, compared to that at 1670 cm⁻¹.

In the deconvoluted spectrum of the biofilm obtained by Ajisawa extraction (Fig. 3c), the results were predominantly intermediate between those obtained for

the cocoon and the biofilm extracted with LiBr. A higher intensity was observed for the band at 1667 cm^{-1} and lower intensity of the bands at 1652 and 1680 cm^{-1} , respectively related to the α -helix and β -turn conformations, despite the fact that the band at 1684 cm^{-1} was fairly broad and intense, impeding more accurate analysis.

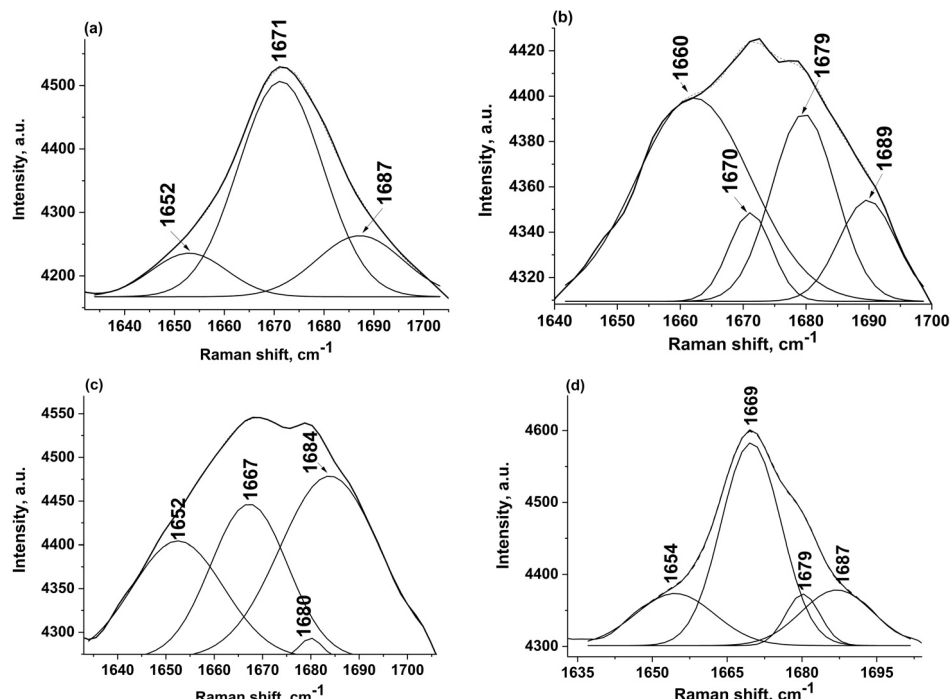


Fig. 3. Deconvoluted Raman spectra of: a) cocoon, biofilms prepared by: b) the LiBr method and c) the Ajisawa method, and d) the freeze-dried hydrogel.

These results show that the structural ordering of the biofilms is the opposite of that encountered in the cocoon, where there is a mixture of β -sheet, α -helix and β -turn conformations, exhibiting greater malleability and stability.

Similar results were obtained in other studies, in which biofilms produced by Ajisawa extraction contained slightly more β -sheets and less β -turns than those produced by solubilization with LiBr.²⁰ Defining the conformation of biofilms is particularly important and advantageous, depending on the applications envisaged. The conformation of the material can significantly influence characteristics such as biodegradation, mechanical and optical properties, and even biological compatibility conditions. For instance, a biofilm with a predominance of β -turns and α -helices would be highly soluble in water and more biodegradable compared to a biofilm with a predominance of secondary structures, such as β -sheets, but this material would be more flexible and mechanically stronger than the other.²⁰

It was observed that the dialysis time and conditions precipitated a rigid solid originating from the gel prepared from the cocoons. Based on the previous characterization of the biofilm Raman spectra, the same spectrum deconvolution procedures were performed for the freeze-dried hydrogel in the 1624–1710 cm⁻¹ range, as shown in Fig. 3d.

The deconvoluted spectrum showed narrower bands than those previously observed in the cocoon and biofilm deconvoluted spectra (Fig. 3a–c). Regarding the spectrum of the solid originating from the cocoons (Fig. 3a), in the deconvoluted spectrum of the hydrogel (Fig. 3d), the relative intensities of the bands remained the same as those in the cocoon spectrum. The band at 1679 cm⁻¹ could be observed, due to the narrower bandwidth obtained by deconvolution.

Considering that the properties of the prepared biofilms can also be better verified by thermal analysis techniques, assuming that the thermal events developed with these techniques should promote a higher or lower degree of structural disorder in the molecular organization of the fibers that form the biomaterial, these materials were subjected to temperature variations and the modifications were monitored by the differential scanning calorimetry (DSC) and thermogravimetric (TG) techniques.

Sacco and de Santana¹⁴ investigated the effect of temperature on the destabilization of the molecular conformation of silk fiber structures using confocal Raman spectroscopy and differential scanning calorimetry (DSC). The results indicated that, for the different cocoon samples, there was a drop in the β -sheet conformation compared to that of the α -helix, and this structural disordering was caused by increased temperature. Similarly, a transition was observed in the conformation from β -sheet to β -turn as a result of the temperature applied.

The DSC curves in the 230–300 °C temperature range for the biofilms obtained by the two extraction methods are shown in Fig. S-2 of the Supplementary material. The biofilms were less stable to heat conditions than the silkworm cocoon. Sacco and de Santana¹⁴ reported that at around 315 °C, the cocoon underwent an endothermal event, related to the thermal process associated with cocoon structure.

The biofilm prepared using LiBr (Fig. S-2a) exhibited an endothermal peak associated with a thermal event with a maximum of 274 °C, and for the Ajisawa biofilm at 280 °C (Fig. S-2b). Thus, the fact that the endothermal event occurred at a lower temperature for the LiBr biofilm compared to the Ajisawa biofilm must mean that the LiBr biofilm was less thermally stable due to the different aggregates present in these materials, due to stabilization of the different molecular conformations for the fibroin fibers as shown in the Raman results.

However, based on the work of Freddi *et al.*,²² the thermal degradation of fibroin biofilm at temperatures lower than 290 °C is a characteristic of amorphous

phous biofilms (silk I), *i.e.*, biofilms that have not been subjected to any kind of physical or chemical treatment to alter the structure to a more crystalline form.

With the aim of better assessing the thermal behavior of these biofilms, thermogravimetric (TG) experiments were conducted.

The thermogravimetric curves for the cocoon, biofilms and freeze-dried hydrogel at temperatures between 20 and 1000 °C, verifying residual mass, and the differential residual mass curves for each material are shown in Fig. 4.

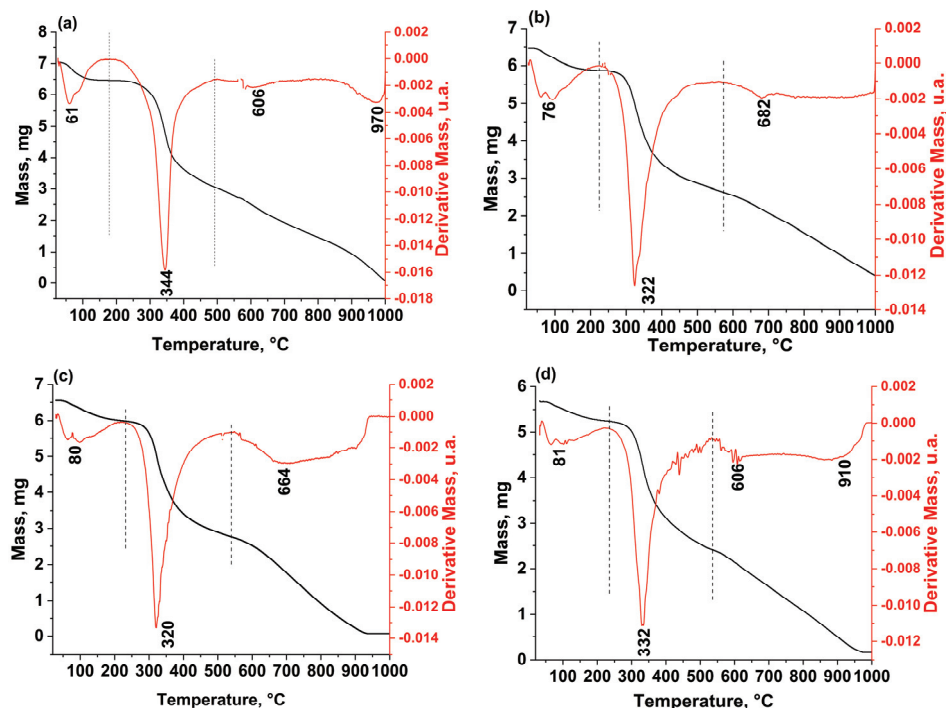


Fig. 4. Thermogravimetric curves of: a) cocoon, biofilms prepared by: b) the Ajisawa method and c) by the LiBr method, and d) the freeze-dried hydrogel.

Losses in mass of 8.1 % were observed for the cocoon (Fig. 4a), 9.4 % for the Ajisawa biofilm (Fig. 4b), 8.5 % for the LiBr biofilm (Fig. 4c) and 7.4 % for the freeze-dried hydrogel (Fig. 4d), at approximate respective maximum temperatures of 61, 76, 80 and 81 °C, which were attributed to water evaporation.

As the thermal process proceeded, different events were observed in the cocoon material, biofilms and the freeze-dried hydrogel. Around 43.5 % of the cocoon material underwent an initial decomposition process at an approximate maximum temperature of 344 °C (Fig. 4a). For the Ajisawa biofilm (Fig. 4b), the values were 40.5 % and 322 °C, and for the LiBr biofilm (Fig. 4c), 42.1 % and 320 °C. In other words, the main thermal degradation process for silk proteins

occurs because of the decomposition of the main structures of the protein molecular skeleton, showing the higher thermal stability of the cocoon material. The freeze-dried hydrogel produced intermediate results for this process, with a loss of 42.7 % at 332 °C (Fig. 4d).

However, another event was initiated close to a temperature of 492 °C, with maxima of 606 and 970 °C, decomposing 42.2 % of the cocoon structure (Fig. 4a). Similarly, at around 574 °C the Ajisawa biofilm (Fig. 4b) loses a further 33.2 % of its mass, whereas at 539 °C the LiBr biofilm (Fig. 4c) loses 41.3 %. This second event is probably attributable to carbonization. The freeze-dried hydrogel once again produced intermediate results, with a 39.7 % loss initiated at 533 °C (Fig. 4d). Residues of all materials were still observed, even at this temperature.

CONCLUSIONS

Using an adapted method from the literature for preparing biofilms by different processes, materials of high quality were prepared in terms of transparency and thermal stability.

Raman spectroscopy was found to be adequate for characterizing the structural ordering of the experimentally produced biofilms.

The results for the most rigid material, the freeze-dried hydrogel, showed a preference for the β -sheet conformation. Biofilms, which are more malleable, can show a tendency to produce a higher quantity of α -helix and β -turn conformations. The two bands related to the β -turn conformation were absent only for the cocoon material, perhaps due to the rigidity of the bonds, as shown by its higher thermal stability.

Based on the thermal analysis and Raman results, it could be inferred that the biofilms with higher amounts of β -sheet conformations could be more thermally resistant.

The fibroin solubilization processes influenced the conformations and structural ordering, as revealed by the different techniques used in this study. The fiber solubilization method for obtaining the fibroin solution can be chosen based on what is most appropriate for the intended application of the material.

SUPPLEMENTARY MATERIAL

Additional data and information are available electronically at the pages of journal website: <https://www.shd-pub.org.rs/index.php/JSCS/article/view/10850>, or from the corresponding author on request.

Acknowledgements. We would like to express our appreciation to the Spectroscopy Laboratory (SPEC) at the PROPPG/UEL Multiuser Center. This study was funded under the Paraná State's SETI project (Silk, the transformative fiber). We would also like to thank the National Council for Scientific and Technological Development for its support.

ИЗВОД
СТРУКТУРНА СТАБИЛНОСТ БИОФИЛМОВА ДОБИЈЕНИХ ОД ВЛАКАНА ЧАУРА
СВИЛЕНЕ БУБЕ

ANA LÚCIA DE SOUZA MADUREIRA FELÍCIO и HENRIQUE DE SANTANA

Departamento de Química, CCE, Universidade Estadual de Londrina, Londrina, PR 86051-990, Brazil

Биофилмови су добијени из чаура свилене бубе, *Bombyx mori*, уклањањем серицина, екстракцијом и солубилизацијом фибринских влакана, дијализом фибринских дисперзија и припремом биофилмова поступком ливења. Транспаренција биофилмова је верификована UV-видљивом спектроскопијом, а термална стабилност термогравиметријском/диференцијално сканирајућом калориметријском анализом (TG/DSC). Након припреме, очвршћивање фибринског раствора припремљеног из чаура и екстрахованог Ajisawa методом је праћено до стабилизације биофилма, применом ослабљене тоталне рефлексије (ATR-FTIR) у функцији времена. Резултати су показали да долази до конформационе промене из свила I (α -хеликс) у свила II (β -раван) структуру. Да би се унапредила карактеризација биофилмова добијених Ajisawa методом и LiBr солубилизацијом фибринских влакана, коришћена је Раманска спектроскопија за верификацију стабилности различитих молекуларних конформација влакана у овим материјалима, поређењем спектра чауре и спектара талога (лиофилизовани хидрогел) преципитираних дијализом 72 сата. Поређењем Раманских спектара биофилмова и то интензитета проширене траке карактеристичне за амид I, могуће је добити информације о конформационим променама између β -равни и флексибилних структура α -хеликса и β -завојнице. Резултати су показали дисперзију ових конформација у добијеним биофилмовима и у спектрима чврстих лиофилизованих хидрогелова, а конформација β -равни је преовлађујућа. TG и DSC криве су показале да материјал са већим садржајем β -равни показује већу термалну отпорност. Резултати добијени у овом раду доприносе бољем разумевању особина материјала који имају широку примену и бројним процесима.

(Примљено 11. јуна, ревидирано 21. јула, прихваћено 23. јула 2021)

REFERENCES

1. S. D. A. Cervantes, D. V. Cervantes, L. M. Olmo, J. L. Cenis, A. A. L. Pérez, *Mater. Sci. Eng., C* **33** (2013) 1945 (<https://dx.doi.org/10.1016/j.msec.2013.01.001>)
2. H. Yamada, H. Nakao, Y. Takasu, K. Tsubouchi, *Mater. Sci. Eng., C* **14** (2001) 41 ([https://dx.doi.org/10.1016/S0928-4931\(01\)00207-7](https://dx.doi.org/10.1016/S0928-4931(01)00207-7))
3. L. D. Koh, Y. Cheng, C. P. Teng, Y. W. Khin, X. J. Loh, S. Y. Tee, L. M. E. Ye, H. D. Yu, Y. W. Zhang, M. Y. Han, *Prog. Polym. Sci.* **46** (2015) 86 (<https://dx.doi.org/10.1016/j.progpolymsci.2015.02.001>)
4. W. I. Abdel-Fattah, N. Atwa, W. A. Ghareib, *Prog. Biomater.* **4** (2015) 77 (<https://dx.doi.org/10.1007/s40204-015-0039-x>)
5. X. Chen, Z. Shao, N. S. Marinkovic, L. M. Miller, P. Zhou, M. R. Chance, *Biophys. Chem.* **89** (2001) 25 ([https://dx.doi.org/10.1016/s0301-4622\(00\)00213-1](https://dx.doi.org/10.1016/s0301-4622(00)00213-1))
6. L. D. Koh, J. Yeo, Y. Y. Lee, Q. Ong, M. Han, B. C. K. Tee, *Mater. Sci. Eng., C* **86** (2018) 151 (<https://dx.doi.org/10.1016/j.msec.2018.01.007>)
7. Y. Qi, H. Wang, K. Wei, Y. Yang, R. Y. Zheng, I. S. Kim, K. Q. Zhang, *Int. J. Mol. Sci.* **18** (2017) 237 (<https://dx.doi.org/10.3390/ijms18030237>)
8. D. N. Rockwood, R. C. Preda, T. Yücel, X. Wang, M. L. Lovett, D. L. Kaplan, *Nat. Protoc.* **6** (2011) 1612 (<https://dx.doi.org/10.1038/nprot.2011.379>)

9. A. Sionkowska, A. Planecka, *Polym. Degrad. Stabil.* **96** (2011) 523 (<https://dx.doi.org/10.1016/j.polymdegradstab.2011.01.001>)
10. S. Krimm, J. Bandekar, *Adv. Protein Chem.* **38** (1986) 181 ([https://dx.doi.org/10.1016/S0065-3233\(08\)60528-8](https://dx.doi.org/10.1016/S0065-3233(08)60528-8))
11. Q. Lu, X. Wang, S. Lu, M. Li, D. L. Kaplan, H. Zhu, *Biomater.* **32** (2011) 1059 (<https://dx.doi.org/10.1016/j.biomaterials.2010.09.072>)
12. R. Nazarov, H. Jin, D. L. Kaplan, *Biomacromolecules* **5** (2004) 718 (<https://dx.doi.org/10.1021/bm034327e>)
13. T. Lefèvre, M. E. Rousseau, M. Pézolet, *Biophys. J.* **92** (2007) 2885 (<https://dx.doi.org/10.1529/biophysj.106.100339>)
14. B. L. Sacco, H. de Santana, *Quím. Nova* **42** (2019) 1014 (<https://dx.doi.org/10.21577/0100-4042.20170413>)
15. M. Preghennella, G. Pezzotti, C. Migliaresi, *J. Raman Spectrosc.* **38** (2007) 522 (<https://dx.doi.org/10.1002/jrs.1675>)
16. M.-E. Rousseau, T. Lefèvre, L. Beaulieu, A. Tetsuo, M. Pézolet, *Biomacromolecules* **5** (2004) 2247 (<https://dx.doi.org/10.1021/bm049717v>)
17. P. Monti, P. Taddei, G. Freddi, T. Asakura, M. Tsukada, *J. Raman Spectrosc.* **32** (2001) 103 (<https://dx.doi.org/10.1002/jrs.675>)
18. P. Monti, G. Freddi, A. Bertoluzza, N. Kasai, M. Tsukada, *J. Raman Spectrosc.* **29** (1998) 297 ([https://dx.doi.org/10.1002/\(SICI\)1097-4555\(199804\)29:4%3C297::AID-JRS240%3E3.0.CO;2-G](https://dx.doi.org/10.1002/(SICI)1097-4555(199804)29:4%3C297::AID-JRS240%3E3.0.CO;2-G))
19. S. D. Aznar-Cervantes, D. Vicente-Cervantes, L. Meseguer-Olmo, J. L. Cenis, A. A. Lozano-Pérez, *Mater. Sci. Eng., C* **33** (2013) 1945 (<https://dx.doi.org/10.1016/j.msec.2013.01.001>)
20. X. Chen, D. P. Knight, Z. Shao, F. Vollrath, *Polym.* **42** (2001) 9969 ([https://dx.doi.org/10.1016/S0032-3861\(01\)00541-9](https://dx.doi.org/10.1016/S0032-3861(01)00541-9))
21. A. Motta, L. Fambri, C. Migliaresi, *Macromol. Chem. Phys.* **203** (2002) 1658 ([https://dx.doi.org/10.1002/1521-3935\(200207\)203:10/11%3C1658::AID-MACP1658%3E3.0.CO;2-3](https://dx.doi.org/10.1002/1521-3935(200207)203:10/11%3C1658::AID-MACP1658%3E3.0.CO;2-3))
22. G. Freddi, G. Pessina, M. Tsukada, *Int. J. Biol. Macromol.* **24** (1999) 251 ([https://dx.doi.org/10.1016/s0141-8130\(98\)00087-7](https://dx.doi.org/10.1016/s0141-8130(98)00087-7)).

SUPPLEMENTARY MATERIAL TO
**Structural stability of biofilms produced from silkworm cocoon
fibers**

ANA LÚCIA DE SOUZA MADUREIRA FELÍCIO and HENRIQUE DE SANTANA*

Departamento de Química, CCE, Universidade Estadual de Londrina, Londrina,
PR 86051-990, Brazil

J. Serb. Chem. Soc. 87 (3) (2022) 331–343

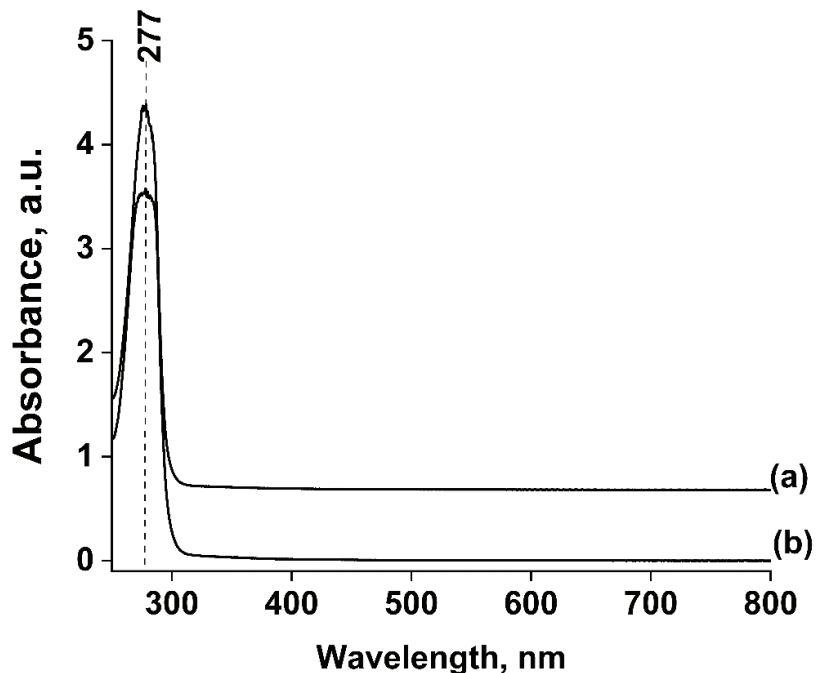


Fig. S-1. UV-Vis spectra of biofilms produced from cocoon material using: a) the Ajisawa and b) the LiBr extraction methods.

*Corresponding author. E-mail: hensan@uel.br

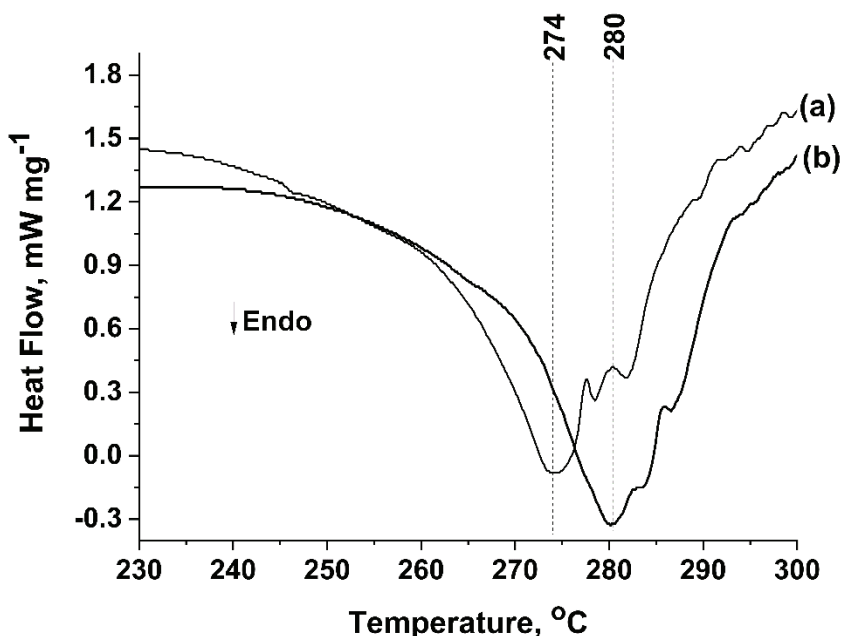


Fig. S-2. DSC curves for biofilms prepared by: a) the LiBr and b) the Ajisawa methods.



Electrocatalytic hydrogen evolution upon reduction of pyridoxal semicarbazone and thiosemicarbazone-based Cu(II) complexes

SALMA A. AL-ZAHRANI¹, VIOLETA JEVTOVIC^{1*}, KHALAF M. ALENEZI¹,
HANI EL MOLL¹, ASHANUL HAQUE¹ and DRAGOSLAV VIDOVIC²

¹Department of Chemistry, College of Science, University of Hail, Ha'il 81451, Kingdom of Saudi Arabia and ²School of Chemistry, Monash University, Clayton, Melbourne, Australia

(Received 20 May, revised 29 June, accepted 2 July 2021)

Abstract: The growing global demand for renewable energy sources has pushed renewable, green energy sources to the forefront, among which the production of hydrogen gas from water occupies a significant place. To realize this goal, researchers across the globe are developing various systems that could swiftly catalyze the hydrogen evolution reaction (HER) in the highest possible yield. In the present work, the electrocatalytic HER performances of pyridoxal semicarbazone- and thiosemicarbazone-based Cu(II) complexes, *i.e.*, $[\text{Cu}(\text{PLSC})\text{Cl}_2]$ and $[\text{Cu}(\text{PLTSC-H})\text{H}_2\text{O}]\text{Br}\cdot\text{H}_2\text{O}$) are reported. It has been unambiguously demonstrated that the complexes exhibit enviable level of HER catalytic activity. The catalytic activity of the complexes was not only the function of central metal but it was also controlled by the nature of the coordinating ligand.

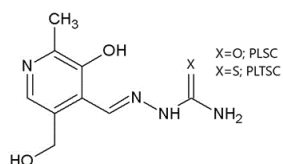
Keywords: renewable energy; cyclic voltammetry; proton-coupled electron transfer.

INTRODUCTION

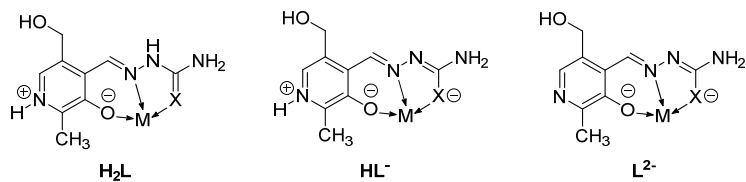
Molecular hydrogen is considered to be one of the best alternatives to non-renewable sources due to its high energy content and environment friendly nature.¹ Owing to its great potential and urgent demand towards a greener future, a plethora of research has been carried out on H₂ production. Among others, the electrocatalytic hydrogen evolution reaction (HER) has been extensively studied in the last decade.^{1–4} One of the key challenges in this area of research is to design and develop suitable electrocatalysts with low kinetic barriers and to drive the reaction at high current densities.⁵ In this context, a large number of organometallic and metal organic frameworks (MOFs) based electrocatalysts have been reported with variable performances.^{5,6} However, it was found that high per-

* Corresponding author. E-mail: v.jevtovic@uoh.edu.sa
<https://doi.org/10.2298/JSC210520050A>

formance was often achieved with the use of catalysts based on expensive metals, such as platinum.⁷ Therefore, realization of low-cost catalysts remains a challenge to the research community leading to the quest for new organic ligands and their earth abundant metal complexes with acceptable electrocatalytic activity.^{8–10} Among varieties of organic ligands, mixed ligand systems based on semicarbazone/thiosemicarbazone and pyridoxal fragments (a form of vitamin B6, Scheme 1) have attracted interest of the researchers due to multi-dimensional applications.¹¹ Basically, PLSC and PLTSC are tridentate ligands that coordinate with metal ions through the phenolic oxygen, the hydrazine nitrogen and oxygen (in the case of PLSC) or sulfur (PLTSC; Scheme 2). Accordingly, these ligands are classified as ONO or ONS ligands. The three common coordination modes of such ligands are depicted in Scheme 2. A zwitterion (H_2L) in the neutral form with deprotonated phenolic OH⁻ group and protonated “pyridine” N atom. Monoanionic form (HL^-) of the ligands PLSC and PLTSC is obtained through deprotonation of enol–thiol forms and dianionic form of ligands is obtained through further deprotonation of pyridine N atom (L^{2-}).



Scheme 1. Structural formulas and abbreviations of pyridoxal semicarbazone (PLSC; $X = O$) and thiosemicarbazone (PLTSC; $X = S$).



Scheme 2. Coordination modes and ligand forms for PLSC and PLTSC ligands.

A thorough literature survey indicated that, although a significant number of transition metals complexes with PLTSC and PLSC has been synthesized,^{11–17} the catalytic activities of such complexes have rarely been studied.^{18–21} Owing to this, it was envisioned that these complexes could be good candidates for cyclic voltammetry (CV) measurements and electrocatalytic hydrogen production (H_2) *via* proton reduction. Motivated by this, herein the electrocatalytic HER performances of pyridoxal semicarbazone- and thiosemicarbazone-based Cu(II) complexes, *i.e.*, $[\text{Cu}(\text{PLSC})\text{Cl}_2]$ and $[\text{Cu}(\text{PLTSC}-\text{H})\text{H}_2\text{O}]\text{Br}\cdot\text{H}_2\text{O}$, are reported.

EXPERIMENTAL

All chemicals were obtained from Sigma–Aldrich or Across Organics and used as received. Solvents were dried according to available literature methods.²² Cyclic voltammetry

experiments were realized using an Autolab PGSTAT 128 potentiostat. The electrochemical cell containing 5 ml of a solution of electrolyte $[\text{NBu}_4][\text{BF}_4]$, 0.2 M in DMF, was degassed with nitrogen gas A conventional three-electrode arrangement was employed, consisting of a vitreous carbon working electrode (GCE, 0.07 cm²), a platinum wire as the auxiliary electrode and Ag/AgCl as the reference electrode. All potentials in the paper are referred to Ag/AgCl scale. Ligands (PLSC and PLTSC) and corresponding Cu(II) complexes were synthesized following a reported procedure.¹¹

Synthesis of PLSC ligand ($\text{PLSC}\cdot\text{HCl}\cdot\text{H}_2\text{O}$)

To a warm mixture of pyridoxal hydrochloride (3.10 g, 15 mmol) and semicarbazide hydrochloride (1.60 g, 15 mmol) in 30 mL water, $\text{Na}_2\text{CO}_3\cdot 10\text{H}_2\text{O}$ (4.5 g, 25 mmol) was added in portions. After stirring for 5 h, the obtained microcrystalline yellow deposit was filtered off, washed with H_2O and dried to realize the final product. Yield: 3.70 g (95 %).

Synthesis of PLTSC ligand ($\text{PLTSC}\cdot 3\text{H}_2\text{O}$)

To a mixture of pyridoxal hydrochloride (2.03 g, 10 mmol) and thiosemicarbazide (0.91 g, 10 mmol) dissolved in 20 mL of methanol, LiOAc (0.70 g, 10 mmol) was added and refluxed for 45 min. The yellow deposit of the ligand was isolated very fast and washed with MeOH. Yield: 2.42 g (82 %).

Synthesis of complex $\text{Cu}(\text{PLSC})\text{Cl}_2$

PLSC·HCl·H₂O ligand (0.10 g, 0.35 mmol) was dissolved in 10 mL of MeOH. To this solution, 0.15 g (0.88 mmol) $\text{CuCl}_2\cdot 2\text{H}_2\text{O}$ was added and warmed. The resulting green solution was filtered off and the obtained gleaming small crystals were washed with MeOH after 25 h. Yield: 0.10 g (79.8 %).

Synthesis of complex $[\text{Cu}(\text{PLTSC-H})\text{H}_2\text{O}]\text{Br}\cdot\text{H}_2\text{O}$

A mixture of PLTSC·3H₂O (0.20 g, 0.7 mmol) and CuBr_2 (0.22 g, 1 mmol) in 30 mL of H₂O was heated until complete dissolution of the reactants. The resulting green solution was left at room temperature for 50 h. The obtained crystals were filtered off and dried under vacuum. Yield: 0.24 g (88 %).

RESULTS AND DISCUSSION

The ligands and their corresponding Cu(II) complexes, *i.e.*, $[\text{Cu}(\text{PLSC})\text{Cl}_2]$ and $[\text{Cu}(\text{PLTSC-H})\text{H}_2\text{O}]\text{Br}\cdot\text{H}_2\text{O}$, were obtained in good yields and purities following a reported procedure.⁸ The molecular compositions of the complexes were determined using various analytical techniques prior to the catalytic studies. It has been reported that the PLSC ligand adapted its neutral form while PLTSC its monoanionic form upon coordination with Cu(II) ion and the formation of the title compounds.¹¹

Cyclic voltammetry of ($[\text{Cu}(\text{PLSC})\text{Cl}_2]$ and $[\text{Cu}(\text{PLTSC-H})\text{H}_2\text{O}]\text{Br}\cdot\text{H}_2\text{O}$)

The studied complexes were further characterized by cyclic voltammetry in DMF solution with 0.2 M tetrabutylammonium tetrafluoroborate, $[\text{NBu}_4][\text{BF}_4]$ and 2.5 mM $[\text{Cu}(\text{PLSC})\text{Cl}_2]$ or $[\text{Cu}(\text{PLTSC-H})\text{H}_2\text{O}]\text{Br}\cdot\text{H}_2\text{O}$. The Cu(II) complex of the *O*-containing ligand exhibited two reduction peaks with E_p^{red} of -0.10 and -1.48 V for $\text{Cu}^{2+}/\text{Cu}^+$ and Cu^+/Cu , respectively. The corresponding

oxidation peaks appear at -0.7 V (retarded because of the resistivity) and 0 V. In addition, a third oxidation peak appeared at -0.25 V that may be attributed to the ligand.²³ However, the two reduction peaks of the copper complex of the PLTSC ligand appeared at -0.50 ($\text{Cu}^{2+}/\text{Cu}^+$) and -1.25 V (Cu^+/Cu), in addition to the reduction peak of the ligand at -0.81 V. Note that the latter reduction peak was attributed to the ligand based on cyclic voltammetry of the free ligand (Fig. 1).²³ The differences in electrochemical behavior between $[\text{Cu}(\text{PLSC})\text{Cl}_2]$ and $[\text{Cu}(\text{PLTSC-H})\text{H}_2\text{O}]\text{Br}\cdot\text{H}_2\text{O}$ are attributed to the presence of sulfur atom in the PLTSC ligand. The corresponding oxidation peaks appeared at -1.0 , -0.7 and -0.45 V.

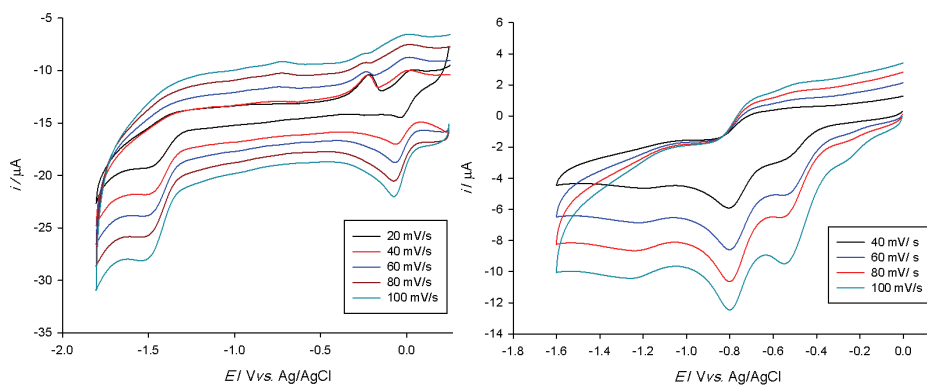


Fig. 1. Cyclic voltammetry of 2.5 mM $[\text{Cu}(\text{PLSC})\text{Cl}_2]$ (left) and 2.5 mM $[\text{Cu}(\text{PLTSC-H})\text{H}_2\text{O}]\text{Br}\cdot\text{H}_2\text{O}$ (right) DMF solutions containing 0.2 M $[\text{NBu}_4]\text{[BF}_4]$ at a carbon electrode vs. Ag/AgCl with different scan rate under nitrogen.

Hydrogen evolution reaction (HER) studies

Both Cu(II) complexes were studied as electrocatalysts for proton reduction into molecular hydrogen using acetic acid as the proton source. The proton reduction occurred at the second reduction peak, where a clear increase of the current at -1.53 and -1.25 V for $[\text{Cu}(\text{PLSC})\text{Cl}_2]$ and $[\text{Cu}(\text{PLTSC-H})\text{H}_2\text{O}]\text{Br}\cdot\text{H}_2\text{O}$, respectively, were noticed (Fig. 2). It is noteworthy that these two voltages were marked, respectively, with shifts of 320 and 600 mV compared to the electrocatalysts-free medium (Fig. 3, Table I). Remarkably, the current increased with the number of acid equivalents. The highest electrocatalytic activity was observed in the presence of twelve equivalents of acetic acid (relative to the catalyst mole number) for the complex with the S-containing ligand, while for the complex with O-containing ligand, the highest activity was achieved in the presence of eight equivalents (Fig. 4). These results confirm the beneficial effect of using S-containing complexes instead of O-containing ones. Evidently, better activity was highlighted for the S-containing copper complex with maximum current 4.5 time higher than the acid-free medium, while a maximum current 3.5 time

higher was observed in the presence of $[\text{Cu}(\text{PLSC})\text{Cl}_2]$ (Fig. 5). Moreover, the current density vs. acetic acid concentration relationship obtained at potentials of -1.53 and -1.25 V for $[\text{Cu}(\text{PLSC})\text{Cl}_2]$ and $[\text{Cu}(\text{PLTSC-H})\text{H}_2\text{O}]\text{Br}\cdot\text{H}_2\text{O}$, respectively, have been plotted. The highest electrocatalytic activity was observed in the presence 20 mM acetic acid, which corresponds to 12 equivalents of acid with respect to the catalyst concentration (Fig. 4).

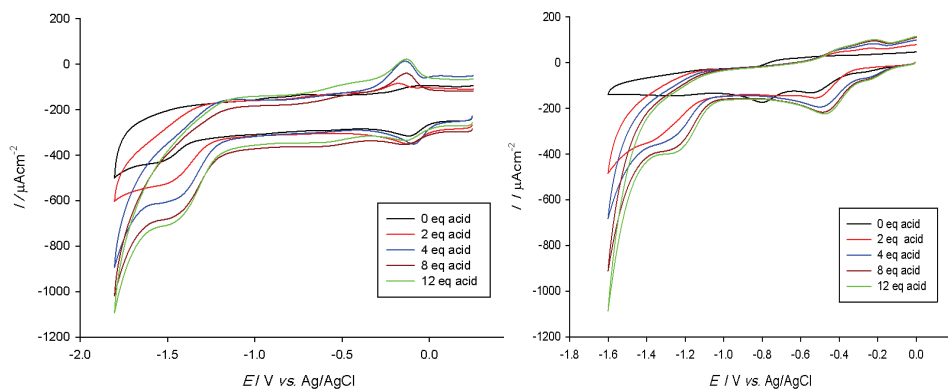


Fig. 2. Cyclic voltammetry of 2.5 mM $[\text{Cu}(\text{PLSC})\text{Cl}_2]$ (left) and 2.5 mM $[\text{Cu}(\text{PLTSC-H})\text{H}_2\text{O}]\text{Br}\cdot\text{H}_2\text{O}$ (right) DMF solutions containing 0.2 M $[\text{NBu}_4]\text{[BF}_4]$, scan rate 100 mV s⁻¹ at a vitreous carbon electrode under N_2 , in the presence of 2-12 equivalents of acetic acid.

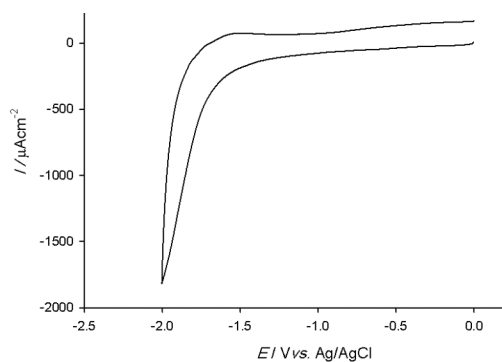


Fig. 3. Cyclic voltammetry obtained in a catalyst-free solution containing 20 mM acetic acid in $[\text{Bu}_4\text{N}]\text{[BF}_4]$ -DMF, scan rate 100 mV s⁻¹ at a vitreous carbon electrode under N_2 .

TABLE I. Potentials of the reduction wave of CH_3COOH vs. Ag/AgCl in the absence or presence of the different complexes and the second reduction peak shift of the studied complexes

DMF solution of CH_3COOH	E / V vs. Ag/AgCl	Shift ^a , mV
Electrocatalysts-free	-1.85	0
In the presence of $[\text{Cu}(\text{PLSC})\text{Cl}_2]$	-1.53	320
In the presence of $[\text{Cu}(\text{PLTSC-H})\text{H}_2\text{O}]\text{Br}\cdot\text{H}_2\text{O}$	-1.25	600

^aCompared to the proton reduction potential in electrocatalyst free medium

The rate constants were estimated using the approach of Dubois and co-worker and the i_{cat}/i_0 data, based on Eq. (1):

$$k_{\text{obs}} = 0.1992(Fv/RTn^2)(i_{\text{cat}}/i_0)^2 \quad (1)$$

where F , v , R , T , i_{cat} and i_0 are the Faraday constant, the scan rate, the gas constant, the temperature, the peak catalytic current and the peak current in the absence of acetic acid, respectively, and n is the number of electrons.²⁴

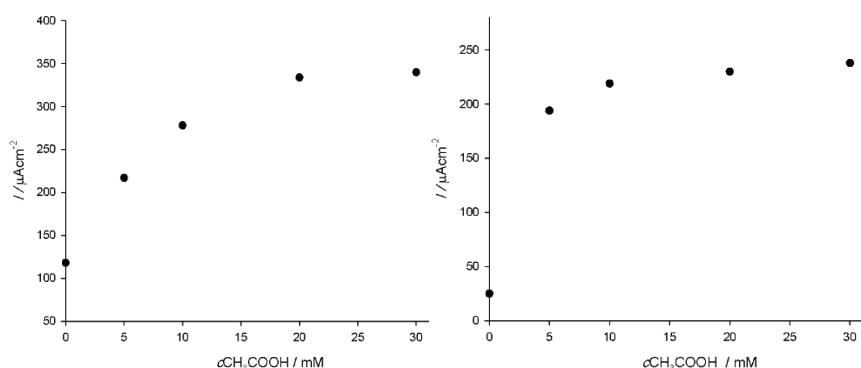


Fig. 4. The current density vs. acetic acid concentration relationship for $[\text{Cu}(\text{PLSC})\text{Cl}_2]$ obtained at a potential of -1.53 V (left) and for $[\text{Cu}(\text{PLTSC-H})\text{H}_2\text{O}]\text{Br}\cdot\text{H}_2\text{O}$ obtained at a potential of -1.25 V (right).

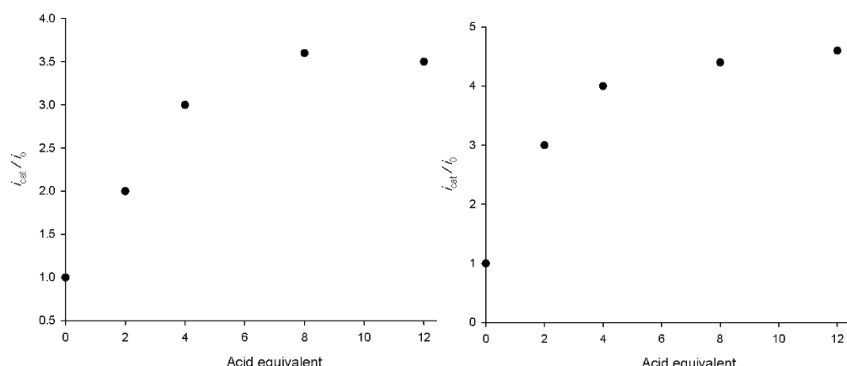


Fig. 5. Effect of the acid concentration on the i_p/i_0 ratio at a vitreous carbon electrode of $[\text{Cu}(\text{PLSC})\text{Cl}_2]$ (left) and $[\text{Cu}(\text{PLTSC-H})\text{H}_2\text{O}]\text{Br}\cdot\text{H}_2\text{O}$ (right) recorded at -1.53 and -1.25 V, respectively (catalytic reduction of the proton peak).

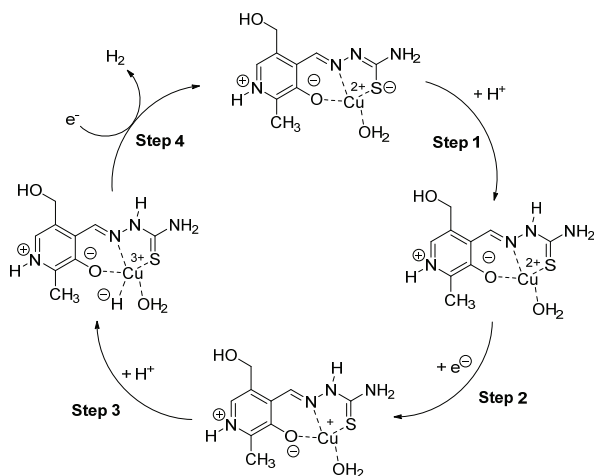
The electrocatalytic rate constants (k_{cat} , 25 °C) in the presence of these complexes at a vitreous carbon electrode are reported in Table II from the magnitude of i_{cat}/i_0 in the acid independent regime.

TABLE II. The rate constant (k_{obs} , 25 °C) for catalysis at vitreous carbon (8 eq. acid)

Complex	i_{cat}/i_0	$k_{\text{obs}} / \text{s}^{-1}$
[Cu(PLSC)Cl ₂]	3.6	10.10
[Cu(PLTSC-H)H ₂ O]Br H ₂ O	9.4	68.50

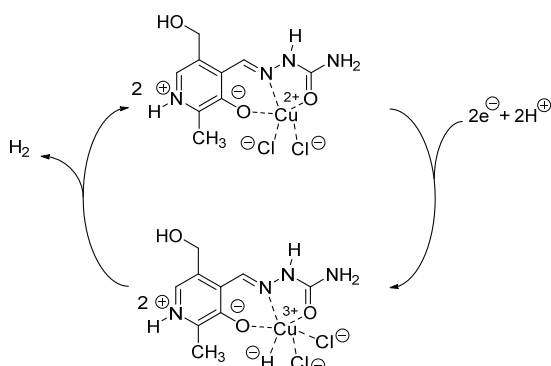
Possible mechanism of HER

As electrochemical analysis has shown, copper in which the PLSC ligand was in its neutral form was much less catalytically active than copper in which the PLTSC ligand was coordinated in the deprotonated form HL⁻. Hence, it is proposed that the catalytic abilities of the complexes primarily depend on the nature and the coordinated form of the ligand, as observed by the CV measurements. Thus, the complex that contains the PTLSC ligand in its mono-anionic form will initially accept a proton at one of the N atoms found at the ligand backbone (Step 1, Scheme 3). This process will then be followed by sequential electron (Step 2) and proton (Step 3) transfers or these two steps could occur in a concerted step, *i.e.*, *via* proton-coupled electron transfer (PCET).^{25,26} Simultaneous heterolytic cleavages of the N–H and Cu–H bonds and electron transfer steps (Step 4, Scheme 3) were proposed to occur to generate a molecule of hydrogen. On the other hand, as the PLSC-containing complex contains the ligand in the neutral form, it is proposed that its electrocatalytic activity occurs primarily at the metal center without involving the ligand and hence lessening its overall activity (Scheme 4). In this case, PCET is depicted for the first step followed by homolytic cleavage of the Cu–H bond, *via* reductive elimination, involving two independent complexes to form molecular hydrogen.²⁶



Scheme 3. Proposed electrochemical generation of H₂ as catalyzed by [Cu(PLTSC-H)H₂O] Br · H₂O. Formal charges for several atoms, including the central metal ion, are depicted for clarity.

Actually, according to the proposed mechanisms depicted in Schemes 3 and 4, it could be assumed that the catalytic ability of $[\text{Cu}(\text{PLTSC-H})\text{H}_2\text{O}] \text{Br}\cdot\text{H}_2\text{O}$ would be twice as high in comparison to that of $[\text{Cu}(\text{PLSC})\text{Cl}_2]$. The ligand protonation would allow for the formation of a single H_2 molecule per catalytic cycle for the former complex, while only half of H_2 per proposed catalytic cycle involving the latter complex. Indeed, if the results of the CV measurements in Table I are examined, it could clearly be observed that the second reduction peak shift is twice as large for the PLTSC-containing complex (600 vs. 320 mV). Similarly, the value for i_{cat}/i_0 (Table II) is also significantly higher for $[\text{Cu}(\text{PLTSC-H})\text{H}_2\text{O}] \text{Br}\cdot\text{H}_2\text{O}$ (9.4) in comparison to $[\text{Cu}(\text{PLSC})\text{Cl}_2]$ (3.6). These observations strongly suggest that in order to create more efficient catalysts based on transition metal complexes incorporating semicarbaone- and thiosemicarbazone pyridoxal ligands, one should strive to synthesize complexes in which the ligands would be coordinated in mono- or di-deprotonated forms.



Scheme 4. Proposed electrochemical generation of H_2 as catalyzed by $[\text{Cu}(\text{PLSC})\text{Cl}_2]$. Formal charges for several atoms, including the central metal ion, are depicted for clarity.

This could possibly be achieved by modifying the pH medium of the solution used in the synthesis of these complexes. Acidic medium during synthesis would favor neutral coordination forms of PLSC and PLTSC ligands.⁸ Certainly, the role of the central metal (in this case copper) is also not completely insignificant. The challenge would be to synthesize complexes containing PLSC and PLTSC ligands with metals such as Ru, Ir or Rh, as these metals have already exhibited excellent activity in numerous catalytic processes (*e.g.*, Wilkinson, Grubbs and Schrock complexes).

CONCLUSIONS

This work presented captivating possibilities that a targeted design of coordination systems could lead to efficient electrocatalysts for the hydrogen evolution reaction. The cyclic voltammetry measurement performed on a couple of $\text{Cu}(\text{II})$

compounds coordinated by either the O-containing PLSC or the S-containing PLTSC ligand showed their undoubted ability to electro-catalyze reduction of the CH₃COOH acidic proton and convert it into molecular hydrogen. The better activity for the complex containing the deprotonated form of the coordinated ligand should also be highlighted. This valuable information would be considered in the future as an extremely useful guideline for the synthesis of electrocatalysts based on PLSC or PLTSC ligands.

Acknowledgement. This research was funded by Scientific Research Deanship at University of Hail, Kingdom of Saudi Arabia, through Project number RG-20072.

ИЗВОД

ЕЛЕКТРОКАТАЛИЗА ИЗДВАЈАЊА ВОДОНИКА НАКОН РЕДУКЦИЈЕ КОМПЛЕКСА БАКРА (II) НА БАЗИ ПИРИДОКСАЛНИХ ПОЛУ- И ТИОСЕМИКАРБАЗОНА

SALMA A. AL-ZAHRANI¹, VIOLETA JEVTOVIC¹, KHALAF M. ALENEZI¹, HANI EL MOLL¹, ASHANUL HAQUE¹
и DRAGOSLAV VIDOVIC²

¹*Department of Chemistry, College of Science, University of Hail, Ha'il 81451, Kingdom of Saudi Arabia*

²*School of Chemistry, Monash University, Clayton, Melbourne, Australia*

Растућа глобална потражња за обновљивим изворима енергије довела је у први план обновљиве, зелене изворе енергије, међу којима производња водоника из воде заузима значајно место. Да би остварили овај циљ, истраживачи широм света развијају катализатор који би могао брзо да катализује реакцију издвајања водоника (HER) у највећем могућем приносу. У овом раду извештавамо о електрокаталитичким HER перформансама комплекса Cu (II) на бази пиридоксалних сеmi- и тиосемикарбазона, тј. ([Cu(PLSC)Cl]₂ и [Cu (PLTSC-H) H₂O]Br·H₂O). Недвосмислено смо показали да комплекси показују завидан ниво HER катализичке активности. Катализичка активност комплекса није била само функција централног метала већ и контролисана врстом координирајућег лиганда.

(Примљено 20. маја, ревидирано 29. јуна, прихваћено 2. јула 2021)

REFERENCES

1. J. Zhu, L. Hu, P. Zhao, L. Lee, K. Wong, *Chem. Rev.* **120** (2020) 851 (<https://doi.org/10.1021/acs.chemrev.9b00248>)
2. J. Yu, Y. Dai, Q He, D. Zhao, Z. Shao, M. Ni, *MRE* **120** (2021)100024 (<https://doi.org/10.1016/j.matre.2021.100024>)
3. Y. She, Z. Lyu, M. Zhao, R. Chen, Q. Nguyen, Y. Xia, *Chem. Rev.* **121** (2021) 649 (<https://doi.org/10.1021/acs.chemrev.0c00454>)
4. Z. Zhou, Z. Pei, L. Wei, S. Zhao, X. Jian,Y. Chen, *Energy Environ. Sci.* **13** (2020) 3185 (<https://doi.org/10.1039/D0EE01856B>)
5. S. Roy, Z. Huang, A. Buhunia, A. Castner, A. Gupta, X. Zou, S. Ott, *J. Am. Chem. Soc.* **141** (2019) 15942 (<https://doi.org/10.1021/jacs.9b07084>)
6. C. Chen, T. Chiou, H. Chang, W. Li, C. Tung, W. Liaw, *Sustain. Energy Fuels* **3** (2019) 2205 (<https://doi.org/10.1039/C9SE00371A>)

7. N. Cheng, S. Stambula, D. Wang, M. Banis, J. Liu, A. Riese, B. Xiao, R. Li, T. Sham, L. Liu, G. Botton, X. Sun, *Nat. Commun.* **7** (2016) 13638 (<https://doi.org/10.1038/ncomms13638>)
8. H. Tang, E. N. Brothers, C. A. Grapperhaus, M. B. Hall, *ACS Catal.* **10** (2020) 3778 (<https://doi.org/10.1021/acscatal.9b04579>)
9. H. Shao, S. K. Muduli, P. D. Tran, H. S. Soo, *Chem. Commun.* **52** (2016) 2948 (<https://doi.org/10.1039/C5CC09456A>)
10. A. Z. Haddad, B. D. Garabato, P. M. Kozlowski, R. M. Buchanan, C. A. Grapperhaus, *J. Am. Chem. Soc.* **138**, **25** (2016) 7844 (<https://doi.org/10.1021/jacs.6b04441>)
11. V. Jevtovic, *Cu, Fe, Ni and V Complexes with Pyridoxal Semicarbazones*, Lap Lambert Publication, Saarbrücken, 2010 (<https://www.amazon.com/complexes-pyridoxal-semicarbazones-properties-structural/dp/3838351339>)
12. V. M. Leovac, V. S. Jevtovic, L. S. Jovanovic, G. A. Bogdanovic, *J. Serb. Chem. Soc.* **70** (2005) 423 (<https://doi.org/10.2298/JSC0503393L>)
13. S.A'Shidhani, M. Al Bouromi, S. Al Ameri, S. Al Ghawi, V. Jevtovic, *Am. J. Chem.* **6** (2016) 8 (<https://doi.org/10.5923/j.chemistry.20160601.02>)
14. V. Jevtovic, D. Vidovic, *Acta Cryst., E* **66(Pt.4)** (2010) 408 (<https://doi.org/10.1107/S1600536810003570>)
15. V. Jevtovic, D. Cvetkovic, D. Vidovic, *JICS* **8** (2011) 727 (<https://doi.org/10.1007/BF03245904>)
16. D. Vidovic, A. Radulovic, V. Jevtovic, *Polyhedron* **30** (2011) 16 (<https://doi.org/10.1016/j.poly.2010.09.022>)
17. N. Knezevic, V. Leovac, V. Jevtovic, S. Grgurie-Sipka, T. Sabo, *Inorg. Chem. Comm.* **6** (2003) 561 ([https://doi.org/10.1016/S1387-7003\(03\)00041-8](https://doi.org/10.1016/S1387-7003(03)00041-8))
18. R. Manikandan, P. Anitha, G. Prakash, P. Vijayan, P. Viswanathamurthi, *Polyhedron* **81** (2014) 619 (<https://doi.org/10.1016/j.poly.2014.07.018>)
19. R. Manikandan, P. Anitha, P. Viswanathamurthi, J. G. Maleck, *Polyhedron* **119** (2016) 300 (<https://doi.org/10.1016/j.poly.2016.09.005>)
20. R. Manikandana, P. Anithaa, G. Prakasha, P. Vijayana, P. Viswanathamurthi, R. Jay Butcher, J. G. Malecki, *J. Mol. Catal., A* **398** (2015) 312 (<https://doi.org/10.1016/j.poly.2016.09.005>)
21. J. Pisk, B. Prugovecki, D. Matkovic-Calogović, R. Poli, D. Agustin, V. Vrdoljak, *Polyhedron* **33** (2012) 441 (<https://doi.org/10.1016/j.poly.2011.12.003>)
22. D. Perrin, W. Armarego, D. Perrin, *Purification of Laboratory Chemicals*, Pergamon, New York, 1988 (<https://doi.org/10.1002/recl.19881071209>)
23. V. Jevtovic, K. Alenezi, H. El Moll, A. Haque, J. Humaidi, S. A. Al-Zahrani, D. Vidovic, *Int. J. Electrochem. Sci.* **16** (2021) 210731 (<https://doi.org/10.20964/2021.07.61>)
24. T. Liu, D. L. Du Bois, R. M. Bullock, *Nat. Chem.* **5** (2013) 228 (<https://doi.org/10.1038/nchem.1571>)
25. B. H. Solis, S. Hammes-Schiffer, *Inorg. Chem.* **53** (2014) 6427 (<https://doi.org/10.1021/ic5002896>)
26. M. Drosou, F. Kamatsos, C. A. Mitsopoulou, *Inorg. Chem. Front.* **7** (2020) 37 (<https://doi.org/10.1039/C9QI01113G>).



Flotator Oxal as the plasticizer for suspension PVC

IRINA P. TRIFONOVA*, JULIA A. RODICHEVA, ANNA E. SHEVELEVA,
VLADIMIR A. BURMISTROV and OSCAR I. KOIFMAN

Research Institute of Macroheterocycles, Ivanovo State University of Chemistry and
Technology, Sheremetevskiy Avenue 7, 153000 Ivanovo, Russia

(Received 17 August, revised 11 October, accepted 9 November 2021)

Abstract: Flotator Oxal, a mixture of dioxane ethers and alcohols, was studied as a plasticizer for suspension PVC in comparison with the well-known dibutyl phthalate (DBP) and di-(2-ethylhexyl) phthalate (DOP). The rheological parameters and gelation ability of the plasticizers were determined, and the values of the storage modulus and tangent of mechanical loss angle in the glassy and rubbery states were measured by the DMA method, and the glass transition temperatures were determined. The deformation-strength properties and rigidity of polymer films were tested before and after light-thermal aging. Oxal was shown to reveal a fairly low viscosity and high gelation properties in relation to PVC. At the same time, its ability to reduce the glass transition temperature and elasticize the polymer in the glassy and rubbery state is somewhat lower than that of phthalate plasticizers. PVC samples plasticized with DBP have the highest resistance to light-thermal aging.

Keywords: phthalates; dynamic viscosity; polyvinyl chloride; DMA method.

INTRODUCTION

Plasticizers play an irreplaceable role in the manufacture of flexible materials based on rigid-chain polymers.¹ Initially, cellulose ethers, poly(vinyl acetate) and its copolymers² were used as plasticizable polymers. Currently, the main consumer of plasticizers is the production of flexible PVC materials, such as films, linoleum, artificial leather, awning materials, etc.³

It is customary to distinguish between internal plasticization associated with the addition of plasticizing fragments into macromolecules of rigid-chain polymers due to covalent bonding^{4–6} and external – by introducing special plasticizers without chemical interaction. Among PVC plasticizers, the most common are esters of organic acids (phthalic, adipic, trimellitic, sebacic, azelaic), as well as phosphoric acid.^{7,8} To reduce volatility, polymer plasticizers are utilized, in

* Corresponding author. E-mail: trifonova@isuct.ru
<https://doi.org/10.2298/JSC210817093T>

particular polyesters.⁹ In addition a large group is made up of the so-called secondary plasticizers (extenders), used in conjunction with primary ones. The most common among them are chlorinated hydrocarbons.³ In recent decades, much attention has been paid to the search for biodegradable plasticizers of various nature,^{10–13} which enables a number of environmental protection and health safety problems to be solved¹⁴ and in some cases to combine plasticizing and the antipyretic function of a biodegradable additive.¹⁵

The most widespread plasticizers based on phthalic acid esters have been used for almost 100 years to change the elastic properties of poly(vinyl chloride).¹ Phthalate plasticizers effectively reduce the pour point and the glass transition temperature of PVC.⁶ Nevertheless, there is a permanent search for new plasticizers that, with high efficiency, would have a lower tendency to diffuse onto the product surface, less volatility at elevated temperatures, and a lower cost.¹

Over the past several decades, the use of a high-boiling by-product Edos (TU 2493-003-13004749-93) as PVC plasticizer has been actively discussed.^{16–21} It is formed in the manufacture of 4,4-dimethyl-1,3-dioxane by condensation of isobutylene with formaldehyde. In one turn, flotator Oxal is the by-product of Edos (technical requirements 2452-015-48158319-2009). This product contains about 50 % dioxane ethers and alcohols and about 50 % mixtures of 1, 2 and 3 atomic alcohols.²⁰

The successful application of flotator Oxal as a plasticizer in the production of plastisols based on emulsion PVC E was described.^{16–18} The influence of Oxal on the properties of composites based on suspension PVC has practically not been studied. Therefore, the estimation of the plasticizing action of Oxal performed in this work seems to be very actual.

EXPERIMENTAL

Materials

Suspension PVC Ongrovil S-5070 was obtained from BORSODCHEM (Hungary). Dibutyl phthalate (DBP) and di-(2-ethylhexyl) phthalate (DOP) were purchased from “Ural plasticizers plant” (Russia) and used without purification. Flotator Oxal T-92 (Technical requirements: 20.59.59-029-05766801-2016) was purchased from “Nizhnekamskneftekhim” (Russia), stabilizer Baerostab UBZ 751 – from “Baerlocher GmbH” (Germany).

Film preparation

To study the mechanical and thermophysical properties of the composites, films were produced from PVC melts. The compositions contained 70.2 % PVC, 1.7 % Baerostab UBZ 751 and 28.1 % plasticizer. Dibutyl phthalate (DBP) and di-2-ethylhexyl phthalate (DOP) were chosen for comparison with Oxal. PVC, plasticizer and stabilizer were mixed, then heated for 30 min at 120 °C. The final mixing and formation of the film were performed on rollers at 150 °C for 5–6 min. To achieve a fixed thickness, the films were pressed at 160 °C and 5 MPa for 4 min, followed by cooling in a mold.

Measurements

Rheological tests of plasticizers were carried out in accordance with ASTM D2983-09 on a Brookfield DV-II+ rotary viscometer equipped with Thermosel, in the range of shear rates from 0 to 186 s⁻¹ and temperatures 22–45 °C. The size of PVC particles was determined using a polarizing microscope POLAM R-211 (magnification 75.6 times).

DMA was performed on a DMA Eplexor 25N (NETZSCH-Gerätebau GmbH) in the tensile-film mode. The specimens 70.0 mm × 7.0 mm × 0.4 mm were measured from –30 to 80 °C with a frequency of 1 Hz and a temperature ramp of 1 °C min⁻¹. The storage modulus E' and $\tan \delta$ were recorded as a function of temperature. The glass transition temperature was determined according to ASTM D7028-07(2015).

The tensile strength and elongation at break were measured using a testing machine 2099-P-5 (“Tochpribor”, Russia) at 25 °C before and after light-heat aging according to ISO527-2:2012. The length of the films was equal to 170 mm and the stretching speed was 25 mm min⁻¹. The measurements of the mechanical properties of the composite films were made with 5 replicates of each composition.

Accelerated aging was realized in accordance with ASTM G151-19 and D3045-18. Ultra-violet irradiation was performed with mercury-quartz lamps DRT-400, exposure time 36 h at 70 °C. The hardness of films before and after UV light-thermal aging was determined on a PMZh-12 M device. The hardness was assumed to be equal to the load required for deflection of an elementary sample bent into a ring by 1/3 of the diameter. Test conditions corresponded to Gost 8977 (ball weight 0.86 g, sample size 20 mm × 95 mm).

RESULTS AND DISCUSSION

Rheological characteristics of plasticizers essentially influence the technological processing parameters of flexible PVC, especially in the case of using plastiols.^{16–18} In this regard, the rheology of the product Oxal was studied in comparison with the most common phthalate plasticizers: dibutyl phthalate (DBP) and di-(2-ethylhexyl) phthalate (DOP) (see Experimental). The values of dynamic viscosity were measured in the shear rate range 0–186 s⁻¹. All plasticizers studied were found to behave like Newtonian liquids.²² The simulation of temperature semilogarithmic dependencies (Fig. 1) according to the Frenkel–Eyring Equation:²³

$$\eta = \frac{N_A \hbar}{V} e^{\frac{-\Delta S^\#_{VF}}{R}} e^{\frac{\Delta H^\#_{VF}}{RT}} \quad (1)$$

where η is the viscosity, V the mole volume, $\Delta S^\#_{VF}$ and $\Delta H^\#_{VF}$ the changes in activation entropy and enthalpy, respectively, of viscous flow, allowed the flow activation parameters to be calculated, which together with the viscosity at 25 °C are presented in Table I.

An analysis of these data indicates a slightly lower viscosity of Oxal (25 °C) than that of DOP, but higher than that of DBP. The free activation energy, $\Delta G^\#_{VF}$, of viscous flow follows the same trends. Simultaneously, the ratio of the activation parameters of Oxal are completely different than those of the phthalate plasticizers (Table I) – lower enthalpy and practically zero entropy of activation. This testifies

to differences in the flow mechanism of the studied fluids. It is known that the value of ΔH^\neq_{VF} is associated with the size of the molecule or its fragment involved in the momentum transfer in viscous flow.²⁴ Therefore, the activation enthalpy of DOP is slightly higher than that of DBP. Thus, a low Oxal value indicates a weaker effect of temperature on the viscosity (Fig. 1) and a smaller volume of the momentum transfer element.

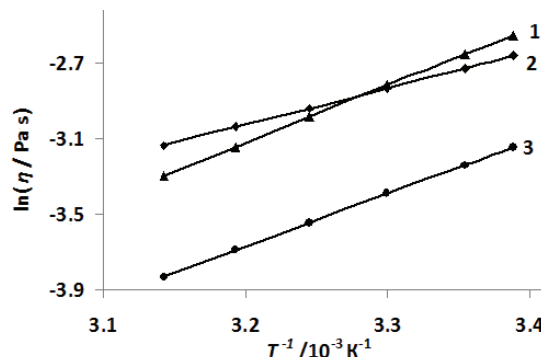


Fig. 1. Temperature dependence of the logarithm of the dynamic viscosity for plasticizers: 1 – DOP, 2 – Oksal, 3 – DBP.

TABLE I. Rheological parameters of the considered plasticizers

Plasticizer	$\eta / \text{mPa s}$ ($\gamma = 27.9 \text{ s}^{-1}$, $t = 25 \text{ }^\circ\text{C}$)	ΔH^\neq_{VF} $\text{kJ} \cdot \text{mol}^{-1}$	ΔS^\neq_{VF} $\text{J} \cdot \text{mol}^{-1} \cdot \text{K}^{-1}$	ΔG^\neq_{VF} $\text{kJ} \cdot \text{mol}^{-1} (t = 25 \text{ }^\circ\text{C})$
DOP	70.5	25.1	29.8	16.2
Oxal	65.4	16.1	0.2	16.1
DBP	39.4	23.9	30.7	14.8

One of the most important properties of a plasticizer is its gelation ability for a given polymer.⁶ The combination of suspension PVC with plasticizers begins with their mechanical mixing and is accompanied by swelling of the polymer particles and an increase in the particle size.³ The ratio of the size of the swollen PVC particles to the size of the initial particles allows the effective absorption of the plasticizer during hot mixing to be evaluated and, consequently, its gelation properties (Table II).

TABLE II. Average particle size of PVC and swelling degree after combining with plasticizer at 120 °C within 30 min

PVC composite	Average particle size, μm	Swelling degree of the PVC particles
Initial PVC	79.6	1
PVC + DBP	143.9	1.81
PVC + DOP	104.1	1.31
PVC + Oxal	149.0	1.87

According to the data in Table II, the gelation properties of Oxal is at the level of DBP – one of the most effective PVC plasticizers.^{3,6} Thus, significant

absorption at the mixing stage allows “dry” blends based on suspension PVC and Oxal to be produced, which could be used in calender and extrusion technological schemes.

The main function of the primary plasticizer is to lower the glass transition temperature and increase the elongation and softness of the polymer compositions.⁶ The most informative method for evaluating the plasticizing effect is dynamic mechanical analysis (DMA), which permits fundamentally important physical-mechanical and thermo-physical parameters to be measured. In this regard, the temperature dependences of the storage modulus (Fig. 2a) and the tangent of the mechanical loss angle $\tan \delta$ (Fig. 2b) were obtained by the DMA method. The values E' in the glassy and rubbery states, as well as the glass transition temperatures t_g corresponding to the maxima on the curves $\tan \delta = f(t)$ are presented in Table III.

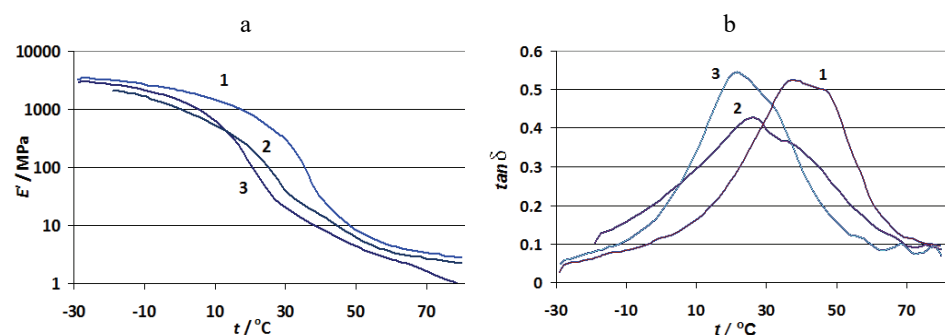


Fig. 2. Temperature dependences of the storage modulus E' (a) and $\tan \delta$ (b) of PVC composites with plasticizers: 1 – Oxal, 2 – DOP, 3 – DBP.

TABLE III. Efficiency of PVC plasticization; Plasticizer content: 28.1 %

Plasticizer	$t_g / ^\circ C$	$\Delta t_g / ^\circ C$	E' / MPa at $-8^\circ C$	E' / MPa at $60^\circ C$
Without plasticizer	80	–	–	–
DBP	20.9	-59.1	2087	2.6
DOP	24.9	-55.1	1513	3.4
Oxal	32.9	-47.1	2620	4.5

Analysis of these data shows that the rigidity of PVC films plasticized with Oxal are higher than those of phthalate plasticized films both in the glassy and in the rubbery state (Table III). At the same time, the efficiency of elasticization of the latter in different relaxation states is different. Thus, DOP provides greater elasticity to the glassy polymer, while DBP provides highly soft for rubbery PVC. The efficiency of plasticizers, estimated by the decrease in the glass transition temperature (Δt_g) of the plasticized polymer relative to the original poly-

mer, decreases in the series DBP > DOP > Oxal simultaneously with a lowering in the modulus (Table III) in the rubbery state.

Along with the characteristics of plasticizers presented above, the deformation and strength parameters of plasticized samples and their behavior during accelerated aging are essential. Therefore, in this work, the tensile strength, elongation, and hardness of plasticized PVC films before and after light-thermal aging (see experimental part) were measured. The results of these tests are listed in Table IV.

TABLE IV. Deformation and strength properties of PVC films before and after light-thermal aging

Composite	Properties before aging			Properties after aging		
	Tensile strength, MPa	Elongation %	Hardness cH	Tensile strength, MPa	Elongation %	Hardness cH
PVC+DBP	22.7	220	18.1	22.3	190	23.2
PVC+DOP	25.6	280	16.3	23.4	243	24.1
PVC+Oxal	33.7	215	55.9	28.6	143	89.4

The data (Table IV) showed a higher rigidity and lower elasticity (elongation) of PVC films plasticized with Oxal, in comparison with those phthalate plasticized. The highest resistance to accelerated light-thermal aging was demonstrated by the samples plasticized with DBP.

CONCLUSIONS

The dynamic viscosity of flootator Oxal was shown to be lower than that of di-(2-ethylhexyl) phthalate (DOP), but higher than that of dibutyl phthalate (DBP). Analysis of the activation parameters of the flow indicates a weaker dependence of the Oxal viscosity on temperature compared to the phthalate plasticizers. Size estimation of PVC particles swollen in the studied plasticizers revealed the high gelation ability of Oxal comparable with that of DBP.

A comparative study of the plasticizing effect by dynamic mechanical analysis (DMA) showed that the lowering the PVC glass transition temperature under plasticizing (Δt_g) decreases in the series DBP > DOP > Oxal, simultaneously with a decrease in the storage modulus in the rubbery state. The data on the mechanical properties exhibit a higher rigidity and lower elasticity of PVC films plasticized with Oxal, in comparison to those with phthalate plasticizers. The highest resistance to accelerated light-thermal aging was demonstrated by the samples plasticized with DBP. Thus, the complete replacement of phthalate plasticizers with Oksal makes it impossible to obtain materials with similar working properties.

Acknowledgements. The work was performed within the framework of the state assignment for the implementation of research work (Topic No. FZZW-2020-0008). The dynamic

mechanical properties survey was conducted using the resources of the Center for the collective use of scientific equipment by Ivanovo State University of Chemistry and Technology.

ИЗВОД

ФЛОТАЦИОНИ РЕАГЕНС „ОКСАЛ“ КАО ПЛАСТИФИКАТОР ЗА СУСПЕНЗИЈУ PVC

IRINA P. TRIFONOVA, JULIA A. RODICHEVA, ANNA E. SHEVELEVA, VLADIMIR A. BURMISTROV
и OSCAR I. KOIFMAN

*Research Institute of Macroheterocycles, Ivanovo State University of Chemistry and Technology,
Sheremetievskiy Avenue 7, 153000 Ivanovo, Russia*

Флотациони реагенс „Оксал“, мешавина етара на бази диоксана и алкохола, проучаван је као пластификатор за суспензију PVC у поређењу са познатим дибутил-фталатом (DBP) и ди-2-етилхексисил-фталатом (DOP). Одређени су реолошки параметри и способност желирања пластификатора, мерене су вредности модула сачуване енергије и тангенса угла механичких губитака у стакластом и гумоликом стању методом динамично-механичке анализе (DMA) и одређене температуре остатакљивања. Својства отпорности на деформацију и крутост полимерних филмова тестирали су пре и после излагања светlostи и температури. Показало се да „Оксал“ показује прилично низак вискоzитет и висока својства желирања код PVC. Истовремено, његова способност да смањи температуру остатакљивања и еластичност полимера у стакластом и гумоликом стању је нешто нижа од способности фталатних пластификатора. PVC узорци пластифицирани помоћу DBP имају највећу отпорност на старење после излагања светlostи и температури.

(Примљено 17. августа, ревидирано 11. октобра, прихваћено 9. новембра 2021)

REFERENCES

1. M. Rahman, C. S. Brazel, *Prog. Polym. Sci.* **29** (2004) 1223 (<https://doi.org/10.1016/j.progpolymsci.2004.10.001>)
2. K. Thinius, *Chemie, Physik und Technologie der Weichmacher*, 2nd ed., VEB Dt. Verl. für Grundstoffindustrie, Leipzig, 1963, p. 896
3. C. E. Wilkes, J. W. Summers, C. A. Daniels, M. T. Berard, *PVC Handbook*, 1st ed., Hanser Publications, Cincinnati, OH, 2005, p. 723 (ISBN 3-446-22714-8)
4. R. Navarro, M. P. Perrino, M. G. Tardajos, H. Reinecke, *Macromolecules* **43** (2010) 2377 (<https://doi.org/10.1021/ma902740t>)
5. V. Najafi, H. Abdollahi, *Eur. Polym. J.* **128** (2020) 109620 (<https://doi.org/10.1016/j.eurpolymj.2020.109620>)
6. V. V. Antic, M. N. Govendarica, J. Djonalagic, *Polym. Int.* **52** (2003) 1188 (<https://doi.org/10.1002/pi.1241>)
7. D. F. Cadogan, C. J. Howick, in: *Ullmann's Encyclopedia of Industrial Chemistry*, B. Elvers, Ed., Wiley-VCH, Weinheim, 2012, pp. 599–618 (ISBN: 978-3-527-32943-4)
8. A. D. Godwin, in *Applied Polymer Science: 21st Century*, C. D. Craver, C. E. Carraher, Jr., Eds., Elsevier, New York, 2000, pp. 157–175 (ISBN 100080434177)
9. *Plastics Additives Handbook*, 5th ed., Hanser Gardner Publications, Cincinnati, OH, 2001, p. 1148 (ISBN-10: 1-56990295-X)
10. M. T. Benaniba, V. Massardier-Nageotte, *J. Appl. Polym. Sci.* **118** (2010) 3499 (<https://doi.org/10.1002/app.32713>)

11. M. Park, I. Choi, S. Lee, S. Hong, A. Kim, S. Jihoon, H.-C. Kang, Y.-W. Kim, *J. Ind. Eng. Chem.* **88** (2020) 148 (<https://doi.org/10.1016/j.jiec.2020.04.007>)
12. H. B. Pyeon, J. E. Park, D. H. Suh, *Polymer Testing* **63** (2017) 375 (<https://doi.org/10.1016/j.polymertesting.2017.08.029>)
13. B. Y. Yu, A. R. Lee, S.-Y. Kwak, *Eur. Polym. J.* **48** (2012) 885 (<https://doi.org/10.1016/j.eurpolymj.2012.02.008>)
14. I. Kostić, T. Andelković, D. Andelković, T. Cvetković, D. Pavlović, *J. Serb. Chem. Soc.* **83**(2018) 1157 (<https://doi.org/10.2298/JSC180423058K>)
15. P. Jia, L. Hu, M. Zhang, G. Feng, Y. Zhou, *Eur. Polym. J.* **87** (2017) 209 (<http://dx.doi.org/10.1016/j.eurpolymj.2016.12.023>)
16. I. L. Glazko, O. P. Gur'yanova, S. V. Levanova, S. A. Kozlova, N. S. Neiman, *Russ. J. Appl. Chem.* **78** (2005) 972
17. A. A. Gudkov, E. M. Gotlib, T. Z. Lygina, *Izv. Vyssh. Uchebn. Zaved. Khim. Khim. Tekhnol.* **47** (2004) 104
18. E. M. Gotlib, R. V. Kozhevnikov, E. S. Ilyicheva, A. G. Sokolova, *Bull. Kazan Technol. Univ.* **4** (2013) 151
19. E. M. Gotlib, A. G. Sokolova, *Composite materials, plasticized with EDOS*, 1st ed., Paleotype, Moscow, 2012, p. 235
20. S. K. Ogorodnikov, G. S. Idlis, *Isoprene production*, Chemistry, Leningrad, 1973, p. 296
21. E. M. Gotlib, *Waste and by-products of national economic production are raw materials for organic synthesis*, Chemistry, Moscow, 1989, p. 212
22. A. Y. Malkin, A. I. Isayev, *Rheology Concepts, Methods, and Applications*, ChemTec Publishing, Toronto, 2012, p. 473 (<https://doi.org/10.1016/C2011-0-04626-4>)
23. Ya. Yu. Frenkel, *The Kinetic Theory of Liquids* Nauka, Moscow, 1975, p. 424
24. M. Y. Dolomatov, G. I. Nizamova, N. A. Zhuravleva, *J. Eng. Phys. Thermophys.* **90** (2017) 1020 (<https://doi.org/10.1007/s10891-017-1652-4>).



Flame retardant characteristics of polymerized dopamine hydrochloride coated jute fabric and jute fabric composites

MEHMET FATİH ÖKTEM^{1*} and BAHADIR AYDAŞ²

¹Department of Metallurgical and Materials Engineering, Ankara Yıldırım Beyazıt University, Ayvalı Mah. 151. Cad. No: 5, Etlik-Keçiören, 06010, Ankara, Turkey and ²Department of Metallurgical and Materials Engineering, Ankara Yıldırım Beyazıt University, Ayvalı Mah. 151. Cad. No: 5, Etlik-Keçiören, 06010, Ankara, Turkey

(Received 8 April, revised 29 July, accepted 8 August 2021)

Abstract: In this paper, fire resistance of natural fabrics and their composites were experimentally investigated. Special interest was given to use bio based materials such as lignin, chlorophosphates, levulinic acid and cardanol in order to exploit their capability to be utilized as flame retardants. Dopamine hydrochloride was polymerized to polydopamine (PDA) and coated to jute fabric surface. Scanning electron microscope (SEM) and thermogravimetric analysis (TGA)/derivative thermogravimetric (DTG) analyses were performed to examine surface morphology and effect of PDA to degradation behaviour of jute fabrics. Real fire behaviour of non-coated and coated fabrics was observed with torch burn test. UL-94 horizontal flame propagation test was also utilized for composite samples. Limiting oxygen index (*LOI*) testing that measures the minimum amount of oxygen required for combustion, was carried out for assessing the ability of the composite samples for their ability against flammability. PDA was seamlessly coated on the surface of the jute fabrics with its surface-active feature without damaging the structure of the fabric as observed in the SEM images. With the support of this coating on the fabric surface, the increase of the decomposition temperature of the material can be clearly seen in TGA/DTG analyses and torch burn test showed the increase in the ignition time. UL-94 horizontal testing resulted in decrease in flame propagation rate of PDA coated composite samples. In addition to this, when the mass loss rates after combustion were examined, it was seen that there is a decrease in mass loss in the coated fabrics. Jute fabrics, a type of natural fabric, can be efficiently coated with PDA, and the fire retardant property of the PDA coating on natural fabrics has been clearly demonstrated.

Keywords: fire resistance; organic coatings; natural fibre composites.

*Corresponding author. E-mail: mfoktem@ybu.edu.tr
<https://doi.org/10.2298/JSC210408063O>

INTRODUCTION

Natural fibres are fibres originated from natural resources, *i.e.*, animals or plants.¹ The use of natural fibres as the reinforcing phase for the composites has become attractive in the recent years because of their low cost, friendly processing, renewability and biodegradability features.² Although having many advantages of using natural fibres in the composites, there are some disadvantages of these fibres, *e.g.*, mechanical, thermal and physical. In the literature more attention is given to the mechanical and physical performance of these fibres than to fire characteristics of natural fibres and their composites.^{3,4}

Like many natural phenomena, the first phase of fire process starts on the surface by ignition. So it is of the utmost importance to concentrate on the interactions happening on the material surface. One of the surface modification methods is coating, and the purpose for coating is to modify a surface to meet the desired requirements by adding a new layer of material or compound. The use of several types of coating has been reported as an effective approach to improve the fire safety of the materials where the thin layers of less than 100 nm could be achieved.⁵

Coatings used as fire retardants protect materials by delaying the ignition time. The applications of the fire retardant coatings are one of the most efficient and easiest methods without making modifications in the intrinsic properties of the host material.⁶ Several types of coatings such as magnesium hydroxide, ammonium polyphosphate, and graphene have been utilized as fire retardants including metallic, organic and inorganic substances respectively.⁷ Recently, organic and toxic free fire retardants are gaining attraction because of health issues.⁸ Baldissera *et al.*⁹ have studied semiconducting polymer as fire retardant on mild steel surfaces. They found out that the coating has improved both anticorrosive and fire protection capabilities of the coated structure. Hybrid organic and inorganic fire retardants for the use in fabrics have been studied by several researchers.^{10–12} In these studies reported success was the synergistic effect of the organic-inorganic compounds improving the flame retardancy and self-extinguishing effects.

Polydopamine (PDA) is a bio based mussel inspired polymer that was discovered in 2007 by Lee and colleagues.¹³ Because of the presence of PDA inside the mussels they have the ability to strongly adhere to the surfaces of other substances. It is reported that as PDA has a similar structure with mussels, and it can easily be coated on any type of organic or inorganic substances.¹⁴

PDA can be used as coating almost on any material where coating thickness of few to one hundred nanometres could be made.¹⁵ As nontoxic and environment friendly material, PDA could be employed as flame retardant coating which contains catechol molecule. In a study made by Cho *et al.*¹⁶ polyurethane (PU) foam was deposited by nanocoatings of PDA to see the effects of PDA thickness

on the flame properties. It was seen that flammability of the PU material was reduced with the increasing PDA thickness. After 3 days of PDA deposition, torch burn experiment was carried out on the sample and it was seen that PU material quickly self-extinguished and preserved its original shape.

Li *et al.*¹⁷ studied flame retardant and antibacterial properties of cotton fabrics coated by hybrid cyclotriphosphazene, PDA and silver nanoparticles. They found out a coating yield of 3.7, 7.2 and 16.9 % by coatings with different flame retardant concentrations such as 10, 30 and 60 g/L on the fabrics. Flame retardancy was considerably improved and excellent antibacterial activities against *Staphylococcus aureus* and *Escherichia coli* were obtained.

Several researchers have reported the studies for flame retardancy and fire phenomena of natural fibre composites.^{18–20} Major chemical constituent of jute is cellulose but it also contains other components such as lignin, hemicellulose and inorganic salts often identified as ash.²¹ These non-cellulosic components play an important role in the properties of jute. For example, lignin, a high molecular weight polymer based on phenyl propene, provides cell wall stiffness.^{22,23} Jute, bast type of fibre, is one of the most commonly used natural fibres and traditional areas of use for the jute fibre are bag, rope and bed production. Jute fibre based natural composites are used in some structural applications such as indoor elements in housing, low cost housing for defense, rehabilitation and transportation. Jute fibres have good insulating properties and the produced parts are used in door/ceiling panels.²⁴ Saleem *et al.*²⁵ manufactured jute reinforced mud bricks by using a compression machine to improve the compressive strength of the samples. They found that after 28 days of drying under sun, compressive strength of jute reinforced mud bricks improved up to 2.75 times compared to that of mud bricks without fibres. Although jute and other natural fibres could be used as reinforcing material in the chopped form, it gives more strength when they are used in woven form.²⁶ By this way, non-directional and randomly distribution disadvantages of the chopped fibres disappear.

Like synthetic fibres, polymers are utilized to form a composite material and this kind of material is called polymer matrix composite. It is reported in the literature that many thermoset and thermoplastic polymers, either bio based or not, are compatible with natural fibres for the composites production.^{27,28} As the operating temperature of natural fiber composites increases, its strength and stiffness decrease. In the elevated temperatures or when exposed to flame, natural fibre composites experience thermal decomposition and combustion. Combustibility of natural fibre composites depends on the nature of its constituents, thermal conductivity, density, structure, humidity and *etc.*²⁰ Polymeric resins are attractive in the natural fibre composites manufacturing due to ease of processing, relatively low cost and suitability to use. However, the utilization of different polymeric resin brings some problems as well too; these hydrocarbon based

materials can be flammable and even toxic and make contribution to flame propagation when in contact with a heat source.²⁹ As was mentioned before, jute like other natural fibres are prone to fire and has low fire resistance. When combining with the polymeric resin to form a composite material, fire resistance of natural fiber composites becomes even worse.

This paper presents the development of fire resistant jute fabric and its composites by PDA coating on the jute fabric. The PDA was obtained by polymerizing dopamine hydrochloride. Reference uncoated jute fabrics and uncoated jute fabric composites were also produced for comparison purposes with their PDA coated jute fabrics and PDA coated jute fabric composite counterparts. Torch burn testing as well as UL-94 horizontal tests were carried out on the samples and SEM, TGA and DTG analysis were also performed. Additionally, *LOI* testing was carried out to observe resistance of the PDA coated composite samples against flammability. The main aim of this study was to produce and test organic and nontoxic coating on a natural fabric, this was achieved by efficient coating with PDA, and fire retardant property of the PDA coated jute fabrics has been demonstrated.

EXPERIMENTAL

PDA coating on jute fabrics

One group of fabrics was used as it is (uncoated), while the other group (for contribution to combustion resistance) was coated with PDA. 100 ml of Tris-HCl buffer solution was prepared with a pH of 8.5. First, dopamine hydrochloride was added to the solution. Dopamine hydrochloride (3-hydroxytyramine hydrochloride) was obtained from Sigma-Aldrich. Subsequently, jute samples were immersed in 1 mg/ml PDA solution and mixed with magnetic stirrer for 12 h at room temperature. Several jute fabrics were (PDA coated and uncoated) utilized for TGA/DTG and SEM analysis while the remaining uncoated and PDA coated fabrics were stored in a shelf with dehumidifier for the composite plate production. The jute fabrics that were used in this study are tight woven 250 g/m². The mass of each 5×5 cm² jute fabric used to produce the composite plate is approximately 0.625 g. The dimensions were measured by a digital calliper and the masses by a precision balance.

Fabrication of composite plates

Jute fabric epoxy composites were prepared by hand lay-up method of 5×5 cm² jute fabrics. In these processes, after the epoxy was applied on the fabrics homogeneously with a brush, the next jute fabric layer was placed on this layer regardless of the weaving direction, and in this way, the epoxy impregnation process continues for 5 layers. The epoxy resin used in this study was obtained from Duratek Company and Duratek 1200 + 2110 epoxy system was used as matrix of the composite.

Hot pressing technique is a widely used manufacturing technique for the production of such composite plates. In this production technique, the temperature and pressure are applied to the sample placed between two flat metal plates. In our study, jute fabrics impregnated with epoxy resin by hand laying method were kept at 100 °C under 0.4 tons pressure for 4 h and turned into a composite plate. In Fig. 1, PDA coating process on jute fabrics and composite plate production phase are given schematically.

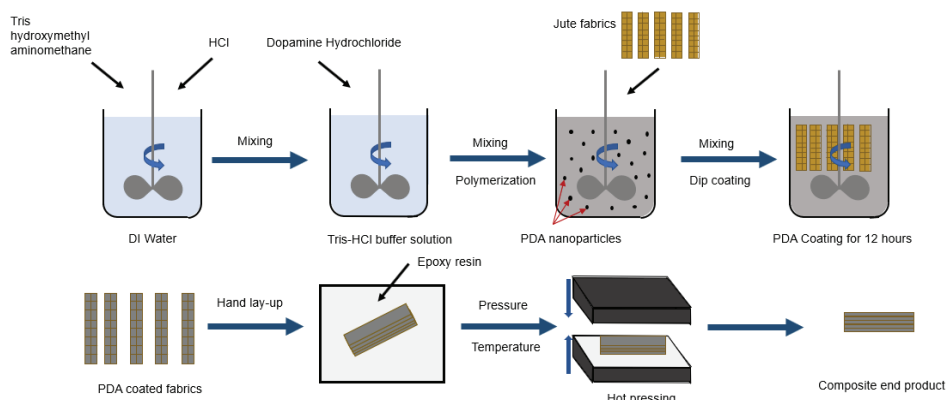


Fig. 1. Schematic representation of PDA coating and composite plate production.

Characterization

Characterization methods were applied to examine the coating on the material surface and the performance of this coating in accordance with the purpose of the study. In this context, SEM (Hitachi SU5000) analyses were performed to examine the layer formed by the PDA coating on the jute fiber surface. Thus, these images gave us information about the surface morphology of PDA coated jute fibers. SEM images of several composite plates were obtained after UL-94 testing.

TGA/DTG (Hitachi STA 7300) analyses were conducted to obtain information about the degradation temperatures and the change in their mass with temperature increase of PDA coated and non-coated jute fibre samples upon 600 °C under N₂ atmosphere.

Finally, the flame behaviour of composite materials and coated jute fabrics was examined with a torch burn test apparatus. With this examination, information about the ignition times of the materials and flame propagation comparisons and the mass loss rates before and after the combustion were obtained.

Torch burn tests

In order to examine the fire retardant effect on PDA coated jute fabrics, two types of samples produced were exposed to flame source at equal distance. For this purpose, a butane torch which provided a blue flame was utilized and the behaviour of the samples (*i.e.*, ignition time and flame propagation time) was analysed visually. This test unlike UL-94 horizontal testing does not give any quantitative data on the propagation rate of the flame, but instead gives qualitative information on the propagation rate of the flame. The torch burn test gave the ignition times of both jute fabrics and its composites.

Underwriters laboratories – 94 (UL-94) horizontal tests

A cabinet was designed and built by the authors for the purpose of performing UL-94 testing. A total of six jute fabric composite samples have been prepared and put to UL-94 horizontal testing for the assessment of the samples' flame propagation behaviour in accordance with ASTM D635. Table I shows the geometrical properties of the samples used in the UL-94 horizontal testing.

After producing six samples, based on the dimensions given in the Table I, a vertical line indicated as L_i was drawn 75 mm away from the edge of each sample with the help of a permanent marker as shown in Fig. 2.

TABLE I. Geometrical properties of samples used in the UL-94 testing

Sample	Sample No.	Thickness, mm	L / mm	W / mm	No. of layers
Uncoated jute-epoxy composite	1, 2, 3	2.5	130	10	5
PDA coated jute-epoxy composite	4, 5, 6	2.5	130	10	5



Fig. 2. Dimensions of sample used for the UL-94 testing.

Limiting oxygen index testing (LOI)

LOI testing is one of the efficient ways to assess the flammability of the materials, by doing this the minimum amount of O₂ needed to burn the material was investigated based on ISO 4589. During the testing, the amount of O₂ required for combustion of PDA coated composite samples (samples 10–12) compared to uncoated composite samples (samples 7–9) was examined. *LOI* testing of composite samples (coated and uncoated composite plates) was carried out with a dimension of 80×10×2.5 mm³. The results are given in results and discussion.

RESULTS AND DISCUSSION

The change in the colour of the fabrics from yellow to dark brown clearly demonstrated the successful coating of the PDA in Fig. 3.

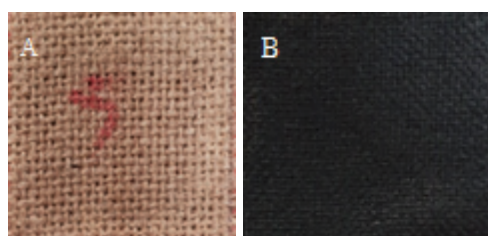


Fig. 3. Photographs of the prepared samples, A) before PDA coating and B) PDA coated fabrics.

The SEM images of the PDA coated jute fabrics are presented in Fig. 4. As seen here, a uniform PDA growth was achieved with no significant change in the fibre structure of the jute fabrics. Additionally, further magnification on the surface of the PDA coated jute fabrics demonstrated the conformal coating of the PDA nanoparticles with no change in the uniform morphology of the fibres (Fig. 4E and F). Moreover, large PDA grains, which were clearly shown in SEM images, demonstrated the strong adhesion of the PDA from bulk to the surface of jute fibres (Fig. 4G and H).

SEM images of PDA coated composite jute plates after UL-94 horizontal testing (Fig. 5A and B) show evidence of good adhesion of the PDA even after the fire has been extinguished. As seen in Fig. 5A, PDA has formed a protective char layer on the fibre surface. For this reason, during the combustion the heat

penetrated less into the interior of the jute fabrics and the fabric material, maintaining its integrity, did not act as a combustible material. In addition, this char layer restricts the passage of flammable gases to the combustion zone even if pyrolysis occurs in the material inside and prevents the strengthening of the flame. Figure 5B shows the distribution of the char layer formed by PDA on the fibres after combustion.

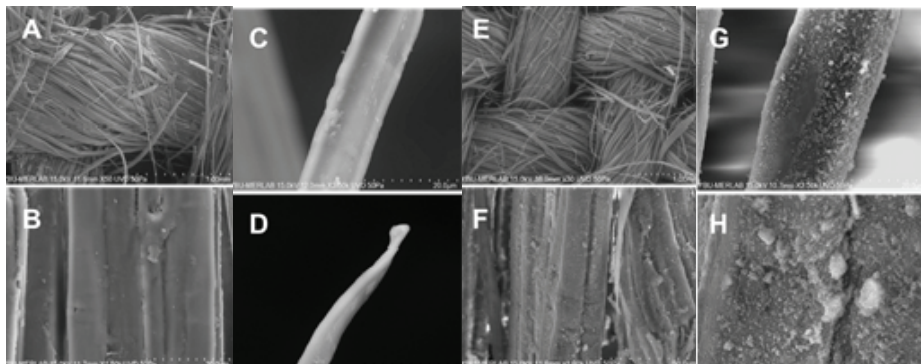


Fig. 4. SEM images of: A)–D) jute fabrics before PDA coating and E)–H) PDA coated jute fabrics.

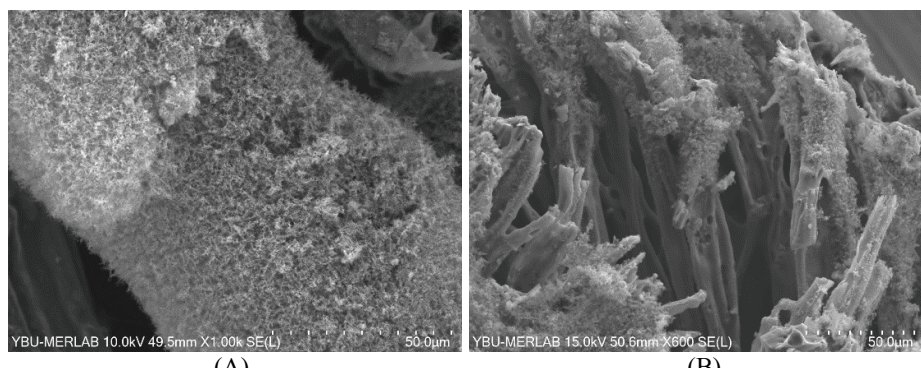


Fig. 5. SEM images of PDA coated composite jute plates and char formation after UL-94 horizontal testing: A) PDA coated single jute fiber char formation after combustion; B) Distribution of char layer on the PDA coated jute fiber after combustion.

In Fig. 6 as can be seen, the TGA curves show two clear mass loss events in the structure of bare jute and PDA coated fabrics. The first mass loss of 6.1 and 1.33 %, in the range of 200 to 320 °C, was measured for bare jute and PDA coated jute samples, respectively. From the DTG curves (Fig. 6A and B), it could be noted that the bare jute and PDA coated jute samples decomposed at 310 and 365 °C for bare jute and PDA coated jute samples, respectively. This phenomenon showed the high amount of mass loss at approximately 310–400 °C for

second stage. Hong *et al.* examined the thermal properties of bamboo fibres by coating PDA, and proved that the degradation temperature of PDA coated bamboo fibres increased compared to the uncoated fibres.³⁰ Moreover, the shifting in the DTG curve of the samples could be caused by the reactive surface of the PDA nanoparticles (*i.e.*, radical scavenging), presences of catecholic groups, as well as reducing the heat release from PDA coated jute samples.³¹

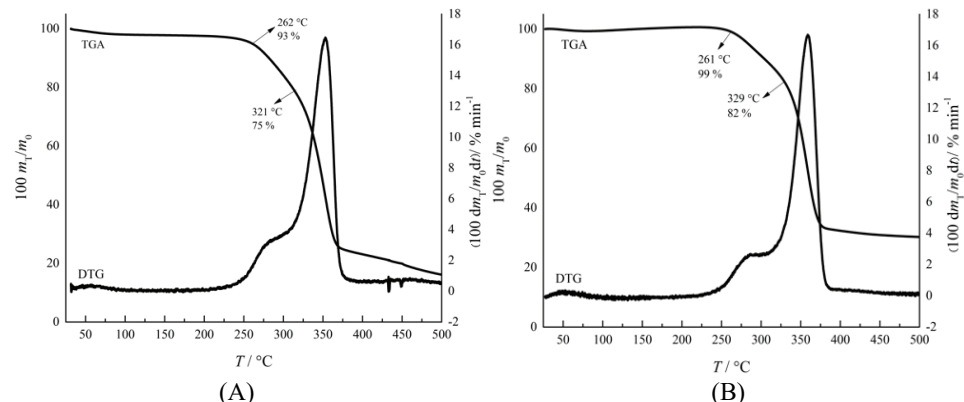


Fig. 6. TGA/DTG analysis of: A) pristine jute fabric and B) PDA coated jute fabric.

Flame retardant behavior

Reference single layer jute and reference composite jute ignited instantly and the flame propagation rate of single layer jute is faster than PDA coated single layer and flame propagation rate of reference composite jute is faster than PDA coated composite jute samples. As shown in the Table II, the ignition times of the PDA coated samples are considerably higher than that of the reference samples. Unlike the reference samples, the flame did not directly contact the surface of the samples, firstly come into contact with PDA coating on the surface.

TABLE II. Some parameters related to the torch burn tests and flame retardant behaviour of samples

Material type	Composition	Ignition time, s	Flame propagation rate comparison	Mass loss rate wt.% s ⁻¹
Reference jute	Single layer pure	4	Faster than single layer coated	2.87
PDA coated jute	Single layer coated	10	Lower than reference jute	2.49
Reference composite jute plate	5 layer coated with epoxy	8	Faster than 5 layer coated with epoxy	0.93
PDA coated composite jute plate	5 layer coated with epoxy	25	Lower than 5 layer with epoxy	0.47

Besides increasing the ignition time, low flame propagation rate is a significant point during fire. Fire tests confirmed that PDA coating decreased flame propagation rate. Fox *et al.* in the flame propagation test of the polyurethane foam and cardboard coated by the PDA, showed that the PDA coating eliminated the flame propagation.³² While the flame propagated on the reference samples rapidly, it showed more slowly propagation behavior on the PDA coated samples. Taking these two results into consideration, the PDA coating clearly demonstrated the flame retardant effect by delaying ignition and reducing flame spread rate. In addition to these results, as seen in the table, mass loss rates have been reduced significantly.

UL-94 horizontal testing was performed inside the cabinet designed and built by the authors. Fig. 7A and B shows the stages of UL-94 horizontal testing of a PDA coated composite sample.



Fig. 7. PDA coated composite plate: A) ignition phase and B) propagation of the flame.

In Fig. 8, the chart showing comparison between uncoated and PDA coated jute–epoxy composite samples' flame propagation rate has been given. In this figure, time to extinguish has been given for a total of six specimens. Three PDA coated jute–epoxy composite and three uncoated jute–epoxy composite plates were put on testing. Time to extinguish resulted 366, 338 and 355 s for PDA coated samples number 4, 5 and 6, respectively, while time to extinguish gave 140, 177 and 101 s for uncoated samples number 1, 2 and 3, respectively. The arithmetic average value of uncoated samples time to extinguish value is calcul-

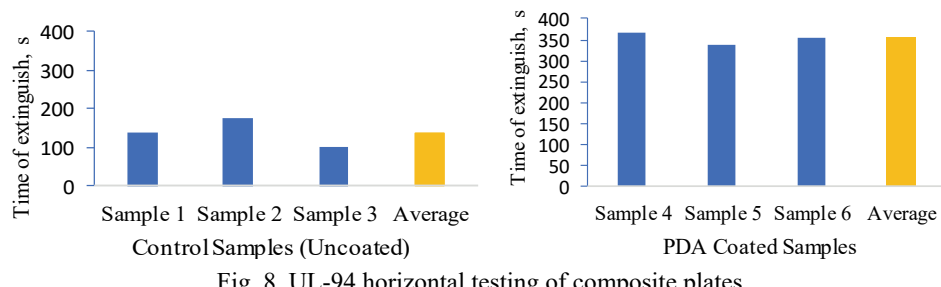


Fig. 8. UL-94 horizontal testing of composite plates.

ated as 139 s and coefficient of variation is 27.33 % while the arithmetic average value of PDA coated samples is calculated as 353 s and coefficient of variation is 3.97 %. The standard deviation of uncoated jute–epoxy composites is 38, while the standard deviation of PDA coated samples is 14.10. When arithmetic average values are compared, it is seen that time to extinguish values of PDA coated samples' flame propagation rate are about 60 % less than that of uncoated samples. UL-94 horizontal testing proved the efficiency of PDA coating on jute fabrics with regard to flame propagation.

LOI results

As given in Fig. 9, uncoated composite samples are the most combustible with 19 % limit amount of O₂ during the testing. PDA coated composite samples with 23 % O₂ content started burning showing better combustion performance than their uncoated counterparts.

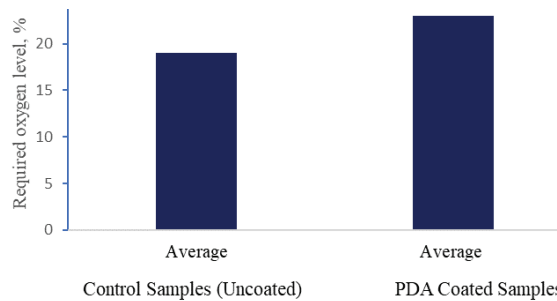


Fig. 9. LOI testing of composite plates.

Wang *et al.* observed an increase in *LOI* value when they coated ammonium polyphosphate and PDA to cotton. Although, in their study, the greater increase showed the effect of ammonium polyphosphate, the *LOI* value which was 26.5 %, increased to 28.5 % with the effect of the PDA coating.³³ Zhang *et al.* produced flax–PLA composite with PDA and iron phosphonate coating. In this study, PDA and iron phosphonate showed fire retardant effect and increased the *LOI* value from 19.1 to 26.1 %.³⁴ This testing is defined as the minimum oxygen percentage needed to sustain flaming combustion. As this value gets higher, a material's ability to resist flammability is said to be improved. Compared with uncoated samples, PDA coated samples have improved resistance against flammability.

CONCLUSION

In this study, dopamine hydrochloride was polymerized to PDA and coated to jute fabric surface. After the dipping method coating process, SEM and TGA/DTG analysis were performed to examine surface morphology and effect of PDA to degradation behaviour of jute fabrics. Additionally, real fire behaviour of non-coated and coated fabrics was observed with torch burn test. *LOI* and UL-94

horizontal testing were also employed for assessing the flame propagation and combustion characteristics of composite plates as well.

As a result of the study, PDA was seamlessly coated on the surface of the jute fabrics with its surface-active feature without damaging the structure of the fibres as observed in the SEM images. With the support of this coating on the fabric surface, the increase of the decomposition temperature of the material can be clearly seen in TGA/DTG analyses and torch burn test showed the increase in the ignition time. In addition to this, when the mass loss rates after combustion were examined, it was seen that there is a decrease in mass loss in the coated fabrics. Jute fabrics, a type of natural fabric, can be efficiently coated with PDA, and the fire retardant property of the PDA coating on natural fabrics has been clearly demonstrated. The results of the UL-94 horizontal test show that flame propagation is significantly slowed down for PDA coated jute fabric composites, while the *LOI* test shows that the amount of oxygen required for the combustion of the PDA coated jute fabric composite material is increased compared to composites made of uncoated jute fabrics. In this case, while PDA coating decreased the flame propagation rate it increased the minimum amount of oxygen required for combustion.

Acknowledgements. This study was partially supported by Scientific and Technical Research Council of Turkey (TUBITAK, Grant No. 119M076). The authors would like to thank to Dr. Kouroush Salimi and Nuray Çelebi for their technical support and assistance.

ИЗВОД

ТКАНИНЕ ОД ЈУТЕ И КОМПОЗИТИ НА БАЗИ ТКАНИНА ОД ЈУТЕ СА СЛОЈЕМ ПОЛИМЕРИЗОВАНИГ ДОПАМИН-ХИДРОХЛОРИДА ПОВЕЋАЊЕ ОТПОРНОСТИ НА САГОРЕВАЊЕ

МЕНХМЕТ ФАТИХ ÖKTEM¹ и ВАХАДИР АЙДАШ²

¹Department of Metallurgical and Materials Engineering, Ankara Yıldırım Beyazıt University, Ayvalı Mah.

151. Cad. No: 5, Etlik-Keçiören, 06010, Ankara, Turkey и ²Department of Metallurgical and Materials Engineering, Ankara Yıldırım Beyazıt University, Ayvalı Mah. 151. Cad. No: 5, Etlik-Keçiören, 06010, Ankara, Turkey

У овом раду је испитивана отпорност на сагоревање природних тканина и њихових композита. Посебна пажња посвећена је биоактивним материјалима, као што су лигнин, хлорофосфати, левулинска киселина и карданол да би се испитала њихова способност успоравања ширења пламена. Допамин-хидрохлорид је полимеризован у полидопамин (PDA) и нанет на површину тканине од јуте. Скенирајућом електронском микроскопијом (SEM) је испитана морфологија површине, а термогравиметријском анализом (TGA) утицај PDA на деградацију тканине од јуте. Отпорност на сагоревање сирове тканине и тканине наслојене PDA је испитана применом горионика. За композите на бази јуте је коришћен и UL-94 хоризонтални тест горења. Границни индекс кисеоника (*LOI*) којим се одређује минимална количина кисеоника потребна за сагоревање је примењен за процену отпорности композитних материјала на сагоревање. SEM анализа је показала присуство танког слоја PDA на површини тканине, без нарушувања њене структуре. Захваљујући овом слоју, температура на којој долази до деградације материјала је пови-

шена, што је утврђено TGA анализом, а време сагоревања је продужено, што је утврђено тестом са гориоником. UL-94 хоризонтални тест горења је показао смањење брзине ширења пламена за узорке наслојене PDA. Додатно, губитак масе након сагоревања је смањен у случају узорака са слојем. Резултати показују да се тканина од јуте, врста природне тканине, може ефикасно препокрити полидопамином, што доприноси побољшању отпорности на сагоревање.

(Примљено 8. априла, ревидирано 29. јула, прихваћено 8. августа 2021)

REFERENCES

1. L. Mohammed, M. N. M. Ansari, G. Pua, M. Jawaid, M. S. Islam, *Int. J. Polym. Sci.* **2015** (2015) 1 (<http://dx.doi.org/10.1155/2015/243947>)
2. S. Chapple, R. Anandjiwala, *J. Thermoplast. Compos. Mater.* **23** (2010) 871 (<https://doi.org/10.1177/0892705709356338>)
3. J. Biagiotti, D. Puglia, J. M. Kenny, *J. Nat. Fibers* **1** (2004) 37 (https://doi.org/10.1300/J395v01n02_04)
4. D. Nabi Saheb, J.P. Jog, *Adv. in Polym. Technol.* **18** (1999) 351 ([https://doi.org/10.1002/\(SICI\)1098-2329\(199924\)18:4<351::AID-ADV6>3.0.CO;2-X](https://doi.org/10.1002/(SICI)1098-2329(199924)18:4<351::AID-ADV6>3.0.CO;2-X))
5. H. Yang, B. Yu, P. Song, C. Maluk, H. Wang, *Composites, B* **176** (2019) (<https://doi.org/10.1016/j.compositesb.2019.107185>)
6. T. Mariappan, Fire Retardant Coatings, *New Technologies in Protective Coatings*, IntechOpen, Rijeka, 2017 (<http://dx.doi.org/10.5772/67675>)
7. Y. Hu, B. Yu, L. Song, *Novel Fire Retardant Polymer and Composite Materials*, Woodhead Publishing, Sawston, 2017 (<https://doi.org/10.1016/C2014-0-01717-0>)
8. K. De Silva, S. Ray, R. Blache, M. Taylor, *Fire Mater.* **41** (2016) 169 (<https://doi.org/10.1002/fam.2376>)
9. A. F. Baldissera, M.R. da Silva Silveira, C. H. Beraldo, N. S. Tocchetto, C.A. Ferreira, *J. Mater. Research Technol.* **8** (2019) 2832 (<https://doi.org/10.1016/j.jmrt.2019.04.022>)
10. Y. Ren, Y. Zhang, J. Zhao, X. Wang, Q. Zeng, Y. Gu, J. *Sol–Gel Sci. Technol.* **82** (2017) 280 (<https://doi.org/10.1007/s10971-016-4273-z>)
11. Y. Ren, Y. Zhang, Y. Gu, Q. Zeng, *Prog. Org. Coat.* **112** (2017) 225 (<https://doi.org/10.1016/j.porgcoat.2017.07.022>)
12. Y. Liu, Y. T. Pan, X. Wang, P. Acuna, P. Zhu, U. Wagenknecht, G. Heinrich, X.Q. Zhang, R. Wang, D.Y. Wang, *Chem. Eng. J.* **294** (2016) 167 (<https://doi.org/10.1016/j.cej.2016.02.080>)
13. H. Lee, S. M. Dellatore, W. M. Miller, P. B. Messersmith, *Science* **318** (2007) 426 (<https://doi.org/10.1126/science.1147241>)
14. H. Wang, J. Cao, F. Luo, C. Cao, Q. Qian, B. Huang, L. Xiao, Q. Chen, *RSC Adv.* **9** (2019) 21371 (<https://doi.org/10.1039/c9ra02861g>)
15. V. Ball, *Front. Bioeng. Biotechnol.* **109** (2018) 6 (<https://doi.org/10.3389/fbioe.2018.00109>)
16. J. H. Cho, V. Vasagar, K. Shanmuganathan, A. R. Jones, S. Nazarenko, C. J. Ellison, *Chem. Mater.* **27** (2015) 6784 (<https://doi.org/10.1021/acs.chemmater.5b03013>)
17. Y. Li, B. Wang, X. Sui, R. Xie, H. Xu, L. Zhang, Y. Zhong, Z. Mao, *Appl. Surf. Sci.* **435** (2018) 1337 (<https://doi.org/10.1016/j.apsusc.2017.11.269>)
18. A. U. R. Shah, M. N. Prabhakar, J.I. Song, *Int. J. Precis. Eng. Manuf.-Green Technol.* **4** (2017) 247 (<https://doi.org/10.1007/s40684-017-0030-1>)

19. T. D. Hapuarachchi, G. Ren, M. Fan, P. J. Hogg, T. Peijs, *Appl. Compos. Mater.* **14** (2007) 251 (<https://doi.org/10.1007/s10443-007-9044-0>)
20. R. Kozlowski, and M. Wladyka-Przybylak, *Polym. Adv. Technol.* **19** (2008) 446 (<https://doi.org/10.1002/pat.1135>)
21. K. Salmeia, M. Jovic, A. Rageisiene, Z. Rukuiziene, R. Milasius, D. Mikucioniene, S. Gaan, *Polymers* **293** (2016) 8 (<https://doi.org/10.3390/polym8080293>)
22. A. Ivanovska, K. Asanovic, M. Jankoska, K. Mihajlovski, L. Pavun, M. Kostic, *Cellulose* **27** (2020) 8485 (<https://doi.org/10.1007/s10570-020-03360-x>)
23. D. Ahuja, A. Kaushik, M. Singh, *Int. J. Biol. Macromol.* **107** (2018) 1294 (<https://doi.org/10.1016/j.ijbiomac.2017.09.107>)
24. M. R. Sanjay, G. R. Arpitha, L. L. Naik, K. Gopalakrishna, B. Yogesha, *Nat. Resour.* **7** (2016) 108 (<https://doi.org/10.4236/nr.2016.73011>)
25. M. A. Saleem, S. Abbas, M. Haider, *Pak. J. Eng. Appl. Sci.* **19** (2016) 83 (https://journal.uet.edu.pk/ojs_old/index.php/pjeas/article/view/285/223)
26. G. M. Arifuzzaman Khan, M. Terano, M. A. Gafur, M. Shamsul Alam, *J. King Saud University – Eng. Sci.* **28** (2016) 69 (<https://doi.org/10.1016/j.jksues.2013.12.002>)
27. H. Dahy, *Sensors* **19** (2019) 738 (<https://doi.org/10.3390/s19030738>)
28. A. Gholampour, T. Ozbakkaloglu, *J. Mater. Sci.* **55** (2020) 829 (<https://doi.org/10.1007/s10853-019-03990-y>)
29. L. Ahmed, B. Zhang, L. C. Hatanaka, M. S. Mannan, *J. Loss Prev. Proc. Ind.* **55** (2018) 381 (<https://doi.org/10.1016/j.jlp.2018.07.005>)
30. G. Hong, Y. Meng, Z. Yang, H. Cheng, S. Zhang, W. Song, *Bioresources* **12** (2017) 8419 (<https://doi.org/10.15376/biores.12.4.8419-8442>)
31. X. Qui, C. K. Kundu, Z. Li, X. Li, Z. Zhang, *J. Mater. Sci.* **54** (2019) 13848 (<https://doi.org/10.1007/s10853-019-03879-w>)
32. D. M. Fox, W. Cho, L. Dubrulle, P. G. Grützmacher, M. Zammarano, *Green Mater.* **8** (2020) 162 (<https://doi.org/10.1680/jgrma.19.00065>)
33. S. Wang, X. Du, S. Deng, X. Fu, Z. Du, X. Cheng, H. Wang, *Cellulose* **26** (2019) 7009 (<https://doi.org/10.1007/s10570-019-02586-8>)
34. L. Zhang, Z. Li, Y. T. Pan, A. P. Yanez, S. Hu, X. Q. Zhang, R. Wang, D. Y. Wang, *Composites, B* **154** (2018) 56 (<https://doi.org/10.1016/j.compositesb.2018.07.037>).



Investigation of selective leaching conditions of ZnO, ZnFe₂O₄ and Fe₂O₃ in electric arc furnace dust in HNO₃

MERT ZORAGA, TUGBA YUCEL, SEDAT ILHAN and AHMET ORKUN KALPAKLI*

*Istanbul University—Cerrahpasa, Engineering Faculty, Metallurgical and Materials
Engineering Department, 34320, Avcilar, Istanbul, Turkey*

(Received 23 May 2020, revised 16 December, accepted 17 December 2021)

Abstract: Electric arc furnace dust (EAFD) includes mainly Zn, Fe, Pb, Ca and Mn-bearing compounds. Thus, EAFD is classified as a hazardous waste. The dissolution behavior of Zn- and Fe-bearing compounds in EAFD in nitric acid solutions was investigated in this work. The composition of Zn- and Fe-bearing compounds in the EAFD was determined as 28.58, 37.96 and 11.33 % for ZnO, ZnFe₂O₄ and Fe₂O₃, respectively. The effect of stirring speed, temperature and HNO₃ concentration on the dissolution rate of ZnO, ZnFe₂O₄ and Fe₂O₃ were investigated and optimum leaching conditions determined. While ZnO was dissolved rapidly, the dissolution rate of ZnFe₂O₄ increased with increasing temperature and HNO₃ concentration. Fe₂O₃ was not soluble in 0.5 M HNO₃ solution at 40 °C, whereas it was dissolved completely in 4 M HNO₃ solution at 80 °C.

Keywords: environmental protection; zinc recovery; leaching; zinc oxide; zinc ferrite.

INTRODUCTION

One of the most important issues with which steel producers are faced is the question of environmental protection. For example, it refers to the necessity to utilize dusts resulting from the process of steel production from scrap in electric arc furnaces, which mainly contain of Zn, Fe, Pb and a considerable amount of harmful elements, such as Cd, As, Cr and F.^{1,2} The world generation of EAFD is estimated to be around 3.7 million tons per year. Plants from Europe generate around 500.000–900.000 tons of dusts per year.¹ Turkey is Europe's 2nd and the world's 8th largest crude steel producer with an annual steel production of 37.3 million tons. While 30 % of the world's steel production (1.7 billion tons) is made in EAF as secondary production, this ratio reaches to 80 % in Turkey.

During the production of 1 ton of steel, 14–20 kg of EAFD is generated as hazardous waste. Recovery of valuable metals from EAFD is important from the

* Corresponding author. E-mail: aok13@iuc.edu.tr
<https://doi.org/10.2298/JSC200523004Z>

economic and environmental points of view. EAFD is an important source for the production of zinc and zinc-bearing chemicals for paint, rubber, natural rubber, cosmetics, stock farming, petroleum products, ceramic, glass and plating.³ The content of the main elements in EAFD varies in the range of 25–45 % of Zn, 20–35 % of Fe, 0.3–6 % of Pb, 1–10 % of Ca, 0.01–0.2 % of Cd, 0.2–0.7 % of Cr, etc., depending on the scrap processed, type of steel to be produced and operating conditions. Zinc is present in EAFD as ZnO and ZnFe₂O₄, and possibly as a complex ferrite, *e.g.*, (Zn,Mn)Fe₂O₄. ZnO is an easily workable form for both the pyrometallurgical and the hydrometallurgical method, but the ferrite form is considerably complex and difficult.^{1,4}

In the literature, different processes (hydrometallurgical or pyrometallurgical method) have been used for the processing of EAFD. The pyrometallurgical processing is usually represented by impure ZnO, which has minimal commercial value.^{5–7} This product has to be further processed by the hydrometallurgical method in order to obtain high purity zinc. Pyrometallurgical methods require some reducing agents and relatively high temperatures to produce raw zinc oxide of low commercial value.⁴ Particular attention is devoted to specific technical challenges emerging in the pyrometallurgical processing of the EAF dust and to the corresponding potential measures for improving the dust recycling by promoting the processing efficiency with the elimination of secondary hazardous pollutants.⁸ Hydrometallurgical processes are mainly based on acid (H₂SO₄, HNO₃, HCl or combined) or alkaline (usually NaOH) leaching.^{1,2,4,9–22} The alkaline leaching processes offer the potential advantage that iron remains largely insoluble. Such processes are limited, however, by their inability to recover zinc from zinc ferrite unless a reducing roast is performed first. Both approaches result in halide-containing solutions. This kind of processing is difficult.¹⁵

Caravaca *et al.* investigated the dissolution of Zn from the EAFD in basic solutions (NaOH), acidic solutions (HCl, HNO₃ and H₂SO₄) and solutions containing ammonia ((NH₄)₂SO₄, NH₄OH, NH₄Cl, (NH₄)₂CO₃) and determined that the recovery of zinc is limited when alkaline leaching is applied due to the presence of zinc ferrite. However, a relatively low iron containing leach solution is obtained.¹¹ Havlik *et al.* studied the recovery of Zn from the EAFD in H₂SO₄ solutions by the hydrometallurgical method and obtained optimum zinc leaching conditions from the EAFD at a leaching temperature of 70–90 °C and an H₂SO₄ concentration of 0.5 M.⁴ Orhan investigated leaching of EAFD in NaOH solutions and reported optimum leaching conditions, at which 85 % of Zn and 90 % of Pb were recovered, as 95 °C, 1/7 solid/liquid ratio, 10 M NaOH and a 2 h leaching time.¹⁷ Peng *et al.* used a reductive roasting method to destroy the ZnFe₂O₄ phase in order to obtain ZnO and Fe₃O₄ under a CO atmosphere and then performed leaching experiments in H₂SO₄ solution at 30–70°C. The shrinking core model was found to be the best to describe the dissolution of iron and zinc from

roasted zinc calcines at 750 °C and activation energies were calculated as 51.40 and 10.01 kJ mol⁻¹ for the leaching of Fe and Zn.²¹

The aim of this work was to investigate the dissolution behavior of ZnO, ZnFe₂O₄ and Fe₂O₃ compounds in the EAFD in HNO₃ solution and to determine the selective leaching conditions. The effect of stirring speed, HNO₃ concentration and temperature on the dissolution were determined.

EXPERIMENTAL

EAFD with a particle size fraction of -150 µm obtained from a steel company was used in the leaching experiments. X-ray fluorescence (XRF, Panalytical Axios–Minerals) and X-ray diffraction (XRD, Rigaku D/Max-2200) analyses were used for the determination of elemental and phase composition of the EAFD. SEM–EDS analyses were performed for the semi quantitative and image analysis of the EAFD and the leach residue.

Dissolution experiments were performed in a water-heated, jacketed borosilicate glass reactor (HWS DN 100, Germany) having a volume of 1 L. A thermostate with water circulation (Julabo MV4, Germany) was used to heat the reactor and to achieve isothermal conditions. The solution in the reactor was stirred with a mechanical stirrer (IKA RW 20 DZM, Germany). The solution temperature in the reactor was measured with a PT100 temperature sensor. A glass pipe including G-3 porous alumina disk at the end was used as a sampler. The dissolution experiments were performed using 5 g of the sample, 0.5–4 M HNO₃ solution, at 40–80 °C and stirring speed of 300 rpm for the determination the effect of the HNO₃ concentration, temperature and stirring speed on the dissolution behavior of the EAFD in HNO₃ solutions. In addition, the dissolution experiments of pure ZnO (Merck) and Fe₂O₃ (Merck) were also performed using 1 g of ZnO, 1 g of Fe₂O₃ (Merck), 0.5 M HNO₃ solution, at 40 °C and stirring speed of 300 rpm for the determination of the ZnO, ZnFe₂O₄ and Fe₂O₃ composition in the EAFD. When isothermal conditions were obtained, the sample weighed in a ceramic crucible was added to the reactor. Liquid samples were taken from the reactor at certain time intervals (5–180 min) and analyzed in an ICP–OES instrument.

RESULTS AND DISCUSSION

Characterization of the EAFD

The results of XRF analysis of the EAFD used in this work are given in Table I. The EAFD mainly includes oxides of Zn, Fe, Pb and Mn.

TABLE I. Chemical composition of the EAFD

Compound	ZnO	Fe ₂ O ₃	PbO	CaO	C	MnO	SiO ₂	MgO	SO ₃	Cl, F	Others ^a
Content, wt.%	41.4	36.5	4.9	3.1	3.0	2.7	1.7	1.5	2.0	0.7	< 2

^aK₂O, Al₂O₃, Cr₂O₃, CuO, P₂O₅, SnO, TiO₂, BaO, NiO, V₂O₅

The XRD diagram of the EAFD and the leach residue obtained from the experiment performed for 180 min using 0.5 M HNO₃ solution at 40 °C and a stirring speed of 300 rpm is presented in Fig. 1. It is seen from the Fig. 1a that the EAFD includes ZnFe₂O₄ (ICDD 22–1012), ZnO (ICDD 36–1451), Fe₂O₃ (ICDD 39–1346) and PbO₂ (ICDD 52–0752). ZnO was not detected in the XRD diagram (Fig. 1b) due to the rapid leaching reaction of ZnO in HNO₃ solution.

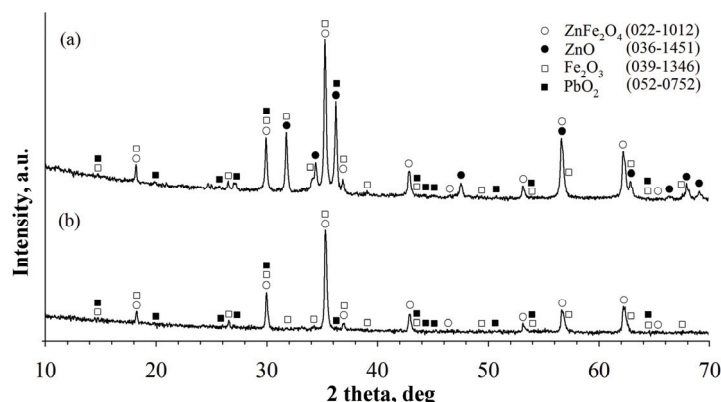


Fig 1. a) XRD diagram of the EAFD, b) the leach residue obtained from the experiment performed for 180 min using 0.5 M HNO_3 solution at 40 °C and a stirring speed of 300 rpm.

After completion of dissolution experiments, it was seen that 38 % of Fe and 86 % of Zn were extracted in the experiment performed for 180 min using 0.5 M HNO_3 solution at 40 °C (Fig. 2). It is possible to determine only the total amount of Fe and Zn in the leach solution using the ICP–OES instrument but not the exact source of Fe and Zn individually. While ZnO and ZnFe_2O_4 are sources for Zn extracted, Fe can be extracted from ZnFe_2O_4 and Fe_2O_3 .

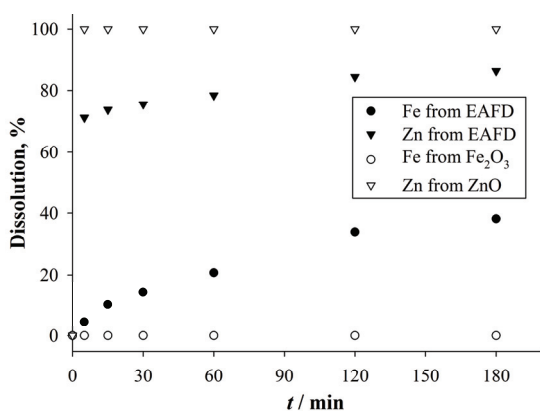


Fig. 2. Dissolution content-time diagram for Fe and Zn from the EAFD, Zn from Fe_2O_3 and Zn from ZnO . (0.5 M HNO_3 , 40 °C and 300 rpm).

The disappearance of peaks of ZnO in the XRD diagram (Fig. 1b) and the low Fe extraction rate obtained from the experiment performed at the lowest temperature (40 °C) and HNO_3 concentration (0.5 M) initiated the question of whether it is possible to determine the composition of ZnO , ZnFe_2O_4 and Fe_2O_3 in the EAFD. Therefore, two separate dissolution experiments were performed

for 180 min using 1 g of Fe_2O_3 (Merck), 1 g of ZnO (Merck), 0.5 M HNO_3 solution at 40 °C and a stirring speed of 300 rpm for the investigation of dissolution behavior of ZnO and Fe_2O_3 (Fig. 2).

ICP-OES analysis shows that ZnO was dissolved totally in 5 min of the reaction, while Fe_2O_3 was insoluble after 180 min of reaction time (no dissolved Fe was measured within the detection limit of the ICP-OES instrument). Thus, source of Fe passed to the leach solution is determined as ZnFe_2O_4 using these findings and dissolution of ZnFe_2O_4 in HNO_3 solutions.²³ It is possible to determine the composition of ZnO , ZnFe_2O_4 and Fe_2O_3 in the EAFD using the results of XRF and ICP-OES analysis as 28.58, 37.96 and 11.33 %, respectively.

Dissolution behavior of the EAFD in nitric acid solutions

Since the dissolution of ZnO in the EAFD was very rapid, the results of the dissolution experiments are presented for ZnFe_2O_4 and Fe_2O_3 as ZnFe_2O_4 dissolved, content–time and Fe_2O_3 dissolved, content–time. The dissolution, content–time diagrams are plotted using the results of the ICP-OES analysis of leach solutions taken from the reactor at defined time intervals.

The effect of stirring speed on the dissolution of EAFD

Dissolution experiments were performed using a 4 M HNO_3 solution at 80 °C for the determination of the effect of stirring speed on the dissolution rate of the EAFD in HNO_3 solutions. The ZnFe_2O_4 dissolved, content–time diagram is shown in Fig. 3.

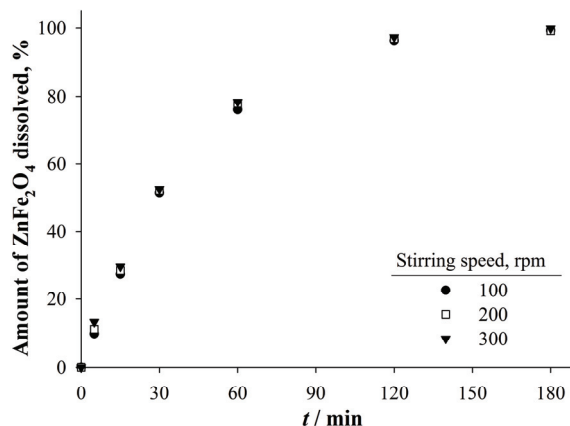


Fig. 3. ZnFe_2O_4 dissolved, content–time diagram for different stirring speeds (4 M HNO_3 and 80 °C).

As could be seen from Fig. 3, the stirring speed had no significant effect on the dissolution rate of ZnFe_2O_4 in the EAFD. Therefore, it was determined that a stirring speed of 300 rpm is adequate to eliminate the resistance of the liquid film

layer around the solid EAFD particles. Thus, a stirring speed of 300 rpm was used in all dissolution experiments.

The effect of temperature and HNO₃ concentration on the dissolution of EAFD

Dissolution experiments were performed using 0.5–4 M HNO₃ solution at temperatures of 40–80 °C and a stirring speed of 300 rpm for the determination of the effect of temperature on the dissolution rate of the EAFD in HNO₃ solutions. ZnFe₂O₄ dissolved, content-time and Fe₂O₃ dissolved, content-time diagrams are shown in Figs. 4 and 5, respectively. As seen from Fig. 4a–d, the dissolution rate of ZnFe₂O₄ increased with increasing temperature and total dissolution of ZnFe₂O₄ was obtained in the experiment performed using 4 M HNO₃ solution at 80 °C and stirring speed of 300 rpm (Fig. 4d).

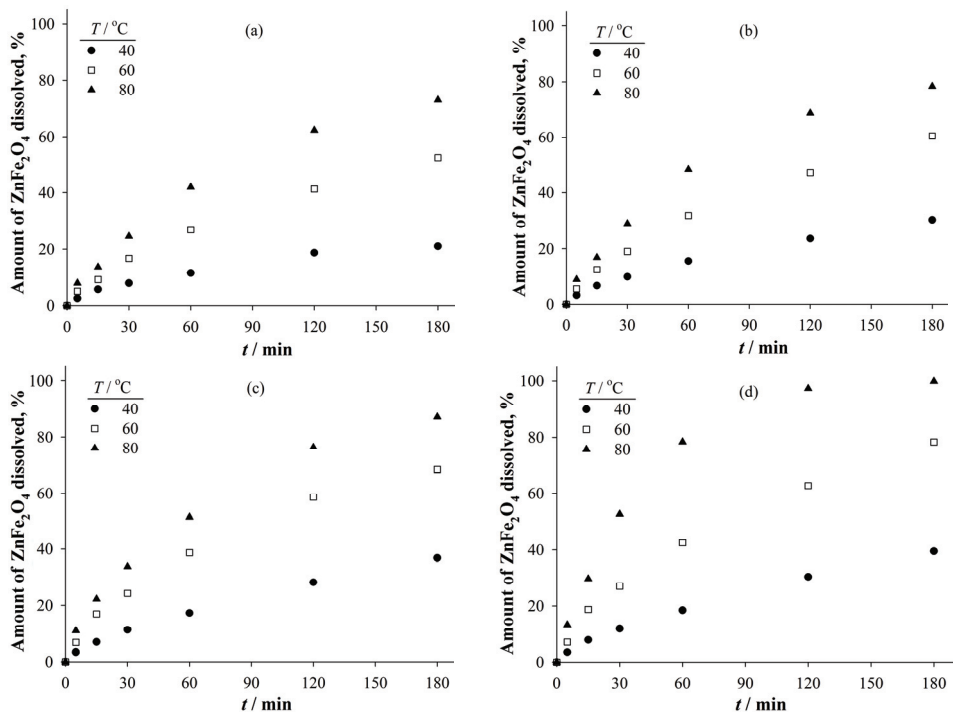


Fig. 4. ZnFe₂O₄ dissolved, content–time diagrams for different temperatures at constant HNO₃ concentration: a) 0.5, b) 1, c) 2 and d) 4 M (stirring speed: 300 rpm).

As shown in Fig. 5a–d, the dissolution of Fe₂O₃ in the EAFD was more dependent on the temperature than that of ZnFe₂O₄ and therefore the dissolution rate of Fe₂O₃ increased with increasing temperature. A dissolution of 99 % was obtained for Fe₂O₃ in the experiment performed using 4 M HNO₃ solution at 80 °C and a stirring speed of 300 rpm (Fig. 5d). However, obtaining high dissolution

rates for Fe together with Zn results in difficulties in the subsequent purification process of Zn in the leach liquor.

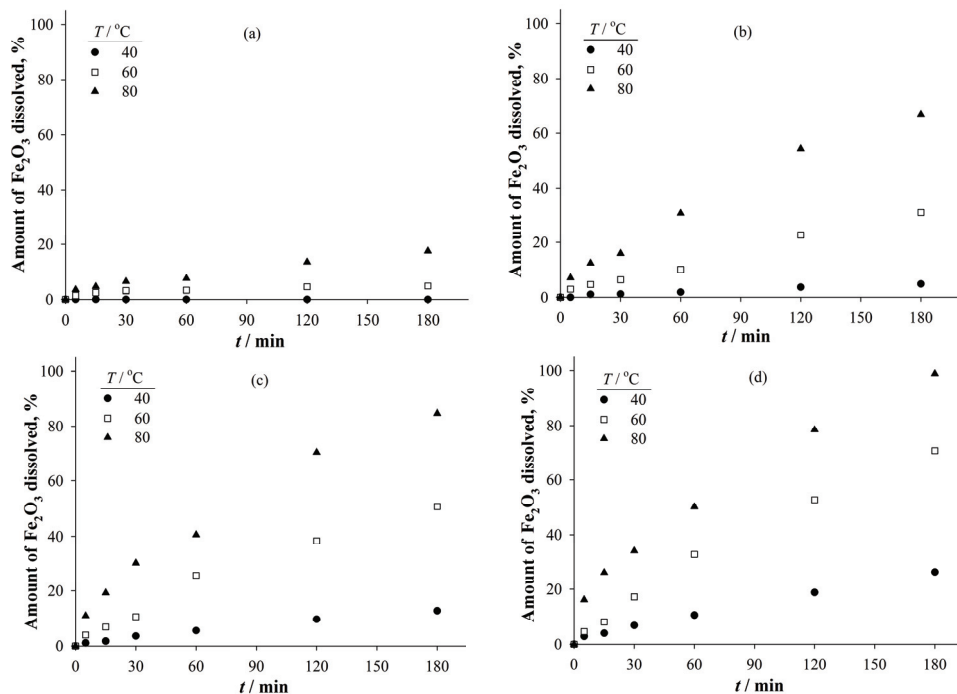


Fig 5. Fe_2O_3 dissolved–time diagrams for different temperatures at constant HNO_3 concentration: a) 0.5, b) 1, c) 2 and d) 4 M (stirring speed: 300 rpm).

A literature survey showed that H_2SO_4 solutions are generally used for the acidic leaching of EAFD. HCl solutions are not preferred due to difficulties in the electrowinning process of leach liquors since Cl_2 gas is generated. Although, it is fact that the use of H_2SO_4 solutions at moderate temperatures lowers the Fe content (1–10 %) in the leach solutions, relatively low Zn dissolution rates (about 60 %) were obtained under these experimental conditions.^{1,4,24–26} Concentrated H_2SO_4 solutions and high temperatures should be used to obtain high Zn dissolution rates. However, dissolution rate of Fe also increases rapidly in this case.

Caravaca *et al.* recovered 70.6 % of Zn and 14.5 % of Fe from EAFD using 5 M HNO_3 solution at 25 °C in 2 h and stated that the presence of zinc ferrites makes acidic leaching more attractive than alkaline leaching in terms of Zn recovery.¹¹ Although, the acidic leach liquor includes a relatively high amount of Fe compared to an alkaline leach liquor, Fe is separated from leach liquor by goethite precipitation at a pH near 2 or by solvent extraction. In this work, 93 % of Zn (100 % of ZnO and 72 % ZnFe_2O_4) and 45 % of Fe (72 % of ZnFe_2O_4 and

17.53 % of Fe_2O_3) were extracted from the EAFD in the experiment performed using 0.5 M HNO_3 solution at 80 °C.

Since the same experimental data were used for plotting the diagrams to determine the effect of the HNO_3 concentration on the dissolution rate of the EAFD in HNO_3 solutions, ZnFe_2O_4 dissolved, content-time (Fig. 6) and Fe_2O_3 dissolved, content-time (Fig. 7) diagrams are plotted only for 60 °C are shown to avoid repetition.

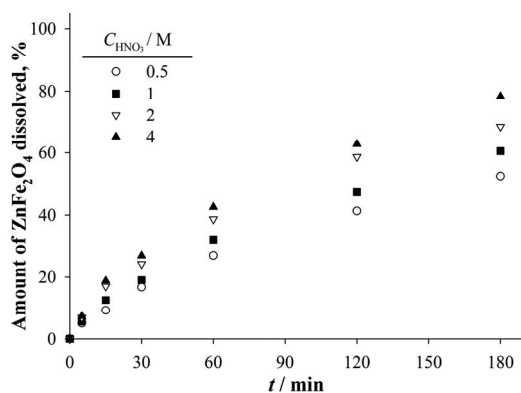


Fig. 6. ZnFe_2O_4 dissolved, content–time diagram for different HNO_3 concentrations at 60 °C.

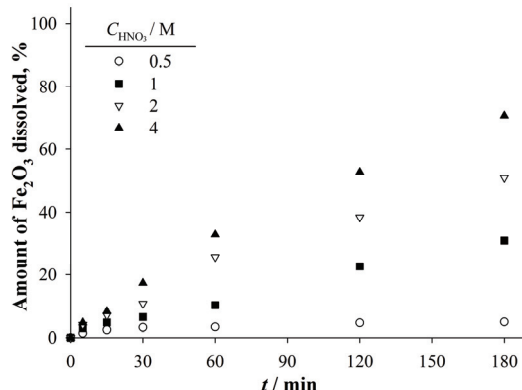


Fig. 7. Fe_2O_3 dissolved, content–time diagram for different HNO_3 concentration at 60 °C.

While the dissolution rate of ZnFe_2O_4 was not affected significantly by the increase in HNO_3 concentration at lower experimental temperatures; increasing temperature resulted in a rise in the effect of the HNO_3 concentration on the dissolution rate of ZnFe_2O_4 (Fig. 4a–d). On the other hand, the dissolution rate of Fe_2O_3 strongly depends on HNO_3 concentration and the dependency increases significantly with increasing temperature (Fig. 5a–d). Therefore, Figs. 6 and 7 show

that the dissolution rate of Fe_2O_3 is more dependent on the HNO_3 concentration than that of ZnFe_2O_4 .

SEM-EDS analysis of the EAFD and the leach residue

SEM-EDS analysis of the EAFD and the leach residue obtained from the experiment performed using 0.5 M HNO_3 at 40 °C are presented in Fig. 8a and b. It could be seen from Fig. 8a that the EAFD consisted of spherical particles with different sizes and fine agglomerated particles with irregular shapes.

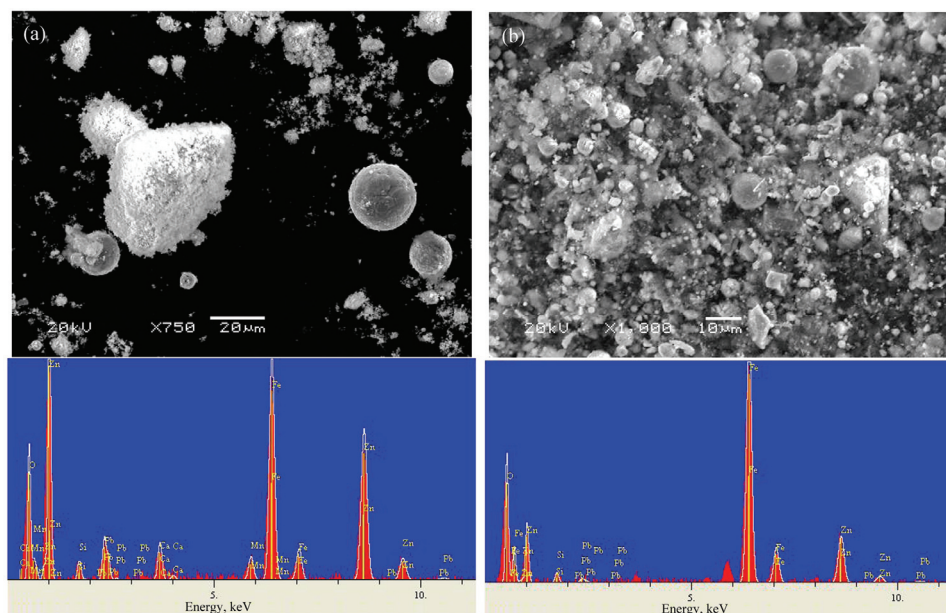


Fig. 8. SEM-EDS analysis of the EAFD and: a) the leach residue and b) obtained from the experiment performed for 180 min using 0.5 M HNO_3 at 40 °C and a stirring speed of 300 rpm.

It was determined from EDS analysis of the EAFD that the particles with spherical shape were rich in iron (Fig. 9b), whereas the particles with irregular shapes were rich in zinc and iron (Fig. 9c). These findings are in good agreement with the XRD analysis of the EAFD (Fig. 1a) and the literature.²⁷ SEM-EDS analysis of the leach residue (Fig. 8b) shows that after the leaching experiment, the particles with spherical shape become more visible and number of the particles with irregular shapes decreases due to higher dissolution rate of particles rich in zinc (ZnO and ZnFe_2O_4) than those rich in Fe_2O_3 .

CONCLUSIONS

It was determined that Fe_2O_3 was not dissolved in 0.5 M HNO_3 solution at 40 °C during a reaction time of 180 min while ZnO reacted rapidly with HNO_3 and was

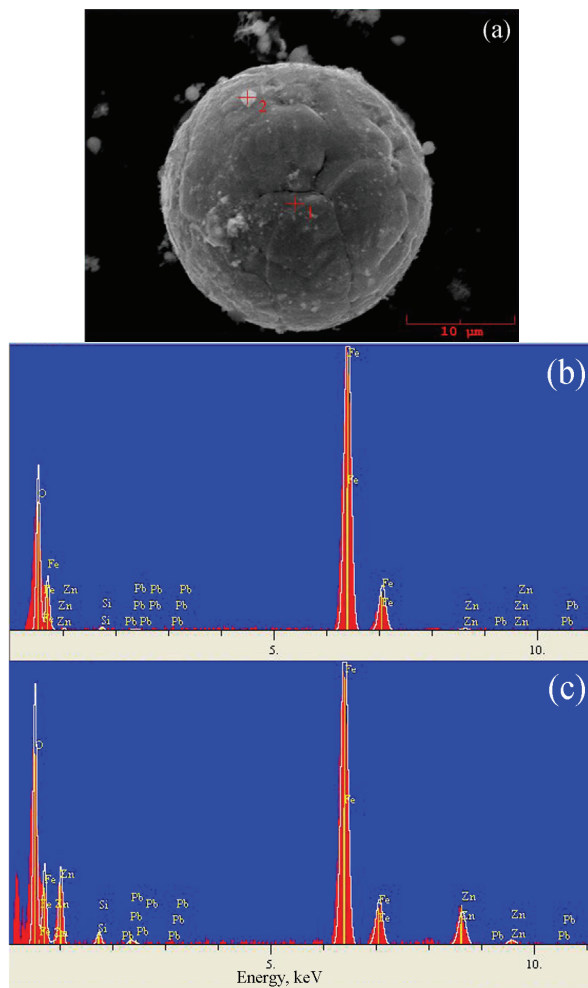


Fig. 9. EDS analysis of the EAFD.

totally dissolved in 5 min reaction time. Thus, it is possible to determine the composition of ZnO, ZnFe₂O₄ and Fe₂O₃ in the EAFD as 28.58, 37.96 and 11.33 %, respectively.

Total dissolution of the ZnFe₂O₄ was obtained from the experiments performed at 80 °C. Although, temperature is effective on the dissolution rate of both ZnFe₂O₄ and Fe₂O₃, dissolution rate of the Fe₂O₃ was more temperature dependent than that of the ZnFe₂O₄.

While the concentration of HNO₃ has slight effect on the dissolution rate of ZnFe₂O₄, the dissolution rate of Fe₂O₃ increased significantly with increasing HNO₃ concentration.

A low HNO_3 concentration (0.5 M) and high experimental temperatures (60-80 °C) should be chosen for the dissolution of the EAFD in HNO_3 solution to minimize the dissolution rate of Fe_2O_3 .

SEM-EDS analysis of EAFD showed that the Fe_2O_3 particles were spherical in shape whereas the shape of ZnO and ZnFe_2O_4 were irregular.

Acknowledgements. This work is a part of research project supported by the Scientific and Technological Research Council of Turkey (TUBITAK, Project No. 118M376). The authors would like to thank TUBITAK for financial support. This work was also supported by the Scientific Research Projects Coordination Unit of Istanbul University-Cerrahpasa (Project No. FDP-2018-31847).

ИЗВОД

ИСПИТИВАЊЕ УСЛОВА СЕЛЕКТИВНОГ ЛУЖЕЊА ZnO , ZnFe_2O_4 И Fe_2O_3 У HNO_3 ИЗ ПРАШИНЕ ЕЛЕКТРОЛУЧНЕ ПЕЋИ

MERT ZORAGA, TUGBA YUCEL, SEDAT ILHAN и AHMET ORKUN KALPAKLI

*Istanbul University-Cerrahpasa, Engineering Faculty, Metallurgical and Materials Engineering Department,
34320, Avcilar, Istanbul, Turkey*

Прашина електролучне пећи (EAFD) углавном укључује једињења која садрже Zn, Fe, Pb, Ca и Mn. Дакле, EAFD је класификован као опасан отпад. У овом раду је испитано понашање растворана једињења која садрже Zn и Fe из EAFD у растворима азотне киселине (HNO_3). Састав једињења која садрже Zn и Fe у EAFD утврђен је као 28,58 % ZnO , 37,96 % ZnFe_2O_4 и 11,33 % Fe_2O_3 . Испитан је утицај брзине мешања, температуре и концентрације HNO_3 на брзину растворана ZnO , ZnFe_2O_4 и Fe_2O_3 и утврђени су оптимални услови лужења. Док се ZnO брзо растворава, брзина растворана ZnFe_2O_4 се повећавала са повећањем температуре и концентрације HNO_3 . Fe_2O_3 није био растворљив у 0,5 M раствору Fe_2O_3 на 40 °C, док је био потпуно растворен у 4 M раствору HNO_3 на 80 °C.

(Примљено 23. маја 2020, ревидирано 16. децембра, прихваћено 17. децембра 2021)

REFERENCES

1. P. Oustadakis, P. E. Tsakiridis, A. Katsiapi, S. Agatzini-Leonardou, *J. Hazard. Mater.* **179** (2010) 1 (<https://doi.org/10.1016/j.jhazmat.2010.01.059>)
2. T. Havlik, M. Turzakova, S. Stopic, B. Friedrich, *Hydrometallurgy* **77** (2005) 41 (<https://doi.org/10.1016/j.hydromet.2004.10.008>)
3. The Union of Chambers and Commodity Exchanges of Turkey, *Turkish Ferrous and Nonferrous Metals Council Report*, 2016, <https://www.tobb.org.tr/Documents/yayinlar/EkonominRapor/Eng/2017%20Economic%20Report.pdf> (accessed 23/10/2018)
4. T. Havlik, B. De Souza, A. M. Bernardes, I.A.H. Schneider, A. Miškufová, *J. Hazard. Mater.* **135** (2006) 311 (<https://doi.org/10.1016/j.jhazmat.2005.11.067>)
5. J. R. Donald, C. A. Pickles, *Can. Metall. Q.* **35** (1996) 255 ([https://doi.org/10.1016/0008-4433\(96\)00009-2](https://doi.org/10.1016/0008-4433(96)00009-2))
6. N. Šrbac, I. Mihajlović, V. Andrić, Ž. Živković, A. Rosić, *Can. Metall. Q.* **50** (2011) 28 (<https://doi.org/10.1179/000844311X552287>)
7. M. H. Morcali, O. Yucel, A. Aydin, B. Derin, *J. Min. Metal.* **48** (2012) 173 (<https://doi.org/10.2298/JMMB111219031M>)

8. X. Lina, Z. Penga, J. Yana, Z. Li, J.Y. Hwang, Y. Zhang, G. Li, *J. Clean. Prod.* **149** (2017) 1079 (<https://doi.org/10.1016/j.jclepro.2017.02.128>)
9. V. N. R. Sarma, K. Deo, A. K. Biswas, *Hydrometallurgy* **2** (1976) 171 ([https://doi.org/10.1016/0304-386X\(76\)90026-8](https://doi.org/10.1016/0304-386X(76)90026-8))
10. M. Cruells, A. Roca, C. Núñez, *Hydrometallurgy* **32** (1992) 213 ([https://doi.org/10.1016/0304-386X\(92\)90119-K](https://doi.org/10.1016/0304-386X(92)90119-K))
11. C. Caravaca, A. Cobo, F. J. Alguacil, *Resour. Conserv. Recycl.* **10** (1994) 35 ([https://doi.org/10.1016/0921-3449\(94\)90036-1](https://doi.org/10.1016/0921-3449(94)90036-1))
12. D. K. Xia, C. A. Picklesi, *Miner. Eng.* **13** (2000) 79 ([https://doi.org/10.1016/S0892-6875\(99\)00151-X](https://doi.org/10.1016/S0892-6875(99)00151-X))
13. Z. Youcai, R. Stanforth, *Miner. Eng.* **13** (2000) 1417 ([https://doi.org/10.1016/S0892-6875\(00\)00123-0](https://doi.org/10.1016/S0892-6875(00)00123-0))
14. N. Leclerc, E. Meux, J. M. Lecuire, *Hydrometallurgy* **70** (2003) 175 ([https://doi.org/10.1016/S0304-386X\(03\)00079-3](https://doi.org/10.1016/S0304-386X(03)00079-3))
15. T. Havlik, B. Friedrich, S. Stopic, *World Metal. – ERZMETALL* **57** (2004) 83 (http://www.metallurgie.rwth-aachen.de/new/images/pages/publikationen/havlik_erzmetall_57_id_9401.pdf)
16. S. Kelebek, S. Yoruk, B. Davis, *Miner. Eng.* **17** (2004) 285 (<https://doi.org/10.1016/j.mineng.2003.10.030>)
17. G. Orhan, *Hydrometallurgy* **78** (2005) 236 (<https://doi.org/10.1016/j.hydromet.2005.03.002>)
18. A. J. B. Dutra, P. R. P. Paiva, L. M. Tavares, *Miner. Eng.* **19** (2006) 478 (<https://doi.org/10.1016/j.mineng.2005.08.013>)
19. R. A. Shawabkeh, *Hydrometallurgy* **104** (2010) 61 (<https://doi.org/10.1016/j.hydromet.2010.04.014>)
20. F. Kukurugya, T. Vindt, T. Havlik, *Hydrometallurgy* **154** (2015) 20 (<https://doi.org/10.1016/j.hydromet.2015.03.008>)
21. N. Peng, B. Peng, H. Liu, D. H. Lin, K. Xue, *Can. Metall. Q.* **56** (2017) 301 (<https://doi.org/10.1080/00084433.2017.1343174>)
22. R. L. Nyirenda, *Miner. Eng.* **4** (1991) 1003 ([https://doi.org/10.1016/0892-6875\(91\)90080-F](https://doi.org/10.1016/0892-6875(91)90080-F)).
23. B. Boyanov, A. Peltekov, K. Ivanov, *Int. J. Chem. Mol. Eng.* **9** (2015) 765 (<https://publications.waset.org/10002705/pdf>)
24. Š. Langová, J. Riplová, S. Vallová, *Hydrometallurgy* **87** (2007) 157 (<https://doi.org/10.1016/j.hydromet.2007.03.002>)
25. Z. Sedláková, D. Orac, T. Havlik, *Acta Metall. Slovaca* **12** (2006) 338 (<https://www.censo.fmmr.tuke.sk/content/clanky/200606.pdf>)
26. T. Havlik, F. Kukurugya, D. Orac, L. Parilak, *World Metal. – ERZMETALL* **65** (2012) 48 (https://www.researchgate.net/publication/279701830_Acidic_leaching_of_EAF_steelmaking_dust)
27. M. C. Da Silva, A. M. Bernardes, C. P. Bergmann, J. A. S. Tenório, D. C. R. Espinosa, *Ironmak. Steelmak.* **35** (2008) 315 (<https://doi.org/10.1179/030192307X232936>).



Spatial and temporal evaluation of the physicochemical quality of domestic/industrial water in the Kırklareli Reservoir (Turkish Thrace)

HÜSEYİN GÜHER¹, BURAK ÖTERLER¹, BELĞİN ÇAMUR ELİPEK¹, OKAN YELER²
and GAZEL BURCU AYDIN^{1*}

¹Trakya University, Faculty of Science, Department of Biology, 22100, Edirne, Turkey and

²Van Yüzüncü Yıl University, Muradiye Vocational School, 65100, Van, Turkey

(Received 1 June, revised 19 August, accepted 7 September 2021)

Abstract: The Kırklareli Reservoir, located in the Meriç-Ergene River Basin, is an important drinking/industrial freshwater resource of the Kırklareli Province. In order to ensure the sustainable use of this important reservoir, its current situation should be examined periodically and evaluated by multivariate analyses. For this reason, water samples were taken between the dates April 2018 and February 2019 at monthly intervals from 3 different stations. The data on the environmental and physicochemical variables (water temperature, dissolved oxygen, pH, salinity, conductivity, total dissolved solids, chlorophyll-*a*, light permeability, fluoride, chloride, NO₂-N, NO₃-N, PO₄, SO₄ and essential/potentially toxic elements) were measured and evaluated according to the classes of surface water quality control regulation of Turkey. The parameters exceeding first-class water quality values (chlorophyll-*a*, pH, NO₂-N, chloride, selenium) were mapped in GIS using the spline integration approach. In addition, the sodium absorption ratio, Kelly index values and magnesium ratio, were calculated to evaluate the water quality for agricultural irrigation water standards. The water quality of the reservoir was evaluated using multivariate analyses (Bray-Curtis similarity index, correspondence analyses, Pearson correlation index). As a result, it was emphasized that the use of the GIS approach is a potential useful method for monitoring the sustainable water quality of the Kırklareli Reservoir, which was determined to have an oligomesotrophic character.

Keywords: water quality; GIS; environmental variables; multivariate analyses.

INTRODUCTION

Due to the increasing need for freshwater resources because of the increasing human population and the increasing pollution of existing resources, studies on the sustainability of water resources have become increasingly important. Espe-

* Corresponding author. E-mail: gburcuaydin@trakya.edu.tr
<https://doi.org/10.2298/JSC210601074G>

cially as water stored in lakes, ponds, dams, and reservoirs is used not only as drinking and industrial water, but also for irrigation of agricultural lands and aquaculture. When considered from this point of view, to determine for what purpose a water resource can be used, first of all, the water quality of the aquatic system should be known.

The physicochemical properties of a water source give important information about the current state of the water. However, considering the temporal and spatial changes of a water resource, monitoring studies are needed for the reliable determination of water quality, which can make interpretation difficult because the data obtained from these studies contain too many variables.¹ Therefore, there is a need for methods that can evaluate multiple factors at the same time and allow the analysis of the whole data set instead of a single one.^{2,3} Multivariate statistical techniques can be used for the assessment of water quality.^{2–10} Thus, it has become increasingly important to use computer-aided data analysis and visualization tools in the studies of temporal and spatial evaluation of the parameters measured for monitoring water quality, and consequently in the studies carried out for the protection, development, and management of water resources.¹¹ In addition, it is expected that water quality monitoring studies in aquatic ecosystems, which require time and financial aid, will continue to ensure sustainable use. This means more time and more money spent. However, the monitoring periods of water quality can be determined by the results of appropriate multivariate analysis of the studies, which are carried out periodically for at least one year in a aquatic ecosystem and include sufficient physicochemical data.

In particular, geographic information system (GIS) is one of the most important software in which graphical and objective features of geographic data in different formats are collected and analysed in a common coordinate system in layers. Therefore, in terms of examining the physicochemical changes in water resources, it is valuable software that enables accurate information to be obtained very rapidly.^{12,13} By facilitating the use of data sources with the help of these methods, it becomes increasing possible to evaluate water quality parameters and determine appropriate strategies in the management of water resources.^{5,14–16} The complexity, which may occur due to the excess of criteria used in the assessment of water quality, has been evaluated using techniques such as GIS and multiple criteria decision making (MCDM) analyses in recent years. Thus, by combining spatial data with other data sources, easy and more reliable results, expressing water quality risks, and estimating spatial distributions, are obtained.^{17–19} In Turkey, GIS and remote sensing systems are emphasized in the monitoring of the quality of water resources, and these programs are being used more.^{1,11,13,19–22}

The Kırklareli Reservoir, which is an artificial lentic ecosystem, is located in the Meriç-Ergene River Basin at Turkish Thrace and it provides important freshwater supplies to the area. As with many freshwater ecosystems, it is reported

that this reservoir is being adversely effected by agricultural and domestic pressure.^{23,24} The Kırklareli Reservoir has an area of 6 km² and a volume of 112 hm³. In previous studies, the contents of pesticides and potentially toxic elements were examined during the spring season.^{23,24}

In this study, the water quality of the Kırklareli Reservoir was evaluated. For this purpose, the physicochemical properties of the reservoir were evaluated using samples obtained at 3 different stations between the dates April 2018 and February 2019 at monthly intervals. The results on dissolved oxygen, water temperature, pH, salinity, conductivity, total dissolved solids, chlorophyll-*a*, light permeability, nitrite nitrogen, nitrate nitrogen, sulfate, phosphate, calcium, magnesium, chloride and some other essential/potentially toxic element (B, Na, Mg, Al, Ca, Cr, Mn, Fe, Co, Ni, Cu, Zn, Se, As, Cd, Ba, Pb) contents in Kırklareli reservoir were determined and compared with the limit values given in the regulation of surface water resources of Turkey.²⁵ In addition, sampling stations and sampling periods were compared using the Bray–Curtis similarity index. Some measured parameters of environmental variables were mapped temporary and spatially using the spatial analysis module of the Arc MAP software in the GIS. In this way, it was aimed to identify and visualize areas with high/low water quality by combining the water quality data obtained from Kırklareli Reservoir under a single water quality index, and to determine the temporal and spatial sampling locations and times by grouping periodic analyses.

MATERIALS AND METHODS

Details about the study area are given in Supplementary material to this paper.

A total of 3 sampling stations (St.) which represent the ecological characters of the lake were chosen to take the water samples. The analyses of some parameters (temperature, pH, conductivity, dissolved oxygen, salinity and TDS) in water samples taken from each station at a depth of approximately 2 m with Nansen water sampler were measured during field studies with Orion Star S/N 610541 model land type multiparameter device. Also, the water samples taken from each sampling stations at monthly intervals by Nansen water sampler were put into 2 L dark glass bottles and transported to the laboratory for other chemical analyses (fluoride, chloride, NO₂-N, NO₃-N, PO₄, SO₄, B, Na, Mg, Al, Ca, Cr, Mn, Fe, Co, Ni, Cu, Zn, Se, As, Cd, Ba, Pb). After the water samples were filtered, the pH levels were lowered by adding HNO₃ and HCl to 10 ml of the sample and were stored for analysis. The ion and metal analyzes of the water taken from each station and in each sampling period were measured in 3 repetitions in Agilent Technologies 7700 XX ICP-MS system device with reference to EPA 200.8 and the average values were obtained.²⁶ By taking 3 times the standard deviation (Std. deviation/square root (*n*)) of blank sample analysis results studied in the measurement limit (*LOD*) intermediate precision conditions in the device in question; the limit of detection (*LOQ*) was calculated by taking 10 times the standard deviation (Std. deviation/square root (*n*)) of the results calculated as a result of intermediate precision studies. In addition, the reproducibility is ensured by 10 independent studies at 2 different concentrations, the reproducibility is ensured by working at 2 different concentrations for 5 days, and the reproducibility and reproducibility values obtained with reference to the validation parameters and

criteria were observed in accordance with the HorRatR (it is a normalized performance parameter indicating the acceptability of methods of analysis with respect to among-laboratory precision (reproducibility)) < 2 criteria for each element component. 10 independent studies at 2 different concentrations were used for the recovery where 80–120 % is sought in the measurements and Grubb values (this value detects outliers from normal distributions) from 10 independent studies at 25 ppb were used for accuracy (<2.29).²⁶ The light permeability at each station in each sampling period was measured by using a Secchi disc and the chlorophyll-*a* values of the water samples were determined by classical spectrophotometric methods.²⁷ The obtained data were evaluated according to the surface water resources control regulation and water quality class of the lake were determined.²⁵ In addition, the sodium adsorption rate value (*SAR*), Kelly index (*KI*) and magnesium ratio (*MgR*), the rates giving information about whether the water is suitable for irrigation or not, of the waters were calculated over the meq/L ratios by using the values of Na, Ca, and Mg ions from the obtained chemical analysis results.^{28,29}

The similarities of the sampling stations and periods in the distribution of the data were grouped by the Bray–Curtis cluster analysis by the BioDiversity Pro 2.0 program, and the results were also supported by the correspondence analysis.³⁰ The relationships between physicochemical parameters were evaluated by Pearson correlation coefficient in the Graphpad PRISM software, trial version. The parameters exceeding the second class quality values according to the Water Pollution Control Regulation²⁵ were mapped by the spatial analysis module using GIS supported in the ArcMap 10.3.1 package program. For this aim, the satellite image of the WGS84-Zone 36 coordinate plane in JPEG format, obtained from Google Earth Pro, connected to the metric coordinate system, was transferred to the ArcMAP, and the stations were digitized and turned into vector data.

RESULTS AND DISCUSSION

Data pertaining to physical and inorganic-chemical parameters (Tables S-I and S-II of the Supplementary material) were evaluated according to the water quality classes included in the surface water resources control regulation.²⁵

Accordingly, in terms of physical and inorganic-chemical parameters, it is observed that the averages of the water temperatures of the stations are at seasonal expectations. However, the pH values vary between 8.1 and 9.3, and these values exceed the second class water quality values.²⁵ The average of the dissolved oxygen values measured at the sampling stations was between 7.4 and 13.7 mg/L and this case indicates that the lake has first class water quality in terms of this parameter, and no significant difference (9.7–9.8 mg/L) was found between the sampling stations (Table S-II). Dissolved oxygen is an important parameter for the sustainability of the self-cleaning capacity of water as well as for aquatic organisms. This parameter, which has a great role in physiological and chemical events, should not exceed first class quality values in aquatic ecosystems for protecting the ecological balance. Although chloride ion values were determined between min. 6.1 mg/L and max. 28.7 mg/L in averages, they were found high at St. 1, especially in summer and autumn seasons. Nevertheless, the chloride ion values did not reach the second class quality (200 mg/L) values in terms of the surface water resources

quality values. The sodium values, which did not show a significant difference between the stations and were detected at low rates, vary between 1.2 and 6.6 mg/L on averages and did not exceed the first class water quality value (125 mg/L). Since the total dissolved substance ratio was between 105 and 158 mg/L at average, and it did not exceed 500 mg/L, it was found in first class water quality. Conductivity values measured in the study were well below the 2500 µS/cm limit determined for drinking water and were between the limits compatible with freshwater characters (determined between 213–322 µS/cm in averages and reached the highest values (304 µS/cm) at the St. 1). However, calcium and magnesium are elements that originate from the soil and rock structure where water is located and must be taken for human biology. Ca and Mg values measured in this study did not exceed the limit values in terms of drinking and using water. The chlorophyll-*a* values measured in the study also did not exceed the eutrophication limit values.

When the nutrient salts, which are among inorganic-chemical parameters, were evaluated, it was observed that the sulfate values did not show a significant difference in the stations, varying in range 9.7–10.3 mg/L in averages. They remained at the first class water quality value specified in the regulation on surface water quality.²⁵ Nitrate nitrogen values were determined as 5 mg/L (min. 0.03, max. 2.1 mg/L in averages), which indicated at first class water quality in the regulation on surface water quality. In terms of phosphate amount, it was observed that the values that should not exceed the limit of 0.1 mg/L increased to 0.7 mg/L only in May, and the station averages did not exceed 0.1 mg/L too much. In terms of nitrite nitrogen, the values generally determined in first and second class water quality decreased to third class water quality at all stations in May. It supports the view that nutrient salts may come from the agricultural or forest areas around the dam lake and they can carry out intensively in May, by runoff.

When looking at the inorganic contamination parameters measured in the study, according to the regulation on surface water quality, the values for Cd (max. 0.1 ppb), Pb (max. 2 ppb), As (max. 1.1 ppb), Cu (max. 2.5 ppb), Cr (max. 11.5 ppb), Co (max. 0.1 ppb), Ni (max. 1.7 ppb), Zn (max. 6.6 ppb), fluoride (max. 120 ppb), Fe (max. 108.6 ppb), Mn (max. 24 ppb), B (max. 57 ppb), Ba (max. 34 ppb) and Al (max 0.1 mg/L) did not exceed the first class water quality values.²⁵ Selenium values approached the limit value at all stations in November. Although it is one of the elements necessary for the human body, it is reported that high selenium ratios can cause disorders in some organs and systems.³¹

According to the Bray–Curtis similarity analysis, while the degree of similarity of the months according to the physicochemical contents was determined > 80 %. Also, correspondence analysis results grouped the sampling periods in 3 different clusters for the physicochemical similarities (Fig. 1).

Accordingly, while December, January and April were a cluster, the other months (excluding February) constituted the second cluster. Although the stat-

ions had some differences especially in terms of parameters exceeding the limit values, it was seen that the similarity rates are over 90 % in terms of their general physicochemical content. The sampling stations St. 1 and St. 2 have found to be the most similar each other (Fig. 2). The reason for this high similarity rate seen in the stations can be explained by the fact that the study area is a small water reservoir, while the fact that the St. 3 is surrounded by agricultural and forest area may have caused it to be small differences from the other stations. Thus, only one station can be used for the monitoring studies which will be performed in this reservoir.

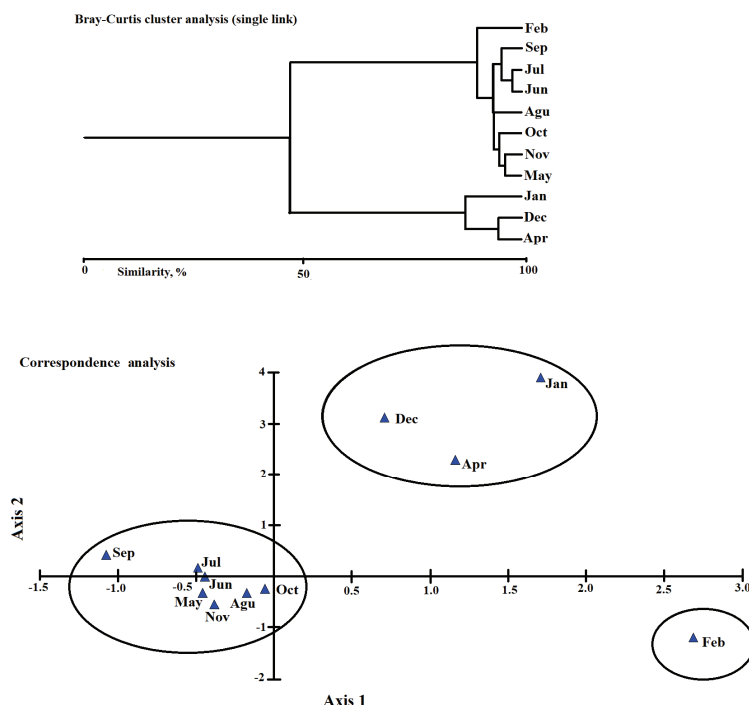


Fig. 1. Monthly similarities according to Bray–Curtis index and cluster analysis.

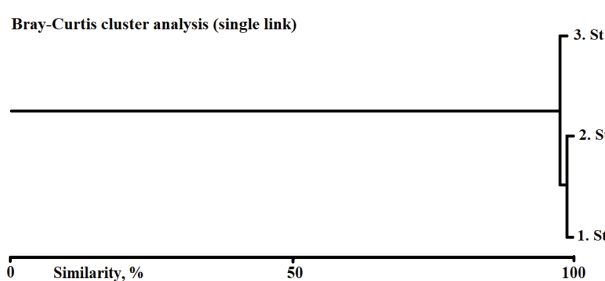


Fig. 2. Similarity of sampling stations according to Bray–Curtis index analysis.

The margin of error is considerably reduced due to GIS using the high-resolution raster data set in water quality monitoring and evaluation studies.¹¹ Based on this idea, the data of pH, nitrite, chloride, and selenium measured in Kirkclareli reservoir lake and found to exceed the first class water quality and the data of chloride value and chlorophyll-*a* distributions of the approaching second class water quality were visualized with the distribution maps created in the spatial analysis results made in the Arc MAP were given in Fig. S-2–S-6 of the Supplementary material.

Accordingly, it was determined that the pH, nitrite nitrogen, selenium, chloride and chlorophyll-*a* values measured at the St. 3 were low, but the chlorophyll-*a* values are low at the St. 1, where the pH was relatively low. Similarly, it was seen that the chlorophyll-*a* values were also high in the St. 3 where the pH value was high. However, at the St. 1, where nitrite nitrogen, chloride and selenium values were high, chlorophyll-*a* values were low. This situation reveals that pH is an important factor in the distribution of algae and supports the view that algae develop faster at high pH values. During periods of algae growth, photosynthesis, respiration, and decay affect the CO₂ level in lakes. This case can cause pH fluctuations. During the periods when photosynthetic microalgae multiply, the pH may rise during the daytime when these organisms fix CO₂.³² It is suggested that selenium limit ratio in drinking water is 10 ppb specified by Turkish Standards Institute.³³ Selenium is known to be released to the environment by means of sewage effluent, agricultural runoff and industrial waste water.³⁴ In this study, selenium was measured at above the limit values at some sampling periods (Table S-I).

It is generally known that there is a relationship between Secchi disc depth and chlorophyll-*a*. Secchi depth in the eutrophic reservoir is partially related to the chlorophyll-*a* content. In the mesotrophic reservoir, the Secchi depth cannot be determined only by algae. In the oligotrophic reservoir, the Secchi depth is neither related to chlorophyll-*a* nor to algae in the water. Inorganic turbidity or colour is an important factor in influencing Secchi depth in a mass of water. High rates of inorganic substances also cause turbidity.^{35,36} The physicochemical data measured in the Kirkclareli reservoir indicate that the lake has an oligomesotrophic character. In this case, a significant relationship between Secchi disk depth and chlorophyll-*a* values cannot be expected.

With respect to the Pearson correlation index relations between the physicochemical variables, the fluoride and nitrite showed positive correlation each other ($r = +0.999, \rho < 0.05$). Chloride had positive correlations with salinity ($r = +0.999, \rho < 0.05$), conductivity ($r = +0.998, \rho < 0.05$) and TDS ($r = +0.999, \rho > 0.05$). Phosphate and chlorophyll-*a* showed positive correlation ($r = +0.997, \rho < 0.05$). TDS had positive correlations with salinity ($r = +0.998, \rho < 0.05$), and conductivity ($r = +0.999, \rho < 0.05$). Also there was positive correlation between DO and water

temperature ($r = +1.00$, $\rho < 0.001$). Electrical conductivity (EC) is generally utilized as a salinity indicator and is directly affected by chloride ions. Thus, it is possible to find a correlation between EC, Cl⁻ concentrations, and salinity as found by many studies and this study.³⁷ It is known that the concentration of chlorophyll-*a* is related to inorganic phosphate concentrations and the Pearson Correlation Index result positive correlation between phosphate and chlorophyll-*a* support it.³⁸

The value of Kelly index (*KI*) is less than 1 in all stations and the water is suitable for irrigation (Table S-I). With respect to the sodium adsorption rate (*SAR*), the value is between 0 and 10 in all stations and the results show that the water is excellent for irrigation (Table S-I). The value of magnesium ratio (*MgR*) is 50 in all stations and is suitable for irrigation (Table S-I).

Since the Kırklareli Reservoir is located in the Ergene Basin, which is an important agricultural and industrial area of Turkey, it is inevitable that there is a pollution load in the other drinking water reserves here and around it. When we look at the previous studies in the field, it is seen that there is a pesticide and ion pollution load originating from agricultural and industrial applications both in Kırklareli Reservoir and other drinking water reservoir around it.^{23,24,39}

So far, there are similar studies in our country by using GIS methods.^{1,11,13,19–22} In these studies, it is aimed to evaluate the potential use of appropriate software tools in water quality determination studies. Thus, it is easier and more understandable to monitor water quality classes with the produced GIS maps. In the study carried out in Lake Gala, it has been summarized more effectively thanks to the GIS that nitrite nitrogen poses the greatest risk in the lake.²² In the study performed in the Damsa Dam Lake, it was easily observed with GIS that it is not suitable in terms of some ions and toxic substances measured from the lake.¹¹ For the efficient use of water reservoirs and their ecological continuity, water quality should be continuously monitored by repeating it at certain periods and necessary interventions should be made in case of pollution.

CONCLUSION

As a result of this study, it was determined that the water quality of Kırklareli Reservoir was generally compatible with the first-class water quality in terms of the parameters measured in the study. Considering the similarities of the sampling periods and stations determined in the study, it was concluded that the sampling periods could be selected seasonally in monitoring the water quality of the Kırklareli reservoir lake, and sampling from two sampling stations (St. 1 and St. 3) would be sufficient. In addition, it should be taken into consideration that GIS can be a more effective evaluation system visually in the data monitoring of surface water resources.

SUPPLEMENTARY MATERIAL

Additional data and information are available electronically at the pages of journal website: <https://www.shd-pub.org.rs/index.php/JSCS/article/view/10811>, or from the corresponding author on request.

ИЗВОД

ПРОСТОРНА И ВРЕМЕНСКА ПРОЦЕНА ФИЗИЧКО-ХЕМИЈСКОГ КВАЛИТЕТА ВОДЕ У
ЗА ПИЋЕ/УПОТРЕБУ У АКУМУЛАЦИЈИ KIRKLARELI (ТУРСКА ТРАКИЈА)

KATARINA SENTA WISSIAK GRM и IZTOK DEVETAK

University of Ljubljana, Faculty of Education, Kardeljeva pl. 16, 1000 Ljubljana, Slovenia

Резервоар Киркларели, који се налази у сливу реке Meriç-Ergene, важан је извор воде за пиће/коришћење у провинцији Kirklareli. Како би се осигурала одржива употреба овог важног резервоара, његово тренутно стање треба повремено прегледати и оценити мултиваријантним анализама. Из тог разлога, узорци воде узимани су на месечном нивоу, од априла 2018. до фебруара 2019. године, са 3 различите станице. Подаци о еколошким и физичко-хемијским варијаблама (температура воде, растворени кисеоник, pH, салинитет, проводљивост, укупне растворене чврсте материје, хлорофил-*a*, пропустљивост светlostи, флуориди, хлориди, NO₂-N, NO₃-N, PO₄, SO₄ и есенцијални/потенцијално токсични елементи) су измерени и оцењени према класама у регулативи контроле квалитета површинских вода Турске. Параметри који премашују вредности квалитета воде прве класе (хлорофил-*a*, pH, NO₂-N, хлорид, селен) мапирани су у географском информационом систему (GIS), уз коришћење Spline интеграције. Такође су израчунати однос апсорпције натријума, вредности Kelly индекса и однос магнезијума да би се проценио квалитет воде за потребе наводњавања у пољопривреди. Квалитет воде у резервоару је оцењиван коришћењем мултиваријантних анализа (Gray-Curtis similarity index, correspondence analyses, Pearson correlation index). Као резултат, закључено је да је коришћење GIS приступа потенцијално корисна метода за праћења одрживог квалитета воде у резервоару Киркларели, за који је утврђено да има олигомезотрофни карактер.

(Примљено 1. јуна, ревидирано 19. августа, прихваћено 7. септембра 2021)

REFERENCES

1. O. Arslan, *Jeodezi, Jeoinformasyon Arazi Yönetimi Derg.* **99** (2008) 5 (https://www.hkmo.org.tr/resimler/ekler/b89a2e980724cb8_ek.pdf) (in Turkish)
2. C. Filik-İşcen, Ö. Emiroglu, S. İlhan, N. Arslan, V. Yilmaz, S. Ahiska, *Monit. Assess. Environ.* **144** (2008) 269 (<https://doi.org/10.1007/s10661-007-9989-3>)
3. C. Tokatlı, A. Çiçek, Ö. Emiroğlu, N. Arslan, E. Köse, H. Dayioğlu, *Environ. Earth Sci.* **71** (2014) 2185 (<https://doi.org/10.1007/s12665-013-2624-4>)
4. K. P. Singh, A. Malik, D. Mohan, S. Sinha, *Wat. Res.* **38** (2004) 3980 (<https://doi.org/10.1016/j.watres.2004.06.011>)
5. K. P. Singh, A. Malik, D. Mohan, S. Sinha, *Anal. Chim. Acta* **538** (2005) 355 (<https://doi.org/10.1016/j.aca.2005.02.006>)
6. S. Shrestha, F. Kazama, *Environ. Model. Software* **22** (2007) 464 (<https://doi.org/10.1016/j.envsoft.2006.02.001>)
7. Y. Zhang, F. Guo, W. Meng, X. Q. Wang, *Environ. Monit. Assess.* **152** (2009) 105 (<https://doi.org/10.1007/s10661-008-0300-z>)

8. T. G. Kazi, M. B. Arain, M. K. Jamali, N. Lalbani, H. I. Afridi, R. A. Sarfraz, J. A. Baig, A. Q. Shah, *Ecotoxicol. Environ. Saf.* **72** (2009) 301 (<https://doi.org/10.1016/j.ecoenv.2008.02.024>)
9. A. Gamble, M. Babbar-Sebens, *Monit. Assess.* **184** (2012) (<https://doi.org/10.1007/s10661-011-2005-y>)
10. J. Badillo-Camacho, E. Reynaga-Delgado, I. Barcelo-Quintal, P. Valle, U. Lopez-Chuken, E. Orozco-Guareno, J. Alvarez-Bobadilla, S. Gomez-Salazar, *JEP* **6** (2015) 215 (<http://dx.doi.org/10.4236/jep.2015.63022>)
11. C. Kalıpçı, H. Cüce, S. Toprak, *Karaelmas Sci. Eng. J.* **7** (2017) 312 (<https://dergipark.org.tr/tr/download/article-file/1329403>)
12. T. Susam, S. Karaman, T. Öztekin, *JAFAG* **23** (2006) 75 (<https://docplayer.biz.tr/14130594-Yuzey-sulari-coografi-bilgi-sistemi-tokat-ili-ornegi-geographic-information-system-of-surface-waters-tokat-province-sample.html>)
13. M. C. Bağdatlı, E. Kalıpçı, G. G. İpek, *Nevşehir J. Sci. Techol.* **6** (2017) 149 (<https://doi.org/10.17100/nevbiltek.336203>) (in Turkish)
14. V. Simeonov, J. A. Stratis, C. Samara, G. Zachariadis, D. Vousta, A. Anthemidis, M. Sofoniou, T. Kouimtzis, *Wat. Res.* **37** (2003) 4119 ([https://doi.org/10.1016/S0043-1354\(03\)00398-1](https://doi.org/10.1016/S0043-1354(03)00398-1))
15. C. Mendiguchia, C. Moreno, D. M. Galindo-Riano, M. Garcia-Vargas, *Anal. Chim. Acta* **515** (2004) 143 (<https://doi.org/10.1016/j.aca.2004.01.058>)
16. N. Lambrakis, A. Antonakos, G. Panagopoulos, *Wat. Res.* **38** (2004) 1862 (<https://doi.org/10.1016/j.watres.2004.01.009>)
17. P. Bolstad, *GIS Fundamentals: A First Text on Geographic Information Systems*, Eider Press, Annecy le Vieux, 2005 (<http://pdfpremiumfree.com/download/gis-fundamentals-a-first-text-on-geographic-information-systems-4th-edition-pdf/>)
18. P. Fu, J. Sun, *Web GIS: principles and applications*, Esri Press, Annecy le Vieux, 2010 (https://www.researchgate.net/publication/297263456_Web_GIS_principles_and_applications)
19. M. Kavurmacı, A. Üstün, *KSU J. Agric. Nat.* **19** (2016) 208 (<https://doi.org/10.18016/ksujns.08103>)
20. S. Girgin, Z. Akyürek, N. Usul, *Development of a Geographical Information System for Water Quality Data Analysis System in Turkey*, 3rd GIS Days in Turkey, 2004, İstanbul, Turkey, October 6–9, Book of Abstracts, Fatih University, İstanbul, 2004, p. 16
21. E. Sener, S. Sener, A. Davraz, *Hydrogeol. J.* **17** (2009) 2023 (<https://doi.org/10.1007/s10040-009-0497-0>)
22. C. Tokatlı, E. Köse, A. Uğurluoğlu, A. Çiçek, Ö. Emiroğlu, *Sigma* **32** (2014) 501 (https://www.researchgate.net/publication/270339895_Use_of_Geographic_Information_System_GIS_to_Evaluate_the_Water_Quality_of_Gala_Lake_Edirne)
23. C. Tokatlı, *J. Eng. Nat. Sci.* **38** (2020) 402 (https://www.researchgate.net/publication/340379057_APPLICATION_OF_WATER_QUALITY_INDEX_FOR_DRINKING PURPOSES_IN_DAM_LAKES_A_CASE_STUDY_OF_THRACE_REGION)
24. C. Tokatlı, *Aquat. Res.* **3** (2020) 134 (<https://doi.org/10.3153/AR20011>)
25. *Turkish Regulations 2015. Regulation on Surface Water Quality Management*, Official Gazette, dated April 15, 2015. No.: 29327 (<http://suyonetimiormansu.gov.tr>) (in Turkish)
26. *EPA Method 200.8: Determination of Trace Elements in Waters and Wastes by Inductively Coupled Plasma-Mass Spectrometry*, U.S. Environmental Protection Agency, Cincinnati, OH, 1994 (<https://www.epa.gov/homeland-security-research/epa-method-2008-determination-trace-elements-waters-and-wastes>)

27. Ö. Egemen, U. Sunlu, *Water Quality*, Ege University, Fisheries Faculty Publications, İzmir, 1999, p. 150 (In Turkish)
28. S. Madhav, A. Ahamad, A. Kumar, J. Kushawaha, P. Singh, P. K. Mishra, *Geol. Ecol. Landsc.* **2** (2018) 136 (<https://doi.org/10.1080/24749508.2018.1452485>)
29. P. Balamurugan, P.S. Kumar, K. Shankar, R. Nagavinothini, K. Vijayasurya, *J. Chil. Chem. Soc.* **65** (2020) 4707 (<http://dx.doi.org/10.4067/S0717-97072020000104697>)
30. N. McAleece, J. D. G. Gage, P. J. D. Lambshead, G. L. J. Paterson, *Biodiversity Professional Statistic Analysis Software*, Jointly Developed by the Scottish Association for Marine Science and the Natural History Museum London, 1997 (<https://biodiversity-pro.software.informer.com/2.0/>)
31. F. Temamoğulları, A. H. Dinçoğlu, *Kafkas Univ. Vet. Fak. Derg.* **16** (2010) 199 (<https://doi.org/10.9775/kvfd.2009.479>)
32. Z. Dubinsky, J. Rotem, *Oecologia* **16** (1974) 53 (<https://doi.org/10.1007/BF00345087>)
33. TS 266 (*Turkish Standard, water intended for human consumption*), 2005 (<http://infogroup.com.tr/media/files/sular.pdf>)
34. ATSDR (*Agency for Toxic Substances and Disease Registry*) 2003. *Toxicological Profile for Selenium*, U.S. Department of Health and Human Services, Atlanta, GA, (<https://www.atsdr.cdc.gov/ToxProfiles/tp92.pdf>)
35. P. L. Brezonik, *Can. J. Fish. Aquat. Sci.* **35** (1978) 1410 (<https://doi.org/10.1139/f78-222>)
36. S. Heddam, *Environ. Process.* **3** (2016) 525 (<https://doi.org/10.1007/s40710-016-0144-4>)
37. H. Peinado-Guevara, C. Green-Ruiz, J. Herrera-Barrientos, O. Escolero-Fuentes, O. Delgado-Rodríguez, S. Belmonte-Jiménez, M. Ladrón de Guevara, *Cien. Inv. Agr.* **39** (2012) 239 (<http://dx.doi.org/10.4067/S0718-16202012000100020>)
38. L. Maslukah, M. Zainuri, A. Wirasatriya, U. Salma, *J. Ecol. Eng.* **20** (2019) 25 (<https://doi.org/10.12911/22998993/108700>)
39. C. Tokathlı, Y. Baştatlı, B. Elipek, *J. Eng. Nat. Sci.* **35** (2017) 750 (https://www.researchgate.net/publication/321965869_WATER_QUALITY_ASSESSMENT_OF_DAM_LAKES_LOCATED_IN_EDIRNE_PROVINCE_TURKEY).

SUPPLEMENTARY MATERIAL TO

**Spatial and temporal evaluation of the physicochemical quality
of domestic/industrial water in the Kırklareli Reservoir
(Turkish Thrace)**

HÜSEYİN GÜHER¹, BURAK ÖTERLER¹, BELĞİN ÇAMUR ELİPEK¹, OKAN YELER²
and GAZEL BURCU AYDIN^{1*}

¹Trakya University, Faculty of Science, Department of Biology, 22100, Edirne, Turkey and

²Van Yüzüncü Yıl University, Muradiye Vocational School, 65100, Van, Turkey

J. Serb. Chem. Soc. 87 (3) (2022) 389–399

STUDY AREA

The study area is located in Kırklareli Province in the Turkish Thrace region approximately 5 km east of the city center (Fig. S-1). Kırklareli reservoir lake that provides drinking and industrial freshwater supplies to the province of Kırklareli is located between 41°44.12'21.1236" N and 27°16'45.8400" E coordinates. It was built on the Şeytandere stream between 1985-1995 for irrigation and flood control.

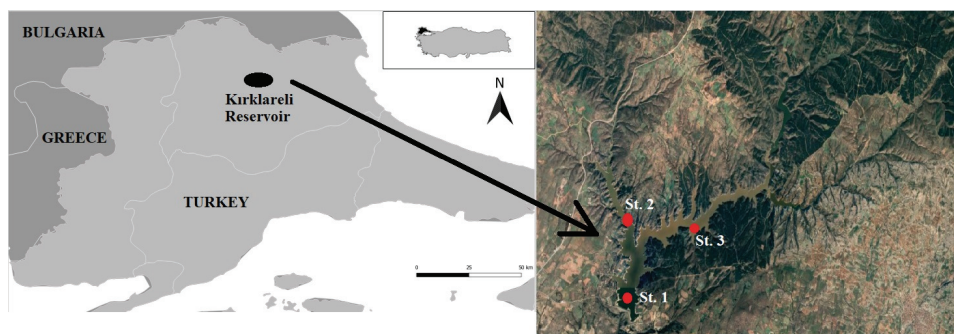


Fig. S-1. Location of Kırklareli Reservoir and the sampling stations.

*Corresponding author. E-mail: gburcuaydin@trakya.edu.tr

Table S-I. Monthly average values of the data obtained from the stations

Element	Content, ppb												
	Apr	May	Jun	Jul	Aug	Sept	Oct	Nov	Dec	Jan	Feb	Ave	SD
B	5.87	8.56	13.06	52.88	50.78	40	57.83	0.96	18.8	20.8	30.26	27.25	±20.32
Na	134	7692	5742	5768	5964	5913	6644	8378	1432	1252	1873	4727.09	±2709.18
Mg	2191	10994	8848	9715	11034	9722	12296	12270	2350	1901	8791	8192	±4056.7
Al	6.68	6.17	15.04	5.28	10.4	7.2	9.7	15.41	5.94	72.9	120.07	24.98	±37.05
Ca	4618	21215	14875	14577	17163	12116	19670	22313	4092	3038	16594	13661	±6926.65
Cr	0.345	3.642	11.519	4.68	3.6	0.827	1.355	2.46	0.912	0.379	1.112	2.8	±3.25
Mn	0.354	1.623	2.944	1.471	2.869	1.8	24.21	6.114	0.475	0.797	2.277	4.08	±6.86
Fe	33	82.67	83.2	104.84	100.21	51.91	83.97	108.66	32.61	66.58	29.46	70.65	±29.83
Co	0.023	0.083	0.128	0.181	0.185	0.11	0.145	0.121	0.032	0.039	0.13	0.11	±0.06
Ni	0.262	0.482	1.717	0.952	0.98	0.577	1.061	0.962	0.69	0.44	1.589	0.88	±0.46
Cu	0.129	0.816	2.55	0.276	0.561	0.933	0.583	0.615	0.207	0.19	0.756	0.69	±0.67
Zn	0.664	2.631	0.531	2.183	2.609	3.017	6.622	5.577	0.785	0.928	3.636	2.65	±2.01
As	0.15	0.623	0.498	0.463	0.585	0.907	1.191	1.182	0.023	0.209	1.077	0.63	±0.41
Se	2.564	9.754	7.273	9.08	11.536	0.3	7.937	16.731	3.013	2.901	0.055	6.47	±5.2
Cd	0.006	0.027	0.041	0.03	0.048	0.057	0.157	0.049	0.009	0.01	0.042	0.04	±0.04
Ba	3.929	21.5	19.639	17.942	19.448	23.31	34.392	32.038	5.951	4.798	29.095	19.28	±10.65
Pb	0.069	0.874	0.685	0.443	0.566	0.51	2.039	0.807	0.069	0.132	0.161	0.58	±0.57
Parameter	Apr	May	Jun	Jul	Aug	Sept	Oct	Nov	Dec	Jan	Feb	Ave	SD
$c_{\text{fluoride}} / \text{mg L}^{-1}$	0.114	0.12	0.099	0.099	0.099	0.108	0.115	0.106	0.112	0.1	0.102	0.11	±0.01
$c_{\text{chloride}} / \text{mg L}^{-1}$	8.18	6.18	11.81	28.71	19.94	15.7	18.54	8.9	9.12	8.16	8.26	13.05	±6.94
$c_{\text{nitrite}} / \text{mg L}^{-1}$	0.04	0.05	0	0.016	0.016	0.002	0.006	0.014	0.025	0.016	0.003	0.02	±0.02
$c_{\text{nitrate}} / \text{mg L}^{-1}$	0.422	0.153	0.209	0.19	0.312	0.039	0.517	0.704	1.496	1.844	2.132	0.73	±0.74
$c_{\text{phosphate}} / \text{mg L}^{-1}$	0	0.784	0	0	0.259	0	0	0.031	0.038	0.032	0.044	0.11	±0.24
$c_{\text{sulfate}} / \text{mg L}^{-1}$	9.94	10.29	9.89	10.15	10.06	10.37	10.12	10.37	10.57	9.71	9.84	10.12	±0.26
Dissolved $\text{O}_2, \text{mg L}^{-1}$	13.7	12	8.5	8.2	8.7	7.4	8.2	9.3	10.1	11.4	11.1	9.87	±1.96
pH	9.447	9.38	9.113	8.86	8.927	8.243	8.227	8.167	8.147	8.203	8.32	8.64	±0.51
Salinity, %	0.166	0.1	0.1	0.186	0.170	0.173	0.204	0.163	0.162	0.146	0.148	0.16	±0.03
$\sigma / \mu\text{S cm}^{-1}$	249.8	250.5	217.5	280.1	245.5	254.3	322.3	241.7	239.9	214.6	213.3	248.14	±31.56
Tot. diss. solids, mg L^{-1}	122.9	120	120	137.7	120.7	125	158.7	118.9	118.1	105.6	105	122.96	±14.78
$c_{\text{chlorophyll-a}} / \mu\text{g L}^{-1}$	4.5	3.33	4.33	9.18	11.55	13.08	5.74	4.62	4.44	2.44	2.3	5.96	±3.66
Light transp, cm	123	125	250	193	166	220	256	336	230	66	140	191.36	±76.76
$T_{\text{water}} / ^\circ\text{C}$	11	12	24	26.5	26.2	22	18	14	9	6	7	15.97	±7.7

TABLE S-II. The average values of the parameters according to the sampling stations

Element	Content, ppb				
	1.St.	2.St.	3.St.	Ave	Accepted limit
B	51.138	15.35	15.958	27.482	1472
Na	4678.35	4765.55	4443.59	4629.16	-
Mg	8165.22	8179.12	7956.86	8100.4	-
Al	22.566	25.94	28.477	25.661	27
Ca	13245.87	13566.14	12936.05	13249.35	-
Cr	2.663	2.941	2.897	2.834	142
Mn	4.193	4.836	3.384	4.138	100
Fe	69.215	69.573	72.212	70.333	101
Co	0.111	0.104	0.106	0.107	2.6
Ni	1.009	0.827	0.843	0.893	34
Cu	0.888	0.601	0.564	0.684	3.1
Zn	2.924	2.484	2.541	2.65	231
As	0.656	0.598	0.63	0.628	53
Se	6.562	6.381	6.129	6.357	10
Cd	0.064	0.029	0.036	0.043	1.5
Ba	19.51	18.553	19.591	19.218	680
Pb	0.722	0.504	0.468	0.565	14
PARAMETER					
$c_{\text{Fluoride}} / \text{mg L}^{-1}$	0.108	0.105	0.104	0.106	I
$c_{\text{Chloride}} / \text{mg L}^{-1}$	22.989	8.108	8.232	13.11	IV
$c_{\text{Nitrite}} / \text{mg L}^{-1}$	0.024	0.013	0.01	0.015	II
$c_{\text{Nitrate}} / \text{mg L}^{-1}$	0.725	0.716	0.803	0.748	I
$c_{\text{Phosphate}} / \text{mg L}^{-1}$	0.088	0.152	0.012	0.084	II
$c_{\text{Sulfate}} / \text{mg L}^{-1}$	10.189	10.109	10.049	10.116	I
Dissolved oxygen, mg L ⁻¹	9.7	9.8	9.7	9.7	I
pH	8.6	8.6	8.5	8.6	III
Salinity, %	0.199	0.144	0.147	0.163	-
Conductivity, $\mu\text{S cm}^{-1}$	304.05	220.87	216.48	247.13	I
Total dissolved solids, mg L ⁻¹	156.1	106.85	106.64	123.2	I
Content of chlorophyll- <i>a</i> , $\mu\text{g L}^{-1}$	6.05	6.23	5.88	6.05	II
Light transparency, cm	192	197	194	194	-
$T_{\text{water}} / ^\circ\text{C}$	15.9	16.2	15.9	16	I
SAR	0.2	0.2	0.1	0.1	Excellent
KI	0.1	0.1	0.08	0.09	Suitable
MgR	50	50	50	50	Suitable

The data of pH, nitrite, chloride, chlorophyll-*a*, and selenium measured in Kırklareli reservoir lake and found to exceed the first class water quality and the data of chloride value and chlorophyll-*a* distributions of the approaching second class water quality were visualized with the distribution maps created in the spatial analysis results made in the Arc MAP were given in Figs. S-1–S-5.

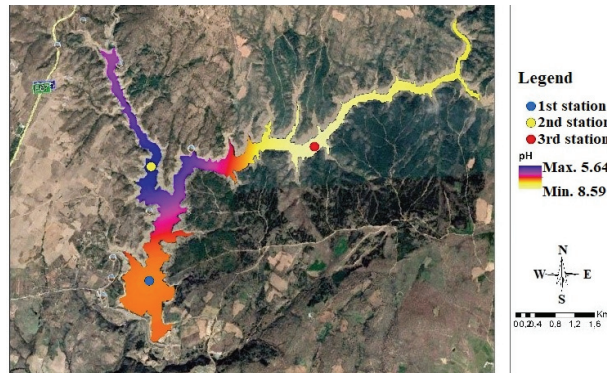


Fig. S-2. Spatial distributions of pH values prepared in Arc MAP.

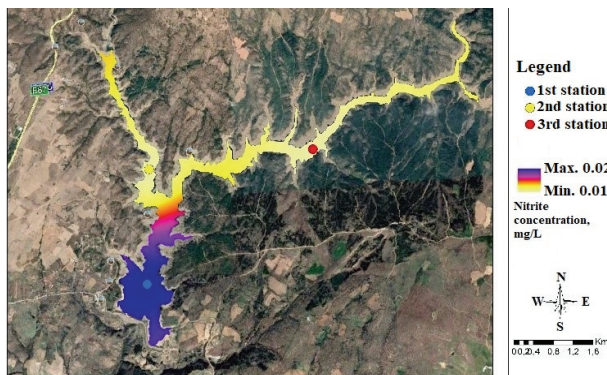


Fig. S-3. Spatial distributions of nitrite values prepared in Arc MAP.

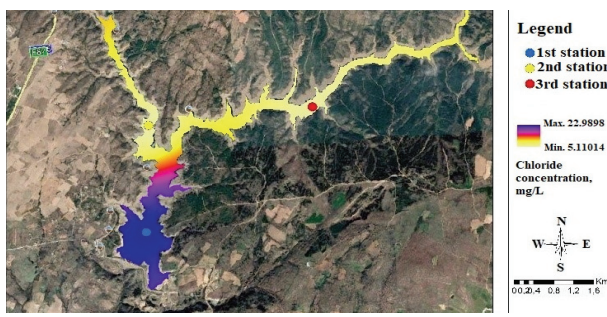


Fig. S-4. Spatial distributions of chloride values prepared in Arc MAP.

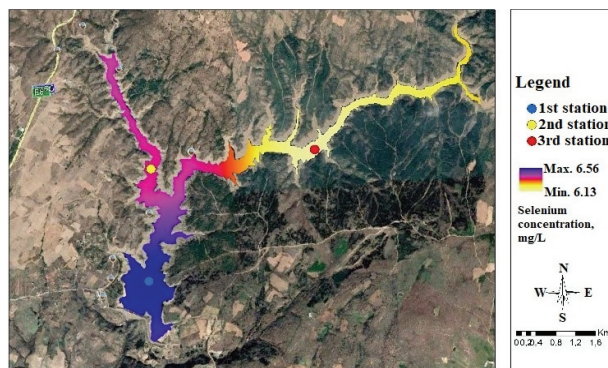


Fig. S-5. Spatial distributions of selenium values prepared in Arc MAP.

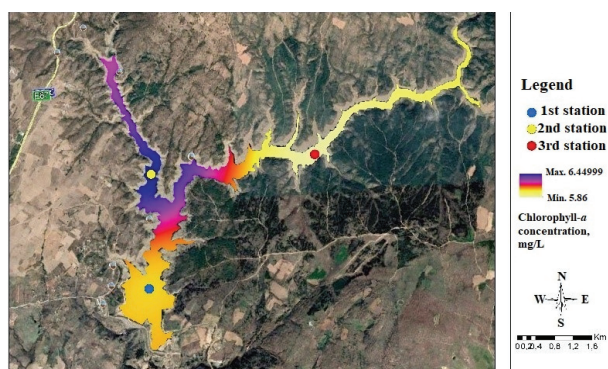


Fig. S-6. Spatial distributions of chlorophyll-a values prepared in Arc MAP.